Title

The Hydrogenation and Dehydrogenation of C2-C4 Hydrocarbons on Pt(111) Monitored In Situ Over 13 Orders of Magnitude in Pressure With Infrared-Visible Sum Frequency Generation

Author

Cremer, P.S.

Publication Date

1996-05-15

LBNL-39148
UC-401

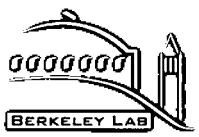

ERNEST ORLANDO LAWRENCE
BERKELEY NATIONAL LABORATORY

The Hydrogenation and Dehydrogenation of C_2-C_4 Hydrocarbons on Pt(111) Monitored *In Situ* Over 13 Orders of Magnitude in Pressure with Infrared-Visible Sum Frequency Generation

P.S. Cremer
Materials Sciences Division
Center for Advanced Materials

May 1996
Ph.D. Thesis

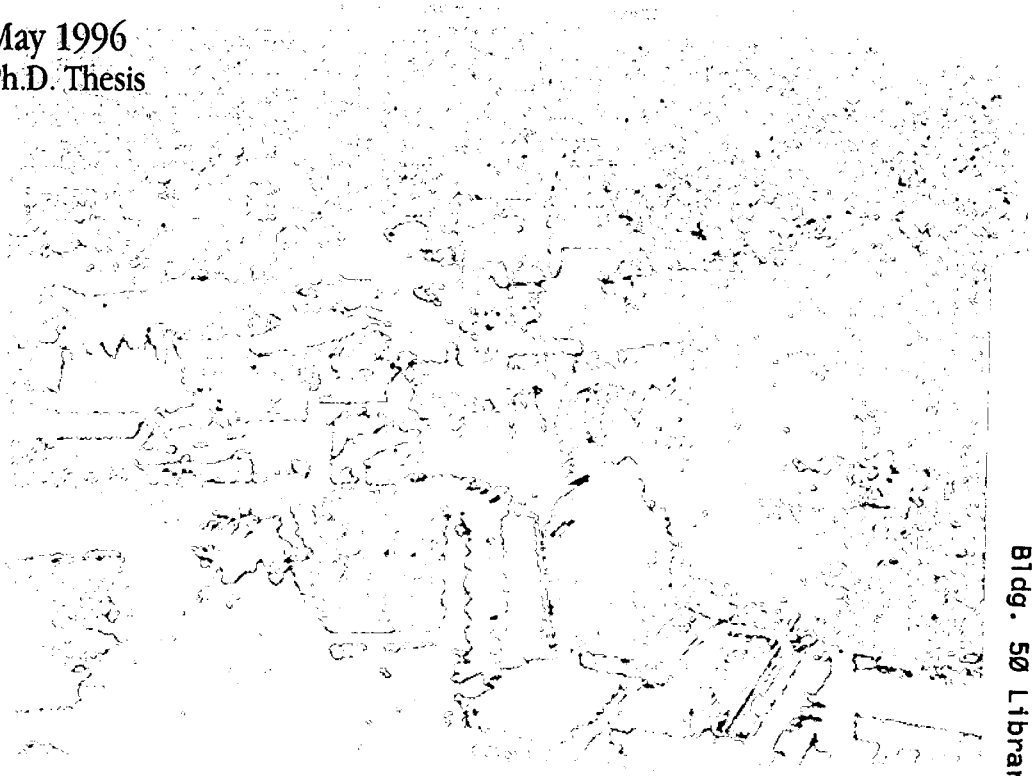

DISCLAIMER

LBL-39148
UC-401

The Hydrogenation and Dehydrogenation of C_2-C_4 Hydrocarbons on Pt(111) Monitored *In Situ* Over 13 Orders of Magnitude in Pressure with Infrared-Visible Sum Frequency Generation

Paul Samuel Cremer
Ph.D. Thesis

Department of Chemistry
University of California, Berkeley

and

Materials Sciences Division
Ernest Orlando Lawrence Berkeley National Laboratory
University of California
Berkeley, California 94720

May 1996

This work was supported by the Director, Office of Energy Research, Office of Basic Energy Sciences, Materials Sciences Division, of the U.S. Department of Energy under Contract No. DE-AC03-76SF00098.

The Hydrogenation and Dehydrogenation of C_2-C_4 Hydrocarbons On Pt(111) Monitored *In Situ* Over 13 Orders of Magnitude in Pressure With Infrared-Visible Sum Frequency Generation

by

Paul Samuel Cremer

B.A. (University of Wisconsin-Madison)

A dissertation submitted in partial satisfaction of the

requirements for the degree of

Doctor of Philosophy

in

Chemistry

in the

GRADUATE DIVISION

of the

UNIVERSITY OF CALIFORNIA, BERKELEY

Committee in Charge:

Professor Gabor A. Somorjai, Chair
Professor Y. Ron Shen
Professor Alexander Pines

1996

The Hydrogenation and Dehydrogenation of C_2-C_4 Hydrocarbons On Pt(111) Monitored *In Situ* Over 13 Orders of Magnitude in Pressure With Infrared-Visible Sum Frequency Generation

by

Paul Samuel Cremer

Abstract

The Hydrogenation and Dehydrogenation of C_2-C_4 Hydrocarbons

On Pt(111) Monitored *In Situ* Over 13 Orders of Magnitude in Pressure

With Infrared-Visible Sum Frequency Generation

by

Paul Samuel Cremer

Doctor of Philosophy in Chemistry

University of California, Berkeley

Professor Gabor A. Somorjai, Chair

The hydrogenation and dehydrogenation of ethylene, propylene, and isobutene were monitored *in situ* during heterogeneous catalysis over Pt(111) between 10^{-10} Torr and 1000 Torr with infrared-visible sum frequency generation (SFG). SFG is a surface specific vibrational spectroscopy capable of achieving submonolayer sensitivity under reaction conditions in the presence of hundreds of Torr of reactants and products.

Olefin dehydrogenation experiments were carried out with SFG under ultra high vacuum (UHV) conditions on the (111) crystal face of platinum. Ethylene chemisorbed on Pt(111) below 230 K in the di-σ bonded conformation (Pt-CH_2CH_2-Pt). Upon annealing the system to form the dehydrogenation product, ethylidyne (M≡CCH_3), evidence was found for an ethylidene intermediate (M=$CHCH_3$) from its characteristic $\nu_{as}(CH_3)$ near 2960 cm^{-1}. This same intermediate was also observed during the dehydrogenation of surface vinyl (M-$CHCH_2$) and acetylene to ethylidyne on Pt(111).

Hydrogenation of ethylene was carried out between 1 Torr and 700 Torr of H_2 while the vibrational spectrum of surface species was monitored with SFG. Simultaneously,

gas chromatography was used to obtain the turnover rate for the catalytic reaction, which could be correlated with the adsorbed intermediate concentration to determine the reaction rate per surface intermediate. Di-σ bonded ethylene, π-bonded ethylene, ethyl groups and ethylidyne resided on the surface during reaction. It was found that the dehydrogenation species, ethylidyne, competed directly for sites with di-σ bonded ethylene. π-bonded ethylene was proposed as the key reaction intermediate. The mechanistic pathway for ethylene hydrogenation involved the stepwise hydrogenation of π-bonded ethylene through an ethyl intermediate to ethane. The concentration of π-bonded ethylene under reaction conditions was approximately 4% of a monolayer. Therefore, the reaction rate was 25 times faster when measured per surface intermediate than per exposed platinum atom.

The hydrogenation of propylene was carried out under the same conditions as ethylene. It was found that propylene hydrogenates from π-bonded propylene through a 2-propyl intermediate to propane on Pt(111). The rate of reaction was approximately 50% slower than that of ethylene hydrogenation. Isobutene, however, was found to hydrogenate almost two order of magnitude slower than propylene on Pt(111). The reason for the dramatic reduction in rate was due to the slow hydrogenation of 2-isobutyl species. Indeed, 1-isobutyl may also be an important mechanistic pathway in isobutane production.

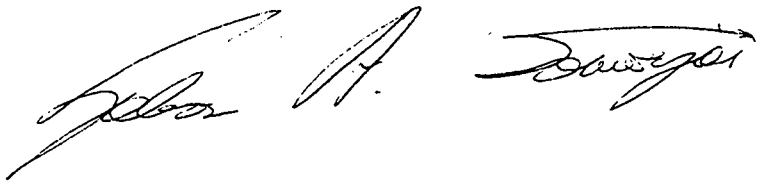

Dedicated to my father, Sheldon E. Cremer,

for teaching me the love of science.

Contents

Acknowledgments

As I look back over my years in graduate school I am overwhelmed by the number of people who have so graciously and patiently helped me. First, I would like to thank my advisor, Prof. Gabor A. Somorjai. The chance to work in his research group was truly an opportunity I will always cherish. Gabor gave me a tremendous amount of encouragement as well the freedom to explore uncharted territory. His advice on scientific matters and life in general have had a profoundly influenced me. I would also like to express my deepest thanks to Prof. Y. Ron Shen. Ron served as my coadvisor and taught me a tremendous amount about nonlinear optics and spectroscopy. I found the collaboration and the ability to work in an interdisciplinary area tremendously rewarding.

I wish to thank Prof. Andrew Gellman for getting me started in the field of surface science and teaching me the "hands on" of ultra high vacuum. I am also greatly indebted to Dr. Colin Stanners, who was the postdoc on the laser project as I arrived in Berkeley. He taught me how to use SFG, HREELS, and the specifics of the laboratory. My further thanks go to Dr. Enrico Magni, who in addition to being a great friend, showed me the world of Reynolds' numbers, batch reactors, flow reactors and chemical engineering.

I wish to acknowledge the tremendous encouragement and advice I received from Prof. Hans Niemantsverdiet, who spent a summer in the lab with me during his sabbatical from the Eindhoven University of Technology. I sincerely value his wisdom in the field of catalysis as well as his patience and friendship. My thanks also go to my classmates Peter Jacobs and Craig Gerken. The many hours we spent discussing topics scientific and otherwise were always enjoyable. I would also like to acknowledge Dr. Rodney Chin who shared the laser with me for more than two and one half years. The time we spent together both inside and outside the lab was always fun. I would like to thank the Somorjai group secretary, Bob Kehr, who went above and beyond to help me in so many

ways. I would like to thank Dr. Howard Fairbrother for thought provoking and informative conversations about "the real world" of science.

In my last two years at Berkeley I have had the chance to work with Xingcai Su, who will be taking over the laser system. It was a pleasure to work with him. His friendship and good nature were always greatly appreciated. I wish Xingcai and the new postdoc, Dina Zhang, with whom I only had a brief chance to overlap, the best of luck! I know that the system will be in good hands with them.

I wish to thank my parents, Joanne and Sheldon Cremer, who were always there for me. Perhaps most importantly I would like to thank my wife, Christine. She has taught me how to enjoy my time outside the lab and added true meaning to my life.

Chapter 1

Introduction

Over the past three decades surface scientists have modeled heterogeneous catalytic reactions on metal single crystal surfaces by undertaking ultra high vacuum (UHV) investigations. The arsenal of UHV techniques available to perform such studies includes: low energy electron diffraction (LEED) for surface crystallography, high resolution electron energy loss spectroscopy (HREELS) and reflection adsorption infrared spectroscopy (RAIRS) for probing surface vibrational modes, Auger Electron Spectroscopy (AES) and X-ray photoemission spectroscopy (XPS) for chemical analysis of the surface, and mass spectrometry for monitoring the desorption of surface species [1]. Many important observations were made in terms of adsorbate ordering, adsorbate-adsorbate interactions, surface restructuring, surface diffusion, mobility, thermal decomposition (such as coking), and specific active sites for reaction [2]. However, the pressure gap between the plethora of vacuum results obtained at 10^{-10} Torr and the characterization of reactions under realistic conditions (atmospheres of reactant gases) still needed to be bridged.

1.1 Bridging the Pressure Gap with SFG

The challenge, in the mid 1990s has been to bridge the pressure gap by developing characterization methods that allow *in situ* monitoring of the surface under realistic reaction conditions. This means that adsorbate identification, concentration, and active site location have to be probed under realistic reaction conditions as well as under ultra high vacuum (a range of thirteen order of magnitude in pressure). To help bridge the gap we have employed infrared-visible sum frequency generation, a surface specific

spectroscopy [3], to monitor late transition metal surfaces at ambient temperatures (~300 K) and pressures (~1 atm) during heterogeneous catalytic reactions such as olefin hydrogenation.

The SFG technique operates by combining an infrared and a visible photon to produce an output at their sum frequency ($\omega_{sf}=\omega_{vis}+\omega_{ir}$). The process essentially consists of infrared adsorption by a vibrational mode coupled with upcovertion via a Raman process [4]. Therefore, for a mode to be SFG active it must obey both the infrared and Raman selection rules. Since only modes which lack centrosymmetry can be simultaneously infrared and Raman active, signal is primarily obtained from interfaces and surfaces where centrosymmetry is always broken, rather from the bulk where it is usually not. In model transition metal single crystal catalysts, the bulk lattices (fcc, bcc, and hcp) possess inversion symmetry. The gas phase above the catalyst is isotropic and possesses inversion symmetry as well. Hence, signal in such systems is only expected from the interface where inversion symmetry is always broken. This makes SFG an ideal tool for obtaining surface specific information during heterogeneous catalytic reactions.

1.2 The Goal: Measuring Active Site Concentrations

The goal of *in situ* heterogeneous catalytic experiments on model transition metal surfaces is to obtain information about reactive surface intermediates concurrently with gas phase kinetic data. The correlation of simultaneously acquired data can ultimately provide the molecular details of catalytic reaction pathways, as well as the relationship between macroscopic turnover rates and surface intermediate concentration. The ability to identify the key surface intermediates and measure their concentration will allow for turnover rate measurements to be calculated per surface intermediate. This contrasts with the traditional method of expressing rates per exposed surface atom of the underlying catalyst [5]. Measurements made per exposed surface atom provide merely a lower bound for the rate of product formation per active site. Indeed, if reactions are

only taking place on 1% of the surface, but doing so at a rate of 100 turnovers/(site·sec) this would yield the same macroscopic turnover number that would be measured for all sites being active at only 1 turnover/(site·sec). An example is shown in figure 1, where only one adsorbed intermediate (π-bonded ethylene) is on the surface in the presence of eight platinum atoms.

The question of active site concentration and the reaction rate per active site (i.e. per surface intermediate) lies at the heart of catalysis. The best and most direct way of determining such information is to investigate both the molecular level detail of the surface and the gas phase kinetics simultaneously.

1.3 Organization of the thesis:

Chapter 2 explains the experimental details of incorporating the infrared-visible sum frequency generation technique into an ultra high vacuum system equipped with a batch reactor. The main area of concentration is on the vibrational information expected from adsorbates on transition metal surfaces.

Chapters 3 and 4 explore the UHV thermal decomposition chemistry on Pt(111) of ethylene and acetylene, respectively [Fig. 2, eqn. 1, 2]. The results indicate that ethylidyne ($M{\equiv}CCH_3$) is most likely formed through an ethylidene ($M{=}CHCH_3$) precursor in both cases.

Chapters 5, 6, 7 deal with the hydrogenation of olefins over Pt(111) monitored *in situ* under atmospheric pressures of reactants near room temperature [Fig. 2, eqn. 3-5]. The results for ethylene hydrogenation indicate that ethylene hydrogenates stepwise from a π-bonded ethylene species, through an ethyl group to ethane (Chapter 5). The concentration of the key intermediate, π-bonded ethylene, was found to be approximately 4% of a monolayer under reaction conditions; hence, the turnover rate per π-bonded ethylene is 25 times faster than the turnover rate per surface platinum atom. In chapter 6 the more complex propylene system is investigated. Propylene hydrogenation on Pt(111)

is found to be approximately 40% slower than ethylene under identical reaction conditions. Spectroscopic evidence revealed that the dominate mechanism for propylene hydrogenation is from the π-bonded species through a 2-propyl group to propane. Chapter 7 explores the chemistry of isobutene and hydrogen. Isobutene hydrogenation also proceed through a π-bonded intermediate; however, the pathway through 2-isobutyl groups was found to be very much impeded compared to the analogous 2-propyl chemistry. The hindrance of the 2-isobutyl pathway caused this reaction to slow down by about a factor of 20 with respect to the propylene rate.

Chapter 8 discusses results for the packing and orientation of L&S 2-butyl alcohol at the BaF_2 interface. Using SFG to monitor relative surface concentrations, it was found that the pure left handed enantiomer could pack more densely on the surface near 308 K than could the racemate. This contrasted with the bulk liquid where nearly identical densities are observed at this temperature.

Chapter 9 shows data for partly deuterated ethanols at the liquid/vapor interface. Comparing the spectra with known Raman and infrared data for the bulk liquid allows the peak assignments to be properly designated. Finally, chapter 10 draws some conclusions about the nature of catalytic reaction intermediates under reaction conditions compared with species more typically seen under ultra high vacuum. Future directions for heterogeneous catalysis with SFG are also discussed.

1.4 References

[1] D. Woodruff and T. Delchar, Modern techniques of Surface Science, Cambridge University Press, 1986

[2] G. Somorjai, Introduction to Surface Chemistry and Catalysis, Wiley, 1994

[3] Y. Shen, Nature, 337 (1989) 519

[4] Y. Shen, Surf. Sci., 299/300 (1994) 551

[5] T. Madey, J. Yates, D. Standstrom, and R. Voohoeve, in Treatise on Solid State Chemistry 6B, ed. B. Hannay, Plenum Press, 1976

1.5 Figure Captions

Fig. 1 Schematic representation of the hydrogenation of ethylene on Pt(111). For the above case, it is clear that the turnover rate measured per surface ethylene would be considerably faster than that measure per platinum atom.

Fig. 2 Schematic summary of the olefin chemistry presented in this thesis.

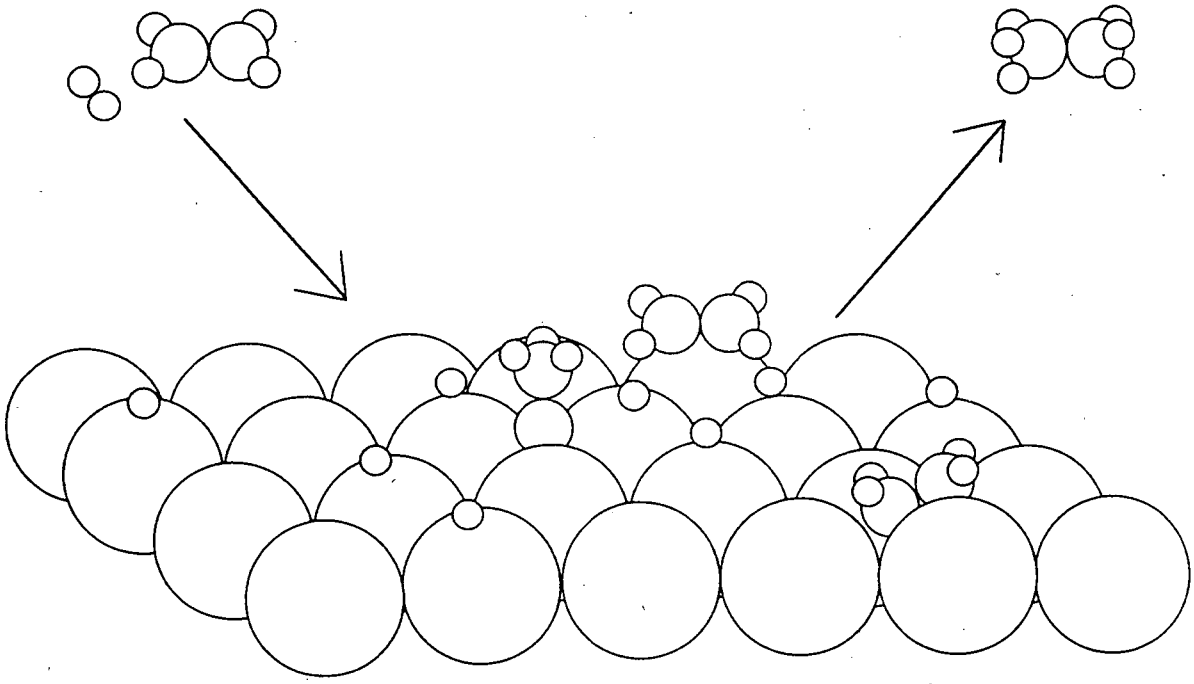

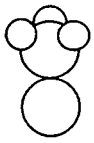

Ethylidyne

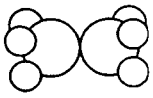

Ethane

Hydrogen

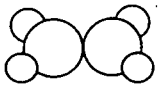

π–Ethylene

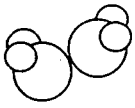

Di-σ Ethylene

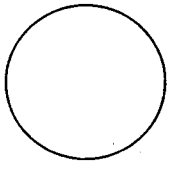

Platinum

Fig. 1

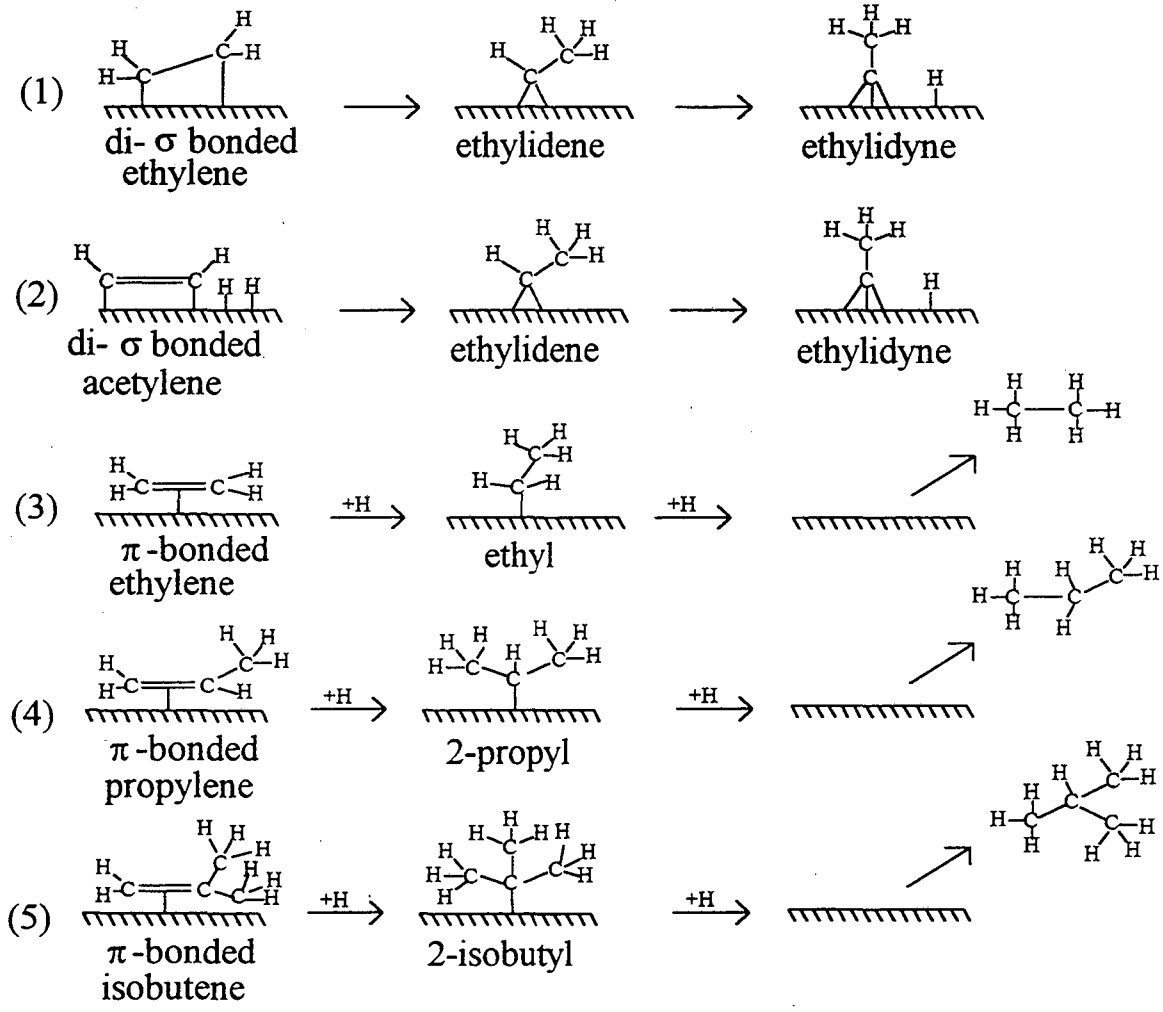
(1)
di- σ bonded ethylene
ethylidene
ethylidyne
(2)
di- σ bonded acetylene
ethylidene
ethylidyne
(3)
π-bonded ethylene
+H
ethyl
+H
(4)
π-bonded propylene
+H
2-propyl
+H
(5)
π-bonded isobutene
+H
2-isobutyl
+H

Fig. 2

Chapter 2

Instrumentation

The purpose of this chapter is to describe the apparatus that was built in our laboratory to couple nonlinear optics to a heterogeneous catalytic batch reactor/UHV setup. In addition, specific applications of sum frequency generation to adsorbates on Pt(111) and Rh(111) samples will be discussed. It is, however, not the goal of this discussion to reiterate the general theoretical and experimental considerations for optical parametric generators/amplifiers or the infrared-visible sum frequency generation experiment, as this has already been done elsewhere many times [1-4].

2.1 The UHV-Batch Reactor

A batch reactor with optical windows was designed and coupled via a gate valve to an ultra high vacuum system [Fig. 1]. The reactor could be charged to 1.5 atmospheres of total pressure and was equipped with a recirculation pump in the reaction loop. The loop contained a septum for gas abstraction and analysis by an HP5890 Series II gas chromatograph. The mixing time of the chamber, τ, was determined to be approximately 3 minutes by following the dilution of a plug of methane gas mix into a background of pure argon. The reactor volume was 62.3 liters and could be pumped out to a base pressure of $5 * 10^{-11}$ Torr by opening a gate valve to an ion and turbomolecular pump.

The reactor was fitted with CaF_2 windows to allow infrared and visible light to pass into it and to allow sum frequency light to pass out to the detector. The sample could be resistively heated to 1000 K and cooled using liquid nitrogen to 120 K under vacuum (250 K under ambient pressure). When the reactor was under vacuum, typical surface

analysis techniques such a mass spectrometer and a retarding field analyzer for Auger and LEED were available. An Ar^+ gun allowed the crystal to be sputtered clean.

A typical example of the kinetic data for the reactor is shown in figure 2a. In this case 1.75 Torr of H_2, 0.25 Torr of ethylene yielded a rate of 1.6 turnovers/(site·sec). The noise level for this measurement was approximately 0.1 turnovers/(site·sec). The background turnover rate was measured by removing the platinum sample from the manipulator. Despite the large size of the system, the turnover rate of the background was determined to be well less than 0.1 turnover/(site·sec) [Fig 2b].

2.2 SFG on Late Transition Metal Single Crystals

The Pt(111) sample used as a model heterogeneous catalyst could be monitored with infrared-visible sum frequency generation (SFG). SFG is a three wave mixing process which involves the addition of infrared (ω_{ir}) and visible light (ω_{vis}) to produce light at the sum of these two frequencies ($\omega_{sf}=\omega_{ir}+\omega_{vis}$) [Fig. 3] [1, 2]. The visible beam is held at fixed frequency while the infrared beam is tuned over the vibrational range of interest. The electromagnetic radiation source for the experiment comes from a passive, active mode locked Nd:YAG laser which outputs a 20 ps pulse at 1064 nm when using #5 dye from Kodak. The repetition rate of the laser is 20 Hz and the total energy per pulse is approximately 50 mJ. The energy is divided into three portions. The first of which is frequency doubled using KD^*P to produce green light at 532 nm. The remaining light is employed to generate infrared light by one of two angle tunable optical parametric generator/amplifier (OPG/OPA) stages capable of producing infrared radiation over most of the range from 1100-4000 cm^{-1}. The first OPG/OPA generates light from 2600 cm^{-1} to 4000 cm^{-1} with a FWHM of 12 cm^{-1} at 2880 cm^{-1} using $LiNbO_3$, while the second OPG/OPA is angle tunable from 1100 cm^{-1} to 2400 cm^{-1} with a FWHM of 4 cm^{-1} by difference frequency generation in a $AgGaS_2$ crystal [3]. The infrared and visible beams are temporally aligned and focused concentrically on the late transition metal catalyst

inside the batch reactor. The spot size of the green beam is approximately 1.55 mm FWHM at the sample and the beam makes an angle of 50° with respect to the surface normal. The input energy is approximately 400 μJ. These values yield a total power of approximately 0.8 gigawatts/cm^2. This regime has been shown experimentally to be at least a factor of 4 below powers that cause either photochemistry or damage the platinum sample even over extended periods of time. The infrared radiation is focused to approximately 1.2 mm inside the green spot at an angle of 56° with respect to the surface normal and the maximum energy out of the OPG/OPA is always used. The infrared power varies widely with frequency. The maximum infrared power is at 2850 cm^{-1}. At this frequency the IR energy at the sample is approximately 275 μJ/pulse when using Kodak #5 dye (approximately 20 ps pulses).

The upcoverted light (ω_{sf}), which is in the blue (450 - 490 nm), is sent through a polarizer and then focused through two anti-stokes Raman edge filters onto the entrance slit of a 20 cm monochrometer. The output from the monochrometer is detected by a Hamamatsu type R647-04 photomultiplier tube. The signal is converted to a voltage, sent to a box car integrator and then stored on a PC. The efficiency of the detection system is approximately 3%. The major loss of signal comes from the monochrometer (25% transmission at 460 nm) and the low quantum efficiency of the photomultiplier tube (20 % at 460 nm).

The signal generated at the surface per laser pulse follows the equation [2]:

$$S(\omega_{sf}) = \frac{8\pi^3 \omega_{sf} \sec^2 \theta_{sf}}{\hbar c^3 (\varepsilon^{sf} \varepsilon^{ir} \varepsilon^{vis})^{1/2}} \left| e'_{sf} \cdot \chi^{(2)} : e'_{ir} e'_{vis} \right|^2 \frac{U_{ir} U_{vis}}{AT} \qquad (1)$$

Where S is the signal, $\chi^{(2)}$ is the nonlinear susceptibility of the medium being probed, ε is the dielectric constant of the probe medium, e' is a unit vector which describes the field polarization, U_{ir} and U_{vis} are the input beam energies, A is the overlap area for the green

and infrared, T is the temporal overlap, and θ_{sf} is the angle the sum frequency output makes with respect to the normal of the probe medium (about 51°).

A typical spectrum of a hydrocarbon species, ethylidyne ($M{\equiv}CCH_3$) on Pt(111) is shown in figure 4a. The spectrum was taken under UHV with both the infrared and visible electric fields polarized normal (or p polarized) to the surface. The sum frequency signal output was also p polarized. This is designated a PPP measurement (where the first P is the designation of the output light, the second P is the designation of the visible light, and the third P is the polarization of the infrared light). The unfitted peak at 2878 cm^{-1} represents approximately 7.6 photons per shot. Taking into account the detection efficiency, there are more than 200 photons generated at the sample per laser shot. This corresponds to $\chi^{(2)}{\approx}10^{-16}$ esu. The terms a, k, ω, θ, and Γ (shown with the spectrum) are parameters from the curve fitting equation and will be discussed on pages 14-15.

The PPP polarization combination consists of four possible nonzero components of the nonlinear susceptibility tensor: $\chi^{(2)}_{zzz}$, $\chi^{(2)}_{yyz}$, $\chi^{(2)}_{yzy}$, and $\chi^{(2)}_{zyy}$. However, because the experiment takes place on a conductor, the electrons inside the metal surface can follow the oscillation of the electric field from the incident light nearly perfectly up to the plasmon frequency of the metal. For the component of the electric field that is in plane with the surface this leads to near perfect cancellation of the field. It is therefore expected that only the $\chi^{(2)}_{zzz}$ component will make a significant contribution to the observable nonlinear susceptibility. To test this, the SSP and SPS polarization were probed. Figure 4b shows the spectrum from di-σ bonded ethylene probed with the SSP polarization combination, which probes χ_{yyz} exclusively. The peak frequency at 2883 cm^{-1} has an intensity corresponding to approximately 0.20 photons/shot. This is down by a factor of 38 from the signal generate from the PPP polarization combination. Figure 4c shows the spectrum for ethylidyne on Pt(111) probed with the SPS polarization combination. This combination probes χ_{yzy} exclusively. As can be seen from the spectrum, the signal was undetectable and therefore down at least three orders of

magnitude from the PPP spectrum. There was also no intensity for the PSS component either which would probe χ_{zyy}. From these experiments it can be concluded that the χ_{zzz} term dominates the response for PPP. Indeed, the only reason why any signal can be seen from SSP (χ_{yyz}) is because the green and blue frequencies are close enough to the plasmon frequency that the cancellation of the electric field is not quite perfect.

The signal generated at the sample is proportional to the square of the second order susceptibility as can be seen from equation 1. As noted above the tensor is reduced to the signal component, χ_{zzz}, on a transition metal catalyst and is related to the microscopic second order polarizability, $\alpha_q^{(2)}$ by the equation:

$$\chi_{zzz}^{(2)} = \sum_q N_q <(\hat{i}\cdot\hat{l})(\hat{j}\cdot\hat{l})(\hat{k}\cdot\hat{m})> \alpha_{lmn,q}^{(2)} \qquad (2)$$

N_q represents the number density of the oscillator q and lmn represent their orientation [4]. As can be seen from the above equation, $\chi^{(2)}{}_{zzz}$ is sensitive to the orientation of second order microscopic polarizability as $\cos^3\theta$. Because the signal is proportional to $\left|\chi_{zzz}^{(2)}\right|^2$, the overall sensitivity of the experiment goes as $\cos^6\theta$. This means that small changes in molecular orientation will have a very substantial affect on the signal observed.

The signal strength is highly dependent on molecular orientation, and changes in coverage may lead to changes in the dynamic dipole or changes in the first order polarizability of the probe species. Therefore, it is quite difficult to use sum frequency spectra for measures of absolute surface coverage. If one has information on what could affect the chemical environment, it is certainly possible to calibrate concentrations to within an order of magnitude, but better than a factor of two would be highly suspect. Further, because experiments of interest in heterogeneous catalysis are conducted on late transition metal surfaces, only the χ_{zzz} term is observable with sufficient strength to be of

practical use. This means that there is insufficient information available to get an estimate of the orientation of the dynamic dipole from these experiments.

For the case of hydrocarbons on Pt(111) there are essentially two sources of $\alpha^{(2)}$, a resonant term, $\alpha^{(2)}_{res}$ from the vibrational modes as well as a nonresonant term, $\alpha^{(2)}_{nr}$, from the top few layers of platinum atoms. For the case in figure 4a there is one vibrational resonance as well as a nonresonant background. Therefore we can write:

$$\chi^{(2)}_{zzz} = N_r < (\hat{i}\cdot\hat{l})(\hat{j}\cdot\hat{l})(\hat{k}\cdot\hat{m}) > \alpha^{(2)}_{lmn,r} + N_{nr} < (\hat{i}\cdot\hat{l})(\hat{j}\cdot\hat{l})(\hat{k}\cdot\hat{m}) > \alpha^{(2)}_{nr} \qquad (3)$$

where the resonant term can be modeled as :

$$\alpha^{(2)}_{lmn,r} = \frac{A'}{\omega_r - \omega_{ir} + i\Gamma} \quad \text{and} \quad A' = \frac{1}{2\omega_r}\frac{\partial\mu}{\partial q}\frac{\partial\alpha^{(1)}_{lm}}{\partial q}$$

The resonance frequency, ω_r, in figure 4a is at 2882 cm^{-1} and as the infrared light, ω_{ir}, is scanned through it, a general Lorentzian lineshape is formed with the damping term represented by $i\Gamma$. A' is comprised of two parts: (1) the change in dipole moment, $\frac{\partial\mu}{\partial q}$, which is the gross selection rule for infrared spectroscopy and (2) the change in first order polarizability, $\frac{\partial\alpha^{(1)}_{lm}}{\partial q}$, which is the gross selection rule for Raman spectroscopy. This is in essence the hart of the sum frequency generation selection rules. For a vibrational mode to be observable it must be both infrared and Raman active. Because, in the dipole approximation, only those modes which lack centrosymmetry can be both infrared and Raman active signal is necessarily obtained from surfaces, but forbidden in centrosymmetric media (such as face centered cubic lattices like platinum and isotropic gas phases). Therefore in the case of heterogeneous catalysis performed on a signal crystal of platinum one derives a vibrational spectrum which is dominated by the modes of the adsorbed surface monolayer.

The nonresonant contribution to the signal is normally modeled by a constant, k, that has some phase relationship, $e^{i\varphi}$, with respect to the resonance term. The lineshape for SFG spectra of a single resonance with a nonlinear background can be modeled by:

$$\left|\chi^{(2)}\right|^2 = \left|\frac{A}{\omega_r - \omega_{ir} + i\Gamma} + ke^{i\varphi}\right|^2 = \frac{A^2 + 2Ak[(\omega_r - \omega_{ir})\cos\varphi - \Gamma\sin\varphi]}{(\omega_r - \omega_{ir})^2 + \Gamma^2} + k^2 \qquad (4)$$

where $A(=A'<>N_r)$, k, ω_r, φ, and Γ are adjustable parameters which can all be determined by fitting. The consequences of a nonresonant background are readily evident from figure 4a:

There is an interference between the nonresonant background and the resonant feature such that the background constructively interferes at frequencies immediately before the peak and destructively interferes at higher frequency. This leads to the dip seen after the resonance feature. Also, the peak maximum occurs slightly before the actual resonance. In this case ω_r=2882 cm^{-1}, but the peak maximum occurs 4 cm^{-1} below this. The relationship between the area under the curve and number density of species on the surface is also a bit complex. For situations where A » k the area under the curve will go as N^2. However, when k » A the area will approximately go as N and in intermediate situations such as figure 2a it will be a mixture of N and N^2 dependence. Despite the fact that signal intensity dependence on number density is not as straight forward as that for linear spectroscopies, there are never the less some distinct advantages. For strong resonance features the signal increases as N^2 as the number density increases, which gives rise to strong signals. However, if the number density is small, the intensity only falls linearly as the coverage approaches zero.

An example of how the changes in k and θ can affect spectra is seen in figure 4d. This is the vibrational spectrum for a saturation coverage of ethylidyne/Rh(111). Most of the difference in lineshape and depth of the interference after the peak (as compared with 2a) are the direct effect of the change in these two parameters. The values change versus

Pt(111) because the electronic structure of Rh(111) leads to changes in the nonresonant background term. It should be noted that the change in the width of line is from changes in Γ, which is not simply a function of the metal. The linewidth is more likely affected by surface order which comes from how the ethylidyne interacts with the metal surface.

For multiple resonances, the interference between the resonances also must be taken into account. A system with two resonant features and a nonresonant background are modeled as follows:

$$\left|\chi^{(2)}\right|^2 = \left|\frac{A}{\omega_{r_a} - \omega_{ir} + i\Gamma_a} + \frac{B}{\omega_{r_b} - \omega_{ir} + i\Gamma_b} + ke^{i\varphi}\right|^2 = \tag{5}$$

$$\frac{A^2}{(\omega_{r_a} - \omega_{ir})^2 + \Gamma_a^{\,2}} + \frac{B^2}{(\omega_{r_b} - \omega_{ir})^2 + \Gamma_b^{\,2}}$$

$$+\frac{2Ak[(\omega_{r_a} - \omega_{ir})\cos\varphi - \Gamma_a \sin\varphi]}{(\omega_r - \omega_{ir})^2 + \Gamma_a^{\,2}}$$

$$+\frac{2Bk[(\omega_{r_b} - \omega_{ir})\cos\varphi - \Gamma_b \sin\varphi]}{(\omega_{r_b} - \omega_{ir})^2 + \Gamma_b^{\,2}}$$

$$+\frac{2AB[(\omega_{r_a} - \omega_{ir})(\omega_{r_b} - \omega_{ir}) + \Gamma_a\Gamma_b]}{[(\omega_{r_a} - \omega_{ir})(\omega_{r_b} - \omega_{ir}) + \Gamma_a\Gamma_b]^2 - [(\omega_{r_a} - \omega_{ir})\Gamma_b + (\omega_{r_b} - \omega_{ir})\Gamma_a]^2}$$

$$+k^2$$

In this case the first two terms represent the Lorentzian contributions of the two resonant features. The third and fourth terms are the interferences between the features and the nonresonant background. The fifth term is the interference between the resonant features and the final term is due to the nonresonant background.

2.3 *In Situ* Catalysis with SFG

The importance of the SFG-batch reactor apparatus is immediately apparent. Vibrational spectroscopy can be performed simultaneously with gas phase kinetic

measurements. The object is to try to correlate turnover rates with specific species present on the surface during catalysis. Specifically, the object is to vary the temperature, pressure, surface pretreatment, etc. to see how this affects both the reaction rate and the nature/concentration of surface adsorbates. Such information may then be used to determine mechanistic pathways, specific reaction sites, and turnover rates with respect to individual intermediate concentrations. The greatest pitfall of such a method is that nonreactant species (such as ethylidyne ($M{\equiv}CCH_3$) in ethylene hydrogenation) could be incorrectly identified as reactant intermediates. Therefore, the best use of batch reactor methods is to rule species *out* rather than *in* as candidates for key reaction intermediates. This can be done for example by carefully varying conditions to lead to large changes in a surface species without significantly changing the turnover rate as was done for di-σ bonded ethylene in ethylene hydrogenation (see chapter 5). The best way to definitively determine if a species is indeed a key intermediate is to follow its signature in a flow mode system.

2.4 References

[1] Y. Shen, Nature, 337 (1989) 519

[2] Y. Shen, Surf. Sci., 299/300 (1994) 551

[3] J. Zhang, J Huang, Y. Shen, and C. Chen, J. Opt. Soc. Am., 10 (1993) 1758

[4] R. Superfine, Ph.D. Thesis, 1991 University of California-Berkeley

2.5 Figure Captions:

Fig 1 The UHV/Batch reactor apparatus coupled to a Nd:YAG laser for *in situ* SFG studies.

Fig. 2 (a) The turnover data for ethylene hydrogenation monitored by gas chromatography with 1.75 Torr H_2, 0.25 Torr C_2H_4 at 295 K. (b) same as the conditions in (a), but without the platinum catalyst

Fig. 3 The SFG experiment

Fig. 4 The SFG spectrum of ethylidyne on Pt(111) at room temperature monitored with (a) PPP, (b) SSP, and (c) SPS polarization combinations. (d) The SFG spectrum of ethylidyne on Rh(111) monitored with the PPP polarization combination.

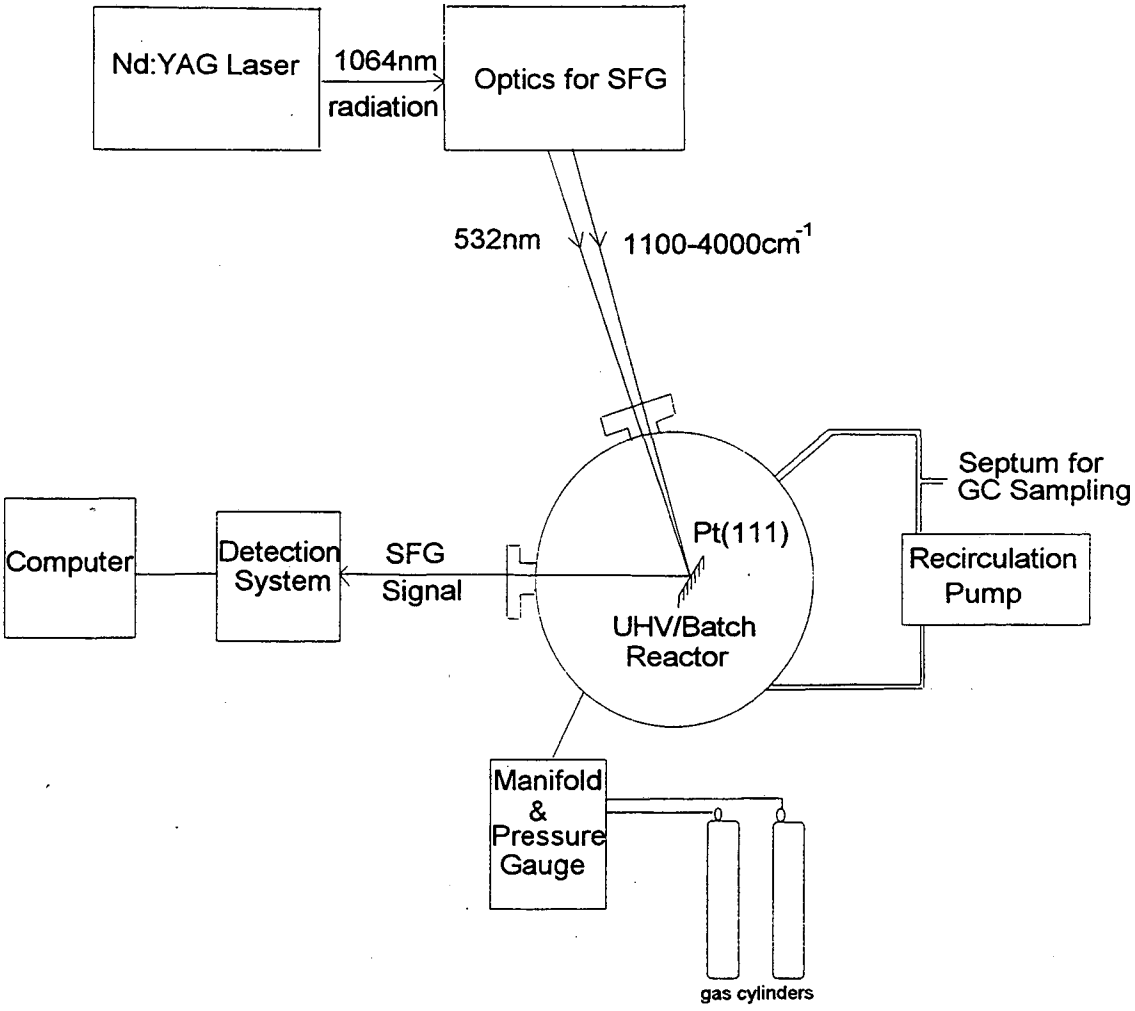
Nd:YAG Laser
1064nm
radiation
Optics for SFG
532nm
1100-4000cm-1
Septum for
GC Sampling
Computer
Detection
System
SFG
Signal
Pt(111)
Recirculation
Pump
UHV/Batch
Reactor
Manifold
&
Pressure
Gauge
gas cylinders

Fig. 1

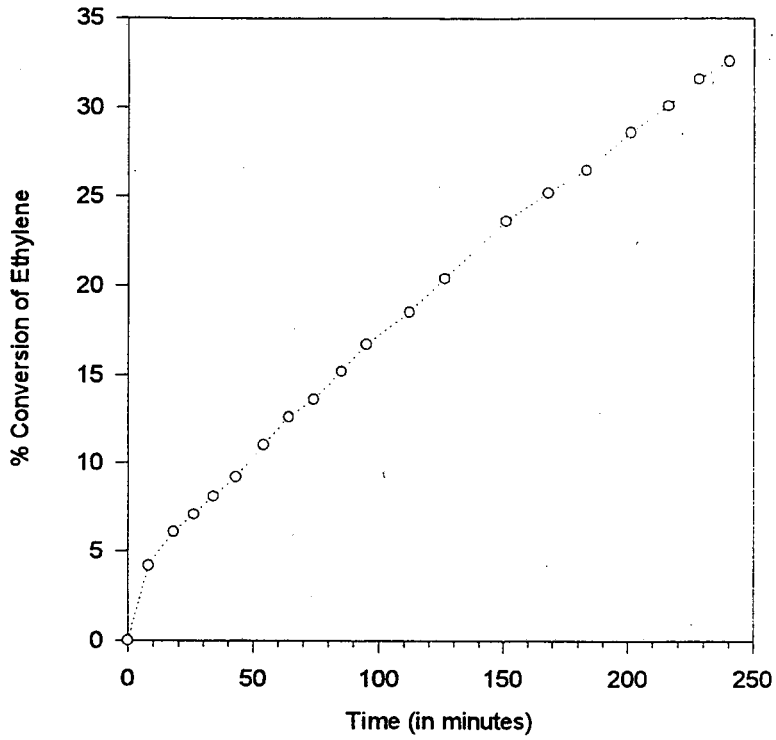
% Conversion of Ethylene
Time (in minutes)
0
5
10
15
20
25
30
35
0
50
100
150
200
250

(a)

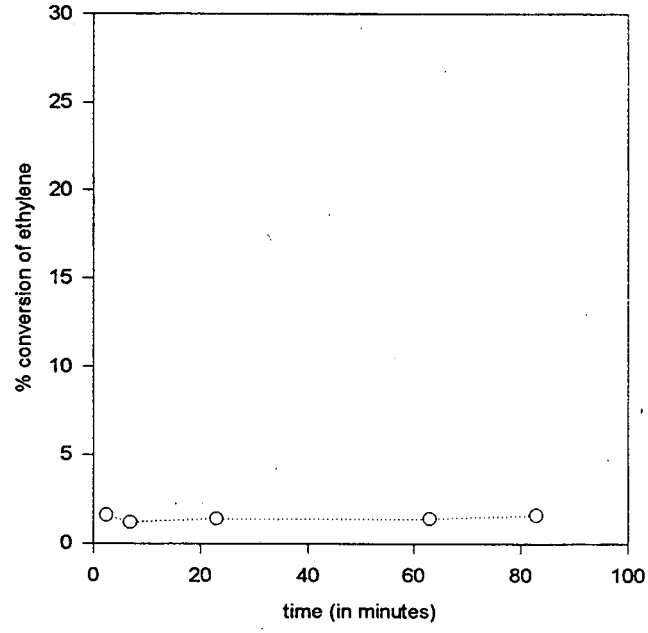
% conversion of ethylene
time (in minutes)
0
5
10
15
20
25
30
0
20
40
60
80
100

(b)

Fig. 2

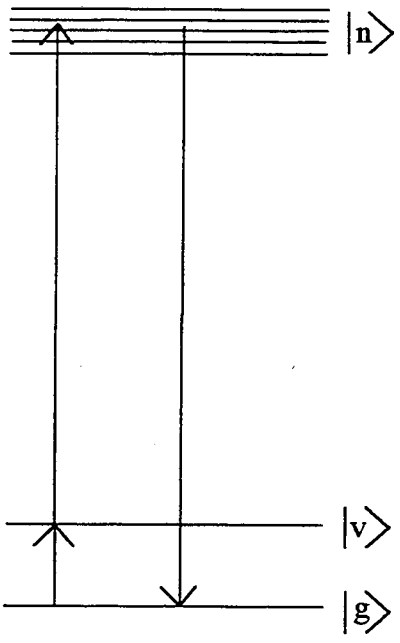

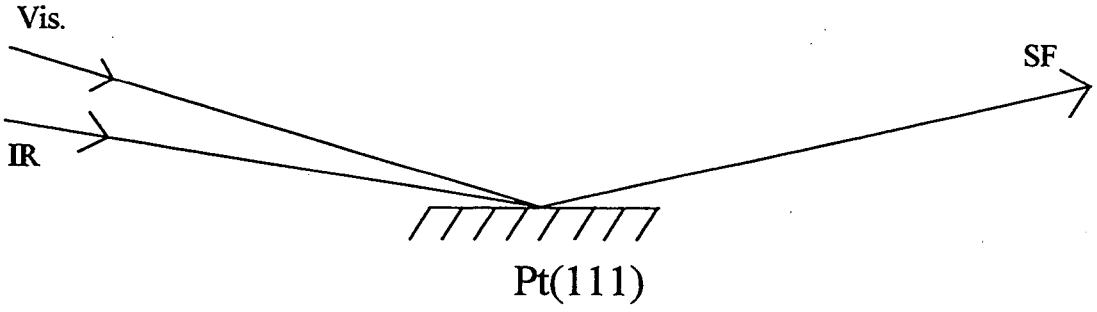

Fig. 3

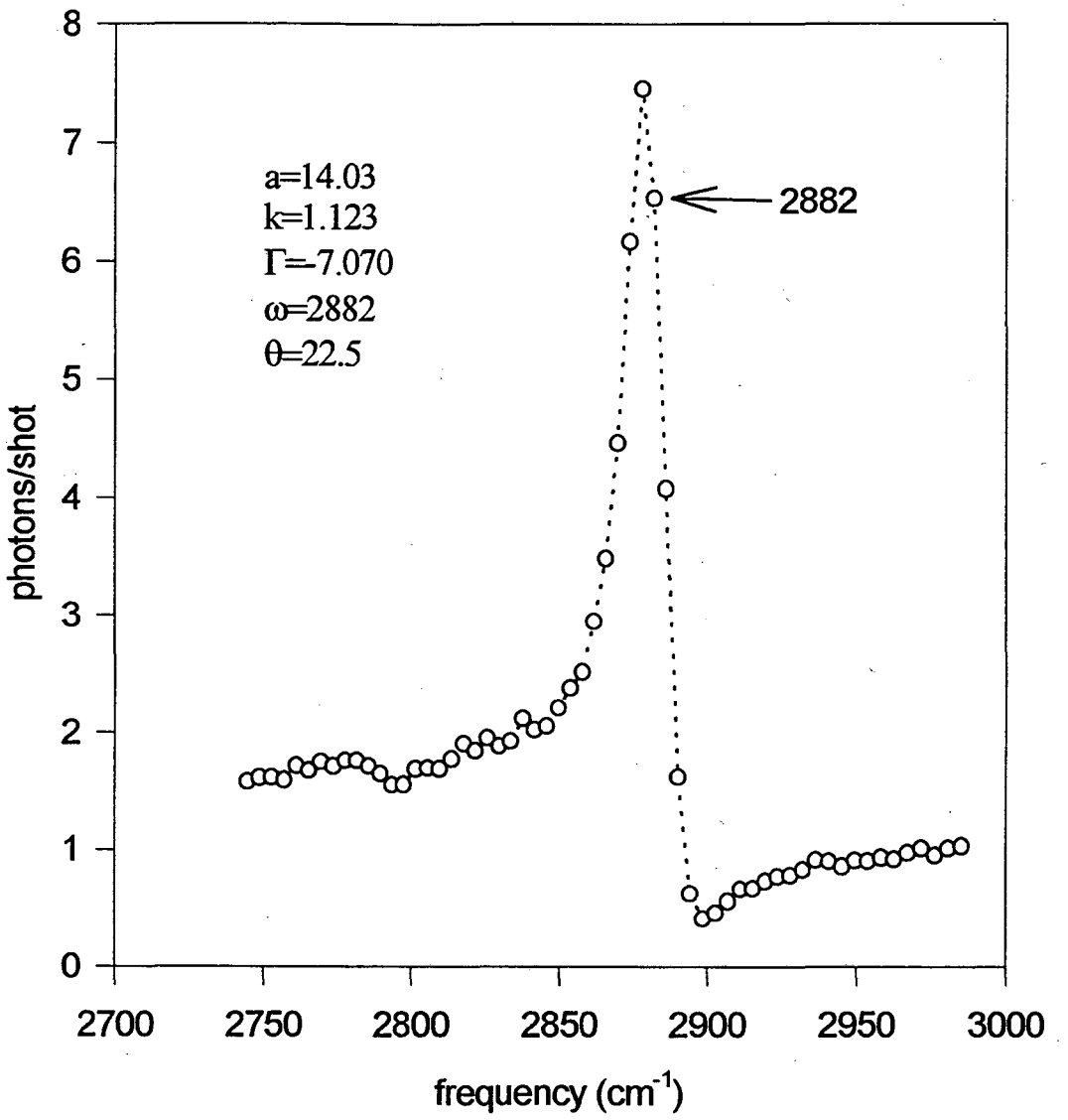
a=14.03
k=1.123
Γ=-7.070
ω=2882
θ=22.5
2882
photons/shot
frequency (cm-1)
0
1
2
3
4
5
6
7
8
2700
2750
2800
2850
2900
2950
3000

Fig. 4a

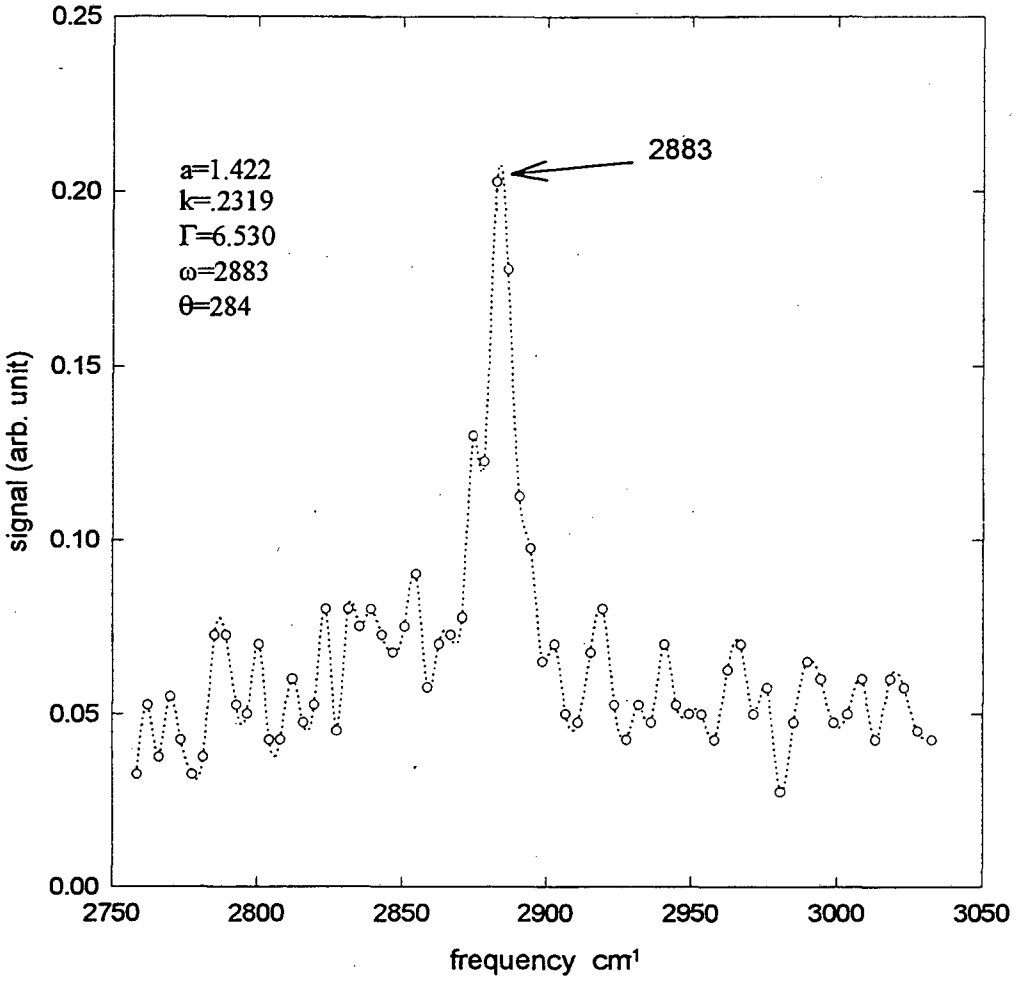
0.25
0.20
0.15
0.10
0.05
0.00
signal (arb. unit)
a=1.422
k=.2319
Γ=6.530
ω=2883
θ=284
2883
2750
2800
2850
2900
2950
3000
3050
frequency cm¹

Fig. 4b

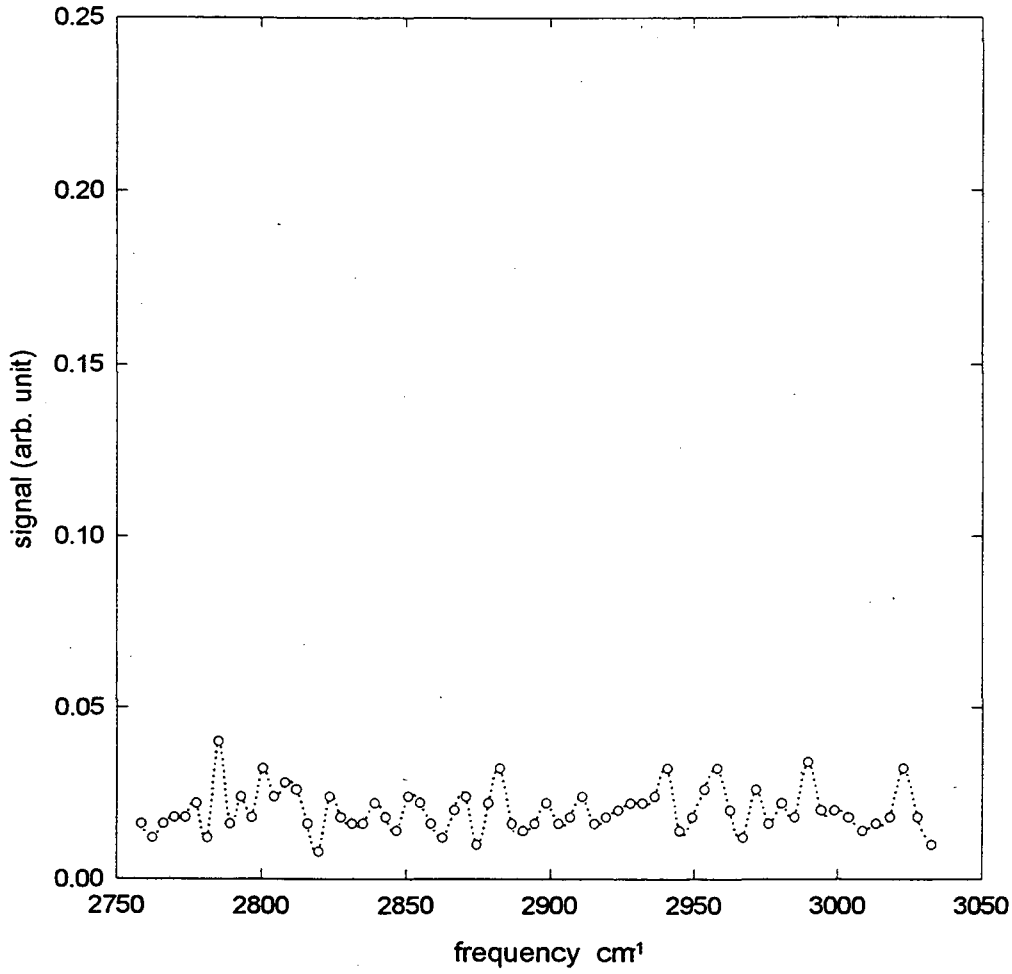
0.25
0.20
0.15
0.10
0.05
0.00
signal (arb. unit)
2750
2800
2850
2900
2950
3000
3050
frequency cm¹

Fig. 4c

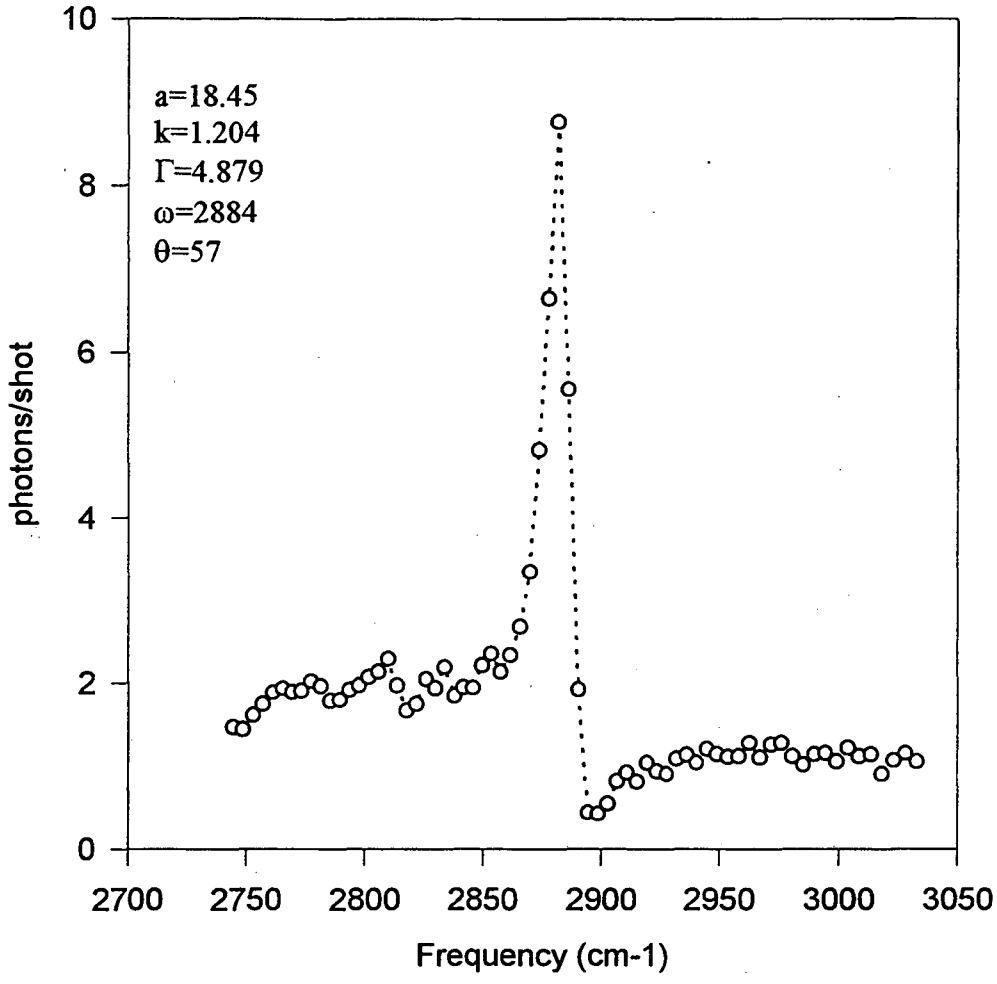
a=18.45
k=1.204
Γ=4.879
ω=2884
θ=57
photons/shot
Frequency (cm-1)
0
2
4
6
8
10
2700
2750
2800
2850
2900
2950
3000
3050

Fig. 4d

Chapter 3

The Thermal Evolution of Ethylene on Pt(111)

The conversion of di-σ bonded ethylene ($-CH_2-CH_2-$) to ethylidyne ($\equiv CCH_3$) on the Pt (111) crystal surface was monitored with infrared-visible sum frequency generation (SFG) in the ν(CH) frequency range. The conversion began around 255K and involved a third stable species that is neither di-σ bonded ethylene nor ethylidyne. This species manifested itself as a peak at 2957cm^{-1} in the vibrational spectrum. Furthermore, we found the same species present during the conversion of vinyl iodide to ethylidyne on Pt(111). The 2957cm^{-1} feature has been assigned to the CH_3 asymmetric stretch of ethylidene and/or ethyl.

1.1 Introduction

When ethylene is chemisorbed on the (111) crystal face of platinum at temperatures in the range of 120K-240K, di-σ bonded ethylene ($-CH_2CH_2-$) forms [1-3]. Annealing this species above 280K causes ethylidyne ($\equiv CCH_3$) to form [4]. Ethylidyne is adsorbed in an FCC threefold hollow site with its C-C axis perpendicular to the surface. Its structure and the relocation of platinum atoms around the site have been reliably determined by tensor LEED - surface crystallography [5]. The transformation of di-σ bonded ethylene to ethylidyne is shown schematically in figure 1. The purpose of this paper is to investigate the mechanism of this transformation by spectroscopic identification of possible intermediate species. To this end we carried out vibrational spectroscopy studies, using the technique of optical sum frequency generation (SFG) on the (111) crystal face of platinum in the temperature range of 202K-352K.

Several different mechanisms involving the formation of a variety of intermediates have been proposed in the literature. These intermediates include ethyl groups (CH_3-CH_2-) [6], vinyl groups ($CH_2=CH-$) [7, 8], ethylidene ($-CH-CH_3$) [9, 10], and vinylidene ($=C=CH_2$) [11, 12]. Because direct spectroscopic evidence for any of these intermediates has been elusive, it has been widely assumed that the rate limiting step for this reaction is either the breaking of the first CH bond in the di-σ bonded species to form vinyl [7, 8] or the isomerization of the adsorbed di-σ bonded species to ethylidene [9, 10].

Although direct spectroscopic evidence has been lacking, some experimental and theoretical studies have pointed to the likelihood of a mechanism involving an

ethylidene intermediate. Windham and Koel have shown spectroscopic evidence for ethylidene formation on Pt(111) when ethylene is coadsorbed with 0.12 monolayers of potassium at 100K and then annealed to 300K [10]. Evidence for an ethylidene species in the potassium promoted system has been further supported by Zhou et al. using secondary ion mass spectroscopy (SIMS) [13]. Some theoretical evidence has also pointed to ethylidene as a possible reaction intermediate. Carter and Koel have made equilibrium thermodynamic estimates of the energetics of the transformation of di-σ bonded ethylene to ethylidyne [9]. These estimates support a mechanism involving ethylidene. However, it should be noted that other theoretical studies did not support this conclusion [12, 14]. In fact some experimental evidence points to vinyl intermediates[7, 8]

In the present work we utilize infrared-visible sum frequency generation to study the ν(CH) portion of the vibrational spectrum (2700-3100cm^{-1}). SFG is a powerful technique for surface vibrational spectroscopy because it is both surface specific and capable of providing resolution on the order of 10cm^{-1} or less. The ν(CH) portion of the vibrational spectrum is extremely valuable because of the frequent difficulty in interpreting the complex structure often found in the 900cm^{-1}-1500cm^{-1} region of the spectrum.

SFG has been described in great detail in the literature [15, 16, 17]. Briefly, it is a second-order nonlinear optical process in which an infrared beam is combined with a visible beam to generate a sum-frequency output. The process is only allowed (in the dipole approximation) in a medium without inversion symmetry. The FCC lattice in the bulk of platinum is centrosymmetric and, therefore, in the case of an organic monolayer adsorbed on Pt(111) the SFG signal may be dominated by the contribution from the interface between the metal and vacuum.

As the IR beam is tuned through vibrational resonances of surface species the effective surface nonlinear susceptibility $\chi_S^{(2)}$ is resonantly enhanced. The SFG signal is proportional to the absolute square of $\chi_S^{(2)}$ and, hence, a vibrational spectrum of the surface species is detected. Formally we can write:

$$\chi_S^{(2)} = \chi_{NR}^{(2)} + \chi_R^{(2)} \qquad (1)$$

$$\chi_R^{(2)} = \sum_q \frac{A_q}{\omega_{ir} - \omega_q - i\Gamma}$$

where $\chi_{NR}^{(2)}, \chi_R^{(2)}, A_q, \omega_q, \omega_{ir,}$ and Γ_q refer to the nonresonant nonlinear susceptibility, resonant nonlinear susceptibility, strength of the q^{th} vibrational mode, q^{th} vibrational mode, infrared laser frequency, and the damping constant of the q^{th} vibrational mode respectively.

Our results indicate the presence of a third species present on the Pt(111) surface during the conversion of di-σ bonded ethylene to ethylidyne. This species gave rise to a vibrational feature which was observed only during the reaction and has been assigned to the CH_3 asymmetric stretch of ethylidene and/or ethyl.

1.2 Experimental

All experiments were carried out in an ultra high vacuum chamber pumped with a turbo pump and an ion pump. The chamber had a base pressure of less than 1×10^{-10} Torr and was equipped with a Varian retarding field analyzer (RFA) for Auger and LEED, a high resolution electron energy loss spectrometer (HREELS), a VG SX300 Mass Spectrometer, and CaF_2 windows to allow the passage of infrared and visible laser beams. The Pt(111) crystal used in this

experiment was spot welded onto the manipulator with platinum wires and was capable of being resistively heated to above 1200K and cooled with liquid N_2 to 115K. Temperature was measured with a Chromel-Alumel thermocouple which was positioned on the edge of the crystal. The sample itself was cut, polished, and then cleaned in UHV following the standard procedures.

A 20 picosecond passive, active mode-locked Nd:YAG laser with a maximum output energy of 50mJ/pulse at 1064nm was used to perform the SFG. A portion of the beam was frequency doubled to 532nm and used as the visible portion of this spectroscopy. The rest of the light was sent to a $LiNbO_3$ optical parametric generator/amplifier arm where it could be frequency tuned from 2650-3900cm^{-1}. The two beams were then focused concentrically onto the Pt(111) sample. Both the green and IR light used in this experiment were p-polarized such that their electric fields had components perpendicular to the surface of the platinum crystal. The sum frequency photons generated from the crystal surface were detected via a photomultiplier tube and the signal was stored on a microcomputer. Figure 2 is a schematic diagram of the instrumentation.

In this experiment 4L of ethylene (Matheson, C.P. grade) were dosed onto clean Pt(111) at 202K. The crystal was cooled to 120K at which point an SFG spectrum was taken. The crystal was then annealed to successively higher temperatures for periods of 60 seconds after which the crystal was allowed to cool to 120K. At the conclusion of each such process an SFG scan was taken at 120K. Additional spectra of di-σ bonded ethylene on Pt(111), ethylidyne on Pt(111), and vinyl iodide (99% pure, Pfaltz and Bauer) on Pt(111) were taken for comparison. All spectra presented in this study represent raw data.

1.3 Results

Figure 3a represents a scan of ethylene adsorbed onto clean Pt(111) at 300K and then flashed to 400K, a procedure which completely decomposes chemisorbed ethylene to ethylidyne. The spectrum shows only one major feature at 2885cm^{-1} (unfitted value) representing the CH_3 symmetric stretch of ethylidyne. A second much smaller feature just under 2800cm^{-1} has been assigned to a Fermi resonance with an asymmetric bending mode [18]. The nonresonant background signal immediately beyond the peak frequency falls below its base line and then returns. This is the interference pattern formed from the interplay between the nonresonant background signal (in this case due primarily to the platinum surface) and the resonant signal from the ethylidyne species. Because of this interaction, the peak of the resonant feature comes at a slightly lower frequency than would otherwise be expected. Signal in a sum frequency experiment is proportional to the square of equation 1; therefore, fitting the data by $|\chi_S^{(2)}|^2$ yields the actual resonant frequency of the main peak in figure 3a at 2886cm^{-1}. All further peaks in this paper have been identified by their fitted value for the resonant frequency.

Figure 3b is a scan of di-σ bonded ethylene that has been adsorbed on Pt(111) at 202K and then cooled to120K before taking the spectrum. The singular feature in this spectrum is at 2904cm^{-1} and has been assigned to a CH_2 symmetric stretch [1-3]. From reflection-adsorption infrared spectroscopy (RAIRS) studies, Hoffman et al. have concluded that the CH_2 asymmetric stretch is also incorporated under this peak [19].

Figure 4 shows a series of eight spectra of di-σ bonded ethylene annealed to successively higher temperature. During the annealing process di-σ bonded ethylene is converted to ethylidyne. Upon annealing di-σ bonded ethylene to 243K for 60 seconds the CH_2 symmetric stretch peak shifts to 2906cm^{-1} and sharpens up, but the spectrum remains otherwise unchanged from the spectrum in figure 3b. The first sign of significant change begins as the sample is annealed to 257K. There is a definite decrease in intensity of the CH_2 symmetric stretch peak and a new feature begins to grow in around 2953cm^{-1}. Further, a shoulder which is assigned to the CH_3 symmetric stretch of ethylidyne develops on the low frequency side of the CH_2 peak.

The ethylidyne shoulder feature increases slightly as the sample is annealed to 265K. The drop off in intensity of the CH_2 peak continues as its frequency shifts to 2916cm^{-1}. The high frequency feature shifts to 2957cm^{-1} and continues to grow. Annealing to 273K for 60 seconds makes the CH_3 symmetric stretch at 2889cm^{-1} of the growing ethylidyne resonance clearly visible. The CH_2 symmetric stretch peak which has now shifted to 2918cm^{-1} has decayed substantially while the high frequency feature continues to grow. At 281K the CH_2 symmetric stretch has almost completely disappeared. The CH_3 symmetric stretch peak of ethylidyne continues to increase in intensity and the 2957cm^{-1} stretch peak starts to decrease.

Annealing to 288K shows continued growth of the ethylidyne peak while the high frequency feature has nearly disappeared. Further annealing to 296K and then 352K leaves only the CH_3 symmetric stretch of ethylidyne.

1.4 Discussion

The CH stretch portion of the vibrational spectrum shows a clear progression from di-σ bonded ethylene to ethylidyne with the appearance of a high frequency feature at 2957cm^{-1} that is only present during the transition (figure 4). The primary objective of this discussion is to identify this feature. There are several candidates for this species, including ethyl, ethylidene, vinyl, and vinylidene. A possible asymmetric stretch mode and a fermi resonance of both di-σ bonded ethylene and ethylidyne must also be considered.

The possibility that the high frequency feature is a fermi resonance can be discounted because its signal would have to grow and attenuate in concert with either the CH_2 or CH_3 symmetric stretch resonance. This is not the case for either the CH_2 or CH_3 mode. The 2957cm^{-1} peak remains until after the CH_2 symmetric stretch intensity is completely gone and actually attenuates as the CH_3 symmetric stretch grows. Further, neither the di-σ bonded ethylene nor the ethylidyne species when present alone on the surface have fermi resonances in the 2957cm^{-1} range.

The high frequency feature in figure 4 is also unlikely to be from an asymmetric stretch mode. Although asymmetric stretches of CH_3 species on Pt(111) are found in this region of the spectrum, they are mostly forbidden in the ethylidyne geometry because of the surface dipole selection rule, which requires the dynamic dipole moment of the species to have some component normal to the surface. In this case (with the C-C bond axis normal to the surface) the asymmetric stretch would be in plane with the surface and would not appear in this spectroscopy. In fact the asymmetric stretch feature is not observed in the pure ethylidyne spectrum (figure 3a).

It also cannot be argued that the high frequency feature is from the CH_2 asymmetric stretch of di-σ bonded ethylene. This is because the high frequency peak is clearly still present *after* the CH_2 symmetric stretch signal has completely vanished. For this feature to be the CH_2 asymmetric stretch, there would have to be a conformation of di-σ bonded ethylene that would only allow the asymmetric stretch to be observed, but not the symmetric one. It is extremely difficult to envision such a conformation of di-σ bonded ethylene on Pt(111). This leads to the conclusion that the high frequency stretch seen during the conversion is due to a species that is neither di-σ bonded ethylene nor ethylidyne, but rather a third species that is only present on the surface during the conversion of the former into the latter.

Both a vinyl group ($-CH=CH_2$) and vinylidene group ($=C=CH_2$) can be ruled out as a candidate for the 2957cm^{-1} feature. Infrared and Raman spectra of vinyl and vinylidene moieties in osmium clusters show that the CH_2 symmetric and asymmetric stretches of these moieties occur too high (2998cm^{-1}, 3052cm^{-1} for vinyl and 2990cm^{-1}, 3052cm^{-1} for vinylidene) to account for this feature and the very weak CH stretch of vinyl is too low (2920cm^{-1}) [20]. Further, a recent RAIRS study by Zaera et al. has shown that vinyl moieties decompose to acetylene and vinylidene by 140K instead of directly converting to ethylidyne [21]. In the RAIRS study heating above 200K caused all spectroscopic features to disappear. This led Zaera to conclude that π-bonded ethylene must be formed around this temperature. The π-bonded ethylene would have its dynamic dipole parallel to the surface and would therefore not be seen by infrared spectroscopy. Zaera accounted for the change in C/H stoichiometry from C_2H_3 to C_2H_4 by proposing either adsorption of H_2 from the background or the evolution of surface hydrogen

from the formation of a minor decomposition product. Upon heating this system above 300K ethylidyne features were observed.

We have also investigated the thermal evolution of the vinyl iodide on Pt(111) system and the spectra are shown in figure 5. The bottom spectrum shows 10L of vinyl iodide dosed on Pt(111) at 132K. At this temperature some of the C-I bonds are broken and vinyl moieties are directly adsorbed on the platinum surface [8]. There are three peaks ($2995cm^{-1}$, $3033cm^{-1}$, and $3068cm^{-1}$) observed for vinyl iodide adsorbed on Pt(111) at 132K. The $2995cm^{-1}$ resonance can be assigned to the CH_2 symmetric stretch of a mixed sp^2/sp^3 hybridized species of either vinyl or vinylidene [20]. The $3068cm^{-1}$ peak may be due to the CH_2 asymmetric stretch of intact vinyl iodide [8]. The $3033cm^{-1}$ feature, however, is harder to identify because it does not correspond well with any frequency from the inorganic cluster models of vinylidene, vinyl, or acetylene [20, 22]. Because there is significant dehydrogenation just above 132K [21], an additional surface species or a Fermi resonance may already be present at this temperature. At any rate all of the peaks in this spectrum come at too high of a frequency to account for the $2957cm^{-1}$ feature seen in the di-σ bonded ethylene to ethylidyne transition.

Upon annealing the vinyl iodide/Pt(111) system to 285K and 295K (middle spectra in figure 5) there is only one peak present which is nearly at the same position as the high frequency feature seen during the transition of di-σ bonded ethylene to ethylidyne in figure 4. Upon further heating to 406K the CH_3 symmetric stretch resonance of ethylidyne is seen at $2878cm^{-1}$ (top spectra in figure 5). This seems to suggest that while vinyl is not the species responsible for the high frequency feature observed in the di-σ bonded ethylene to ethylidyne conversion, vinyl decomposes through the *same* intermediate(s) in its

transformation to ethylidyne as is found by directly dosing and then annealing ethylene . This is quite reasonable in light of the finding by Zaera that vinyl converts to π-bonded ethylene before converting to ethylidyne [21].

We assign the 2957cm^{-1} feature to the CH_3 asymmetric stretch mode of ethylidene and/or ethyl. There is a preponderance of evidence which supports this assignment. In a RAIRS study of deuterated and nondeuterated ethyl iodide on Pt(111) Hoffman et al. have shown that ethyl groups give rise to three features in the CH stretch region at 2857cm^{-1}, 2914cm^{-1}, and 2952cm^{-1}. The highest frequency feature has been assigned to the CH_3 asymmetric stretch of the terminal methyl group [19]. We have repeated this work using our SFG system and obtained the same results. Hoffman et al. have shown that ethyl groups may adopt either an upright or flat geometry on the (111) surface of platinum. It is in the latter case that the CH_3 asymmetric stretch is most prominent in their vibrational spectra (dipole selection rule). The orientation was shown to be coverage dependent with flat lying species predominant at low surface coverages.

In the case of ethylidene moieties, osmium cluster work by Anson et al. has shown that the CH_3 asymmetric stretch comes at 2950cm^{-1} and is the strongest feature in the CH stretch region for this species [23]. Further, in the case of K promoted Pt(111), where ethylidene has been identified as the stable intermediate in ethylene decomposition to ethylidyne, a peak in the CH stretch portion of the HREELS spectrum was seen at 2955cm^{-1}[10]. The CH stretch frequencies and assignments of ethyl iodide on Pt(111) (from ref 19) and ethylidene moieties in $[(CH_3CH)Os_2(CO)_8]$ (from ref 23) are given in table 1.

It is significant that no intensity is seen in the 2850-2857cm^{-1} range (corresponding to a CH_3 symmetric stretch) during the presence of the 2957cm^{-1}

feature. This is a demonstration of the orientational sensitivity of SFG on metal surfaces. The signal intensity of a vibrational mode in our SFG experiments scales as $\cos^6\theta$ [24], where θ is the angle between the surface normal and the direction of the dynamic dipole moment of the surface species. In the case of upright ethylidene moieties the CH_3 symmetric stretch mode would make a 55° angle with respect to the surface normal, whereas the CH_3 asymmetric stretch mode would make a 35° angle with respect to the normal. This difference in angle would lead to nearly an order of magnitude greater signal intensity for the CH_3 asymmetric mode in an SFG experiment. For ethyl groups, low coverages (flat lying) showed little or no intensity in the 2857cm^{-1} region even in RAIRS experiments where signal intensity scales only as $\cos^2\theta$ [19]. Therefore, it would be expected that flat lying ethyl groups would not give rise to a peak in the 2857cm^{-1} region of an SFG spectrum where the orientational sensitivity is even more extreme.

Another significant observation from figure 4 is the blue shift of the 2906cm^{-1} feature. One possible explanation is that the changing surface coverage of di-σ bonded ethylene causes this phenomenon. We have carried out experiments on the coverage dependence of the CH_2 symmetric stretch frequency which show that there is indeed a shift from 2924cm^{-1} at low coverage up to 2904cm^{-1} at saturation. Another possibility is that the shift is due to intensity from another vibrational mode of the intermediate species. This would be easiest to explain in terms of an ethylidene intermediate. For an ethylidene moiety that has its methyl group tilted close to the surface and its hydrogen pointing nearly straight up, one might expect to see some intensity from the weak CH stretch mode. This would also explain the lack of intensity near 2850cm^{-1}, because the CH_3 symmetric stretch would be nearly parallel to the Pt surface. It would, however, be more

difficult to explain the blue shift of the 2906cm^{-1} peak in terms of an ethyl group. This is because an additional feature at 2857cm^{-1} is not seen. The 2857cm^{-1} intensity would be from a Fermi resonance of the 2914cm^{-1} feature and should scale with it.

Because small amounts of ethane have been detected to desorb from the surface during ethylidyne formation [25, 26], we postulate that some ethyl species may exist during the conversion of di-σ bonded ethylene to ethylidyne. However, studies of ethyl moieties have shown that ethyl groups decompose to form di-σ bonded ethylene and ethane at temperatures above 250K on the Pt(111) surface [27, 28]. Our spectra of the conversion show that the 2957cm^{-1} feature is present on the surface without any di-σ bonded ethylene at 281K and 288K (figure 4). This requires ethyl groups to survive for minutes under severe dehydrogenation conditions after all the di-σ bonded ethylene is gone. Further, our vinyl iodide spectra show that the same CH_3 asymmetric stretch signal occurs even under the condition of 25% less initial surface hydrogen. For these reasons we favor an ethylidene interpretation of the 2957cm^{-1} feature.

An ethylidene interpretation of the 2957cm^{-1} stretch leads to two important conclusions. Ethylidene would be a likely intermediate in the conversion of di-σ bonded ethylene to ethylidyne and the breaking of the CH bond on the α-carbon of ethylidene would be the rate limiting step in this reaction.

The mechanisms in figure 6 illustrate three possible pathways for ethylene decomposition to ethylidyne that involve an ethylidene intermediate. In the first mechanism di-σ bonded ethylene is hydrogenated to an ethyl group followed by stepwise dehydrogenation of the α-carbon. We reject this mechanism because work on ethyl chloride by Lloyd et al. has shown that ethyl groups first dehydrogenate on

Pt(111) to yield di-σ bonded ethylene rather than dehydrogenate directly to ethylidyne [28, 29].

In the second mechanism a CH bond on the di-σ bonded ethylene breaks to form a vinyl group. This vinyl group undergoes hydrogenation at the CH_2 carbon to form ethylidene. Ethylidene then dehydrogenates to form ethylidyne. This too can be ruled out on the basis of the vinyl iodide work by Zaera et al. which shows that vinyl decomposes readily to vinylidene and acetylene at temperatures around 140K [21].

The last mechanism involves only two steps. First, a hydrogen atom undergoes a 1,2 shift to form ethylidene. This is followed by a dehydrogenation step to form ethylidyne. Such a mechanism is consistent with experimental data and indeed involves the least number of steps. Therefore, in agreement with Carter and Koel we favor this last mechanism.

Clearly there is a third species present on Pt(111) during the dehydrogenation of di-σ bonded ethylene to ethylidyne. For the reasons stated above we believe that it is more likely that this species is ethylidene than ethyl, however, both species would show very similar spectral features in the CH stretch range. In addition, optical sum frequency generation has proven to be an excellent new technique for investigating the surface chemistry of this reaction.

1.5 Conclusion

Surface vibrational spectra of the transformation of di-σ bonded ethylene to ethylidyne have been recorded after each of eight annealing steps. The spectra show that in addition to the CH_3 and CH_2 symmetric stretch features from ethylidyne and di-σ bonded ethylene (respectively) there is a high frequency feature around 2957cm^{-1}

during the transformation process. We have assigned this feature to the CH_3 asymmetric stretch of ethylidene and/or ethyl. Therefore, there is a third stable species present on the surface during the conversion of di-σ bonded ethylene to ethylidyne on Pt(111).

1.6 References

[1] J. Demuth, Surf. Sci. **80**, 867 (1979)

[2] H. Ibach and S. Lehwald, J. Vac. Sci. Technol., **15**, 407 (1978)

[3] H. Steininger, H. Ibach, and S. Lehwald, Surf. Sci., **117**, 685 (1982)

[4] see ref. in H. Ibach and D. Mills, Electron Energy Loss Spectroscopy and Surface Vibrations, Academic Press (1982)

[5] U. Starke, A. Barbieri, N. Materer, M. Van Hove, and G. Somorjai, Surf. Sci., **286**, 1 (1993)

[6] B. Bent, Ph.D. Thesis, University of California at Berkeley, (1986)

[7] F. Zaera, JACS, **111**, 4240 (1989)

[8] Z. Liu, X. Zhou, D.A. Buchanan, J. Kiss, and J. White, JACS, **114**, 2031 (1992)

[9] E. Carter, and B. Koel, Surf. Sci. **226**, 339 (1990)

[10] R. Windham, and B. Koel, J. Phys. Chem., **94**, 1489 (1990)

[11] A. Baro, H. Ibach, Vide, Couches Minces, Suppl., **201**, 458 (1980)

[12] D. Kang and A. Anderson, Surf. Sci., **155**, 639 (1985)

[13] X. Zhou, X. Zhu, and J. White, Surf. Sci., **193**, 387 (1988)

[14] P. Ditlevsen, M. Van Hove, and G. Somorjai, Surf. Sci., **292**, 267, (1993)

[15] X. Zhu, H. Suhr, Y.R. Shen, Phys. Rev., **B35**, 3047 (1987)

[16] Y.R. Shen, The Principles of Nonlinear Optics (Wiley, New York, 1984)

[17] Y.R. Shen, Nature, **337**, 519 (1989)

[18] I. Malik, V. Agrawal, and M. Trenary, J. Chem. Phys., **89**, 3861 (1988)

[19] H. Hoffman, F. Zaera, Surf. Sci., **262**, 141 (1992)

[20] J. Andrews, S. Kettle, D. Powell, and N. Sheppard, Inorg. Chem, **21**, 2874 (1982)

[21] F. Zaera, N. Bernstein, JACS, **116**, 4881 (1994)

[22] J. Coffer, H. Drickamer, J. Park, R. Roginski, J. Shapley, J. Phys. Chem., 94, 1981 (1990) and references therein

[23] C. Anson, N. Sheppard, D. Powell, J. Norton, W. Fischer, R. Keiter, B. Johnson, J. Lewis, A. Bhattacharrya, S. Knox, and M. Turner, JACS, 116, 3058 (1994)

[24] J. Hunt, Ph.D Thesis, University of California at Berkeley, (1988)

[25] R. Windham, M. Bartram, and B. Koel, J. Phys. Chem, 92, 2862 (1988)

[26] P. Berlowitz, C. Megiris, J. Butt, and H. Kung, Langmuir, 1, 206 (1985)

[27] M. Pansoy-Hjelvik, R. Xu, Q. Gao, K. Weller, F. Feher, and J. Hemminger, Surf. Sci., 312, 97 (1994) and references therein

[28] K. Lloyd, B. Roop, A. Campion, J. White, Surf. Sci., 214, 227 (1989)

[29] this argument is stated in ref. 10

1.7 Figure Captions

Figure 1 The decomposition of ethylidyne on Pt(111)

Figure 2 Apparatus for UHV-SFG

Figure 3 (a) 4L of ethylene dosed on Pt(111) at 300K and flashed to 400K
(b) 4L of ethylene dosed on Pt(111) at 202K, spectrum taken at 120K

Figure 4 4L of ethylene dosed on Pt(111) at 202K is annealed stepwise from 243K to 352K.

Figure 5 10L of vinyl iodide dosed on clean Pt(111) at 130K and then annealed to 285K, 295K, and 406K

Figure 6 Three possible dehydrogenation mechanisms for di-σ bonded ethylene to ethylidyne through an ethylidene intermediate

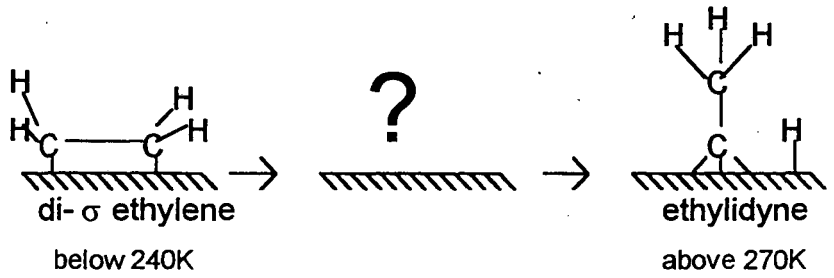
H
H
H
H
C
C
di- σ ethylene
below 240K
?
H
H
H
C
C
H
ethylidyne
above 270K

Fig. 1

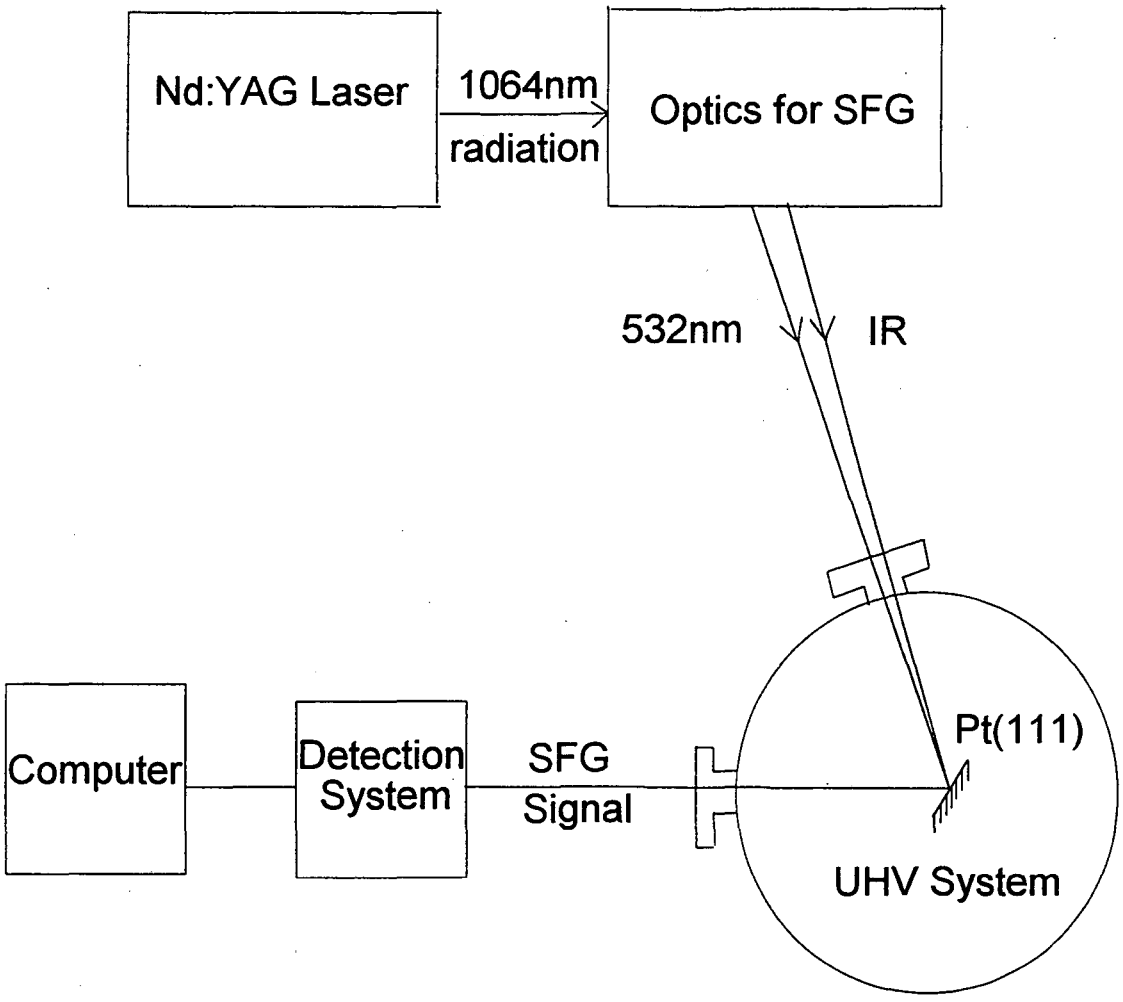
Nd:YAG Laser
1064nm
radiation
Optics for SFG
532nm
IR
Pt(111)
Computer
Detection System
SFG
Signal
UHV System

Fig. 2

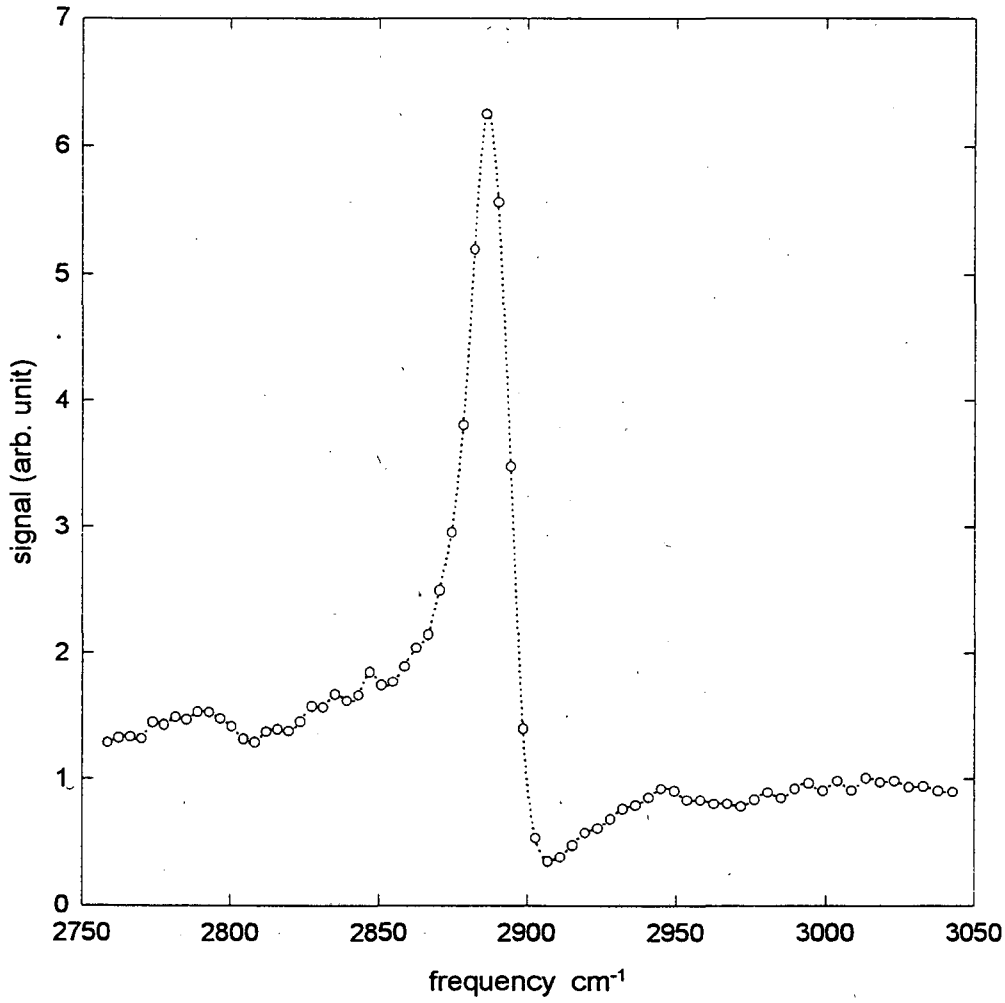
signal (arb. unit)
frequency cm-1
0
1
2
3
4
5
6
7
2750
2800
2850
2900
2950
3000
3050

Fig. 3a

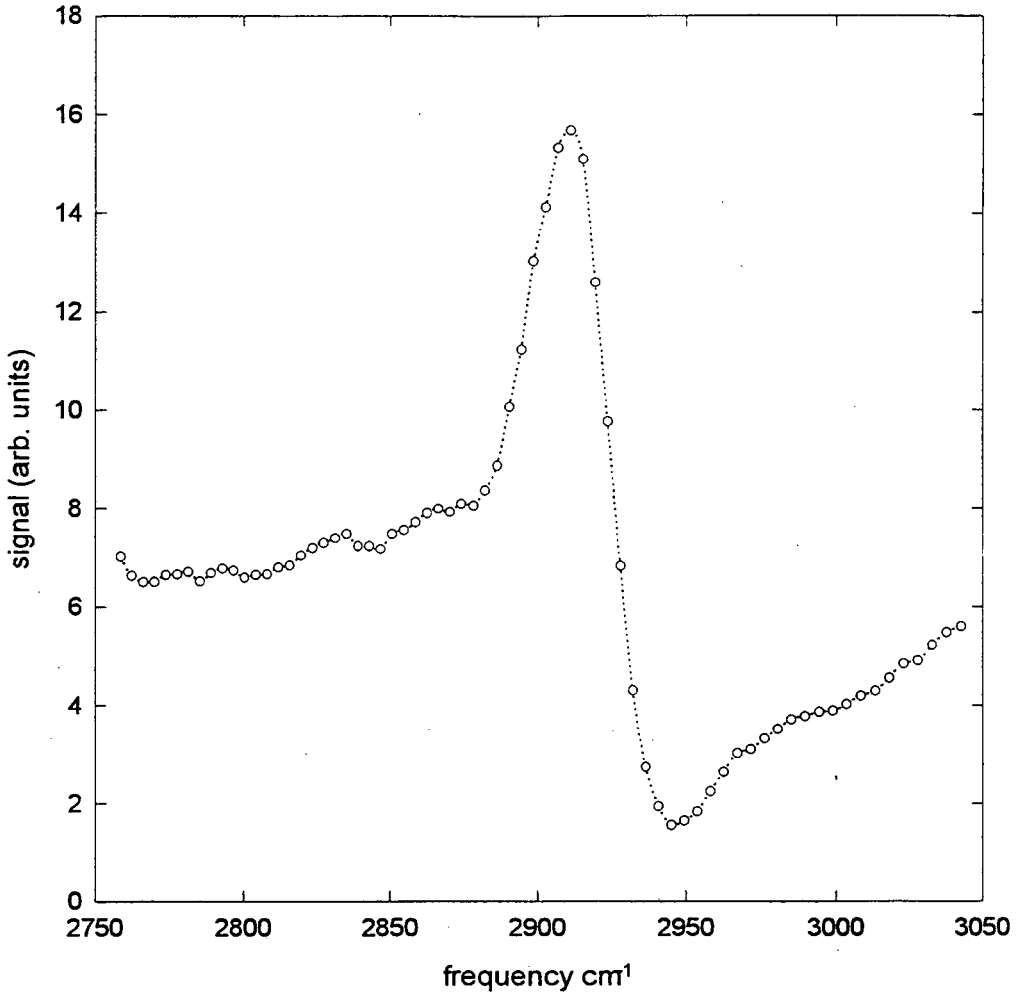
18
16
14
12
10
8
6
4
2
0
signal (arb. units)
2750
2800
2850
2900
2950
3000
3050
frequency cm1

Fig. 3b

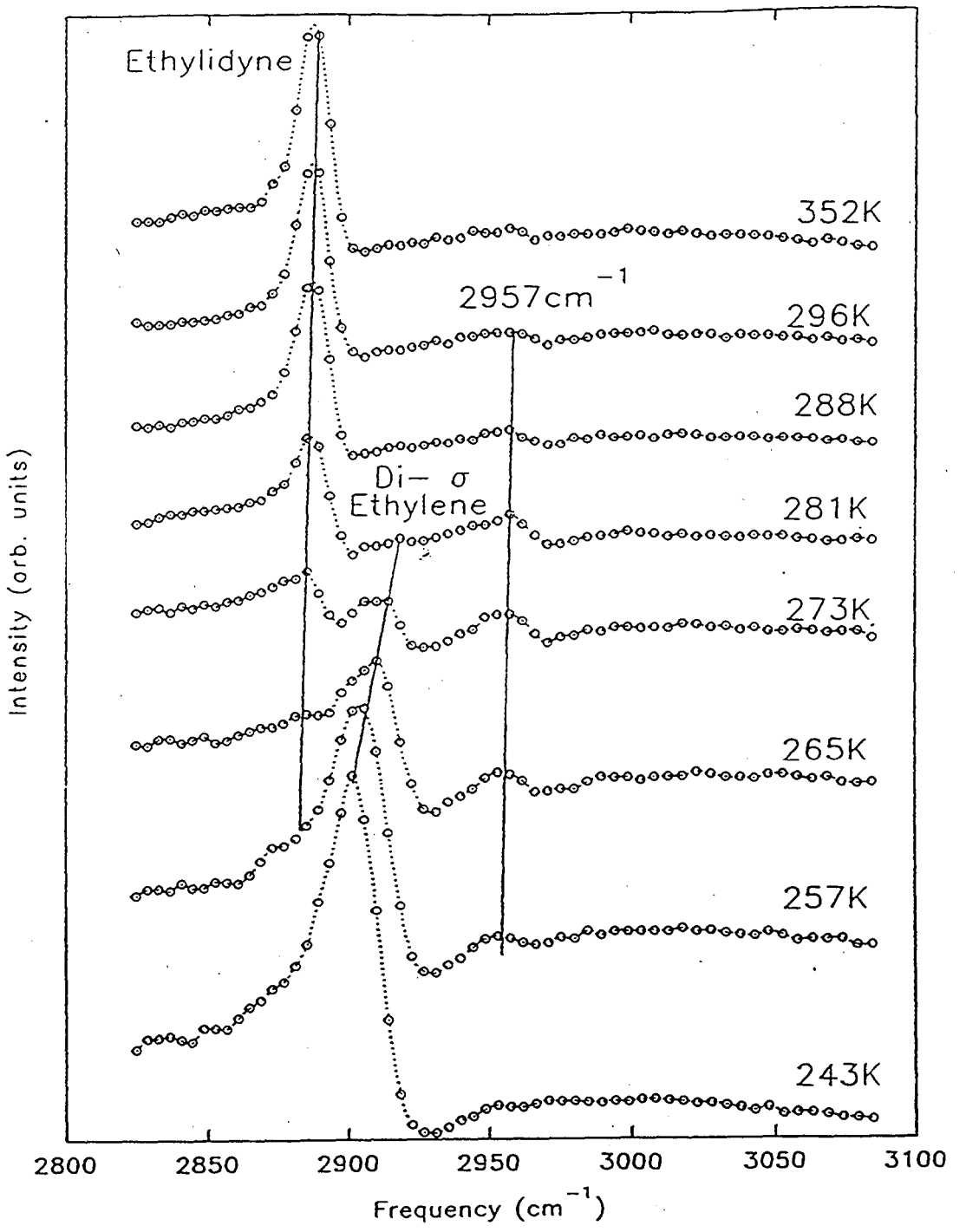
Ethylidyne
352K
2957cm^{-1}
296K
288K
Di- σ
Ethylene
281K
273K
265K
257K
243K
Intensity (arb. units)
2800
2850
2900
2950
3000
3050
3100
Frequency (cm^{-1})

Figure 4

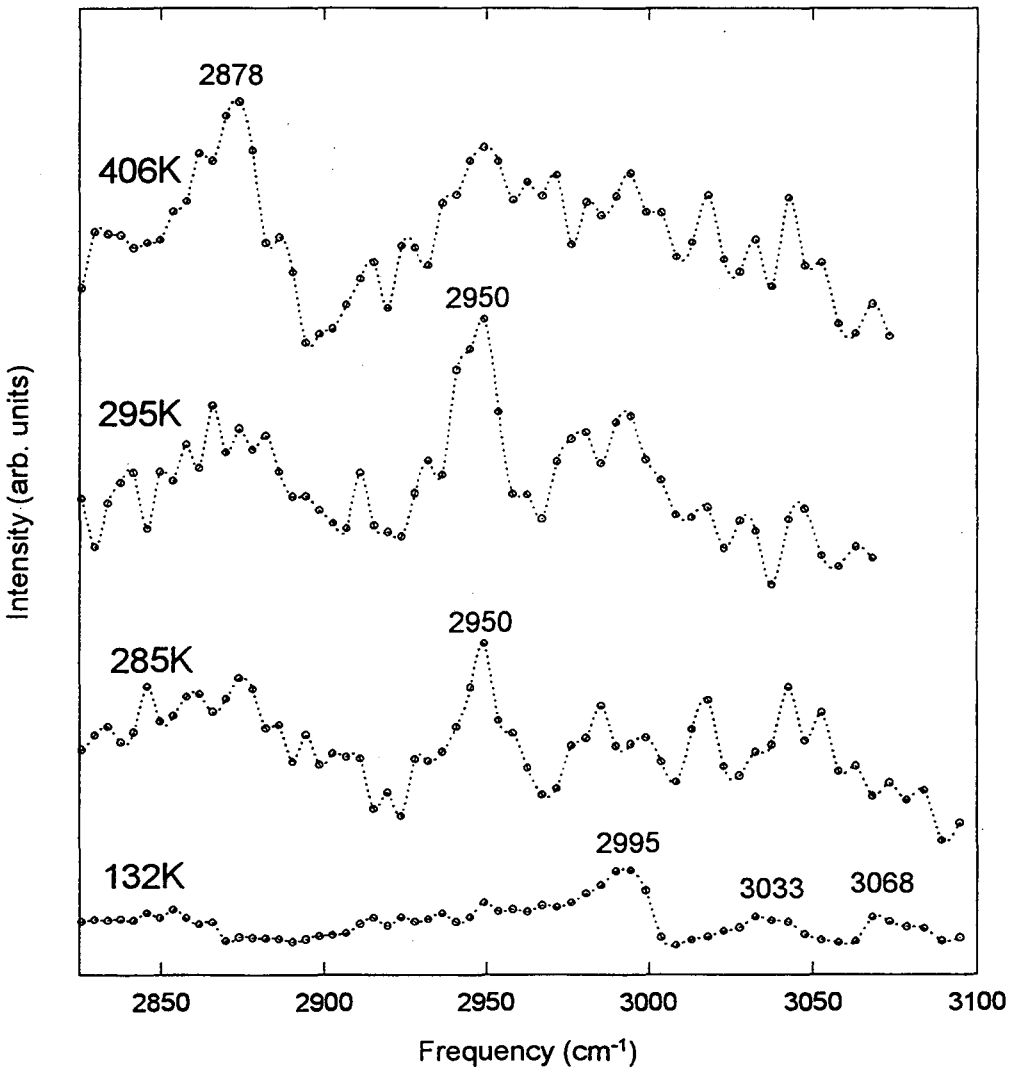
2878
406K
2950
295K
2950
285K
2995
132K
3033
3068
Intensity (arb. units)
2850
2900
2950
3000
3050
3100
Frequency (cm-1)

Fig. 5

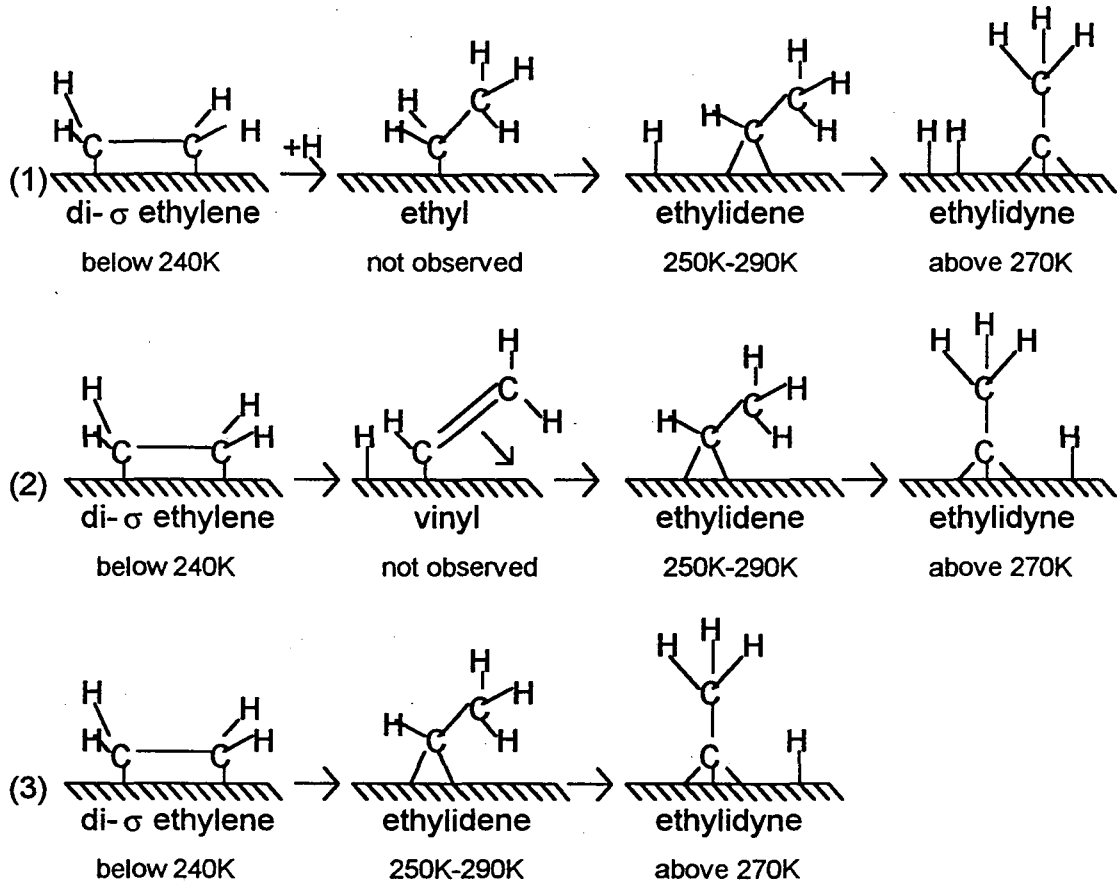
(1)
di-σ ethylene
below 240K
+H
ethyl
not observed
ethylidene
250K-290K
ethylidyne
above 270K
(2)
di-σ ethylene
below 240K
vinyl
not observed
ethylidene
250K-290K
ethylidyne
above 270K
(3)
di-σ ethylene
below 240K
ethylidene
250K-290K
ethylidyne
above 270K

Figure 6

Table 1: Frequencies of Ethyl and Ethylidene Moieties (in cm^{-1})

[$(CH_3CH)Os_2(CO)_8$]	Assignment	CH_3CH_2/Pt(111)	Assignment
2950	$\nu_{as}(CH_3)$	2952	$\nu_{as}(CH_3)$
2916	$\nu(CH)$	2914	$\nu_s(CH_3)$
2905/2850	$\nu_s(CH_3)$	2857	$2\delta_a(CH_3)$

Chapter 4

The Thermal Evolution of Acetylene on Pt(111)

The thermal evolution of acetylene was followed on the (111) surface of platinum in the CH stretch range of the vibrational spectrum using infrared-visible sum frequency generation. It was found that acetylene adsorption at 190 K gave rise to several peaks between 2950-3000 cm^{-1} suggesting that a variety of adsorbates were present including: ethylidene ($M{=}CHCH_3$), η^2-μ_3-CCH_2 vinylidene, as well as adsorbed acetylene. The presence of species with C_2H_4 stoichiometry was strong evidence that a disproportionation reaction must already occur at this temperature. Above 300 K a μ-vinylidene species was formed and remained coadsorbed with ethylidene until both began to decompose near 350 K. By 381 K ethylidyne was the only observable species on the surface.

4.1 Introduction

The adsorption and decomposition of acetylene on Pt(111) was first studied over twenty years ago by low energy electron diffraction. It was noted that if the clean Pt(111) surface was exposed to acetylene and annealed above room temperature, a 2x2 surface structure could be formed [1]. Subsequently, ethylene was found to exhibit similar behavior. By comparing electron energy loss spectra (HREELS) with organometallic cluster analogs it was determined that the surface species formed from both acetylene and ethylene was ethylidyne, ($M{\equiv}CCH_3$) [2]. This species is sp^3 hybridized and resides in the fcc three fold hollow site on the Pt(111) surface [3]. The preponderance of evidence for the mechanism of ethylidyne formation from ethylene favors an ethylidene intermediate [Fig 1] [4].

The thermally induced rearrangement of acetylene/Pt(111) to ethylidyne has received much less attention because annealing in the absence of hydrogen cannot lead to ethylidyne formation by a stoichiometric reaction. A disproportionation reaction is required, whereby a decomposition species, probably ethnyl (M-CCH) [also called acelylide], must be formed simultaneously to provide the necessary hydrogen to produce ethylidyne [Fig. 2]. HREELS studies of acetylene decomposition by Avery found that ethylidyne formed between 300-400 K, but no clear spectroscopic evidence could be found for the vinylidene ($M{=}CCH_2$) species that was believed to be an important mechanistic intermediate [5].

Thermal desorption mass spectroscopy indicated that ethylidyne formation from acetylene was unaccompanied by hydrogen evolution. Detailed studies of the thermal desorption species from acetylene/Pt(111) by Megiris et al. show that the first hydrogen desorption peaks occurred near 490 K [6], well after ethylidyne had been formed. Some intact acetylene was found to desorb near 150 K and small quantities of ethylene were evolved in three peaks at 250, 275, and 460 K. Evidence was also noted for a very small

quantity of methane (a cracking product) near 310 K, however no ethane or any higher hydrocarbons were found to desorb.

A study of the thermally induced rearrangement of acetylene that was monitored by SFG vibrational spectroscopy will be presented in this paper. The vibrational spectra give strong evidence for the formation of several stable intermediates on the surface leading up to ethylidyne formation. These species are identified as ethylidene ($M{=}CHCH_3$) and μ-vinylidene ($M{=}C{=}CH_2$) [Fig. 3].

4.2 Experimental

After, exposing the clean Pt(111) surface to a saturation coverage of acetylene (4 L) at 191 K, a scan of the CH stretch range of the vibrational spectrum was taken between 2800 and 3100 cm^{-1}. The surface was then annealed to a series of predetermined temperatures for 60 seconds after which the crystal was allowed to recool below 191 K and another vibrational spectrum was obtained. This process was repeated between 191 and 381 K at temperature intervals of approximately 25 K. It was independently verified via control experiments that the results were identical for immediately annealing to a predetermined temperature and arriving to the same temperature over a series of heating cycles.

4.3 Results

Figure 4 shows the vibrational spectrum for a saturation exposure of acetylene on Pt(111) at 191 K. Three peaks at 2960 cm^{-1}, 2976 cm^{-1}, and 2990 cm^{-1} dominate the spectrum, while some weak intensity near 2900 cm^{-1} can also be seen just above the noise. The 2960 cm^{-1} feature is characteristic of a $\nu_{as}(CH_3)$ [7]. For signal from the asymmetric stretch of a methyl group to be observed, the species must be inclined with respect to the surface normal. This is because of the metal dipole selection rule, which states that for a mode to be surface active it must have some component of the dynamic

dipole normal to the surface. All dipole components in the plane of the metal are canceled by an image dipole in the metal surface. The 2960 cm^{-1} is therefore assigned to an ethylidene species ($M{=}CHCH_3$). An ethyl assignment would also be possible, but the lack of surface hydrogen makes this less unlikely. Further, the 2960 cm^{-1} feature was noted to survive to quite high temperatures (at least 356 K, Figs. 5a-e), well above where ethyl is known to decompose.

The strongest intensity at 2976 cm^{-1} in figure 4 is difficult to match to an osmium cluster analog, but may be from the ν(CH) of acetylene [8], while the 2990 cm^{-1} feature can be from adsorbed μ_3-η^2-acetylene, μ_3-η^2-vinyl, or μ_3-η^2-vinylidene [Fig 3] [9]. Both the 2976 cm^{-1} and 2990 cm^{-1} features seem to arise from $sp^{2.5}$ hybridization, which gives rise to frequencies in this range as demonstrated by osmium cluster work. The intensity near 2900 cm^{-1} can be assigned to the $\nu_s(CH_2)$ from di-σ bonded ethylene [4], which correlates well with the onset of ethylene desorption that TPD evidence provides just above this temperature.

Annealing the system up to room temperature causes only minor changes in the peaks observed [Fig. 5a]. The first sign of significant decomposition occurs near 313 K [Fig. 5b]. At this point the 2950-3000 cm^{-1} range simplifies with a 2960 cm^{-1} shoulder on the sharp 2976 cm^{-1} feature. There is a small new feature at 3033 cm^{-1}, which is most readily assigned to the $\nu_s(CH_2)$ of μ-vinylidene [Fig. 3] by comparison with the frequency from the corresponding osmium cluster [10]. Further heating to 339 K causes a dramatic drop in the intensity of the 2976 cm^{-1} feature, but the 2960 and 3033 cm^{-1} peaks are still present at approximately the same strength [Fig. 5c]. Annealing to 356 K causes the complete disappearance of the 2976 cm^{-1} feature accompanied by the formation of ethylidyne with its characteristic $\nu_s(CH_3)$ showing up at 2884 cm^{-1} [Fig. 5d] [11]. Under these conditions ethylidyne coexists on the surface with ethylidene at 2960 cm^{-1} and μ-vinylidene at 3033 cm^{-1}. Further annealing of the surface to 385 K causes the higher frequency features to disappear completely and only the ethylidyne

feature remains [Fig. 5e]. The ethylidyne feature has strengthened significantly from the 356 K spectrum. The intensity of this feature represents a coverage of approximately 0.8 ML as judged from comparing the curve fitted peak strength from this spectrum with know calibrations for ethylidyne at saturation coverage (0.25 ML) [4].

4.4 Discussion

(a) Surface Stoichiometry and Hydrogen Production

The decomposition of acetylene on Pt(111) gives rise to a rich variety of spectral features in the CH stretch range. Even at low temperatures a mixture of surface species are present. The features in figure 3, such as the methyl asymmetric stretch at 2960 cm^{-1} of ethylidene ($M{=}CHCH_3$), indicate that significant CH bond breaking and forming already occurs below 200 K. This is consistent with the thermal desorption data by Megiris et al., which indicates that the onset of ethylene desorption is just below 200 K [6]. Avery showed using reactions with deuterium that hydrogen from the gas phase can be ruled out as making a significant contribution to the formation of ethylidyne [5]. Therefore, ethnyl ($M\text{-}C{\equiv}CH$) or other surface residue must already exist on the surface to accommodate the presence of other adsorbed species with higher hydrogen/carbon ratios.

Evidence for an ethnyl species cannot be directly obtained from the SFG spectra apparently because of the lack of a surface normal component of the ν(CH) dynamic dipole. This was confirmed by control scans in the 3156 cm^{-1} range (not shown) where its ν(CH) signal would be expected [9]. However, Avery noted evidence for this species during acetylene decomposition in the HREELS spectrum from a weak signal at 750 cm^{-1} [5]. Other possible surface residues include methylidyne ($M{\equiv}CH$); however, the formation of this species requires breaking of the C-C bond. The TPD data does shows evidence for a very small amount of methane production [6], which would indicate carbon-carbon bond breakage (perhaps occurring at defect sites). This route, however, is

probably not mechanistically important at the temperatures under which these experiments were performed.

If it is assumed that ethnyl formation is the major source for surface hydrogen, then for every C_2H_4 moiety observed on the surface, three C_2H species must be formed. Further, each ethylene which desorbs from the surface requires the formation of three ethnyl groups. This means that the overall stoichiometry on the surface is less than C_2H_2 even below 200 K. Indeed, spectroscopic evidence for a small amount of adsorbed ethylene exist at 190 K from the weak feature near 2900 cm^{-1} [Fig 4]. The evolution of enough surface hydrogen to form ethylene and ethylidene necessarily means that the disproportionation reaction has already begun far below the temperature at which ethylidyne is formed [Fig 4].

(b) The Surface Reaction Mechanism

The appearance of the 3033 cm^{-1} peak is the first new feature that appears in the spectrum upon annealing. The activation barrier to its formation is most likely the rearrangement of acetylene to form μ-vinylidene via a 1,2 hydrogen shift. Evidence for this comes from the corresponding decline of the 2974 and 2990 cm^{-1} peaks as the higher frequency feature grows in.

By 339 K only three species appear to be on the surface: ethylidene, acetylene, and μ-vinylidene. All are present prior to the formation of any ethylidyne, and hence must all be considered as possible candidate species to its formation. However, the acetylene feature at 2976 cm^{-1} has been in constant decline since 331 K and completely disappears by 356 K, a temperature at which the ethylidyne is not yet fully formed. Therefore, it can be reasonably ruled as the direct ethylidyne precursor. Both the ethylidene and μ-vinylidene are present as ethylidyne begins to form near 356 K. Of these two candidates, the ethylidene species is more likely to be the direct ethylidyne precursor.

The decision to favor the ethylidene pathway over μ-vinylidene is based on analogy with our earlier studies of ethylidyne formation from di-σ bonded ethylene and vinyl groups [4]. During vinyl decomposition to ethylidyne, the presence of μ-vinylidene was detected at low temperature (140 K), although ethylidene was not found until much higher temperature. The 3033 cm^{-1} feature from μ-vinylidene disappeared upon annealing to 200 K, while the ethylidene peak was found to grow in near room temperature. Heating above room temperature caused the ethylidene peak to disappear and the ethylidyne $\nu_s(CH_3)$ at 2884 cm^{-1} to grow in. The presence of significant amount of CCH_2 in the case of acetylene chemistry may explain why vinylidene does not decompose below 350 K. Indeed, CCH_2 species may serve to block the important sites for further vinylidene reactions.

The μ-vinylidene species was not observed in the case of di-σ bonded ethylene decomposition to ethylidyne [4]. Instead, as the characteristic 2904 cm^{-1} feature from di-σ bonded ethylene disappeared, only the $\nu_{as}(CH_3)$ feature of ethylidene was observed (in addition to signal from ethylidyne). In this case, the ethylidene feature disappeared near room temperature as the ethylidyne overlayer seemed to be completed by 296 K. Again, the reason for the lower conversion temperature probably stems from the lack of surface CCH, which must block the fcc three fold hollow sites in which ethylidyne is formed.

Ethylidyne formation from ethylidene in the case of acetylene/Pt(111) requires that two acetylene molecules decompose to C_2H for each ethylidene formed [Fig. 5]. Ethylidene cannot be directly formed form acetylene, but must go through an unobserved vinyl intermediate. This chemistry would require that sufficient surface hydrogen is produced (presumably from ethnyl formation) for some remaining acetylene species to proceed through a rate limiting vinyl step to the more stable ethylidene species. Such chemistry would ultimately lead to only 1/3 of the acetylene molecules forming

ethylidyne, assuming an initial coverage of 0.25 monolayers of acetylene. This is indeed in agreement with our observation of .08 ML ethylidyne formed.

4.5 Conclusion

Ethylidyne is formed near 350 K on the surface of Pt(111) from the thermal rearrangement reaction of adsorbed acetylene. Even at low temperatures (below 200 K), C-H bonds are broken and C_2H_4 species such as ethylidene and di-σ bonded ethylene are formed. Annealing the system near 339 K yields a mixture of μ-vinylidene and ethylidene. Upon further heating above 350 K, ethylidyne is formed from the ethylidene species. The net reaction most likely involves three acetylene molecules undergoing disproportionation to form one ethylidyne and two ethnyl molecules.

4.6 References

[1] W. Weinberg, H. Deans, and R. Merrill, Surf. Sci., 41 (1974) 312

[2] P. Skinner, M. Howard, I. Oxton, S. Kettle, D. Powell, and N. Sheppard, J. Chem. Soc. Faraday Trans., 15 (1978) 407

[3] U. Starke, A. Barbieri, N. Materer, M. Van hove, and G. Somorjai, Surf. Sci., 286 (1993) 1

[4] P. Cremer, S. Stanner, J. Niemantsverdriet, Y. Shen, and G. Somorjai, Surf. Sci., 328 (1995) 111

[5] N. Avery, Langmuir, 4 (1988) 445

[6] C. Megiris, P. Berlowitz, J. Butt, H. Kung, Surf. Sci., 159 (1985) 184

[7] C. Anson, N. Sheppard, D. Powell, J. Norton, W. Fischer, R. Keiter, B. Johnson, J. Lewis, A. Bhattacharraya, S. Knox, and M. Turner, J. Am. Chem. Soc., 116 (1994) 3058

[8] The 2976 cm^{-1} peak could be red shifted from the 2990 cm^{-1} feature seen in most osmium cluster spectra if there is a slight change in site

[9] J. Evans and G. McNulty, J. Chem. Soc. Dalton Trans., (1984) 79

[10] J. Evans and G. McNulty, J. Chem. Soc. Dalton Trans., (1983) 639

[11] I. Malik, V. Agrawal, and M. Trenary, J. Chem. Phys., 89 (1988) 3861

4.7 Figure Captions

Fig. 1 Schematic of the decomposition of di-σ ethylene to ethylidyne on Pt(111).

Fig. 2 The disproportionation reaction of acetylene to ethnyl and ethylidyne on Pt(111).

Fig. 3 Schematic representations of adsorbed acetylene, vinylidene, vinyl, ethylidene, ethylidyne species.

Fig. 4 The SFG spectrum of a saturation coverage (4 L) of acetylene adsorbed on Pt(111) at 191 K.

Fig. 5 Vibrational spectra of the thermal evolution of acetylene on Pt(111). The system was annealed to (a) 288 K, (b) 313 K, (c) 339 K, (d) 356 K, and (e) 381 K for 60 seconds and then allowed to cool below 191 K where an SFG scan was performed

Fig. 6 The proposed pathway for acetylene decomposition to ethnyl and ethylidyne on Pt(111).

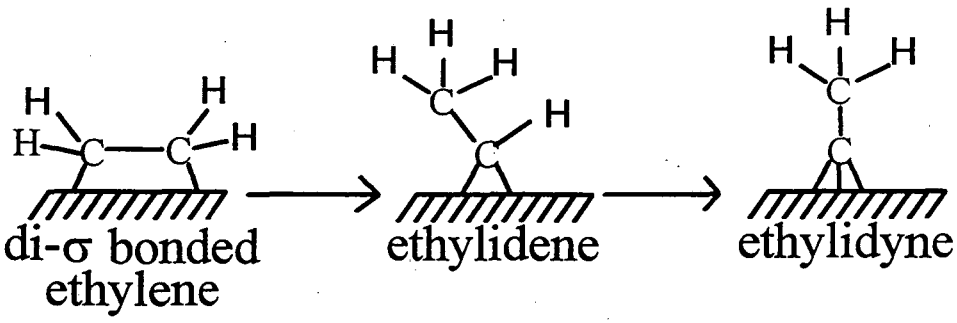
H
H
H
H
C
C
H
H
H
H
H
C
C
H
H
H
H
C
C
di-σ bonded
ethylene
ethylidene
ethylidyne

Fig. 1

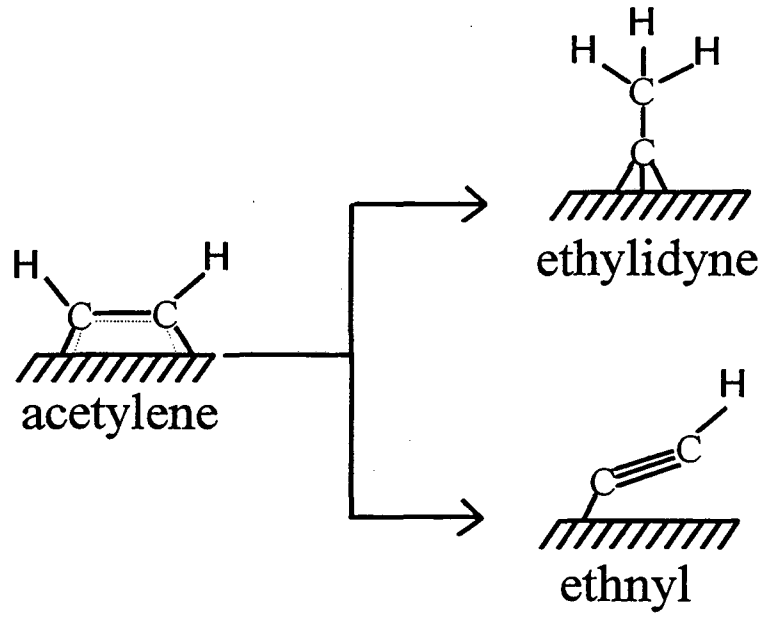

Fig. 2

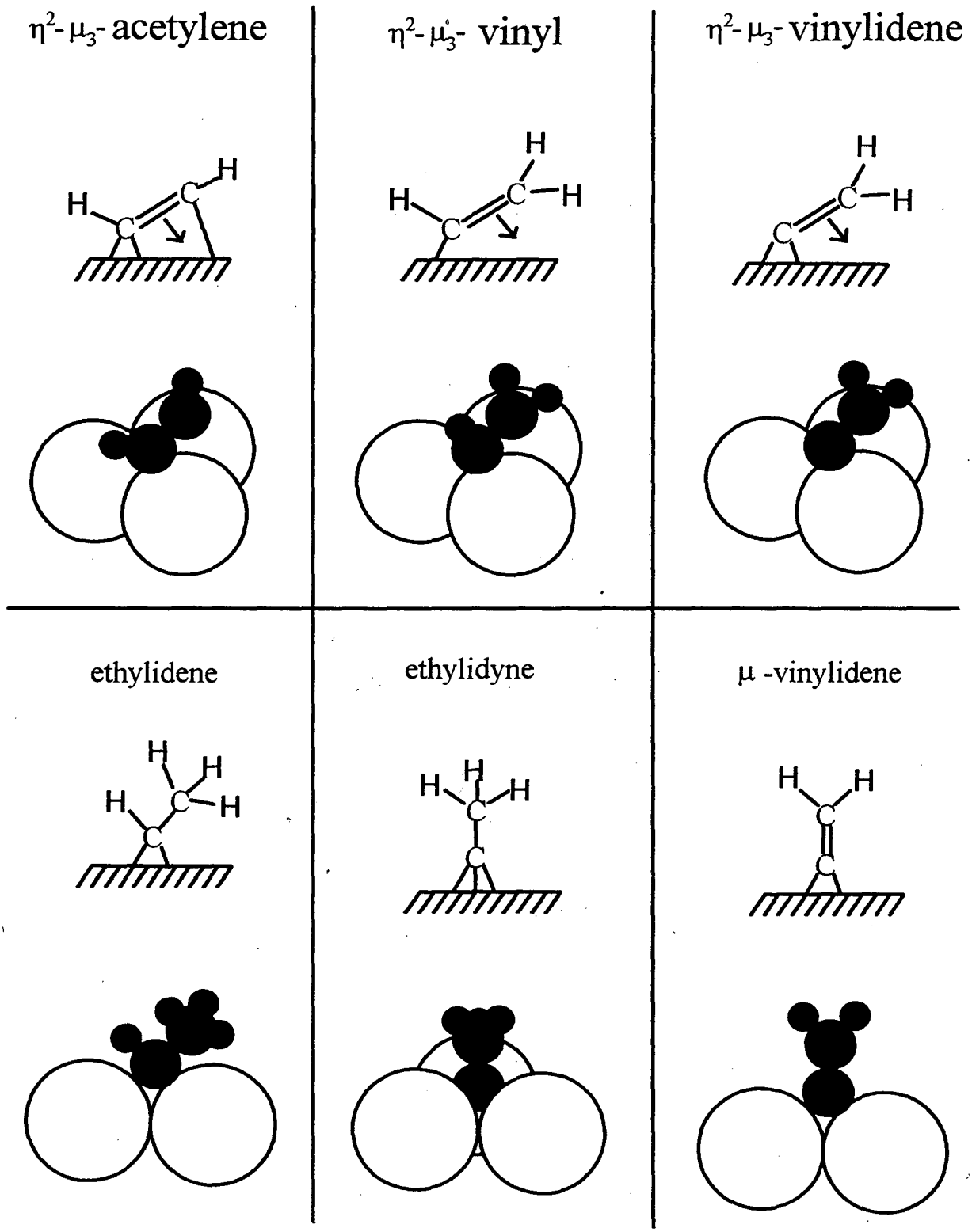
η²-μ₃-acetylene
η²-μ₃-vinyl
η²-μ₃-vinylidene
ethylidene
ethylidyne
μ -vinylidene

Fig. 3

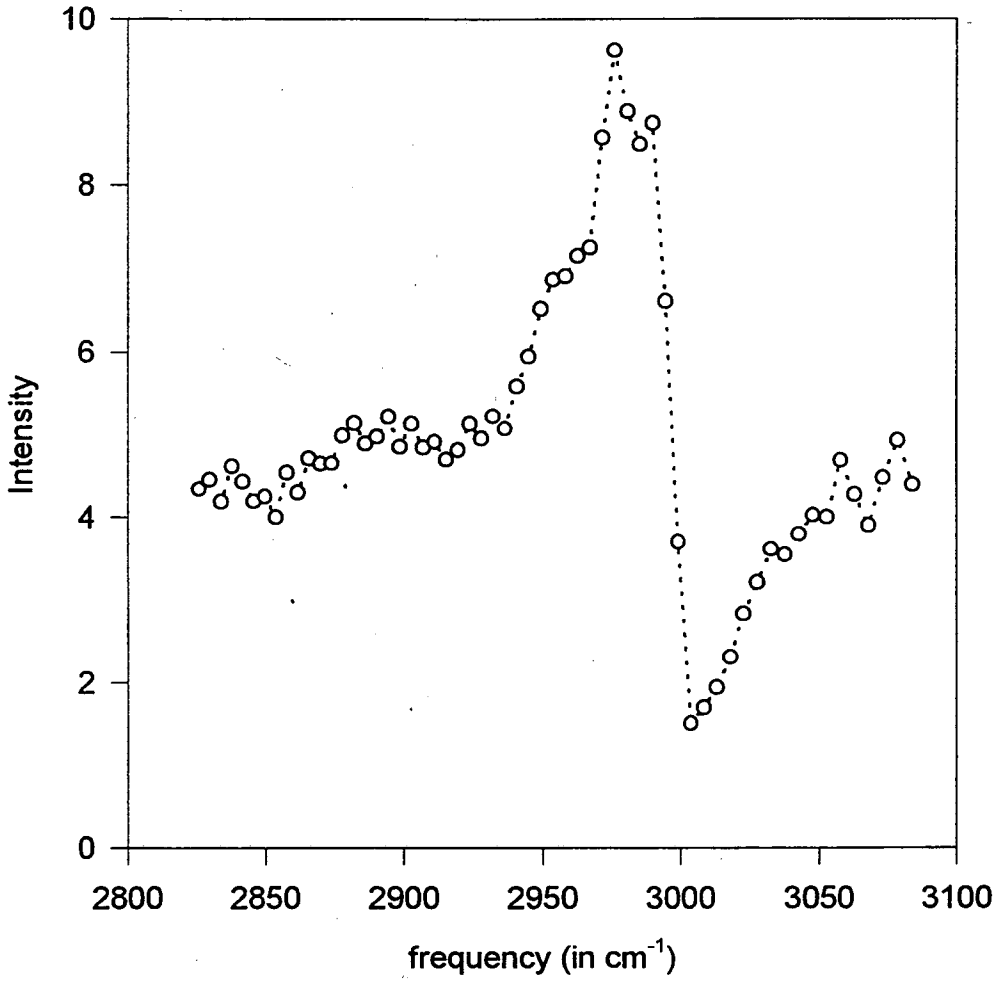
10
8
6
4
2
0
Intensity
2800
2850
2900
2950
3000
3050
3100
frequency (in cm-1)

Fig. 4

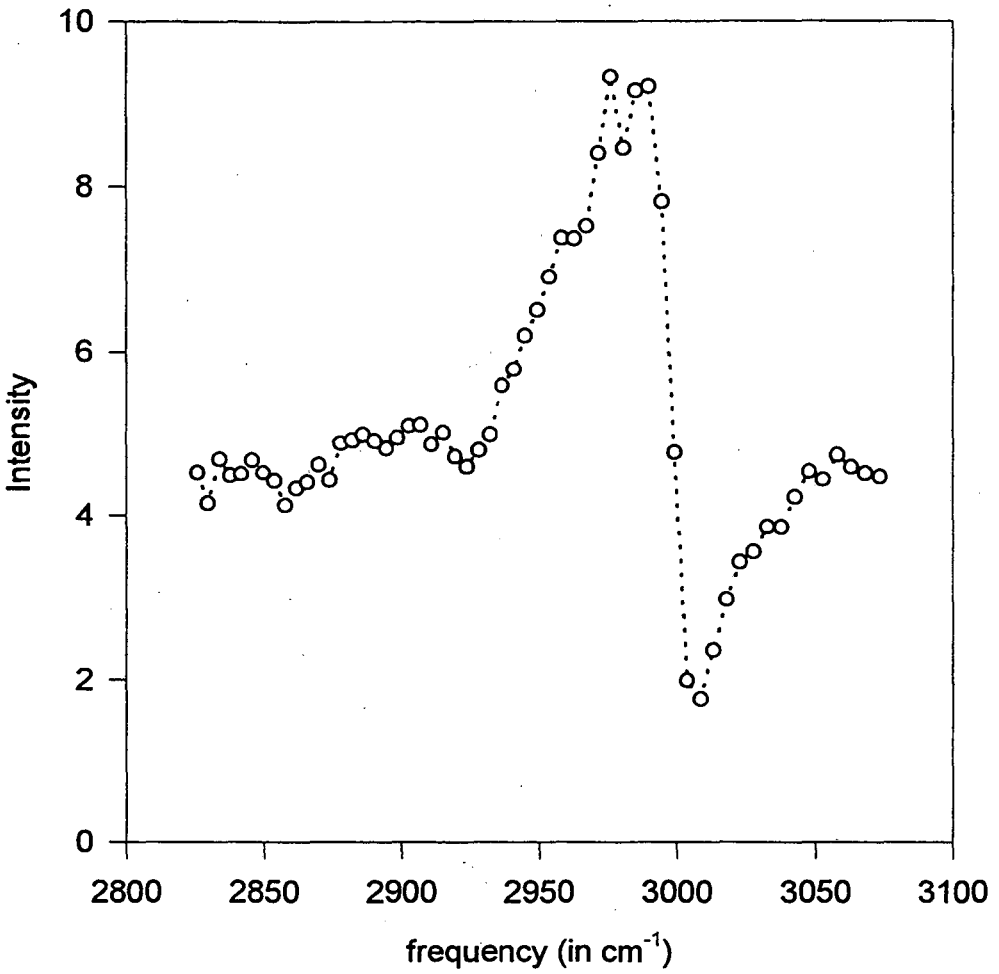
10
8
6
4
2
0
Intensity
2800
2850
2900
2950
3000
3050
3100
frequency (in cm-1)

Fig. 5a

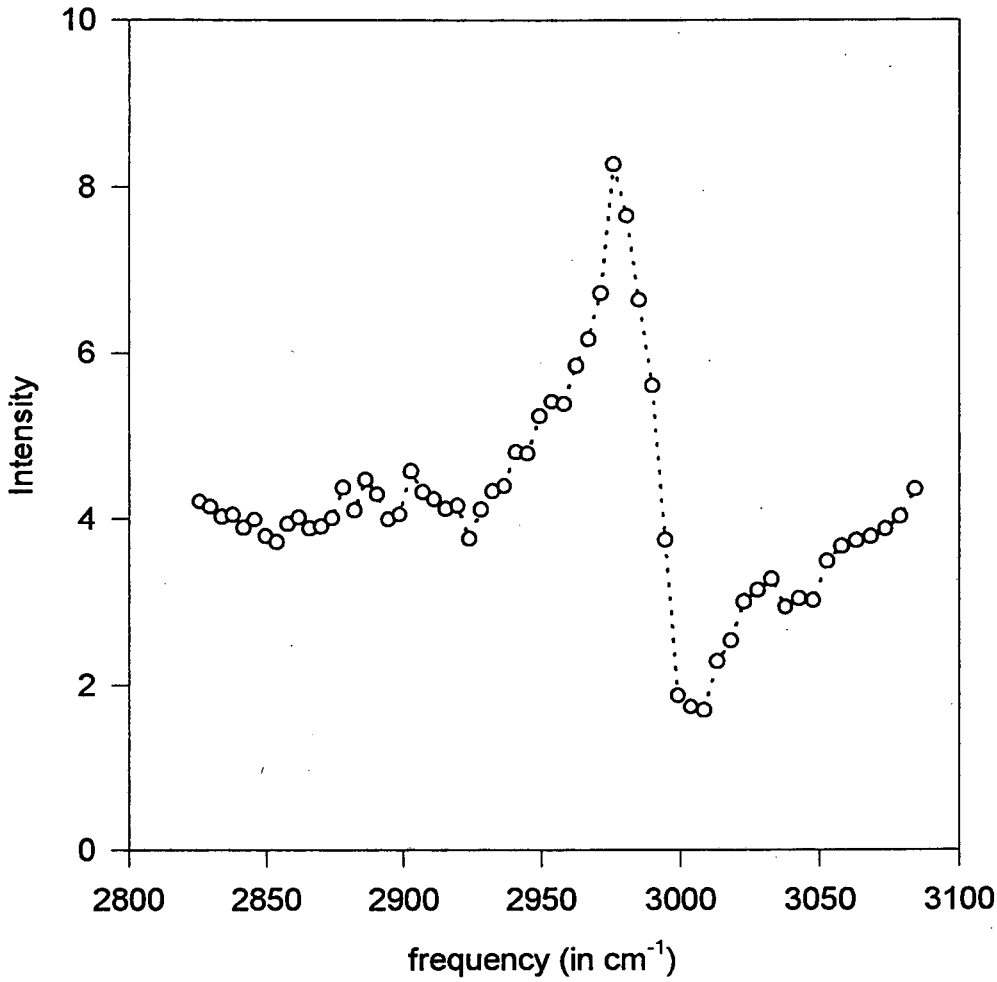
10
8
6
4
2
0
Intensity
2800
2850
2900
2950
3000
3050
3100
frequency (in cm-1)

Fig. 5b

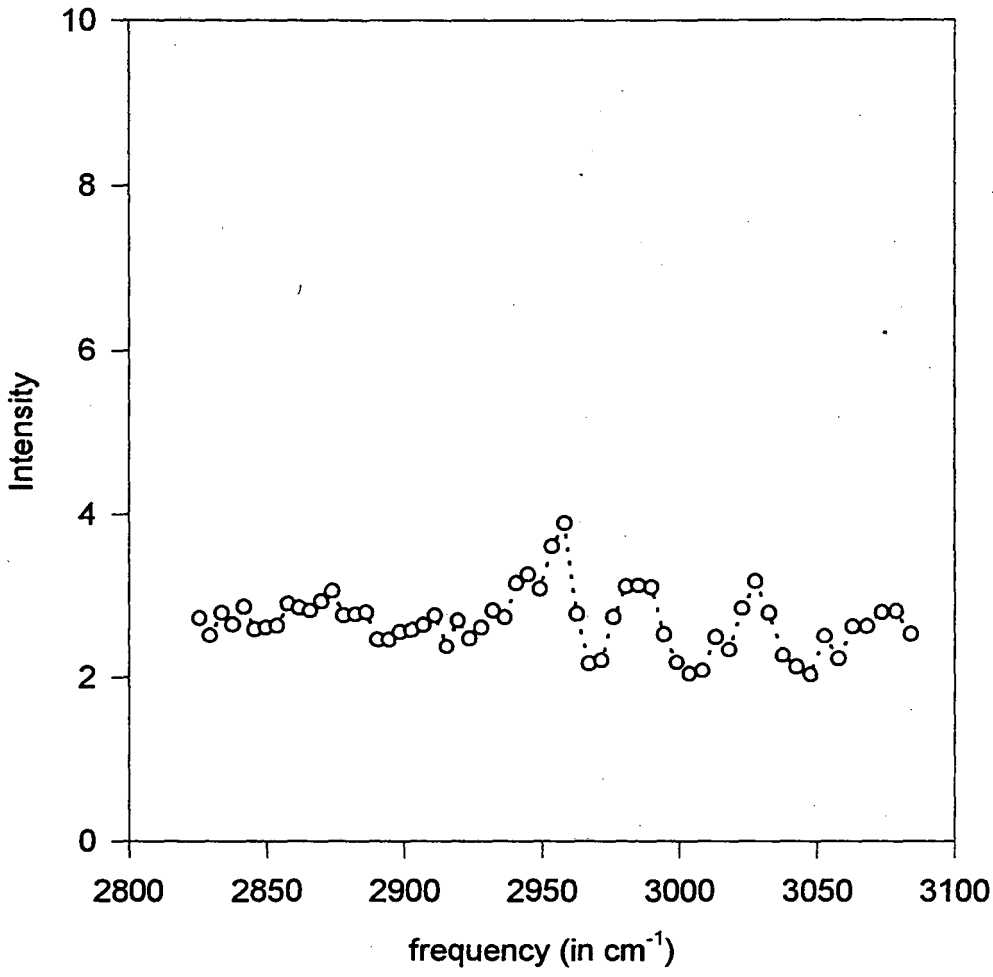
10
8
6
4
2
0
Intensity
2800
2850
2900
2950
3000
3050
3100
frequency (in cm-1)

Fig. 5c

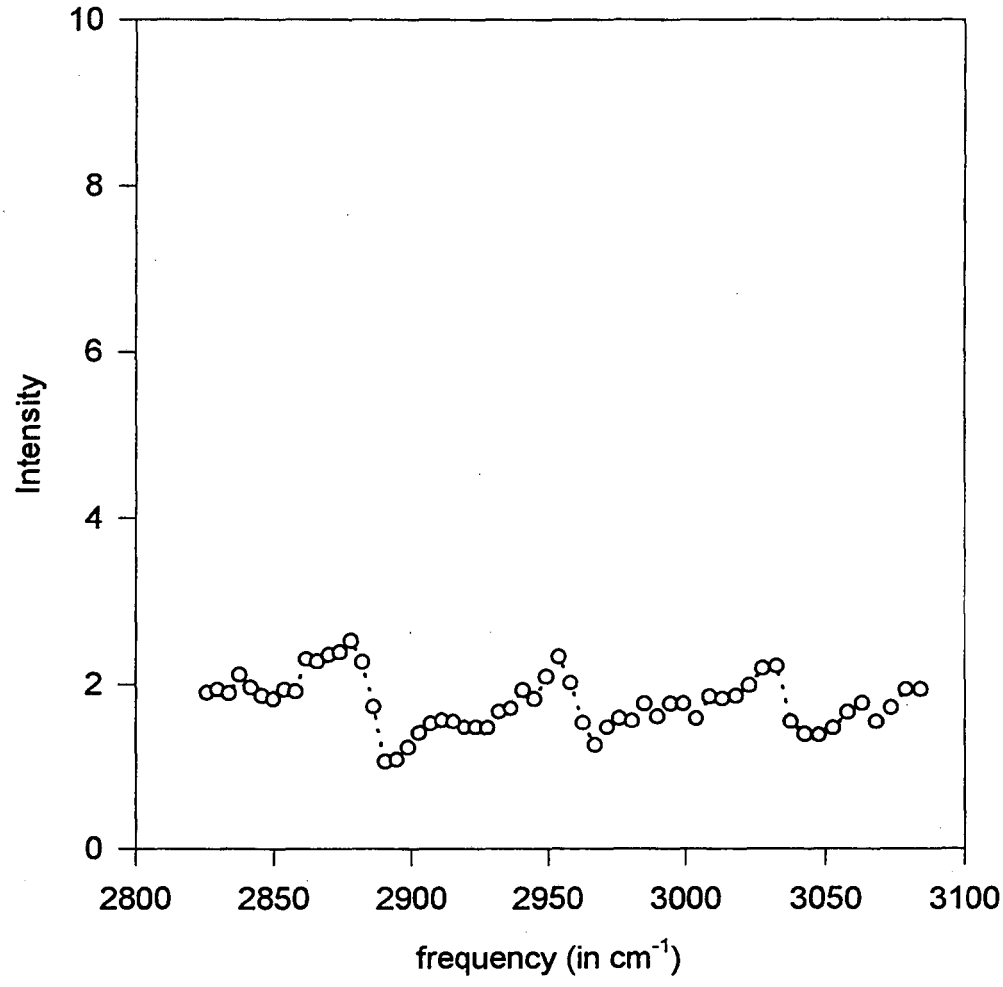
10
8
6
4
2
0
Intensity
2800
2850
2900
2950
3000
3050
3100
frequency (in cm-1)

Fig. 5d

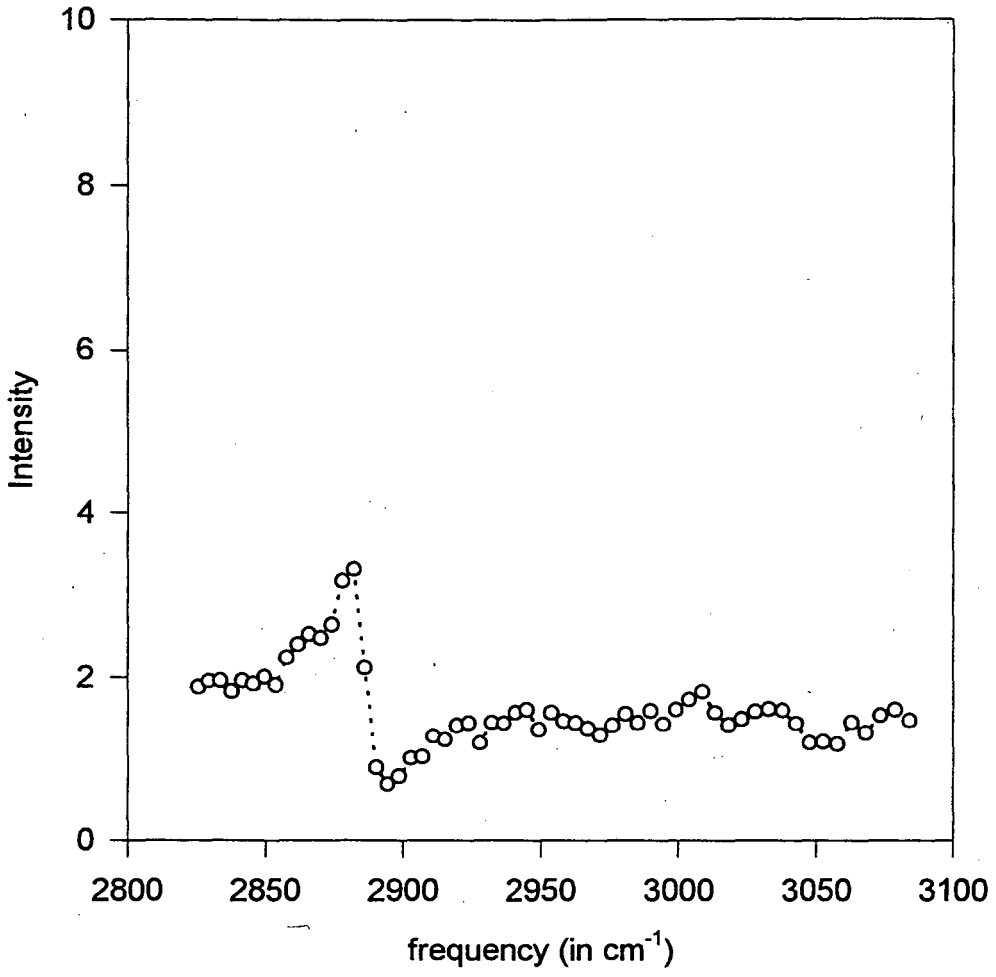
10
8
6
4
2
0
Intensity
2800
2850
2900
2950
3000
3050
3100
frequency (in cm-1)

Fig. 5e

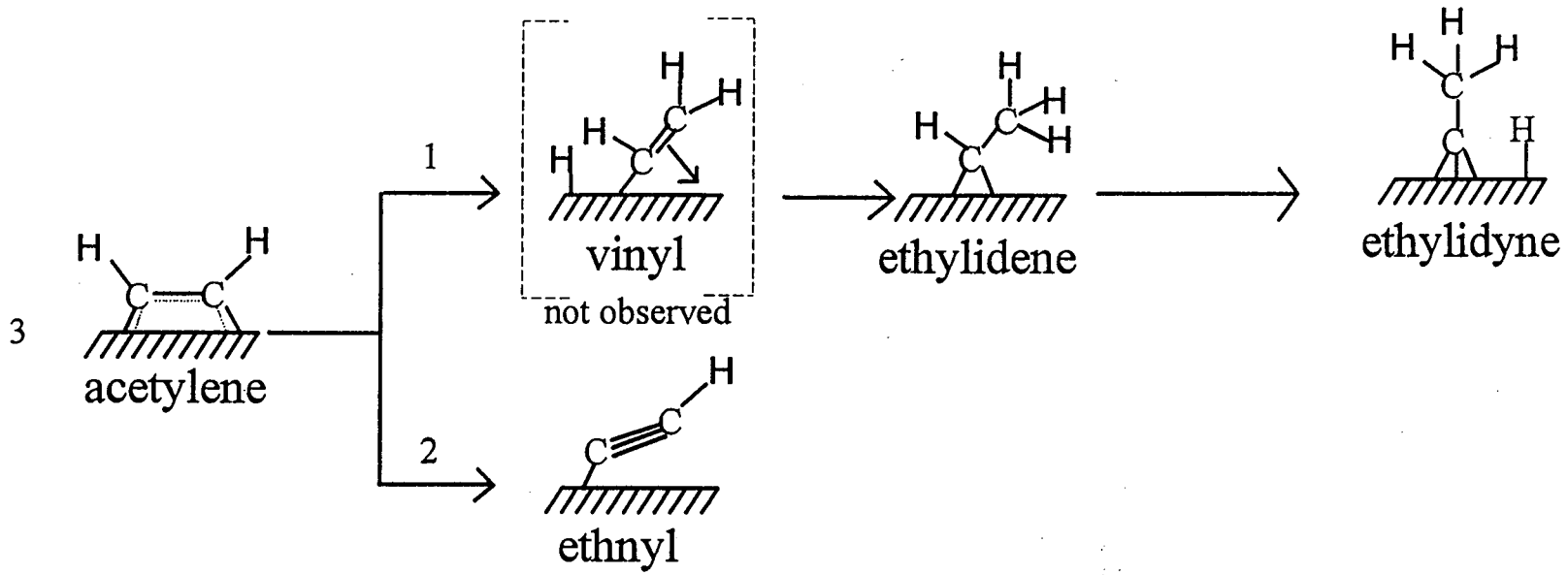
3
acetylene
1
2
vinyl
not observed
ethnyl
ethylidene
ethylidyne

Fig. 6

Chapter 5

The Hydrogenation of Ethylene on Pt(111)

Infrared-visible sum frequency generation (SFG) has been used to monitor the surface vibrational spectrum *in situ* during ethylene hydrogenation on Pt(111). Measurements were made near one atmosphere total pressure of ethylene and hydrogen and at 295 K. Kinetic information was obtained simultaneously with the surface vibrational spectroscopy by monitoring the reaction rate with gas chromatography. The macroscopic turnover rate and surface adsorbate concentration could then be correlated. During the reaction ethylidyne, di-σ bonded ethylene, ethyl, and π-bonded ethylene were observed on the surface in various amounts depending on conditions. Ethylidyne, a spectator species during hydrogenation, competed directly for sites with di-σ bonded ethylene and its surface concentration could be shown to be completely uncorrelated with the rate of hydrogenation. In contrast, π-bonded ethylene did not compete for sites with the ethylidyne overlayer and was observed on the surface regardless of the surface concentration of ethylidyne. Evidence points to the π-bonded species as being the primary intermediate in ethylene hydrogenation on Pt(111). The surface concentration of this species is about 0.04 ML during reaction. Thus, the turnover rate per reaction intermediate is 25 times faster than the turnover rate if measured per surface platinum atom.

5.1 Introduction

A mechanism for the hydrogenation of the simplest olefin, ethylene, over a platinum surface was first proposed in the 1930's by Horiuti and Polanyi (Fig. 1) [1]. According to their model, ethylene chemisorbs on the clean metal surface by breaking one of the carbon carbon double bonds. This species, which forms two sigma bonds with the underlying metal substrate, is then stepwise hydrogenated through an ethyl intermediate to ethane. Evidence for an ethyl intermediate was found in the 1950's by Kemball et al. using deuterium labeling that showed ethylene molecules readily exchange hydrogen atoms during the hydrogenation process [2]. Kinetic studies showed that the rate at which ethylene hydrogenates is independent of the structure of the underlying metal atoms and therefore it is called a structure insensitive reaction [3]. The reaction has been observed to vary between half order and first order in hydrogen (depending upon temperature) and to be zero or slightly negative order in ethylene [4].

Surface science investigations of the mechanism for ethylene hydrogenation began in the 1970's with model studies of ethylene adsorption on low miller index faces of platinum under ultra high vacuum (UHV) conditions. Ethylene adsorbed on Pt(111) in the absence of hydrogen was monitored with a variety of techniques that revealed the presence of several distinct surface species. Ultraviolet photo emission spectroscopy (UPS) showed that ethylene physisorbs through its π-orbital on clean Pt(111) below 52 K [5]. This species is referred to as π-bonded ethylene (Fig. 2a). Its binding site has yet to be determined by low energy electron diffraction (LEED) surface crystallography, but analogy to organometallic cluster chemistry tends to favor an atop site [6, 7].

When heated above 52 K, ethylene irreversibly breaks the π-bond and forms two sigma bonds to the surface metal atoms and is called di-σ bonded ethylene (Fig. 2b). This species is sp^3 hybridized [8] and resides in an fcc three fold hollow site on the Pt(111) surface as determined by LEED [9]. Saturation coverage is 0.25 monolayers (ML) [10];

which means there is one di-σ bonded ethylene molecule for every four underlying platinum surface atoms.

Above 240 K di-σ bonded ethylene dehydrogenates to ethylidyne ($M{\equiv}CCH_3$) by transferring one hydrogen from one carbon to the other and losing a hydrogen (Fig. 2c) [11]. The dehydrogenation is accompanied by hydrogen atom recombination to H_2, which then desorbs from the surface as molecular hydrogen near room temperature and can be readily monitored by thermal desorption mass spectrometry. Like di-σ bonded ethylene, ethylidyne is also adsorbed in an fcc three fold hollow site as determined by LEED, however its C-C bond axis is normal to the surface [12]. Scanning tunneling microscopy (STM) reveals that ethylidyne cannot be imaged unless the surface is cooled to 220 K [13]. This suggests that the species is highly mobile on the surface at room temperature, most likely moving between three fold sites. Ethylidyne has a saturation coverage of 0.25 ML [10] and upon annealing the ethylidyne/(Pt(111) system above 500 K further dehydrogenation to graphitic precursors (such as C_2H and CH) takes place. Finally, above 700 K the hydrocarbon fragments decompose to graphite [13].

In order to determine the role of each of the surface species in ethylene hydrogenation, their chemistry has been studied in the presence of hydrogen under reaction conditions. Several groups have investigated the role of ethylidyne. Davis et al. hydrogenated ^{14}C labeled ethylidyne on Pt(111) with near atmospheric pressure of H_2. Their results indicated that the rate of hydrogenation of the ethylidyne was several orders of magnitude slower than the overall turnover rate of hydrogenation of ethylene to ethane indicating that ethylidyne was not directly involved in the reaction [14]. Beebe et al. monitored ethylene hydrogenation over a Pd/Al_2O_3 supported catalyst *in situ* by using transmission infrared spectroscopy. By varying the ratio of ethylene to hydrogen it was observed that hydrogenation occurred over surfaces both with and without an ethylidyne ($\equiv CCH_3$) overlayer [15]. Rekoske et al. have repeated the transmission infrared work on Pt/Cab-O-Sil and concluded that the ethylidyne was not involved in the reaction in the

case of a supported platinum catalyst [16]. All evidence strongly suggests that ethylidyne is a spectator species not involved in ethylene hydrogenation.

The roles of chemisorbed and physisorbed ethylene have also been examined. Using transmission infrared spectroscopy, Moshin et al. have shown that both π-bonded and di-σ bonded ethylene are hydrogenated when H_2 is flowed over a Pt/Al_2O_3 catalyst precovered with these species [17]. Further, they found that upon annealing a surface covered with π-bonded and di-σ bonded ethylene in the absence of hydrogen only the di-σ bonded species was converted to ethylidyne while the π-bonded ethylene remains unaffected.

None of the infrared spectroscopy studies described above, however, allowed the monitoring of surface intermediates of ethylene hydrogenation when ethylene was flowing. This is because gas phase ethylene greatly interferes with the infrared spectroscopy experiments [16]. Hence, all experiments in which di-σ and π-bonded ethylene were monitored required that ethylene be removed from the gas phase in order to make observations. In order to avoid this problem, nonlinear optical methods are employed in this study. Sum frequency generation (SFG) as a surface specific vibrational spectroscopy is an ideal choice, because it generates virtually no signal from the gas phase [18-20]. Therefore, it can be used to obtain surface vibrational spectra *in situ* under steady state reaction conditions when all the reactants and products are present over a wide range of pressures and temperatures.

In this paper we report SFG studies carried out simultaneously with gas phase turnover rate measurements of ethylene hydrogenation to ethane on the Pt(111) crystal surface near room temperature and atmospheric pressure. These studies permit the identification of the molecular species present on the surface at different hydrogen to hydrocarbon ratios and provide insight into how the turnover rate depends on the nature of the species that are present. A mechanism for ethylene hydrogenation is proposed

with the molecular details of the process that greatly amplify the model proposed by Horiuti and Polanyi.

5.2 Experimental

(1) UHV, Reactor, and SFG Apparatus

All experiments were performed in a UHV/batch reactor system on a Pt(111) single crystal (Fig. 3). The crystal was cut, polished, and oriented using the normal procedures. The UHV system was pumped by a turbo pump and an ion pump and had a base pressure of less than 1×10^{-10} Torr. The crystal could be heated resistively to over 1300 K and cooled with liquid nitrogen to approximately 115 K. The UHV system was equipped with an electron gun for argon ion bombardment, a retarding field analyzer for LEED and Auger, and a mass spectrometer. In addition, the chamber has two CaF_2 windows which were used to allow tunable IR and green light into the chamber as well as to allow sum frequency light to go out to a photomultiplier tube.

The light used for SFG was generated by a passive, active mode locked Nd:YAG laser with a 20 ps pulse width. A portion of the output was sent to an optical parametric generator/amplifier stage where infrared light between 2600 -4000 cm^{-1} was generated. This light was then combined at the Pt(111) sample with 532 nm light that was frequency doubled from the 1064 nm Nd:YAG fundamental. Although both the apparatus used in this experiment [11] to perform the sum frequency generation experiments and the technique itself [18-20] have been described elsewhere, it should be noted that for vibrational modes to be active in SFG they must obey both the Raman and IR selection rules. Only modes which lack centrosymmetry can in the dipole approximation simultaneously obey both rules. In the experiments described in this paper the gas phase (which is isotropic) and the fcc lattice of the bulk platinum sample possess inversion symmetry and give nearly zero contribution to the signal. The dominant contribution is generated at the platinum surface, where inversion symmetry is always broken.

Atmospheric pressure experiments were undertaken in a batch reactor which could be isolated from the turbo pump and the ion pump via a gate valve (Fig. 3). Gas pressures were monitored by a Baratron gauge that was capable of measuring pressures between 100 mTorr and 1000 Torr. The gases in the reactor were constantly mixed by a recirculation pump and samples could be withdrawn from the reaction loop and analyzed in an HP 5890 series II gas chromatograph equipped with a 115-3432 GSQ column for the separation of ethylene from ethane.

(2) UHV Calibration Experiments to Identify Various Adsorbates

To aid in the assignment of the spectroscopic features from surface adsorbates present during catalysis, several high vacuum analogs were prepared on the pristine platinum surface with which to compare. Fig. 4a shows the SFG vibrational spectrum of a saturation coverage of di-σ bonded ethylene on Pt(111) in the CH stretch region. The peak at 2904 cm^{-1} is the $\nu_s(CH_2)$ of the methylene groups. The system was prepared by exposing the clean Pt(111) surface to 4 L(angmuir) of ethylene at 200 K. The dip of the baseline below its initial level following the spectral feature is due to the interference between the nonresonant background from the platinum metal and the resonant signal from the di-σ bonded species. All vibrational spectra in this paper contain this artifact of the sum frequency generation experiment. Because of the interference between the resonant and the nonresonant signals, the background signal may be suppressed for several hundred wavenumbers following a major peak. Also, the resonant features are slightly red shifted and their exact frequencies must be determined by fitting.

The di-σ bonded species is stable on the surface in UHV up to 240 K at which temperature it dehydrogenates to ethylidyne ($M{\equiv}CCH_3$). Ethylidyne can also be formed by directly exposing ethylene to Pt(111) between 240-450 K. The spectrum of a saturated coverage of ethylidyne/Pt(111) formed at 300 K in UHV is shown in Fig. 4b.

The major spectral feature is the $\nu_s(CH_3)$ peak of ethylidyne's terminal methyl group at 2884 cm^{-1}.

Ethyl groups can be formed on Pt(111) by exposing the clean surface to ethyl iodide and then annealing the surface above 170 K to begin breaking some of the C-I bonds [21]. The spectrum of ethyl/Pt(111) at 193 K is shown in Fig. 4c. Several CH stretch features are observable on the surface. The two lower frequency features (2860 cm^{-1} and 2920 cm^{-1}) have been assigned to a fermi resonance and the $\nu_s(CH_3)$ respectively. The higher frequency peak near 2970 cm^{-1} is the $\nu_a(CH_3)$ of undissociated CH_3CH_2I [22].

UHV calibration of the π-bonded species were made by exposing the clean Pt(111) surface to a near saturation coverage of O_2 at 300K. This surface was then further exposed to ethylene at 120 K to yield a mixture of π-bonded and di-σ bonded ethylene [23, 24]. The SFG spectra of the adsorbates is shown in Fig. 4d. The larger peak at 2915 cm^{-1} corresponds with di-σ bonded ethylene and the 2995 cm^{-1} feature is associated with the $\nu_s(CH_2)$ of π-bonded ethylene. This is in good agreement with transmission infrared data on supported platinum catalysts showing intensity for π-bonded ethylene near 3000 cm^{-1} [17, 25, 26]. The intensity of the $\nu_s(CH_2)$ is fairly weak in the SFG experiment because the surface metal dipole selection rule requires the presence of a surface normal component of the dynamic dipole for the species to be observable. In the case of π-bonded ethylene, the $\nu_s(CH_2)$ is nearly in plane with the metal surface; hence, the signal observed is small. The total coverage of ethylene from both species is roughly 0.16 ML [23]. Fitting the peaks suggests that approximately 0.10 ML is from di-σ bonded ethylene and 0.06 ML from π-bonded ethylene. All calibration results for ethyl, ethylidyne, di-σ bonded ethylene, and π-bonded ethylene are in good agreement with infrared values in the literature.

(3) Sample Preparation

Before performing high pressure studies, the Pt(111) crystal was cleaned with cycles of Ar^+ sputtering and annealing, after which sample cleanliness was checked by Auger electron spectroscopy. The sample was then isolated from vacuum via a gate valve at which time pure hydrogen was introduced into the reactor. Hydrogen was always introduced first, followed by ethylene. This insured that hydrocarbon contaminants did not poison the crystal.

5.3 Results

(1) High Pressure Ethylene Hydrogenation

Ethylene hydrogenation experiments were carried out over a range of hydrogen pressures from less than 2 Torr H_2 to over 700 Torr of H_2. The ethylene pressure was kept lower than that of hydrogen under all circumstances. However, the absolute partial pressure of ethylene was not critical to the experiment because the reaction was conducted in the regime where it is known to be zero order in ethylene (except where noted). Control experiments were performed to verify that this was indeed the case. It was at intermediate pressures that the richest surface chemistry was observed (100 Torr H_2). The SFG spectrum obtained during ethylene hydrogenation at 295 K with 100 Torr H_2, 35 Torr ethylene, and 625 Torr He is shown in Fig. 5a. The dominant feature in the spectrum was the CH_3 symmetric stretch of ethylidyne at 2878 cm^{-1}. The intensity of the peak corresponded to a coverage of 0.15 ML or 60% of saturation coverage. Just above the ethylidyne peak the CH_2 symmetric stretch of di-σ bonded ethylene was observed at 2910 cm^{-1}. The peak from the di-σ bonded ethylene represented approximately 0.08 ML.

In addition to these two prominent features a weak and broad hump around 3000 cm^{-1} from π-bonded ethylene was observed. The intensity is weak because the dynamic dipole of the molecule's $\nu_s(CH_2)$ is nearly in plane with the metal surface. Although this

feature is weak, it was consistently reproducible over numerous experimental trials. The coverage of this species was about 0.04 ML based on the calibration coverage of Fig. 4d. The spectrum in Fig. 5a remained unchanged for hours showing that the composition of adsorbates on the surface remained unchanged over the lifetime of the experiment.

While vibrational spectra were being recorded, the gas phase composition was monitored by gas chromatography (GC). GC measurements of ethane production revealed a turnover rate (TOR) of 11±1 ethylene molecules per surface platinum atom per second; that is 11 ethylene molecules were converted to ethane per second for every exposed platinum atom.

Fig. 5b shows the vibrational spectrum of the catalytic Pt(111) surface immediately after evacuation of the reactor. The only spectral feature which remained was from ethylidyne. Further, the intensity of the ethylidyne peak increased to that of saturation coverage (0.25 ML). This increase in the ethylidyne peak was due to the dehydrogenation of di-σ bonded ethylene to ethylidyne after the hydrogen had been removed from the gas phase (analogous to what has been shown to occur under UHV conditions). The π-bonded species might also dehydrogenate to form ethylidyne, but presumably needs to go through a di-σ bonded intermediate first in order to do so. This clearly demonstrates that at 300 K π-bonded ethylene and di-σ bonded ethylene are only present on the surface in the presence of hydrogen and ethylene. As soon as the reactant gases are removed the species either decompose or desorb.

In order to determine the effect of a saturation coverage of ethylidyne on the reaction, experiments were carried out on a surface that was precovered with ethylidyne. The ethylidyne/Pt(111) system was prepared by dosing the clean platinum surface with 4 L of ethylene in UHV at 295 K. The crystal was then exposed to similar experimental conditions as in Fig. 5a. Fig. 5c shows the vibrational spectrum for the UHV prepared ethylidyne/Pt(111) system exposed to 100 Torr H_2, 35 Torr ethylene, and 625 Torr He at 295 K. The measured turnover rate under these conditions was 12 ±1 molecules per

platinum sites per second. This rate is almost identical to the previous conditions; however, the vibrational spectrum looks quite different. The ethylidyne peak at 2878 cm^{-1} is much stronger than in the previous case, while the $\nu_s(CH_2)$ from di-σ bonded ethylene is much smaller. Curve fitting the small di-σ bonded ethylene feature revealed that it represented less than 0.02 ML. This corresponds to more than a factor of four drop in the di-σ bonded ethylene concentration from the previous case without ethylidyne preadsorption. By contrast, the feature from π-bonded ethylene was present and appeared to be quite similar in intensity to the previous case.

The decrease in the concentration of di-σ bonded ethylene without a decrease in the rate of hydrogenation argues strongly against di-σ bonded ethylene being an important intermediate in ethylene hydrogenation. It appears the di-σ bonded species compete directly for sites with ethylidyne. Once ethylidyne species are formed they apparently block the adsorption sites for di-σ bonded ethylene. Because it is known from previous studies on supported catalyst surfaces that the presence or absence of ethylidyne has no affect on the rate of ethylene hydrogenation [15,16], di-σ bonded ethylene also can be ruled out as an important intermediate in ethylene hydrogenation. Indeed, if di-σ bonded ethylene had been an important intermediate, then ethylidyne would be a poison for ethylene hydrogenation.

In contrast to the behavior of the di-σ bonded species, the concentration of π-bonded ethylene was unaffected by the ethylidyne concentration. Therefore, the π-bonded species is likely to be a key intermediate in ethylene hydrogenation.

(2) Effects of higher and lower hydrogen pressures

The ethylene hydrogenation reaction was also carried out at higher pressures of hydrogen and ethylene (Fig. 6). These conditions (723 Torr H_2, 38 Torr ethylene, and 295 K) gave rise to a surface that was not saturated by ethylidyne or other hydrocarbon species in contrast to what was observed using 100 Torr H_2. It is significant to note that

there is little change in intensity of the peak corresponding to π-bonded ethylene; however, there is a drop in intensity of other spectral features as compared with Figs. 5a and 5c. Some di-σ bonded ethylene and ethylidyne were observable under these conditions, but two additional peaks (marked with arrows) at 2850 cm^{-1} and 2925 cm^{-1} were also visible. These features correspond quite well with those seen in the calibration measurements for ethyl/Pt(111) and can be assigned to the presence of the half hydrogenated ethyl intermediate on the surface in large enough quantity to be observed. The turnover rate measured for ethane formation was 61 ±3 molecules per platinum site per second under these conditions reflecting 0.81 order of this reaction with respect to hydrogen. This is in excellent agreement with literature values at this temperature [4].

At lower pressures of hydrogen and ethylene (1.75 Torr H_2, 0.25 Torr ethylene, and 758 Torr Ar) the spectrum observed showed that the surface had nearly a saturation coverage of ethylidyne from the onset of reaction with only a small concentration of di-σ bonded ethylene present (Fig. 7). As the reaction continued, the di-σ bonded ethylene peak slowly disappeared and after 200 minutes the only spectroscopic feature present was from ethylidyne. The turnover rate was 1.6 molecules per platinum site per second and remained unchanged over the course of the reaction (i.e. did not change with the observed decrease in concentration of di-σ bonded ethylene). It should also be noted that the π-bonded ethylene species could not be observed under these circumstances presumably because its concentration was too low. Due to the low reactant pressures used in this case, the reaction order is somewhat negative in ethylene, which is consistent with the surface not being saturated with the hydrocarbon intermediate species, π-bonded ethylene. Despite this, the surface remained saturated with the spectator species, ethylidyne.

Unlike the medium pressure case (100 Torr H_2), preadsorbing ethylidyne had very little affect on the nature and concentration of surface species seen in Figs. 6 and 7. Under the highest pressure conditions (>700 Torr H_2) preadsorbed ethylidyne was

quickly hydrogenated off the surface under reaction conditions in agreement with supported catalyst work under similar conditions. At low pressures of hydrogen, ethylidyne was present at saturation coverage regardless of whether it was preadsorbed or not.

(3) Hydrogenation of di-σ bonded ethylene at low H_2 pressure (~10^{-5} Torr) and low temperature (240 K)

Although it was determined under high pressure conditions that di-σ bonded ethylene was not responsible for the observed rate of ethylene hydrogenation, it remained unclear as to whether this species was merely hydrogenating at a very slow rate or completely static on the surface. To answer this question UHV experiments were conducted on the hydrogenation rate of a saturated coverage of di-σ bonded ethylene at 240 K, a temperature at which this molecule is stable on the Pt(111) surface.

Fig. 8a shows spectra for increasing coverages of di-σ bonded ethylene at 200 K on Pt(111) up to saturation coverage. As the exposure of ethylene is increased, the CH_2 symmetric stretch feature increased in intensity and shifts in frequency from 2924 cm^{-1} for low exposure to 2904 cm^{-1} as the saturation coverage of 0.25 ML is reached.

Fig. 8b shows spectra of an initial saturation coverage of di-σ bonded ethylene after exposure to increasing dosages of hydrogen at 235 K. As the exposure to hydrogen is increased, the CH_2 symmetric stretch at 2904 cm^{-1} begins to attenuate and shift to higher frequency. The feature could be almost completely removed at 235 K after exposure to 30,000 L of hydrogen. The attenuation of the signal with increasing exposure to hydrogen demonstrates the hydrogenation of di-σ bonded ethylene under UHV conditions. The blue shift in the peak is due to the coverage dependence of the frequency as shown in Fig. 8a. No other features appeared during UHV hydrogenation of ethylene. This result clearly demonstrates that although di-σ bonded ethylene is not hydrogenating

fast enough to be responsible for the turnover rate seen under atmospheric conditions, it indeed is hydrogenating on the surface under conditions where it is present.

5.4 Discussion

Vibrational spectroscopy using sum frequency generation permits the detection of submonolayer quantities of species under reaction conditions even in the presence of high reactant and product pressures in the gas phase. Specifically, the vibrational spectra taken during ethylene hydrogenation reveal the presence of ethylidyne, di-σ bonded ethylene, π-bonded ethylene and ethyl groups at various concentrations depending upon specific reaction conditions.

(1) ethylidyne and di-σ bonded ethylene

The lack of any direct role of ethylidyne ($M{\equiv}CCH_3$) in the mechanism for ethylene hydrogenation has already been well documented [14-16], however the SFG results suggest that stagnant ethylidyne blocks the sites for di-σ bonded ethylene adsorption on the catalytic Pt(111) surface. This result corresponds well with LEED surface crystallography which has shown that di-σ bonded ethylene and ethylidyne reside in the same surface site, the fcc three-fold hollow [9,12].

Three distinct spectroscopic features were seen on the Pt(111) surface during ethylene hydrogenation at 295 K with 100 Torr hydrogen and 35 Torr ethylene: di-σ bonded ethylene, π-bonded ethylene, and ethylidyne (Fig. 5a). When the reaction was carried out on an initially clean surface, the concentration of di-σ bonded ethylene that could be observed was about 8% of a monolayer. However, if the platinum surface was saturated with ethylidyne, very little di-σ bonded ethylene was observed under catalytic conditions (Fig. 5c) and the rate of hydrogenation, as measured by gas chromatography, was independent of the surface concentration of the di-σ bonded ethylene species. Under reaction conditions of 1.75 and 100 Torr H_2, the platinum three fold sites remained near

saturation coverage of ethylidyne + di-σ bonded ethylene. Hence the total concentration of these species was always near 0.25 ML. This means that both of these species were adsorbing far faster than they could be hydrogenated. At higher pressures of hydrogen (~700 Torr) the surface became mostly free of these asorbates. However, this does not mean that ethylidyne and di-σ bonded ethylene are hydrogenated at the same rate. UHV experiments (Fig. 8b) clearly showed that the di-σ bonded species can be hydrogenated under the relatively modest conditions of 235 K and 10^{-5} Torr of H_2. By contrast, even under room temperature conditions with 1 atm H_2, previous authors have demonstrated that ethylidyne hydrogenates very slowly [14].

The chemistry of di-σ bonded ethylene can be modeled as follows (Fig. 9): on a closed packed platinum surface, which is not saturated with ethylidyne, di-σ bonded ethylene may adsorb. Di-σ bonded ethylene is hydrogenated in the presence of hydrogen to ethane (fast pathway) or dehydrogenates to ethylidyne (slow pathway). Ethylidyne may also be hydrogenated, but does so much more slowly than di-σ bonded ethylene. Under steady state conditions at 295 K with 100 Torr H_2 and 35 Torr C_2H_4 a near saturation coverage of ethylidyne is favored. At higher pressures of hydrogen (over 700 Torr), di-σ bonded ethylene and ethylidyne are hydrogenated at a fast enough rate that the surface is not saturated with these species.

(2) π-bonded ethylene

Figs. 5a reveals the presence of π-bonded ethylene on the platinum surface when the hydrogenation of ethylene to ethane was detectable. The π-bonded feature was present under reaction conditions (figure 5a), but disappeared upon removal of the reactants (figure 5b). Unlike di-σ bonded ethylene the presence of this peak did not appear to be related to the ethylidyne coverage. It appears that this species was present at roughly the same intensity for the conditions displayed in both Figs. 5a and 5c, where the rates of

reaction are nearly identical. All experimental evidence indicates that π-bonded ethylene is the dominant reaction intermediate that hydrogenates to ethane.

The surface coverage of π-bonded ethylene under reaction conditions is about 4% percent of a monolayer. This means that the turnover rate per ethylene molecule is a factor of 25 higher if reported per surface intermediate than if it is reported per platinum atom. This is clearly significant, because it means that not all platinum atoms on the surface are active at any given time. However, the number of active sites is still far too high for this reaction to be primarily occurring at defect sites. Indeed, numerous studies have shown that ethylene hydrogenation is a structure insensitive reaction and, therefore, the specific location at which key reaction steps take place must be at sites that are available on all crystallographic planes of platinum. The π-bonded ethylene molecule, being of key mechanistic importance, must reside on such a site. We propose atop adsorption on the surface metal atoms (Fig. 10). This is consistent with organometallic cluster analogs of the π-bonded surface species [6,7].

Bowker et al. suggested that there is a correlation between the atop site for hydrogenation on heterogeneous catalysts and the chemistry of the homogenous phase Wilkinson's catalyst, $RhCl(PPh_3)_3$. [27]. In the case of the homogenous catalyst there is only one metal atom (in this case a rhodium atom) site available, which only allows for atop hydrogenation. Hence, the chemistry is quite similar in both the heterogeneous and homogenous case.

(3) ethyl groups

The ethyl species only becomes visible under the highest hydrogen pressure conditions in these experiments (Fig. 6). This demonstrates the high degree of reversibility in the incorporation of the first hydrogen into adsorbed ethylene. Indeed UHV studies by Zaera et al. have shown that ethyl groups can readily undergo β-hydride elimination to yield di-σbonded ethylene and adsorbed hydrogen [28]. This may explain the difficulty in

detecting ethyl species in transmission infrared experiments on supported platinum catalysts. In the only literature report of an ethyl group, Del La Cruz et al. present data for the introduction of 3×10^{-5} Torr of hydrogen onto ethylene covered Pt/SiO_2 which led to several very weak features in the infrared transmission spectrum [29]. The authors tentatively assigned these to an ethyl group. Their study creates conditions that are the low pressure equivalent of the present SFG work, where the increase in hydrogen pressure shifts the equilibrium for the addition of the first hydrogen into adsorbed π-bonded ethylene far enough toward the formation ethyl groups to permit their detection.

(4) mechanism for ethylene hydrogenation

It has been observed that ethylene hydrogenation occurs at the same rate regardless of whether ethylidyne is present or absent. Therefore, the ability of hydrogen and π-bonded ethylene to adsorb must be unaffected by the presence of this species. STM studies have demonstrated that ethylidyne is very mobile on Pt(111) at room temperature [13]. Further, extended Hückel calculations carried out for an ethylidyne molecule on a platinum surface showed a low barrier for diffusion (~0.2 eV) [30]. This suggests that, when present, ethylidyne may move far enough out of the way for ethylene to physisorb on a single platinum atom.

We propose a model in which hydrogen dissociately chemisorbs on a clean or ethylidyne covered platinum surface (Fig. 11). This step is followed by the physisorption of ethylene on single atom sites to form π-bonded ethylene. If ethylidyne is present, it may move out of the way in order to accommodate the adsorption of the π-bonded ethylene. Although the two species reside in different sites, this may be necessary because of steric hindrance. Physisorbed ethylene is then stepwise hydrogenated through an ethyl intermediate onto ethane. All steps up to the incorporation of the second hydrogen are highly reversible.

5.5 Conclusion

Both π-bonded ethylene and di-σ bonded ethylene are present on the Pt(111) surface under certain catalytic conditions where ethylene is being hydrogenated to ethane. However, the concentration of di-σ bonded ethylene can be decreased dramatically by the presence of a spectator species, ethylidyne, without any corresponding decrease in the reaction rate. Therefore, the surface concentration of di-σ bonded ethylene is uncorrelated with the rate of ethane formation and this species is not an important reaction intermediate in the hydrogenation of ethylene. A mechanism involving the hydrogenation of π-bonded ethylene is suggested instead. The relative hydrogenation rates of the species adsorbed on the surface during ethylene hydrogenation are:

π-bonded ethylene » di-σ bonded ethylene » ethylidyne

5.6 References

[1] I. Horiuti and M. Polanyi, Trans. Faraday Soc., **1934**, 30, 1164

[2] C. Kemball, Proc. Chem. Soc., **1956**, 735

[3] J. Schlatter and M. Boudart, J. Catal., **1972**, 24, 482

[4] R. Cortright, S. Goddard, J. Rekoske, and J. Dumesic, J. of Catal., **1991**, 127, 342

[5] A. Cassuto, J. Kiss, and J. White, Surf. Sci., **1991**, 255, 289

[6] J. Evans and G. McNulty, J. Chem. Soc. Dalton Trans., **1984**, 79;
M. Grogan and K. Nakamoto, JACS, **1966**, 88, 5454

[7] C. Anson, N. Sheppard, D. Powell, B. Bender, and J. Norton, J. Chem. Soc. Faraday Trans., **1994**, 90, 10, 1449

[8] H. Ibach and S. Lehwald, Surf. Sci., **1982**, 117, 685

[9] R. Döll, C. Gerken, N. Materer, M. Van Hove, and G. Somorjai, in preparation

[10] K. Griffiths, W. Lennard, I. Mitchell, P. Norton, G. Pirug, and H. Bonzel, Surf. Sci. Lett., **1993**, 284, L389

[11] P. Cremer, C. Stanners, J. Niemantsverdriet, Y. Shen, G. Somorjai, Surf. Sci., **1995**, 328, 111

[12] U. Starke, A. Barbieri, N. Materer, M. Van Hove, G. Somorjai, Surf. Sci., **1993**, 286, 1

[13] T. Land, T. Michely, R. Behm, J. Hemminger, G. Comsa, J. Chem. Phys., **1992**, 97, 9, 6774

[14] S. Davis, F. Zaera, B. Gordon, and G. Somorjai, J. of Catal., **1985**, 92, 250

[15] T. Beebe and J. Yates, JACS, **1986**, 108, 663

[16] J. Rekoske, R. Cortright, S. Goddard, S. Sharma, J. Dumesic, J. Phys. Chem., **1992**, 96, 1880

[17] S. Mohsin, M. Trenary, H. Robota, J. Phys. Chem., **1988**, 92, 5229

[18] X. Zhu, H. Suhr, and Y. Shen, Phys. Rev. B, **1987**, 35, 3047

[19] Y. Shen, The Principles of Nonlinear Optics (Wiley, New York, 1984)

[20] Y. Shen, Nature, **1989**, 337, 519

[21] F. Zaera, Surf. Sci., **1989**, 219, 453

[22] H. Hoffman, P. Griffiths, and F. Zaera, Surf. Sci., **1992**, 262, 141

[23] H. Steiniger, H. Ibach, and S. Lehwald, Surf. Sci., **1982**, 117, 685

[24] A. Cassuto, M. Mane, M. Hugenschmidt, P. Dolle, and J. Jupille, Surf. Sci., **1990**, 237, 63

[25] Y. Soma, J. Catal., **1979**, 59, 239

[26] C. Del La Cruz, N. Sheppard, J. Chem. Soc., Chem Commun., **1987**, 1854

[27] M. Bowker, J. Gland, R. Joyner, Y. Li, M. Slin'ko, and R. Whyman, Catal. Lett., **1994**, 24, 293

[28] F. Zaera, JACS, **1989**, 111, 8744

[29] C. De la Cruz and N. Sheppard, J. Mol. Struc., **1991**, 247, 25

[30] Z. Nomikou, M. Van Hove, and G. Somorjai, submitted to Langmuir

5.7 Figure Captions

Fig. 1: Horiuti-Polanyi mechanism for ethylene hydrogenation on platinum.

Fig. 2: The thermal evolution of adsorbed ethylene on Pt(111). The dehydrogenation proceeds from (a) π-bonded ethylene at low temperature through (b) di-σ bonded ethylene to (c) ethylidyne.

Fig. 3: The UHV/batch reactor apparatus for *in situ* catalysis.

Fig. 4: UHV spectra of saturation coverages of (a) di-σ bonded ethylene at 202 K on Pt(111) (b) ethylidyne at 300 K on Pt(111) (c) ethyl groups at 193 K on Pt(111) and (d) a mixture of di-σ and π-bonded ethylene at 120 K on O/Pt(111).

Fig. 5: (a) SFG spectrum of the Pt(111) surface during ethylene hydrogen with 100 Torr H_2, 35 Torr C_2H_4, and 615 Torr He at 295 K. (b) The vibrational spectrum of the same system after the evacuation of the reaction cell. (c) The SFG spectrum under the same conditions as (a), but on a surface which was precovered in UHV with 0.25 ML of ethylidyne.

Fig. 6: The hydrogenation of ethylene on Pt(111) with 727 Torr H_2 and 60 Torr C_2H_2 at 295 K. The two peaks marked with arrows are features characteristic of an ethyl species.

Fig. 7: The hydrogenation of ethylene on Pt(111) with 1.75 Torr H_2 0.25 Torr C_2H_4 and 758 Torr Ar at 295 K. The upper SFG spectrum was taken after 25 minutes and the lower spectrum after 200 minutes.

Fig 8: (a) SFG spectra of di-σ bonded ethylene on Pt(111) as a function of ethylene exposure. The 0.1 L exposure represents low coverage while the 4.1 L spectrum is of a saturation coverage. (b) SFG spectra of a saturation coverage of di-σ bonded ethylene on Pt(111) at 235 K as a function of hydrogen exposure. (note: 1 L=10^{-6} Torr x sec)

Fig 9: The schematic representation of the reaction channels for di-σ bonded ethylene on Pt(111) during ethylene hydrogenation at 295 K.

Fig 10: (a) The proposed bonding site for π-bonded ethylene on Pt(111) and the bonding site for two organometallic analogs (b) Zeise's salt, $K[Cl_3Pt(C_2H_4)]\cdot H_2O$, and (c) an osmium complex.

Fig 11: Proposed mechanism for ethylene hydrogenation on Pt(111).

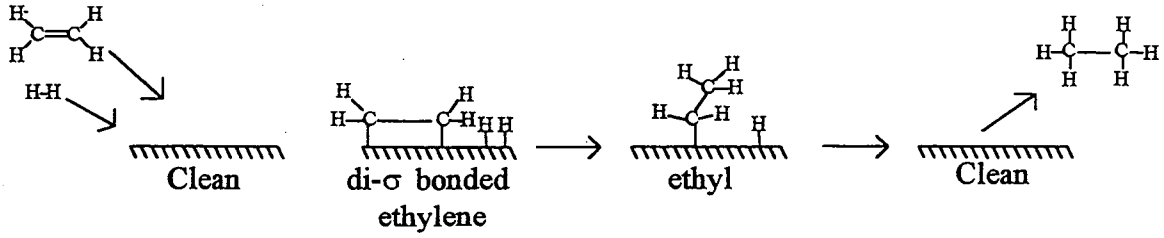

Fig. 1

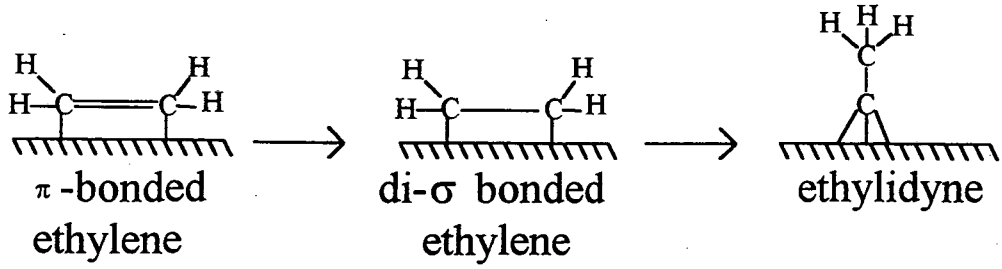

(a) (b) (c)

Fig. 2

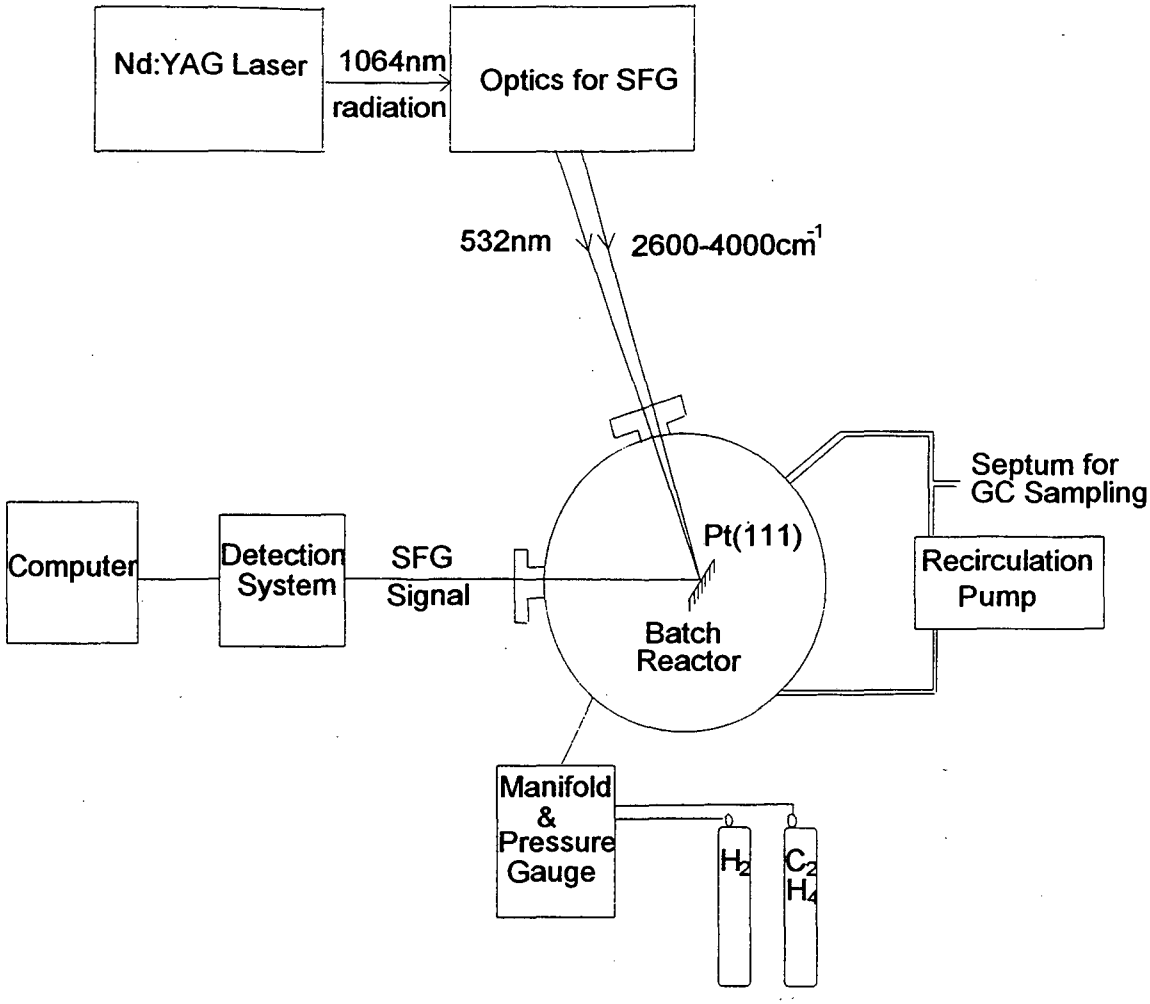
Nd:YAG Laser
1064nm
radiation
Optics for SFG
532nm
2600-4000cm-1
Septum for
GC Sampling
Computer
Detection
System
SFG
Signal
Pt(111)
Recirculation
Pump
Batch
Reactor
Manifold
&
Pressure
Gauge
H2
C2
H4

Fig. 3

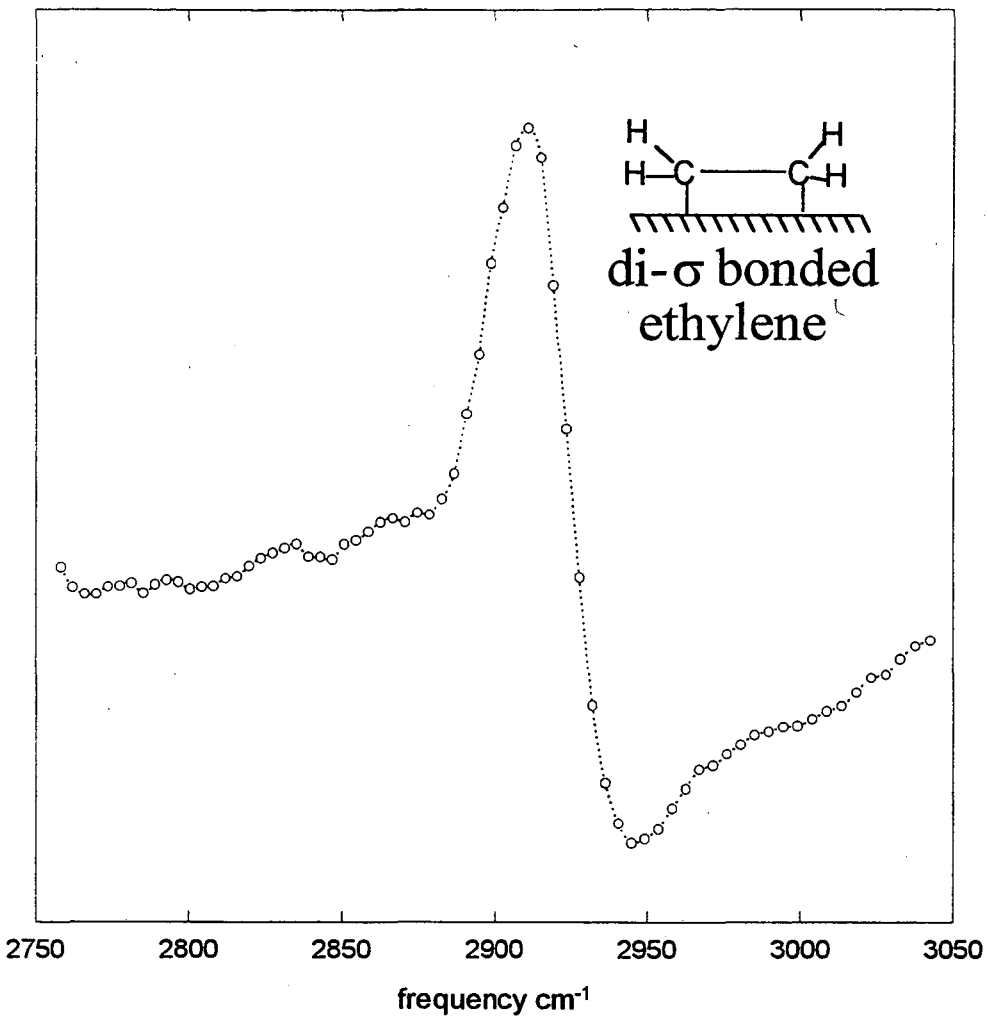
H
H
C
C
H
H
di-σ bonded
ethylene
2750
2800
2850
2900
2950
3000
3050
frequency cm-1

Fig. 4a

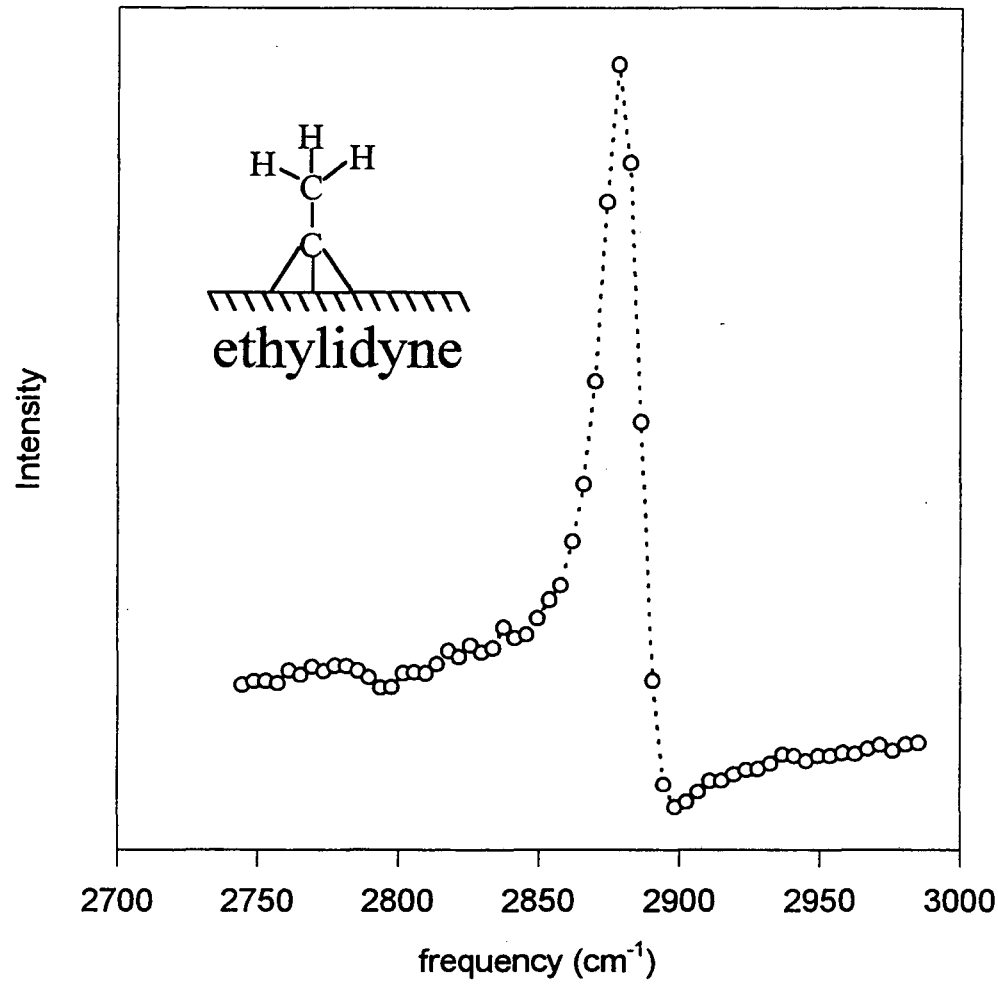
H
H
H
C
C
ethylidyne
Intensity
2700
2750
2800
2850
2900
2950
3000
frequency (cm-1)

Fig. 4b

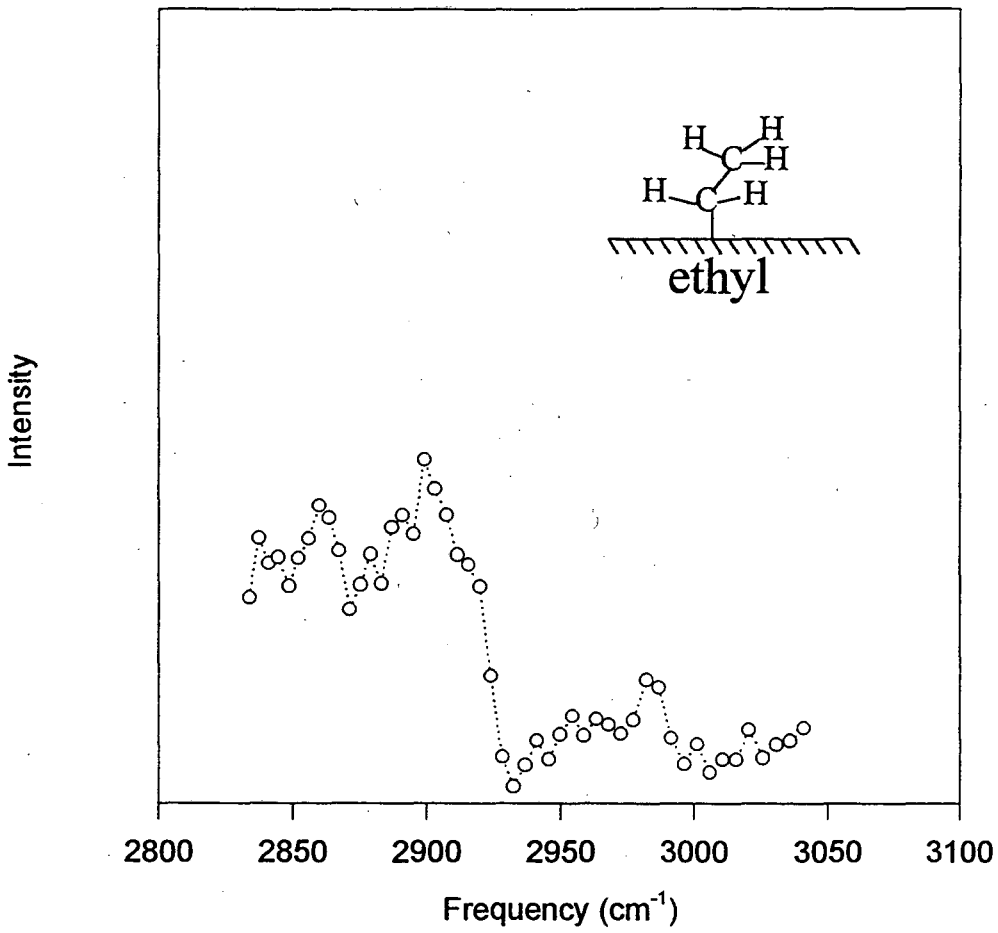
H
H
H
H
H
H
ethyl
Intensity
2800
2850
2900
2950
3000
3050
3100
Frequency (cm-1)

Fig. 4c

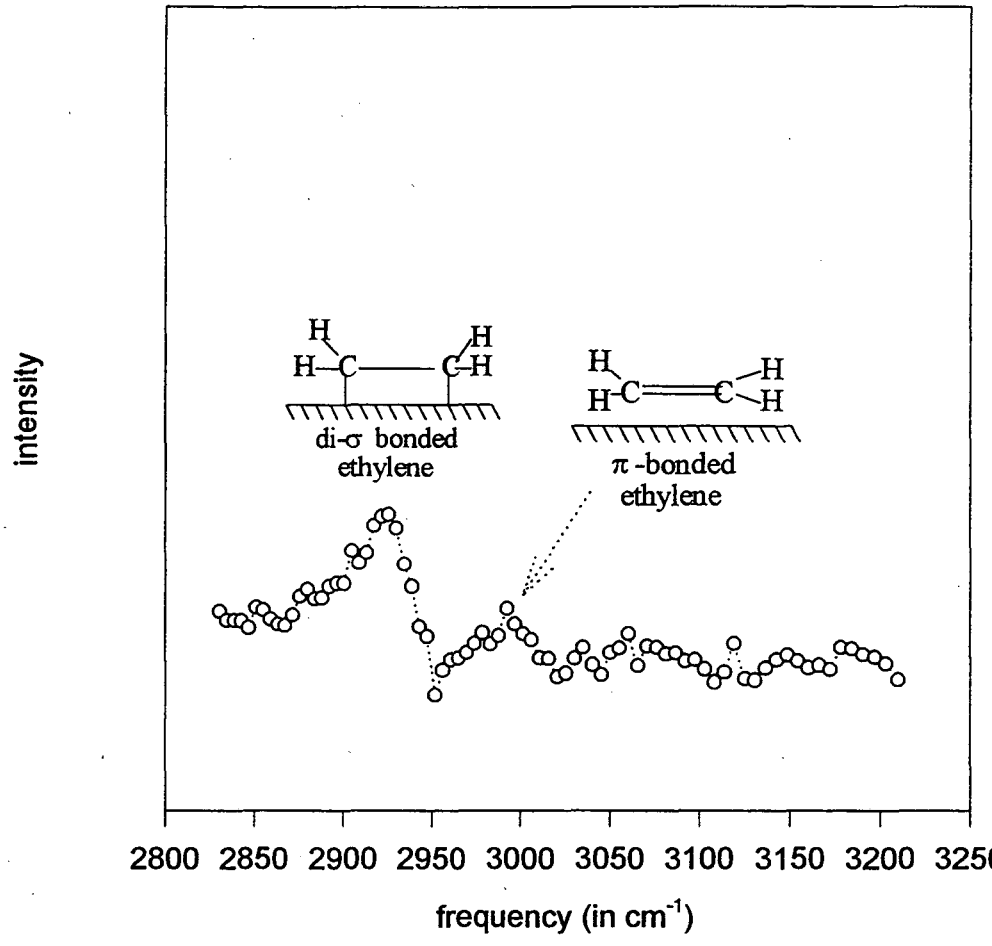
intensity
di-σ bonded
ethylene
π -bonded
ethylene
2800 2850 2900 2950 3000 3050 3100 3150 3200 3250
frequency (in cm-1)

Fig. 4d

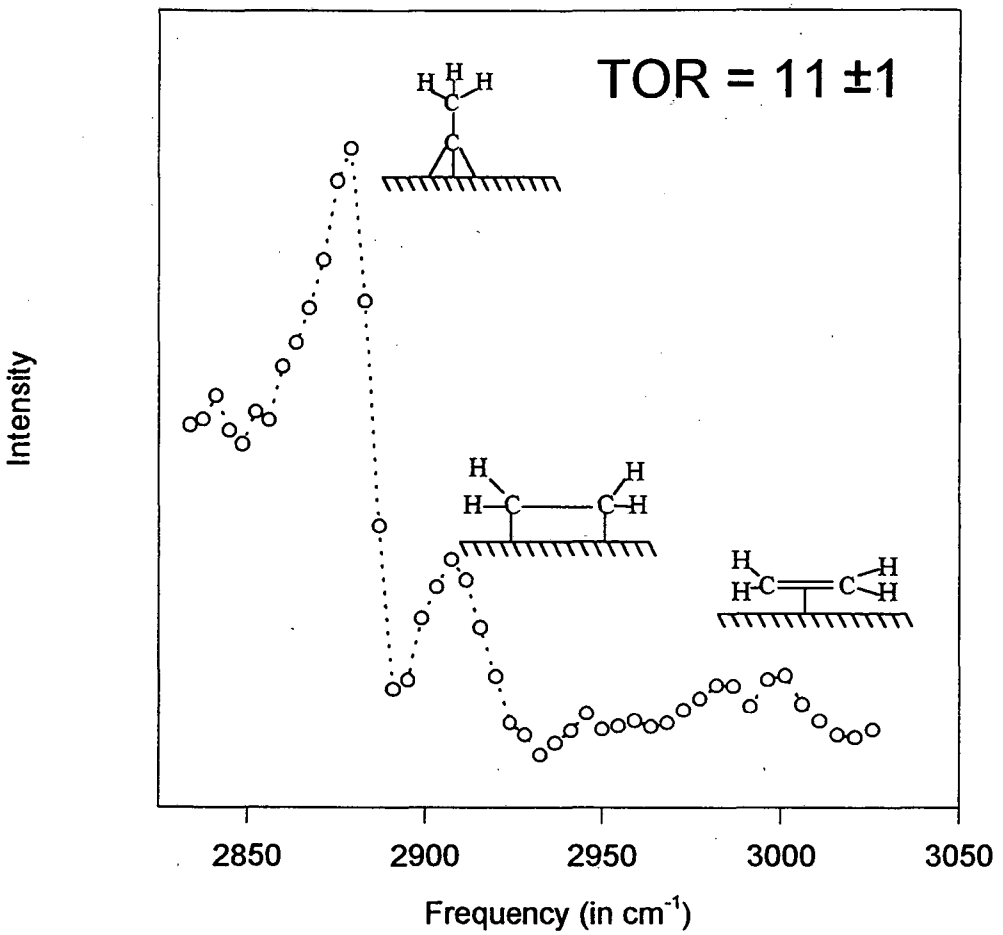

Fig. 5a

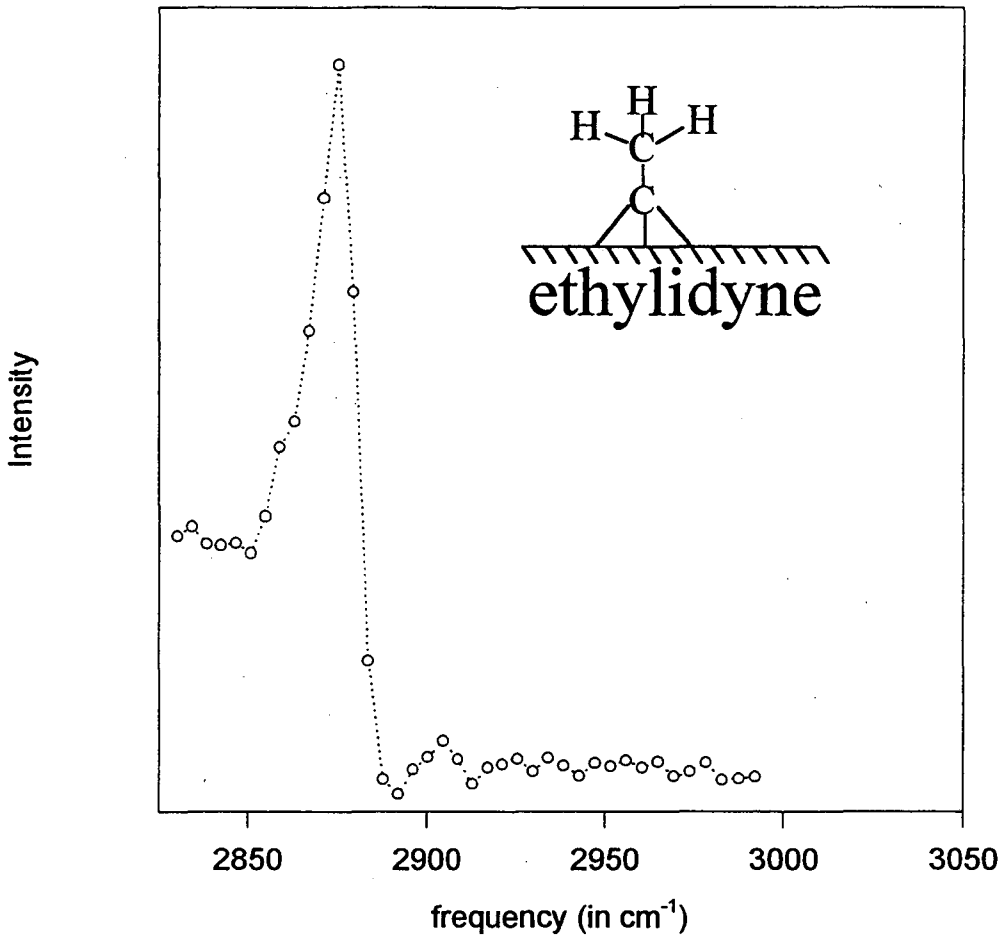
Intensity
H
H
H
C
C
ethylidyne
2850
2900
2950
3000
3050
frequency (in cm-1)

Fig. 5b

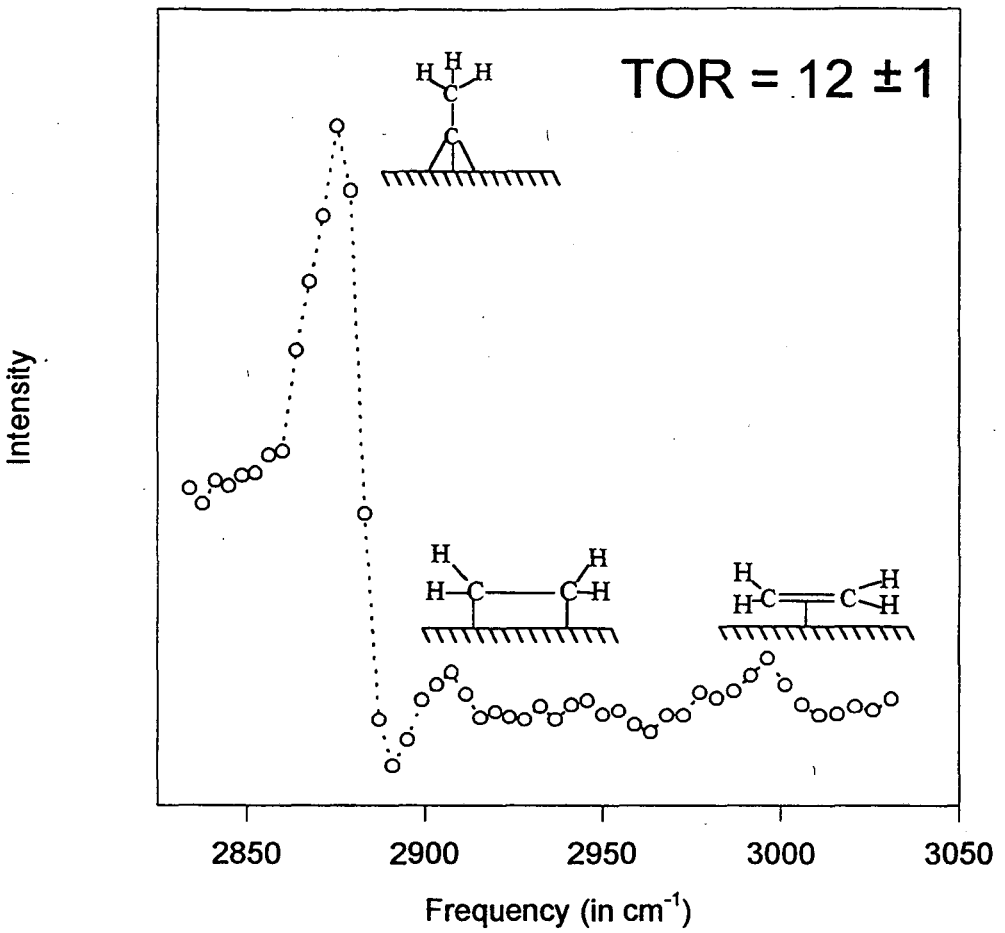

Fig. 5c

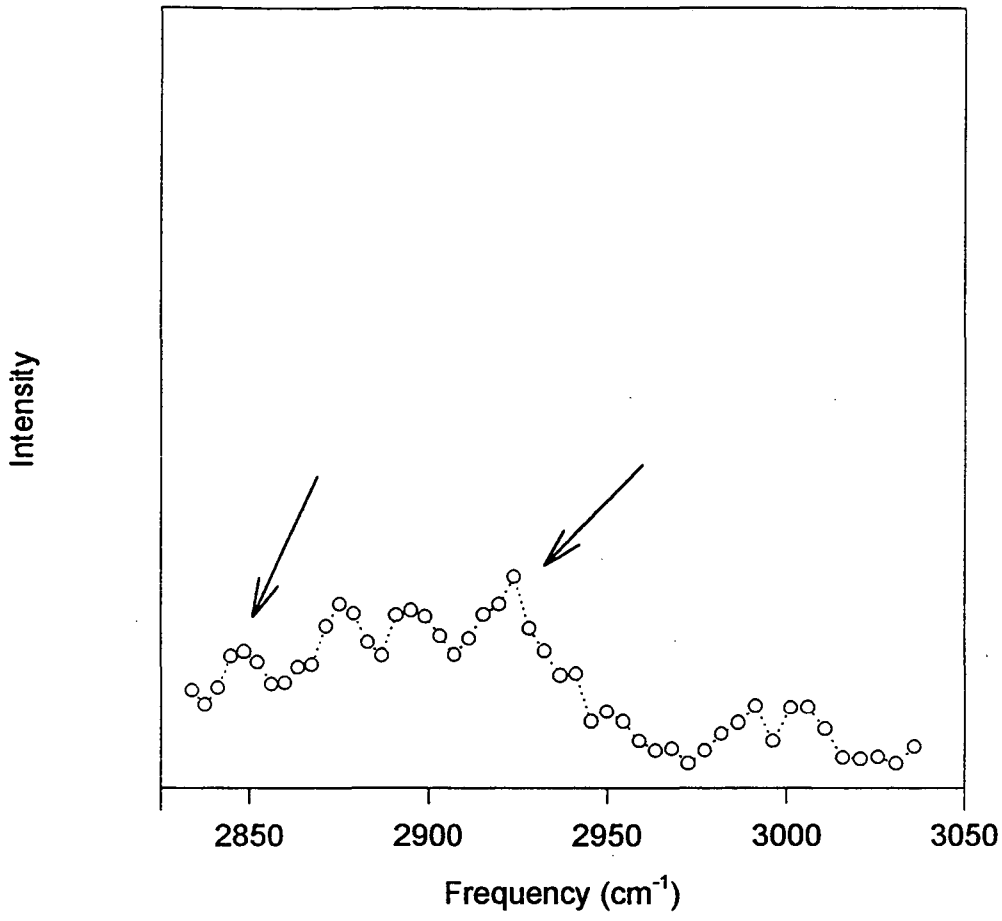

Fig. 6

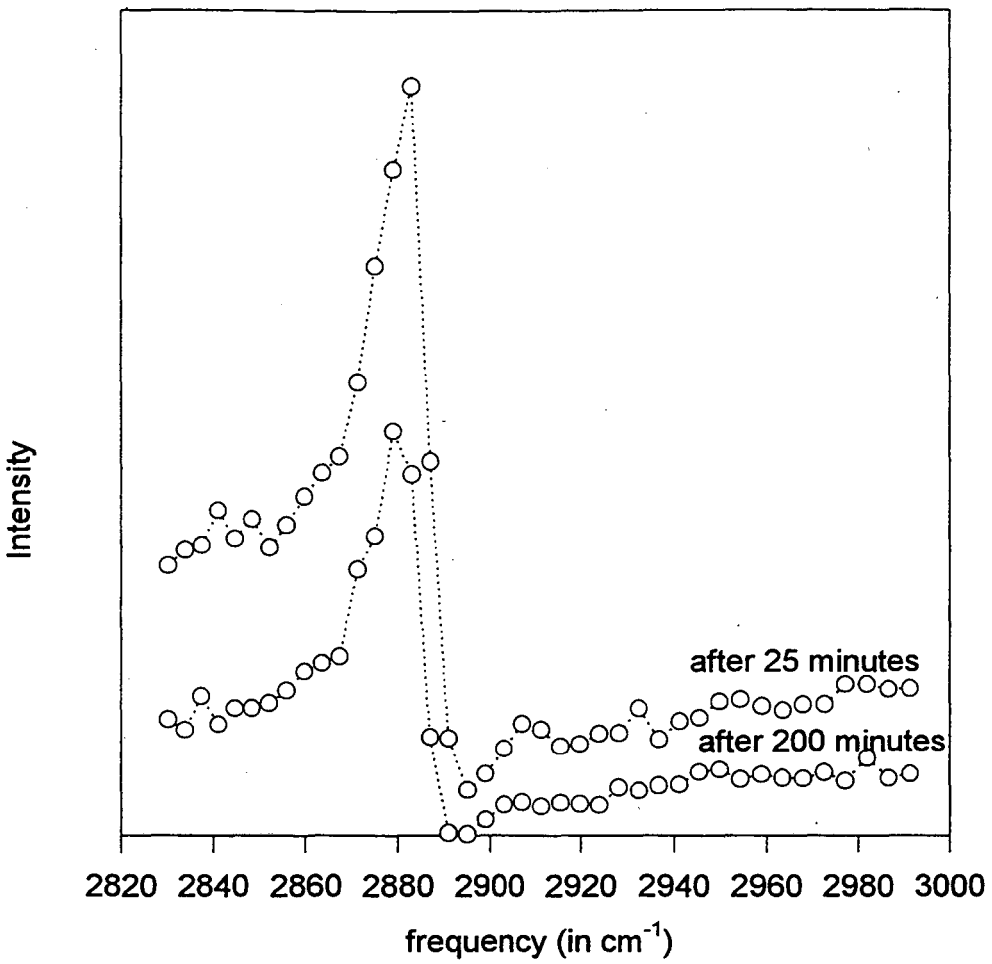
Intensity
after 25 minutes
after 200 minutes
2820 2840 2860 2880 2900 2920 2940 2960 2980 3000
frequency (in cm-1)

Fig. 7

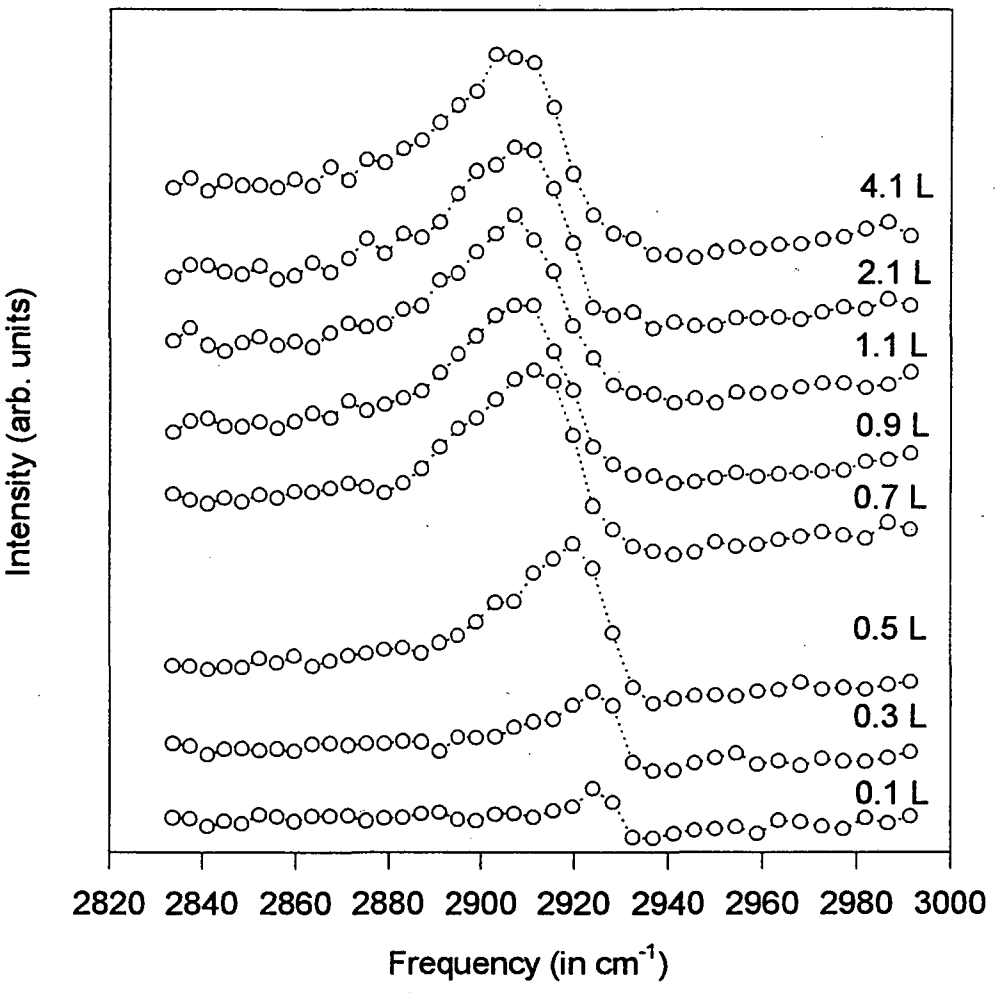
4.1 L
2.1 L
1.1 L
0.9 L
0.7 L
0.5 L
0.3 L
0.1 L
Intensity (arb. units)
2820 2840 2860 2880 2900 2920 2940 2960 2980 3000
Frequency (in cm-1)

Fig. 8a

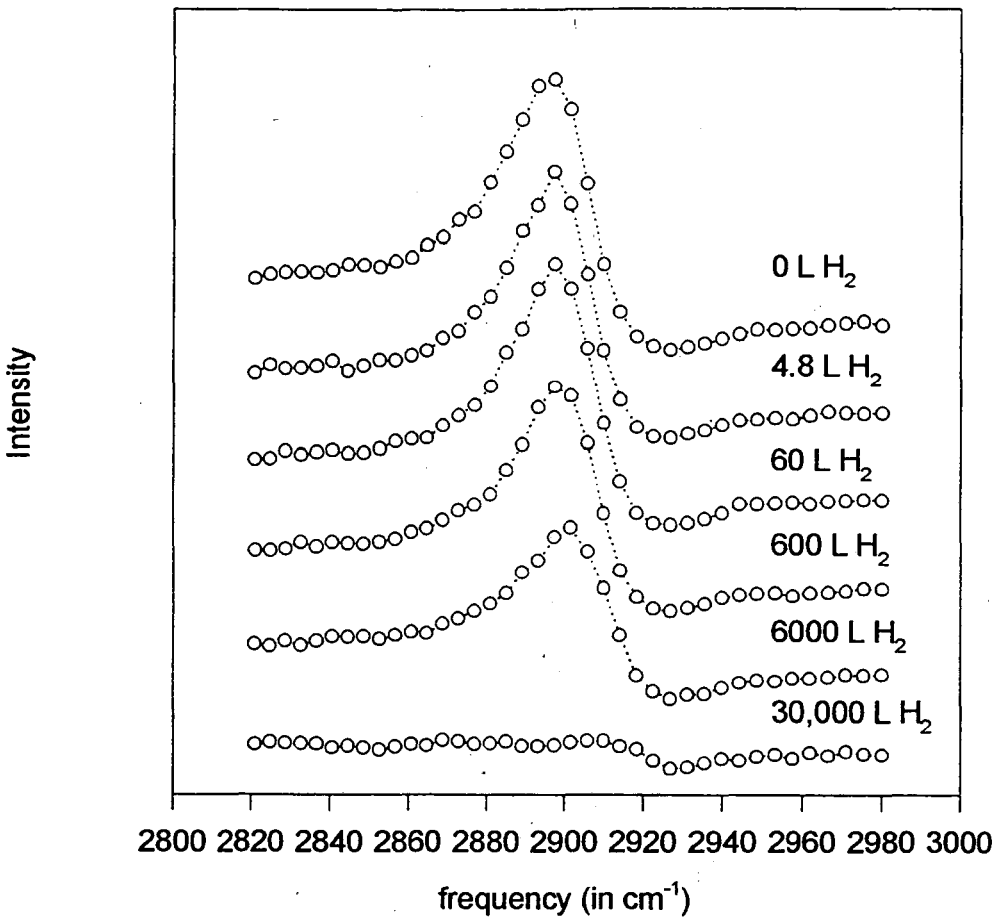
Intensity
0 L H2
4.8 L H2
60 L H2
600 L H2
6000 L H2
30,000 L H2
2800 2820 2840 2860 2880 2900 2920 2940 2960 2980 3000
frequency (in cm-1)

Fig. 8b

slow pathway

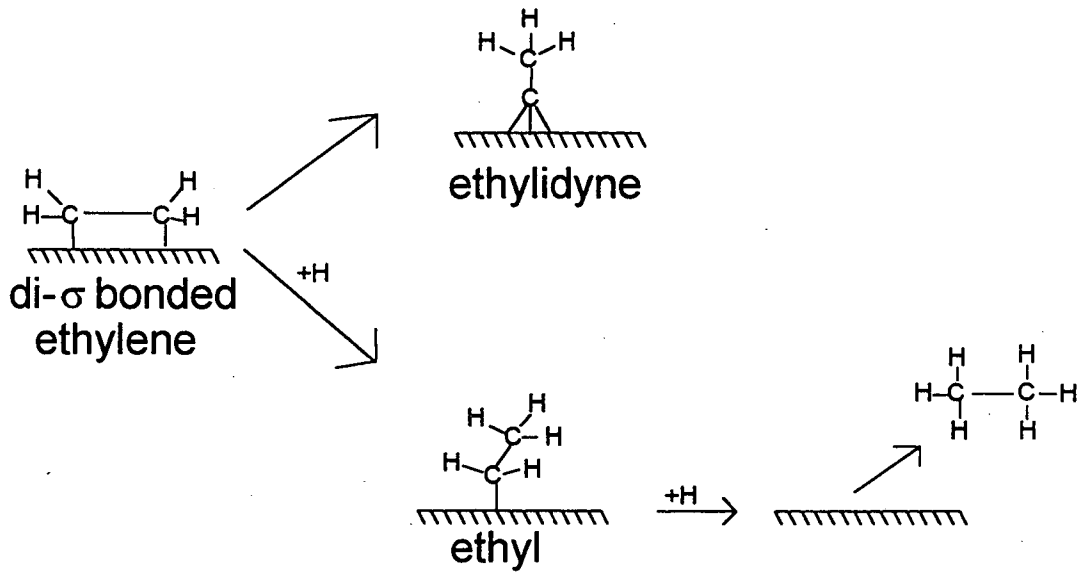

fast pathway

Fig. 9

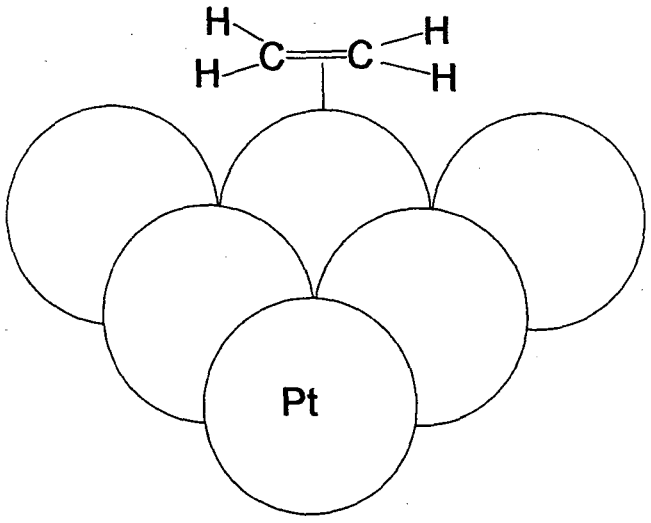

(a) π– ethylene/Pt(111)

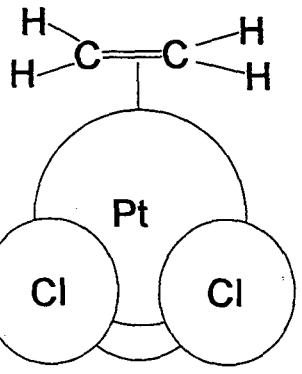

(b) Zeise's Salt

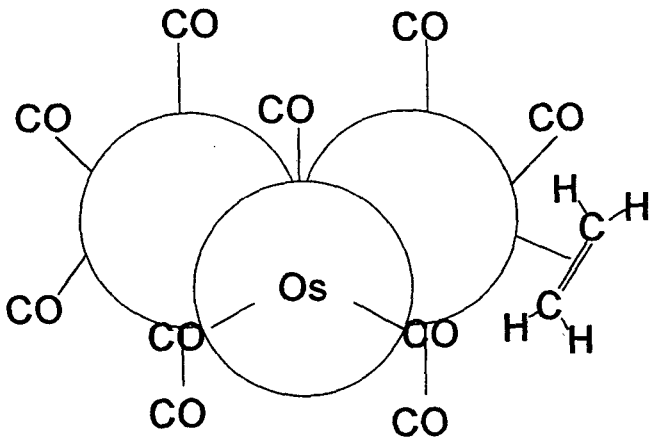

(c) $[Os_3(CO)_{11}(C_2H_4)]$

Fig. 10

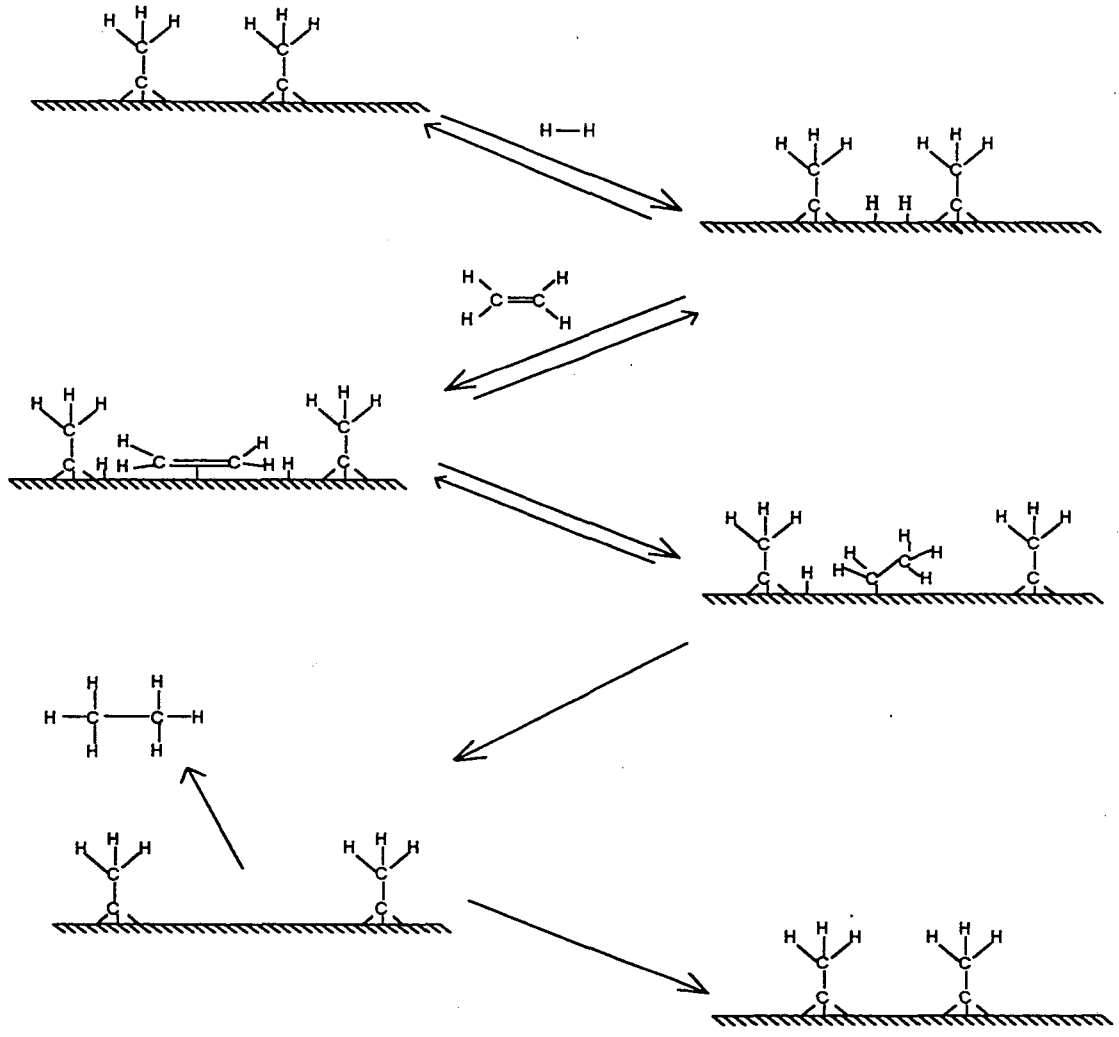

Key:

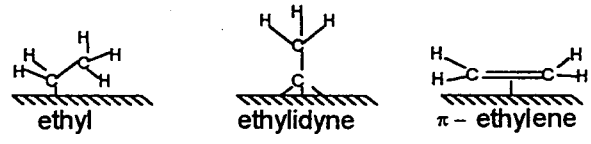

Fig. 11

Chapter 6

The Hydrogenation and Dehydrogenation of Propylene on Pt(111)

The reactions of adsorbed propylene on Pt(111) in the presence and absence of hydrogen have been studied over 13 orders of magnitude in pressure on Pt(111) using infrared-visible sum frequency generation (SFG). In the presence of near ambient pressures of hydrogen and propylene at 295 K, propylene hydrogenation was observed to proceed from a physisorbed intermediate (π-bonded propylene) through a 2-propyl species (Pt-$CH(CH_3)_2$) to propane. Under UHV conditions in the absence of hydrogen di-σ bonded propylene was found to dehydrogenate to propylidyne just below room temperature and then to vinyl methylidyne (M≡$CCHCH_2$) at 450 K on the way to graphite formation.

6.1 Introduction

Infrared-visible sum frequency generation (SFG), a surface specific vibrational spectroscopy, is an ideal technique for studies of surface reaction intermediates at low and high temperature as well as at low and high reactant pressures [1]. In fact, at high pressures of reactant gases, SFG is one of the few available techniques for monitoring submonolayer concentrations of surface species *in situ* during heterogeneous catalytic reactions on single crystal surfaces [2]. We have therefore exploited this method to monitor the surface species formed during propylene hydrogenation over a platinum single crystal surface near atmospheric pressure in order to gain a molecular understanding of the elementary mechanistic steps involved in olefin hydrogenation chemistry.

While there is an abundant literature on the hydrogenation of ethylene [2-11], relatively few surface science investigations have been undertaken on the hydrogenation of higher olefins. In the investigations undertaken, ultra high vacuum (UHV) experiments have shown that propylene adsorbs in a di-σ bonded conformation (Fig 1a) on clean Pt(111) below 220 K [12]. Upon heating, hydrogen is evolved around room temperature and the species geometry changes to that of propylidyne (Fig 1b) analogous to the room temperature formation of ethylidyne ($M{\equiv}CCH_3$) from ethylene [13]. Above room temperature the adsorbed propylidyne dehydrogenates to graphitic precursors and finally to graphite around 800 K.

Kinetic studies of propylene hydrogenation on platinum near ambient pressure reveal that the reaction is approximately 0.5 order in hydrogen and zero order in propylene at 300 K with an activation energy of about 10.4 Kcal/mol [14, 15]. *Ex situ* studies of the species adsorbed on a Pt/SiO_2 catalyst after propylene and hydrogen adsorption reveal the presence of propylidyne, di-σ bonded propylene, and π-bonded propylene (Fig 1c). The π-bonded species is only weakly adsorbed, bonding to the metal through the propylene's π molecular orbital [16].

By analogy with the case for ethylene, heterogeneously catalyzed propylene hydrogenation is assumed to be initiated by the dissociative adsorption of hydrogen on the metal surface along with the physisorption and/or chemisorption of propylene (Fig 2). However, the possible number of reaction pathways for propane formation from propylene is greater than for ethylene hydrogenation, because stepwise hydrogenation of propylene may proceed either through a 2-propyl intermediate or a 1-propyl intermediate depending on whether the first hydrogen is added to the terminal carbon or the internal carbon of the olefin (Fig. 2). Another conceivable pathway for hydrogenation would be for propylene to chemisorb onto the metal followed by a 1,2 hydrogen shift to propylidene before hydrogen addition at the α-carbon begins.

6.2 Experimental

The Pt(111) crystal used in this experiment was oriented, cut, polished, and cleaned using the normal procedures. All experiments were carried out in a batch reactor attached to an ultra high vacuum chamber with a base pressure below $1x10^{-10}$ Torr. The chamber was equipped with a retarding field analyzer for Auger electron spectroscopy (AES) and low energy electron diffraction (LEED), a mass spectrometer, and an Ar^+ gun for cleaning the surface by Ar^+ bombardment. In addition the chamber also was equipped with CaF_2 windows to allow infrared and green light to enter the chamber in order to perform the SFG experiment (Fig 3).

A passive active mode locked Nd:YAG laser at 1064 nm with a pulse width of 20 ps, a pulse energy of 50 mJ, and a repetition rate of 20 Hz was used to generate the high intensity radiation needed for SFG. The 1064 nm fundamental from the laser was split into two parts. The first portion was frequency doubled to 532 nm and the second was angle tuned from 2600-4000 cm^{-1} by employing a $LiNbO_3$ optical parametric generation/amplification (OPG/OPA) stage. The two beams were then focused

concentrically onto the Pt(111) sample. The sum frequency output was measured with a photomultiplier tube and stored on a micro computer.

When atmospheric pressure studies were performed, the batch reactor was isolated from UHV via a gate valve. The reactor could then be pressurized to over one atmosphere of total pressure. The pressure in the reaction cell was monitored by a Baratron gauge with a range from 100 mTorr to 1000 Torr. The batch reactor was equipped with a reaction loop that contained a recirculation pump and a septum for gas abstraction and GC analysis. The gas was analyzed by an HP 5890 series II gas chromatograph which could easily detect 1 ppm of propane in propylene. Using GC sampling to follow the gas phase composition allowed for kinetic measurements to be made simultaneously with SFG surface monitoring.

6.3 Results

(a) SFG Study of the Thermal Decomposition of Propylene under UHV Conditions on Pt(111)

Figure 4a shows the vibration spectrum under UHV of di-σ bonded propylene on Pt(111) at 187 K in the CH stretch range. The system was prepared by exposing the clean platinum surface to 4 L of propylene at this temperature. Two prominent peaks can be seen at 2825 cm^{-1} and 2880 cm^{-1}. The lowering of the baseline level after the resonances is an artifact of the sum frequency experiment and has been described in detail elsewhere [17]. The higher frequency peak is assigned to the $\nu_s(CH_3)$ of the terminal methyl group while the lower frequency feature is a Fermi resonance with a deformation mode. There is also some very weak intensity near the region of 2880 cm^{-1} from either $\nu_s(CH_2)$ or $\nu(CH)$ that can be revealed by performing the identical experiment with CD_3CHCH_2 (Fig 4b).

Exposing the clean platinum (111) crystal face to 4 L of propylene at 310 K leads to the formation of a saturation coverage of propylidyne ($M{\equiv}CCH_2H_3$) by dehydrogenation

(Fig 4c). Its SFG spectrum shows three prominent ν(CH) range peaks at 2855 cm^{-1}, 2920 cm^{-1}, and 2960 cm^{-1}. The most intense feature at 2960 cm^{-1} can be assigned to the $\nu_a(CH_3)$ of the terminal methyl group, while the 2920 cm^{-1} feature is the $\nu_s(CH_3)$. The small feature at 2855 cm^{-1} is due to a Fermi resonance. Deuterating the methyl group reveals weak intensity near 2880 cm^{-1} from CH_2 modes (Fig 4d). By analogy with ethylidyne, propylidyne most likely adsorbs in the fcc three fold hollow site on Pt(111), as determined by LEED analysis [13].

Figure 5a shows the thermal evolution of propylene on Pt(111) from di-σ propylene to propylidyne. The spectra were obtained by exposing the clean platinum crystal to a saturation exposure of propylene (4 L) at 187 K. The crystal was then annealed to successively higher temperatures for 30 seconds periods. At the end of each annealing cycle the crystal was then allowed to cool below 187 K and an SFG scan was taken. The spectra reveal that the di-σ species begins to dehydrogenate around 231 K and completely transforms to propylidyne by room temperature.

Figure 5b shows the further dehydrogenation of propylidyne at higher temperatures. As the propylidyne covered surface is heated above 390 K, the propylidyne moieties begin to dehydrogenate and several new features grow in around 2900 cm^{-1} and 3000 cm^{-1}. The feature near 3000 cm^{-1} is probably an olefinic species formed from the dehydrogenation of propylidyne. The most likely way such an olefinic species could be formed is from the loss of a hydrogen at the terminal methyl group as well as from its neighboring methylene. This would lead to the formation of vinyl methylidyne ($M{\equiv}CCHCH_2$) as shown schematically in Fig 5c. When the surface is heated further, the spectral features become weaker as graphitic precursors are formed.

(b) The Vibrational Spectra of 1-Propyl and 2-Propyl Surface Moieties and Their Hydrogenation in UHV

Both 1-propyl ($Pt\text{-}CH_2CH_2CH_3$) and 2-propyl ($Pt\text{-}CH(CH_3)_2$) moieties can be formed on Pt(111) by adsorbing their respective iodides and heating the surface to break the carbon-iodine bond. Figure 6a shows the vibrational spectrum for 1-propyl/Pt(111). The system was prepared by a saturation dose of 1-propyl iodide (10 L) at 140 K, which was annealed for 10 seconds to 190 K. The annealing process should break some of the C-I bonds leaving intact 1-propyl moieties on the surface by analogy with the thermal chemistry of ethyl iodide on Pt(111) [18]. Three major peaks are seen in the spectrum at 2875 cm^{-1}, 2934 cm^{-1}, and 2974 cm^{-1}. These may correspond to a fermi resonance, the $\nu_s(CH_3)$, and the $\nu_a(CH_3)$ respectively, however, all assignments are very tentative.

The vibrational spectrum of 1-propyl/Pt(111) can be altered dramatically by performing the identical experiment at lower coverage. Figure 6b shows the vibrational spectrum under identical conditions, but with an exposure of propyl iodide below saturation coverage (4 L). The changes in the vibrational spectrum probably result from a change in orientation of the 1-propyl moieties on the surface. This is again analogous to the behavior of ethyl groups which have been shown to lie down at low coverage, but stand up near saturation coverage [19]. The spectrum is now dominated by the 2875 cm^{-1} peak while the intensity of the 2974 cm^{-1} feature has decreased dramatically. The intensity of the 2934 cm^{-1} feature is nearly unaltered, but a new feature at 2810 cm^{-1} is now clearly present.

Hydrogenation of 1-propyl moieties was also carried out from an initially saturated overlayer of 1-propyl iodide by exposing the crystal to 1.4×10^{-5} Torr of hydrogen while annealing the sample to 190 K for 100 sec (Fig 6c). The crystal was allowed to cool below 140 K and an SFG spectrum was taken. The spectrum before hydrogenation is superimposed for comparison. The spectral features exhibit a slight changed relative to the unexposed system with a 20% reduction in the intensity, presumably from

hydrogenation of 1-propyl to propane. Control experiments revealed no desorption of 1-propyl groups or changes in the vibrational spectrum under similar conditions in the absence of hydrogen.

The thermal evolution of 1-propyl iodide is shown in figure 6d. The species can be seen to dehydrogenate from the alkyl though di-σ bonded propylene to propylidyne (Fig. 6e).

All experiments performed with 1-propyl iodide were repeated with 2-propyl iodide. The spectrum for a saturation exposure of 2-propyl on clean Pt(111) annealed to 190 K is shown in figure 7a. It should also be noted that the overall SFG intensity at saturation coverage is somewhat smaller for 2-propyl than that for 1-propyl. The three dominant features in this case are at 2838 cm^{-1}, 2863 cm^{-1}, and 2913 cm^{-1}. Additionally there may be some weak intensity near 2950 cm^{-1}. The 2863 cm^{-1} could be assigned to the $\nu_s(CH_3)$ and the 2913 cm^{-1} is possibly due to the $\nu(CH)$. Low coverage conditions give rise to similar spectral features, but in different ratios (Fig 7b). Surprisingly, the strongest feature is at 2838 cm^{-1} with virtually no intensity near 2863 cm^{-1}. It is unclear in this case whether the 2863 cm^{-1} or the 2838 cm^{-1} is the $\nu_s(CH_3)$. The feature at 2913 cm^{-1} is still present at roughly the same ratio with respect to the overall lower frequency signal.

The hydrogenation of 2-propyl/Pt(111) is shown in figure 7c. In this case the overall intensity of the signal is attenuated by approximately 40% upon exposure to 1400 L of H_2 at 190 K and there is little change in the relative ratios of the spectral features.

The thermal evolution of 2-propyl is shown in figure 7d. The spectra reveal that 2-propyl dehydrogenates through di-σ bonded propylene and finally to propylidyne (Fig. 7e).

(c) *In Situ* SFG Studies of Propylene Hydrogenation Near Atmospheric Pressure

Catalytic hydrogenation experiments were conducted near atmospheric pressure of propylene and hydrogen at 295 K. Many of the species seen on the surface at high pressure could be directly identified by their fingerprint obtained in UHV. Simultaneously with the SFG surface measurements, the gas phase was monitored by gas chromatography to obtain information on reaction rates.

Propylene hydrogenation was carried out over almost two decades of hydrogen pressure. Under the highest pressure conditions, 723 Torr H_2 and 40 Torr of propylene, a total of seven distinct peaks are observed (Fig 8a). The largest peak at 2830 cm^{-1} corresponds well to a 2-propyl group while the high frequency peak at 3050 cm^{-1} is most likely from π-bonded propylene [16]. The small peak at 2960 cm^{-1} can be assigned to the decomposition species, propylidyne. The features between 2860 cm^{-1} and 2940 cm^{-1} are more difficult to identify, but may be from 1-propyl, 2-propyl, and/or di-σ bonded propylene. Gas chromatography revealed the turnover rate (TOR) of propylene hydrogenation under these conditions was 29 propane molecules formed per exposed platinum atom per second.

The concentration of various surface species may be compared on a relative basis. The signal intensity of the π-bonded features is expected to be smaller than that of the di-σ bonded species for equal concentrations, because of both the surface metal dipole selection rule and the SFG selection rules [2]. Despite this, it is clearly seen that the intensity of π-bonded propylene is larger than that of di-σ bonded propylene; therefore, the concentration of the former is almost certainly larger.

The dominance of spectral features from 2-propyl species over 1-propyl species leads to the conclusion that there is a larger amount of 2-propyl on the surface. This can be concluded because spectral features for 2-propyl are at least three times stronger than those for 1-propyl. This is despite the fact that 1-propyl has a slightly larger SFG cross sections (for equal surface concentrations) under UHV (Figs. 6a, 6b, 7a and 7b). It

should be noted that peaks from the 2-propyl species more closely resemble the low coverage vacuum fingerprint than the saturation vacuum fingerprint (Figs. 7a and 7b).

(d) Hydrogenation at Lower Pressures

When the reaction was carried out at lower hydrogen pressure, 100 Torr H_2, 40 Torr propylene, and 617 Torr He at 295 K, both the reaction rate and surface vibrational spectrum changed dramatically compared with the pervious case (Fig 8b). The turnover rate (TOR), as determined by gas chromatography, dropped to 8.6 molecules/(site·sec) and there was a dramatic increase in the 2960 cm^{-1} and 2920 cm^{-1} peaks corresponding to propylidyne. The 3050 cm^{-1} peak from π-bonded propylene is a bit weaker as is the intensity around 2830 cm^{-1} from 2-propyl. However, more intensity can now be seen from the 2863 cm^{-1} feature suggesting a possible net reorientation of 2-propyl species. The peak intensity just below 2900 cm^{-1} increased and can reasonably be assigned to di-σ bonded propylene. The increase in propylidyne and di-σ bonded propylene features along with a corresponding decrease in turnover rate helps to rule these species out as important intermediates in propylene hydrogenation.

As the pressure of the reactants is further decreased to 13.5 Torr H_2, 5 Torr propylene, and 746 Torr He (Fig 8c), the TOR slows to 3.3 molecules/(site·sec). This is nearly an order of magnitude decrease in reaction rate in comparison to the highest pressure conditions and the surface is almost completely covered with the decomposition product, propylidyne, as seen from the three major peaks in the spectrum at 2850 cm^{-1}, 2915 cm^{-1}, and 2960 cm^{-1}. The broad intensity near 2850 cm^{-1} is probably from a small concentration of 2-propyl contributions at 2830 cm^{-1} and 2863 cm^{-1}. The 2913 cm^{-1} feature from 2-propyl is probably helping to strengthen the 2920 cm^{-1} feature from propylidyne.

(e) The Effect of Preadsorbed Propylidyne

To probe the effect of a preadsorbed layer of propylidyne on the reaction, a saturation coverage of this species was formed under UHV conditions by exposing the clean Pt(111) crystal to 4 L of propylene. The propylidyne/Pt(111) system was then exposed to 103 Torr H_2, 40 Torr propylene, and 760 Torr He at 295 K (Fig 8d). The TOF was 8.4 mol/(site·sec); hence, nearly identical to that of Fig 8b. Furthermore, the SFG spectrum looks almost the same as figure 8b. This demonstrates that the amount of propylidyne adsorbed on the surface comes quickly to equilibrium during the hydrogenation process regardless of how much propylidyne is initially adsorbed on the surface.

6.4 Discussion

(a) The Behavior of Propylidyne and Di-σ Bonded Propylene

The vacuum chemistry of propylene on Pt(111) bears a close relationship to that of ethylene [17]. Like ethylene, propylene chemisorbs on platinum below 200 K by breaking the carbon-carbon double bond to form di-σ bonded propylene. It forms the corresponding alkylidyne upon annealing to room temperature. However, the onset of di-σ bonded propylene decomposition appears to occur at a slightly lower temperature than that for di-σ bonded ethylene. The di-σ bonded propylene shows significant decomposition upon annealing to 231 K (Fig 5a), whereas the first sign of di-σ bonded ethylene decomposition has been previously shown to appear above 240 K [17]. Another significant departure is at higher temperature where propylidyne begins to further dehydrogenate near 400 K. This is in contrast to ethylidyne, which is still stable well beyond this temperature. The apparent source of the decomposition is the terminal methyl group and its adjacent methylene which undergo dehydrogenation to form vinyl methylidyne ($M{\equiv}CCHCH_2$) (Fig 5c).

The stability of propylidyne also appears to differ from that of ethylidyne in the presence of hydrogen. Under medium pressure conditions, 100 Torr H_2 and 40 Torr propylene, a UHV formed overlayer of propylidyne could be easily hydrogenated, leading to the same spectroscopic result as when the experiment was performed on an initially clean Pt(111) surface. This is in contrast to ethylidyne, which remains undisturbed on the surface even during extended periods of ethylene hydrogenation under nearly identical conditions [2, 20]. The reason for the relative ease of hydrogenation of propylidyne versus ethylidyne may stem from the fact that the β-carbon in propylidyne is a secondary carbon whereas the β-carbon is primary in ethylidyne. The secondary carbon could facilitate the incorporation of hydrogen to form propylidene under reaction conditions. A greater rate of alkylidene formation from propylidyne versus ethylidyne may in turn lead to a faster overall rate of propylidyne hydrogenation with respect to that of ethylidyne.

(b) 1-Propyl and 2-Propyl Surface Chemistry on Pt(111)

The chemistry of propyl iodide is quite similar to that of ethyl iodide. In the case of ethyl iodide, it is known that the C-I bond begins to break on Pt(111) above 170 K, leaving ethyl groups on the surface [18]. As in the case of ethyl groups, propyl group orientation is very sensitive to coverage compared to that of other adsorbate species. This is presumably because of the ability of these species to reorient themselves on the surface from a lying down configuration at low coverage to one in which they are forced to stand up at higher coverage.

(c) Mechanism for Propylene Hydrogenation

The hydrogenation of propylene on Pt(111) shows clear evidence for proceeding from physisorbed propylene to propane through a 2-propyl intermediate (top of Fig 2). The hydrogenation rate of π-bonded olefins has already been shown to be several orders of magnitude more rapid than that of di-σ bonded olefins in the case of ethylene [2]. Therefore, extending this analogy to adsorbed propylene, the key hydrogenation pathway

would be expected to proceed through π-bonded ethylene, because not only should the rate of hydrogenation per π-bonded propylene be faster than per di-σ bonded propylene, but also the concentration of π-bonded propylene is substantially larger.

π-bonded propylene species may incorporate a hydrogen at either the terminal or internal carbon of the alkene. Our results show that there is a much larger concentration of 2-propyl groups on the surface than 1-propyl groups during reaction (Fig. 8a). This is in agreement with previous studies on surfaces as well as gas phase work. Klein et al. demonstrated in the early 1960's that solid alkene hydrogenation to alkyl radicals by gas phase hydrogen atoms takes place preferentially at the terminal carbon [21, 22]. The gas phase results showed ratios of at least 12:1 in favor of initial hydrogen addition at the terminal carbon. Recent work on Cu(100) at 100 K under UHV by Yang et al. has shown that 1-butene incorporates a hydrogen atom at the terminal carbon 3 times more preferentially than at the internal one [23]. Both of these results are in good agreement with the present observation of high concentrations of 2-propyl groups versus 1-propyl groups during propylene hydrogenation on Pt(111). The dominance of terminal addition in the solid alkene work, however, seems to be even stronger than that observed on the surface.

If 2-propyl groups can incorporate hydrogen at roughly the same rate or faster than 1-propyl groups then the dominant pathway to propane formation on Pt(111) would be through 2-propyl. Alternatively, if the 1-propyl groups are hydrogenated much faster than the 2-propyl groups, it would be conceivable that this route to propane formation is competitive despite the low surface concentration of this species during reaction.

Hydrogenation of 2-propyl moieties was observed to be slightly faster than that of 1-propyl under vacuum in the presence of iodide at 190 K (Figs. 6c and 7c). This is expected to be the case because the bond between an internal carbon and the underlying metal should be slightly weaker than for the carbon metal bond from a terminal carbon. If it is assumed that the breaking of this bond represents the activation barrier for alkyl

hydrogenation, then 2-propyl groups should hydrogenate faster than 1-propyl groups over a wide range of pressures and temperatures.

(d) Kinetics and the rate limiting step

As the pressure of hydrogen is lowered in the propylene hydrogenation reaction, fewer 2-propyl groups and π-bonded propylene species are observed on the surface, and at the same time, a build up of the decomposition species, propylidyne, is seen. This seems to correlate well with the decrease in turnover rate from 29 to 8.6 molecules/(site·sec) as the pressure of hydrogen is decreased from 723 Torr to 100 Torr. From these results the kinetic order of this reaction is 0.63 in hydrogen, which is in good agreement with the expectation of half to first order hydrogen pressure dependence from theoretical considerations [24] as well as experimental observation [14].

The expectation of half to first order reaction kinetics in hydrogen stems from the assumption that the rate limiting step of this reaction is the incorporation of the second hydrogen into the molecule (fig 9). The large build up of 2-propyl groups on the surface under the highest hydrogen pressure conditions is strong evidence for this species being rate limiting. Interestingly, this is in contrast to ethylene hydrogenation, where only a very small concentration of ethyl groups has been observed over a wide range of pressures and temperatures [2]. One possible reason for the relatively high concentration of 2-propyl groups in propylene hydrogenation versus the relatively small build up of ethyl groups during ethylene hydrogenation again may stem from the fact that the carbon attached to the surface in the propyl case is a secondary carbon while the carbon attached to the surface in the case of ethyl is only primary.

In ethylene hydrogenation, the relatively small surface concentration of ethyl groups probably means the hydrogenation of this species is rate limiting in fewer cases than 2-propyl is in propylene hydrogenation. Under conditions of 100 Torr H_2 and 35 Torr ethylene, only chemisorbed and physisorbed ethylene are observed, while the

concentration of ethyl groups remained too small to detect [2]. This difference in intermediate concentrations in ethylene and propylene hydrogenation could lead to different reaction orders in hydrogen depending upon specific conditions.

6.5 Conclusion

SFG has been used to monitor reaction intermediates in propylene hydrogenation under high pressures of reactants while turnover rates were also monitored. The wide variety of possible hydrogenation pathways can be narrowed down to one dominant mechanism for propane formation. This mechanism involves stepwise hydrogen addition to π-bonded propylene through a 2-propyl intermediate to propane. Under UHV conditions propylene was observed to decompose to propylidyne and then to vinyl methylidyne in the absence of hydrogen

6.6 References

[1] Y. Shen, Nature, 337 (1989) 519

[2] P. Cremer, X. Su, Y. Shen, G. Somorjai, J. Am. Chem. Soc. in press

[3] T. Beebe and J. Yates, J. Am. Chem. Soc., 108 (1986) 663

[4] S. Moshin, M. Trenary, H. Robota, J. Phys. Chem., 92 (1988) 5229

[5] J. Schlatter and M. Boudart, J. Catal., 24 (1972) 482

[6] C. Kemball, Proc. Chem. Soc., (1956) 735

[7] Y. Soma, J. Catal., 59 (1979) 239

[8] C. Del La Cruz, N. Sheppard, J. Chem. Soc., Chem. Commun., (1987) 1854

[9] I. Horiuti and M. Polanyi, Trans. Faraday Soc., 30 (1934) 1164

[10] R. Cortright, S. Goddard, J. Rekoske, and J. Dumesic, J. of Catal., 127 (1991) 342

[11] P. Cremer, G. Somorjai, J. Chem. Soc. Faraday Trans. 91, 20 (1995) 3671

[12] N. Avery and N. Sheppard, Proc. R. Soc. London A 405 (1986) 1

[13] R. Koestner, J. Frost, P. Stair, M. Van Hove, and G. Somorjai, Surf. Sci. 116 (1982) 85

[14] L. Lok, N. Gaidai, S. Kiperman, Kinetika i Kataliz, 32, 6 (1991) 1406

[15] P. Otero-Schipper, W. Wachter, J. Butt, R. Burwell, and J. Cohen, J. of Catal., 50 (1977) 494

[16] G. Shahid and N. Sheppard, Spectrochimica Acta, 46A, 6 (1990) 999

[17] P. Cremer, C. Stanners, J. Niemantsverdriet, Y. Shen, and G. Somorjai, Surf. Sci., 328 (1995) 111

[18] F. Zaera, Surf. Sci., 219 (1989) 453

[19] H. Hoffman, P. Griffiths, and F. Zaera, Surf. Sci., 262 (1992) 141

[20] S. Davis, F. Zaera, B. Gordon, and G. Somorjai, J. of Catal., 92 (1985) 250

[21] R. Klein and M. Scheer, J. Phys. Chem, 62 (1958) 1011

[22] R. Klein, M. Scheer, and J. Waller, J. Phys. Chem, 64 (1960) 1249

[23] M. Yang, A. Teplyakov, B. Bent, in preparation

[24] R. Van Santen and J. Niemantsverdriet, *Chemical Kinetics and Catalysis*, Plenum Press, New York, 1994

6.7 Figure Captions

Fig 1: Adsorbed propylene moieties on Pt(111).

Fig 2: Possible surface pathways for the formation of propane from propylene on Pt(111)

Fig 3: SFG-catalysis apparatus for monitoring surface intermediates *in situ* during propylene hydrogenation.

Fig 4: (a) A saturation coverage of di-σ bonded propylene on Pt(111) formed at 187 K exposing the clean surface to 4 L of propylene. (b) Same as in (a), but with CD_3CHCH_2 as the exposure gas. (c) A saturation coverage of propylidyne on Pt(111) formed at 310 K by exposure of the clean surface to 4 L of propylene. (d) Same as in (c), but with CD_3CHCH_2 as the exposure gas.

Fig 5 (a) The thermal evolution of a saturation coverage of di-σ bonded ethylene on Pt(111). (b) The thermal evolution of a saturation coverage of propylidyne on Pt(111). (c) The mechanistic pathway for propylene dehydrogenation under UHV.

Fig 6 (a) 10 L of 1-propyl iodide (saturation coverage) on Pt(111) at 140 K after being flashed to 190 K (b) low coverage of 1-propyl iodide on Pt(111) at 140 K after being flashed to 190 K (c) 1-propyl groups before exposure to H_2 (O) and after exposure to 1400 L H_2 at 190 K (□)

Fig 7 (a) 10 L of 2-propyl iodide (saturation coverage) on Pt(111) at 140 K after being flashed to 190 K (b) Low coverage of 2-propyl iodide on Pt(111) at 140

K after being flashed to 190 K (c) 2-propyl groups before exposure to H_2 (O) and after exposure to 1400 L H_2 at 190 K (□)

Fig 8 (a) The *in situ* SFG vibrational spectrum of the Pt(111) surface during propylene hydrogenation at 295 K with 723 Torr H_2 and 40 Torr C_3H_6. The gas phase turnover rate (TOR) was simultaneously measured to be 29 molecules of propylene converted to propane per surface platinum site per second. (b) Same conditions as (a), but with 100 Torr H_2, 40 Torr C_3H_6, and 617 He. TOR = 8.6. (c) Same conditions as (a), but with 13.5 Torr H_2, 5 Torr C_3H_6, and 746 Torr He. TOR = 3.3. (d) Same conditions as (b), but with a UHV preadsorbed saturation coverage of propylidyne. TOR = 8.4.

Fig 9 The two key intermediate steps in the process of propylene hydrogenation on Pt(111)

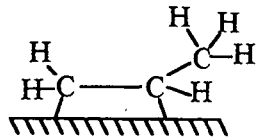

di-σ bonded propylene

(A)

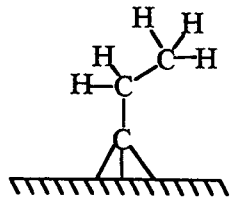

propylidyne

(B)

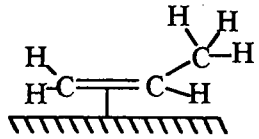

π-bonded propylene

(C)

Fig. 1

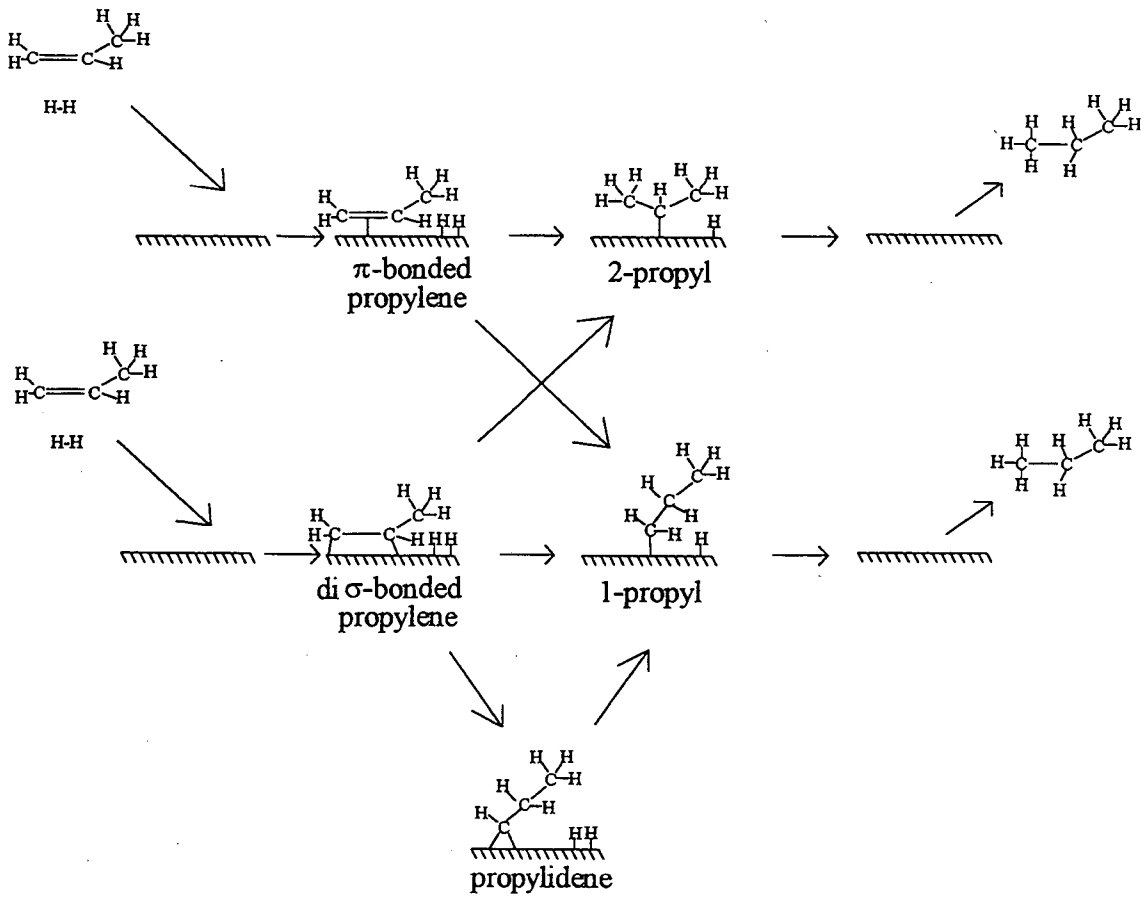
H-H
π-bonded
propylene
2-propyl
H-H
di σ-bonded
propylene
1-propyl
propylidene

Fig. 2

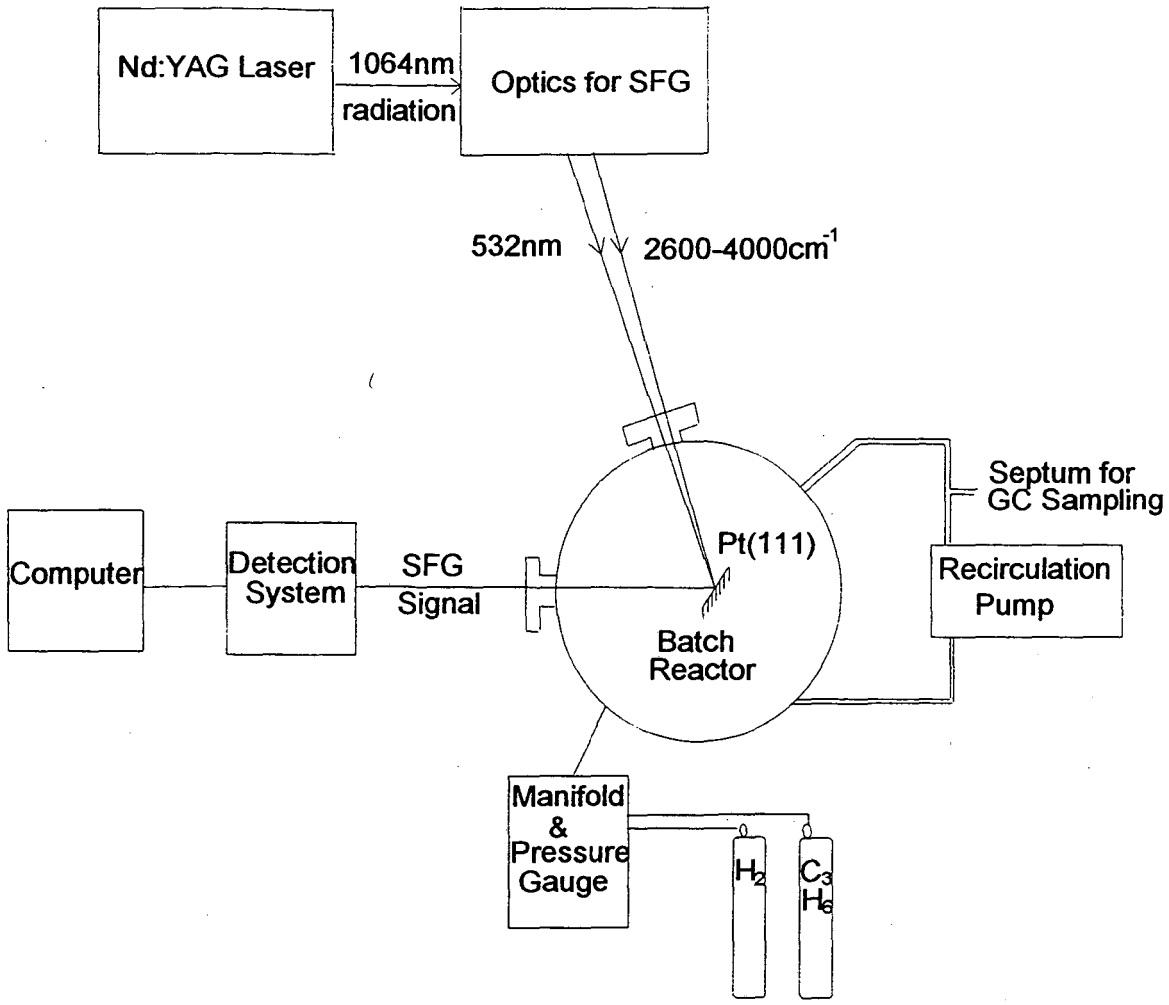
Nd:YAG Laser
1064nm
radiation
Optics for SFG
532nm
2600-4000cm-1
Septum for
GC Sampling
Computer
Detection
System
SFG
Signal
Pt(111)
Recirculation
Pump
Batch
Reactor
Manifold
&
Pressure
Gauge
H2
C3
H6

Fig. 3

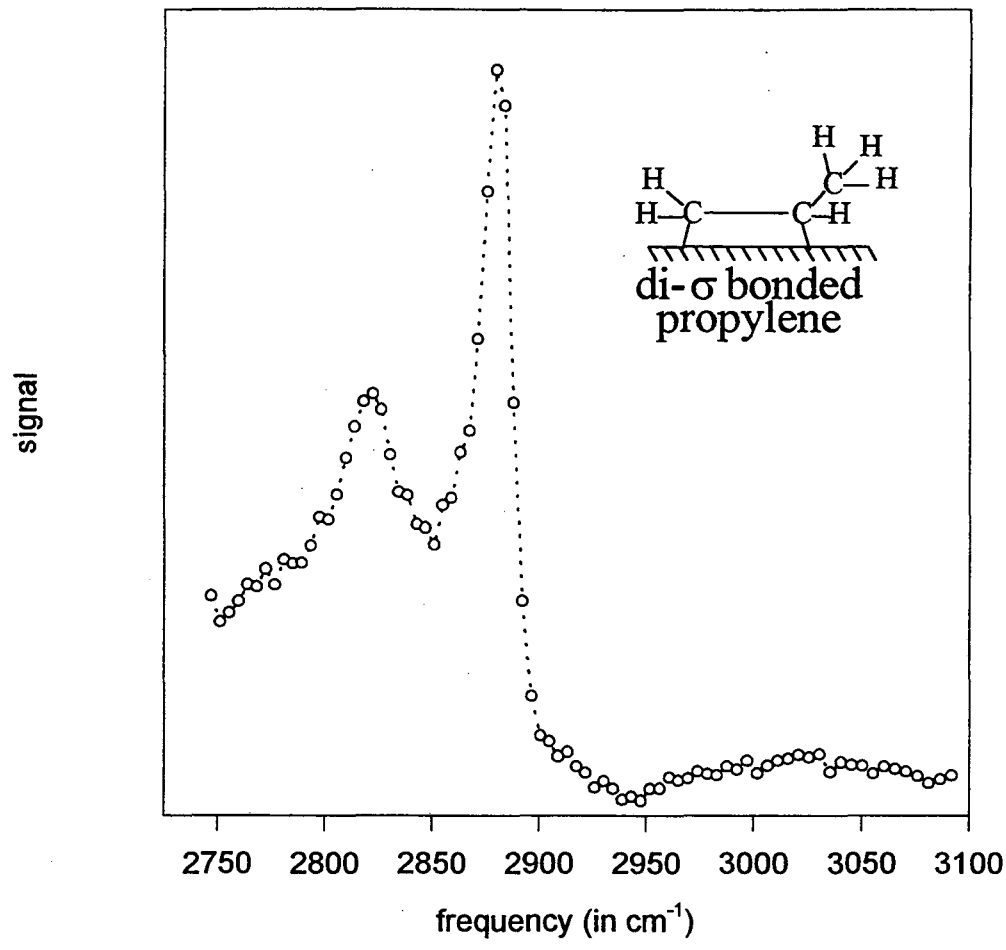
signal
di-σ bonded
propylene
2750
2800
2850
2900
2950
3000
3050
3100
frequency (in cm-1)

Fig. 4a

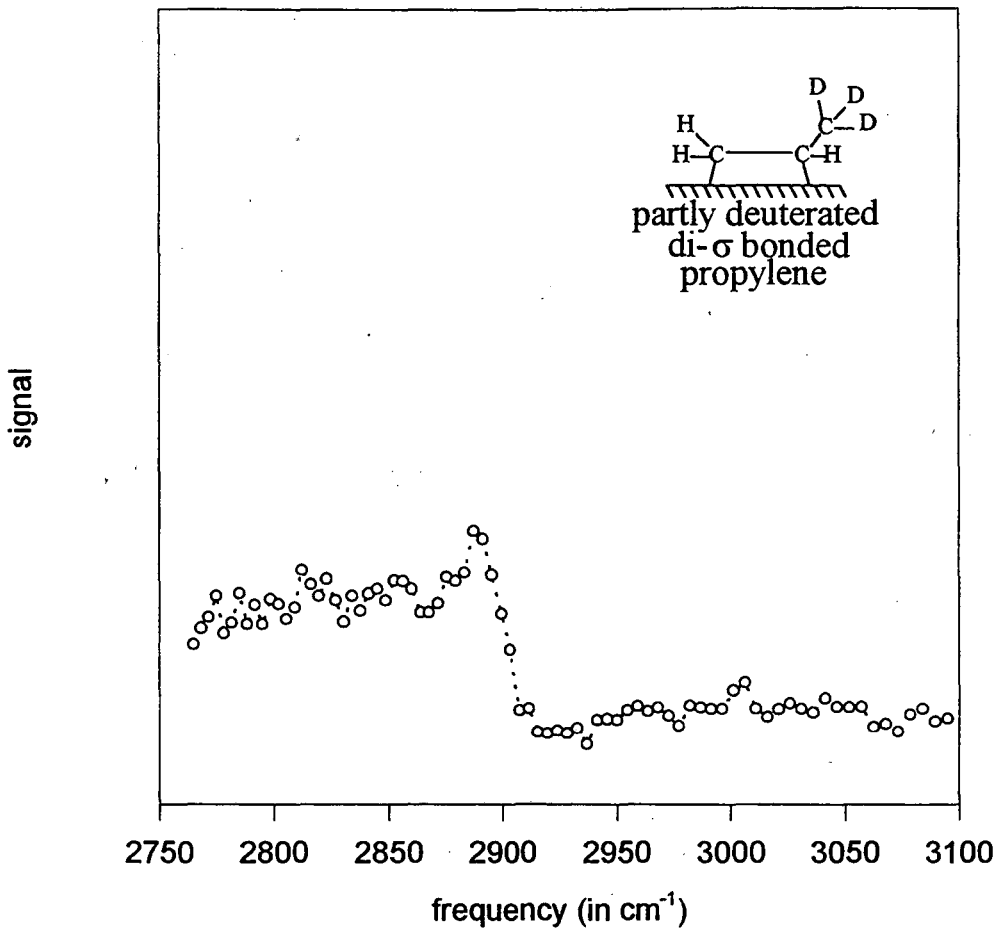
partly deuterated
di-σ bonded
propylene
signal
2750
2800
2850
2900
2950
3000
3050
3100
frequency (in cm-1)

Fig. 4b

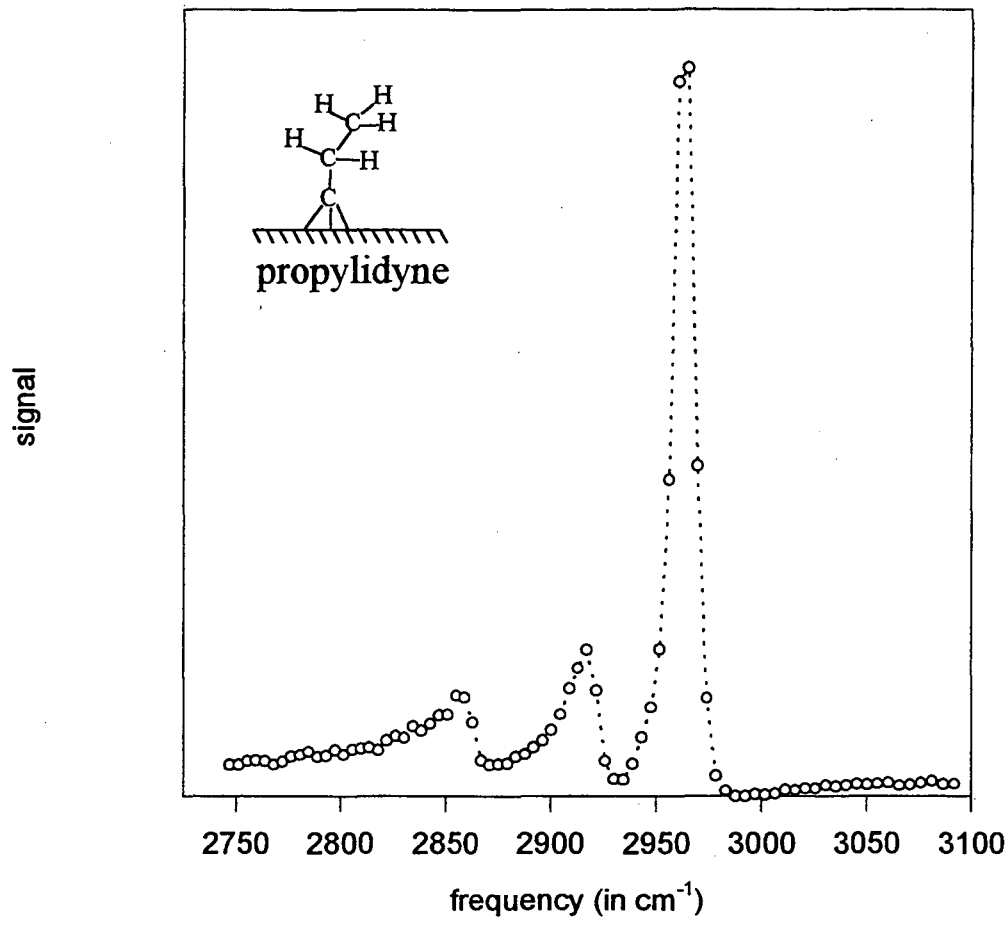
propylidyne
signal
2750
2800
2850
2900
2950
3000
3050
3100
frequency (in cm-1)

Fig. 4c

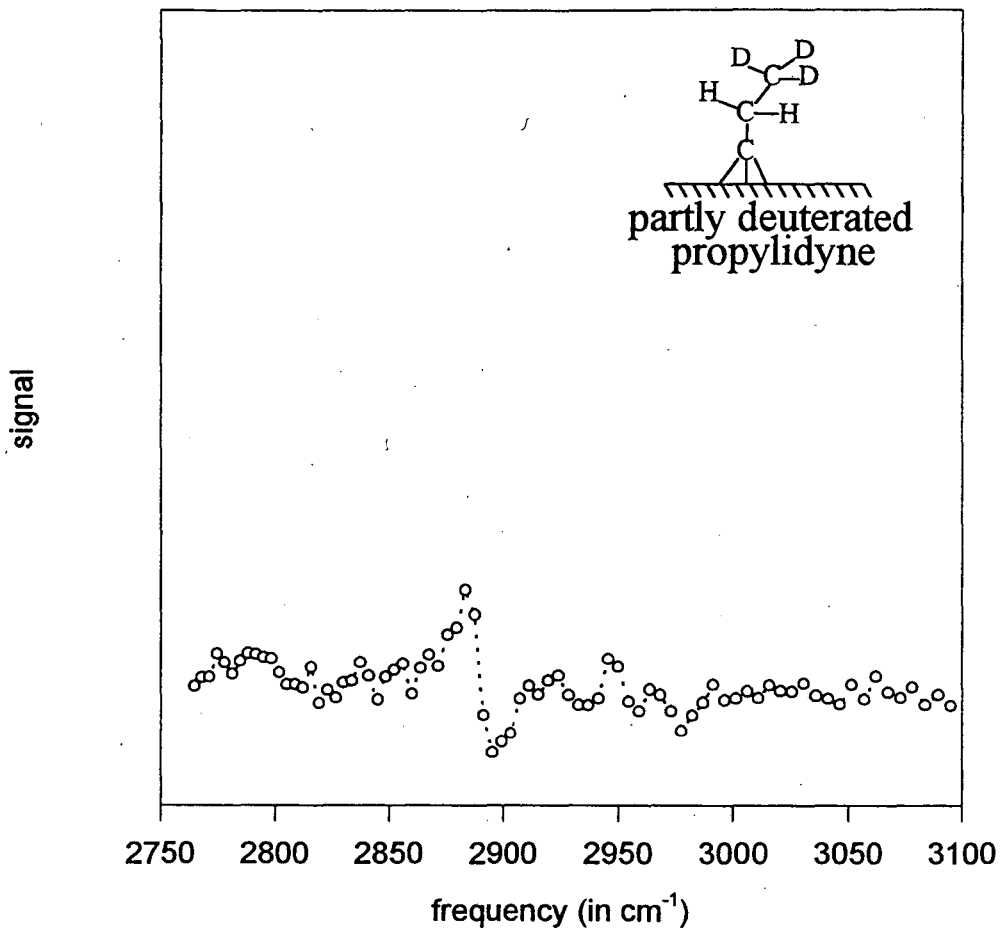
D
D
D
H
C
H
C
partly deuterated
propylidyne
signal
2750
2800
2850
2900
2950
3000
3050
3100
frequency (in cm-1)

Fig. 4d

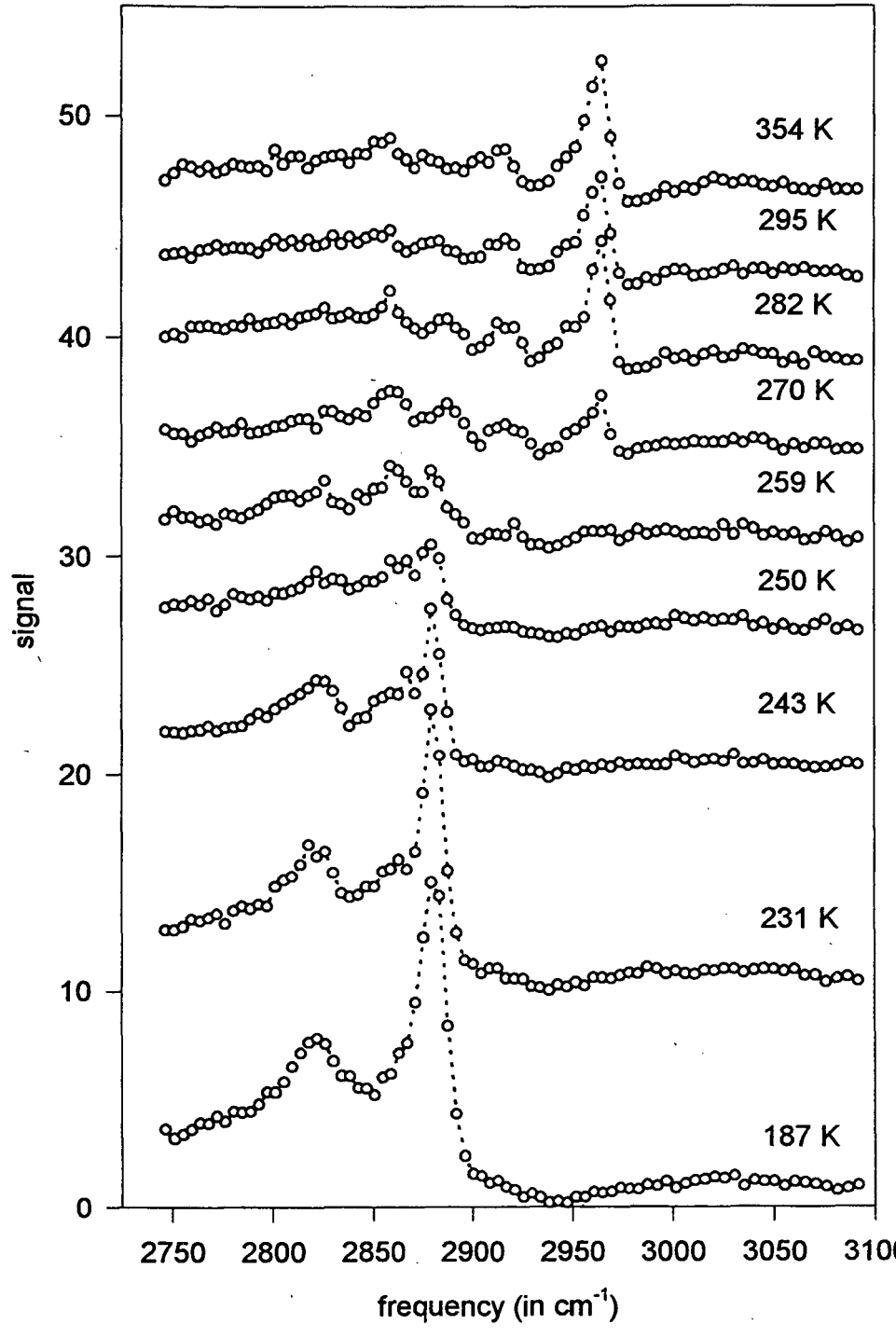
354 K
295 K
282 K
270 K
259 K
250 K
243 K
231 K
187 K
signal
0
10
20
30
40
50
2750
2800
2850
2900
2950
3000
3050
3100
frequency (in cm-1)

Fig. 5a

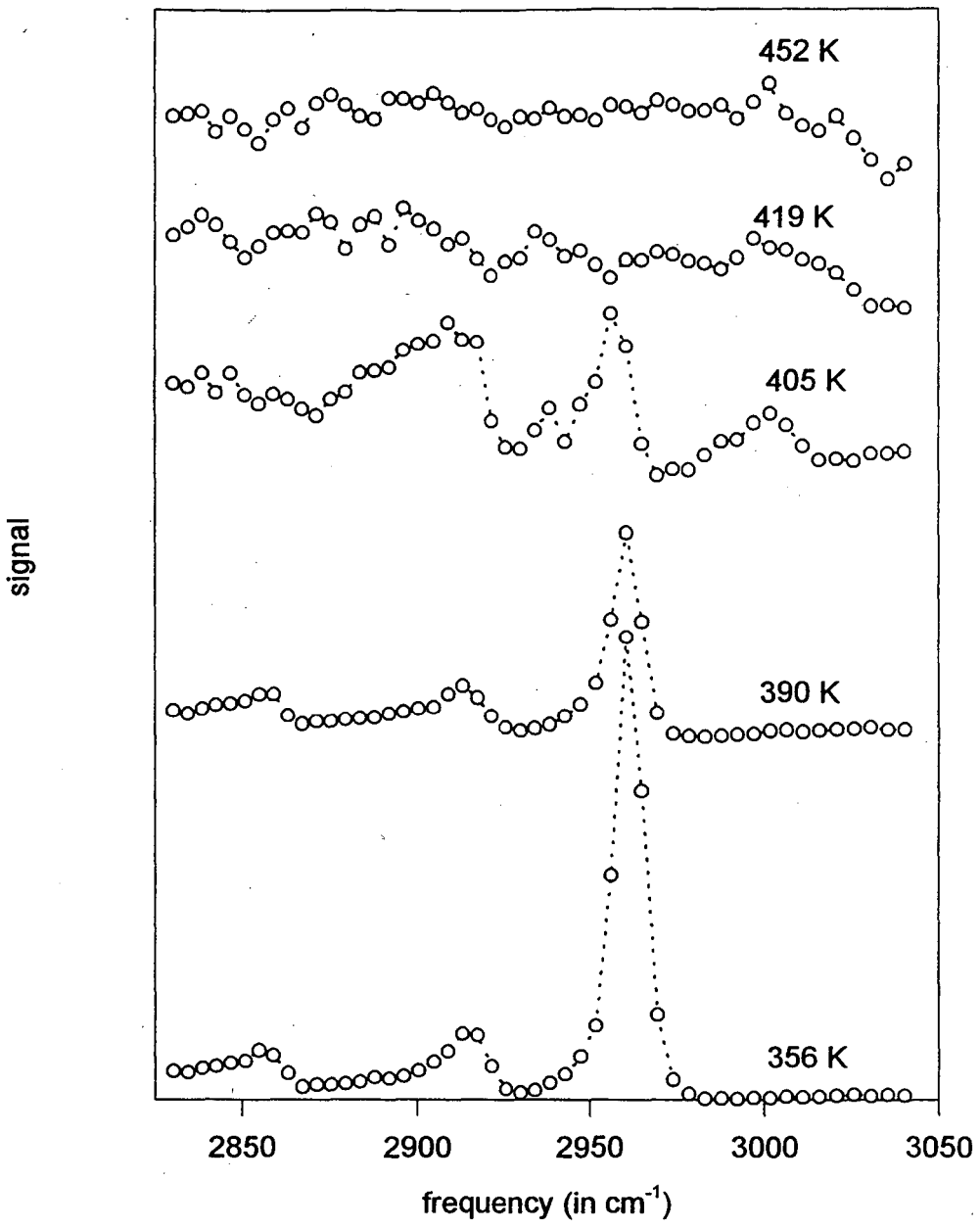
452 K
419 K
405 K
390 K
356 K
signal
2850
2900
2950
3000
3050
frequency (in cm-1)

Fig. 5b

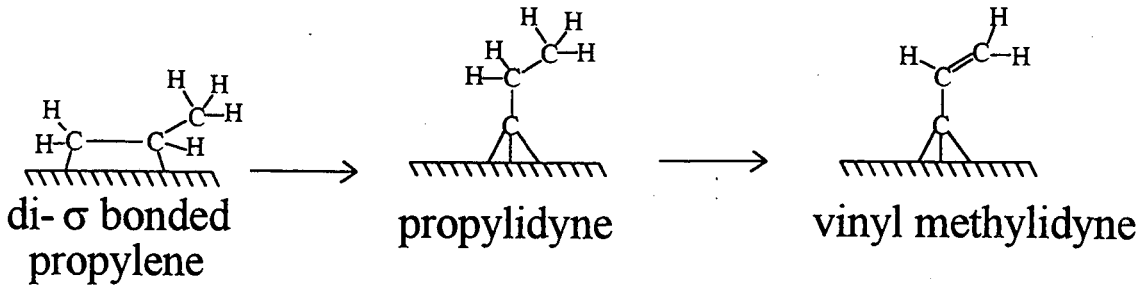

Fig. 5c

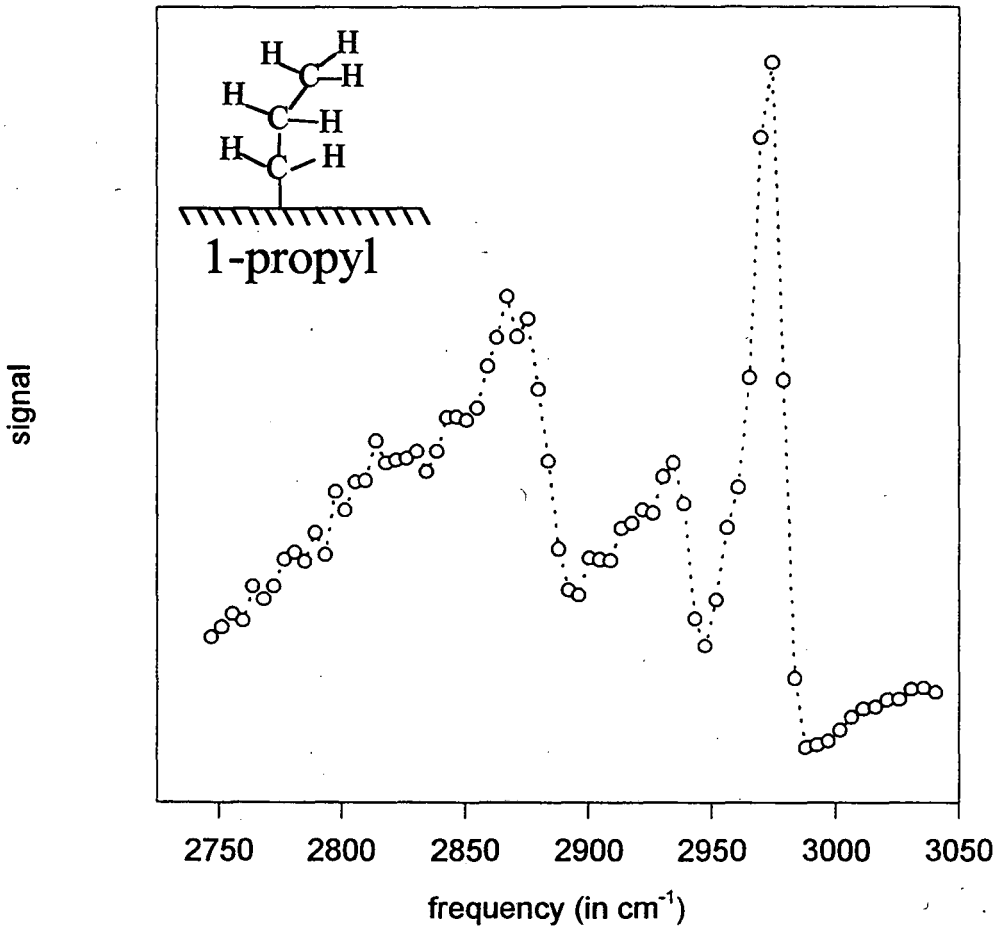
1-propyl
signal
2750
2800
2850
2900
2950
3000
3050
frequency (in cm-1)

Fig. 6a

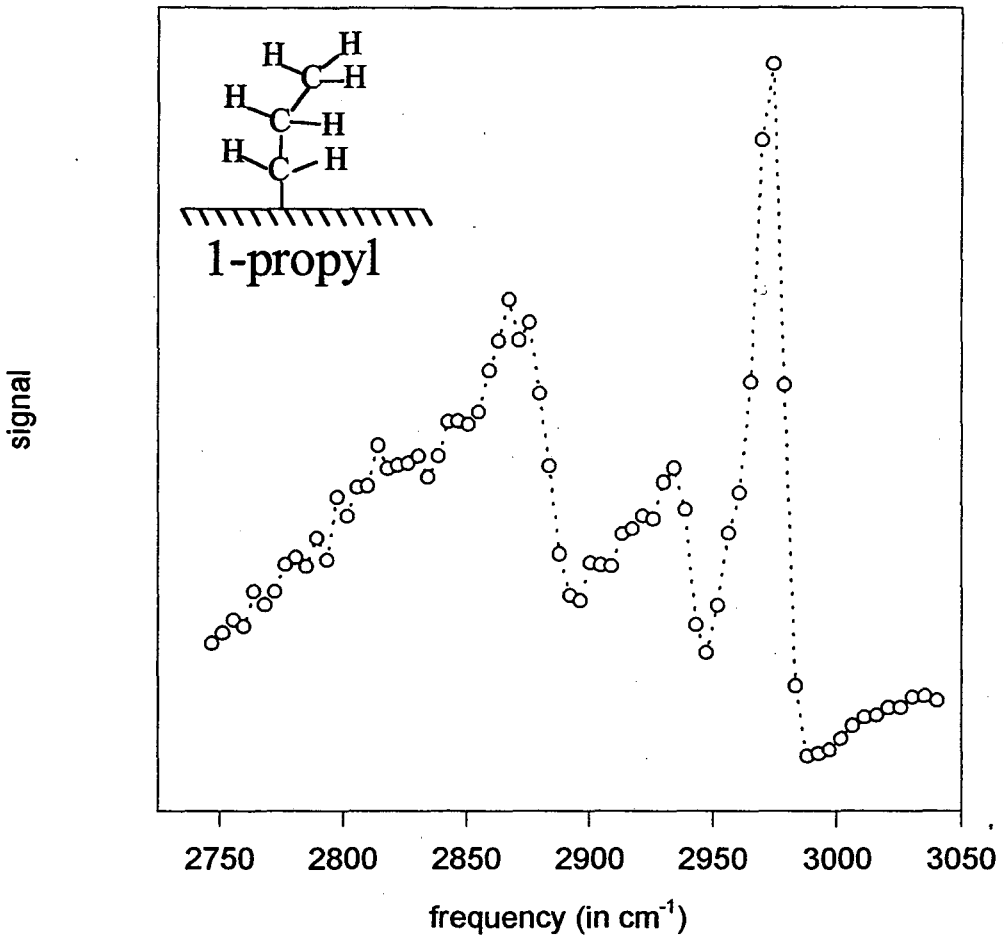
1-propyl
signal
2750
2800
2850
2900
2950
3000
3050
frequency (in cm-1)

Fig. 6b

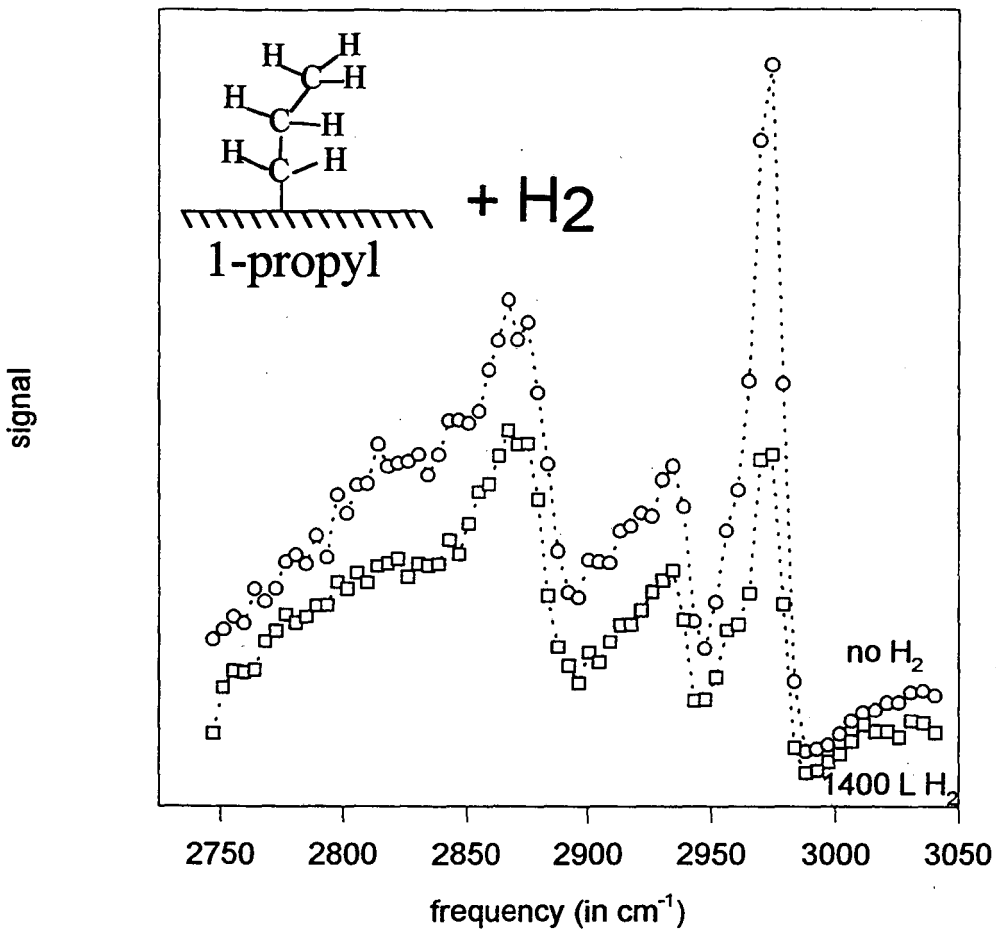
+ H2
1-propyl
signal
no H2
1400 L H2
2750
2800
2850
2900
2950
3000
3050
frequency (in cm-1)

Fig. 6c

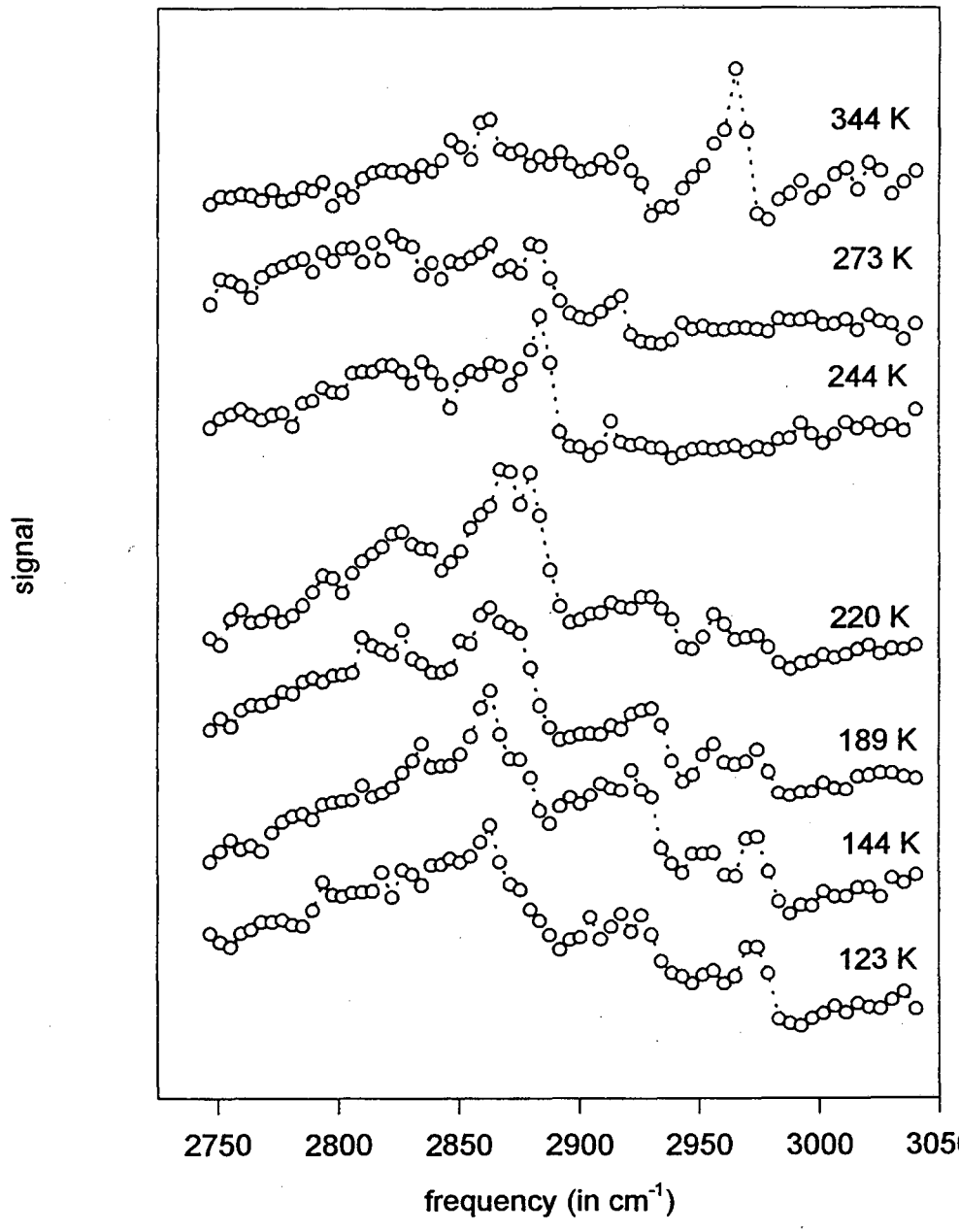
344 K
273 K
244 K
220 K
189 K
144 K
123 K
signal
2750
2800
2850
2900
2950
3000
3050
frequency (in cm-1)

Fig. 6d

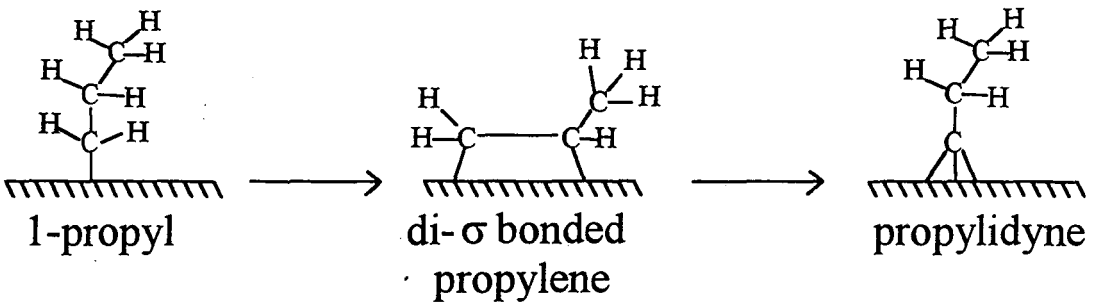

Fig. 6e

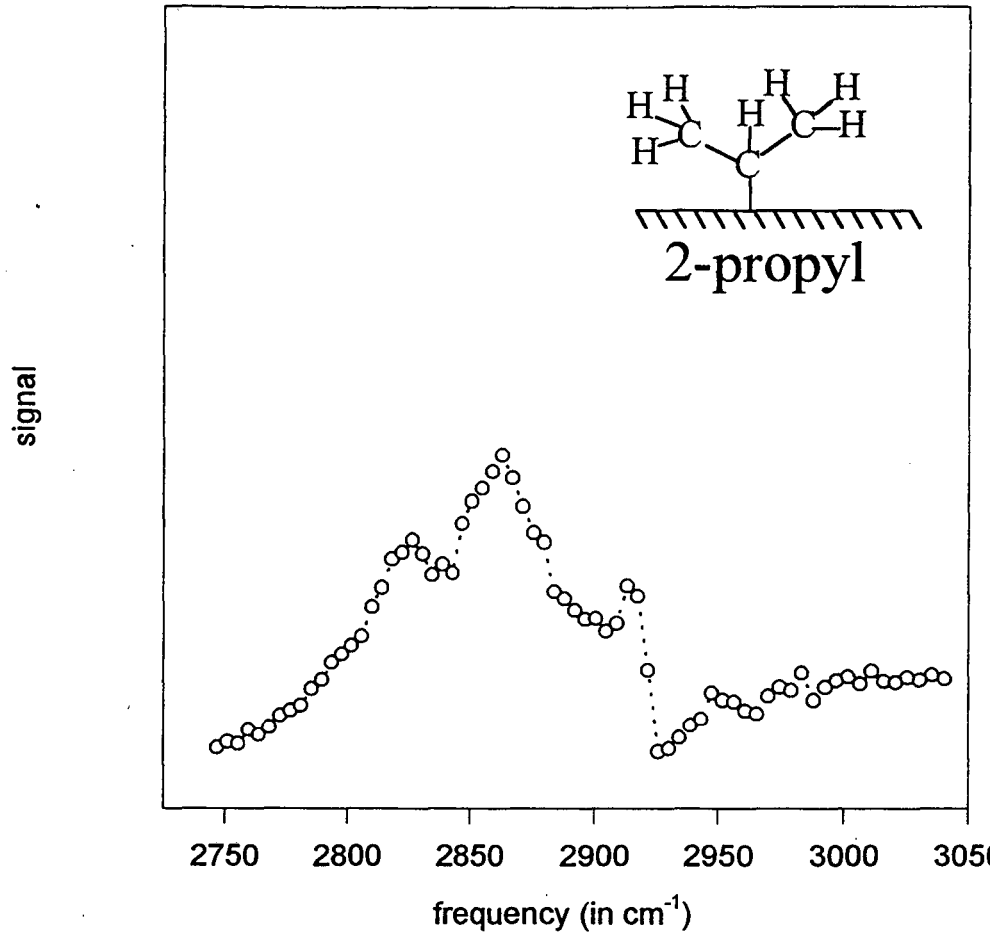
2-propyl
signal
2750
2800
2850
2900
2950
3000
3050
frequency (in cm-1)

Fig. 7a

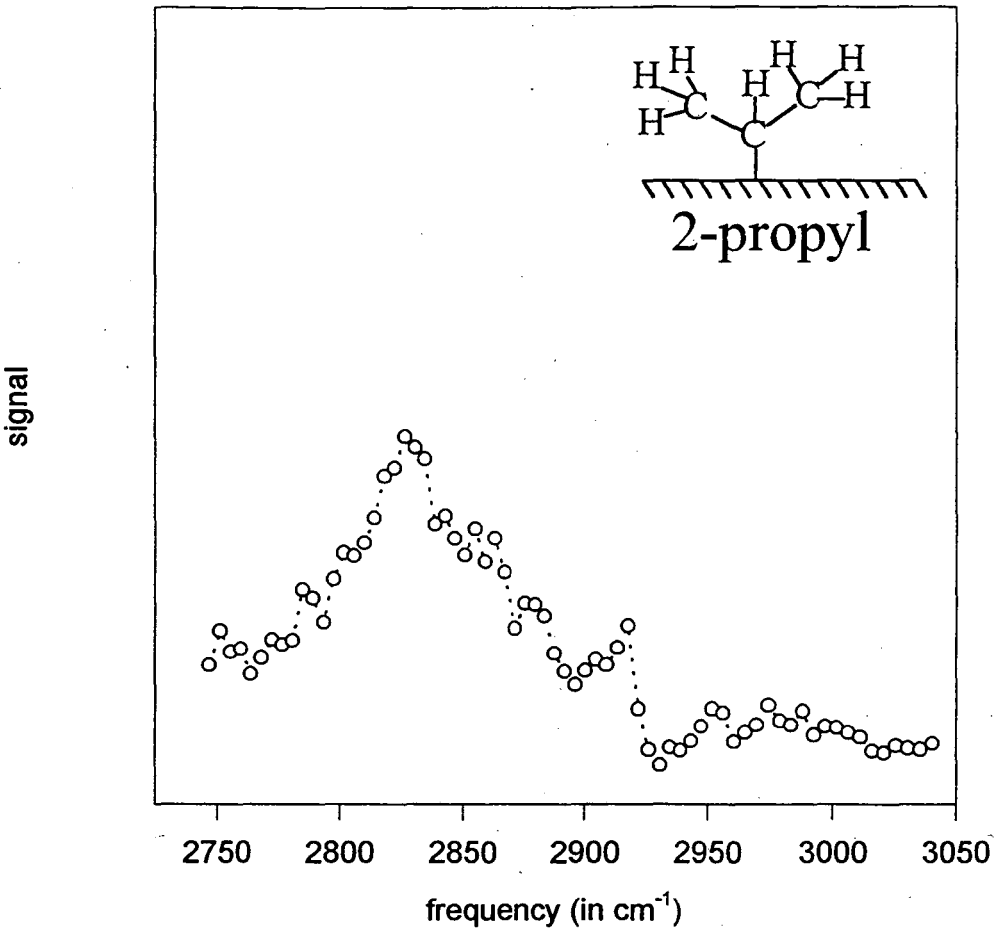
2-propyl
signal
2750
2800
2850
2900
2950
3000
3050
frequency (in cm-1)

Fig. 7b

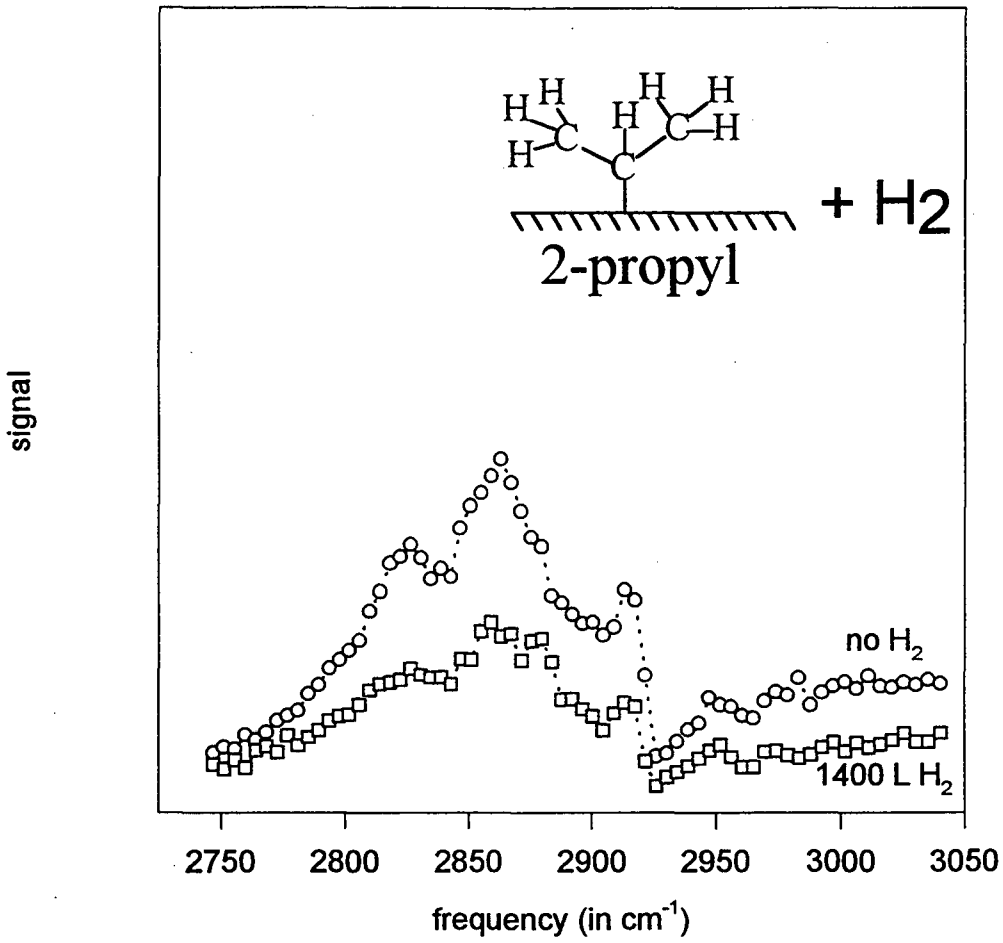
+ H2
2-propyl
signal
no H2
1400 L H2
2750
2800
2850
2900
2950
3000
3050
frequency (in cm-1)

Fig. 7c

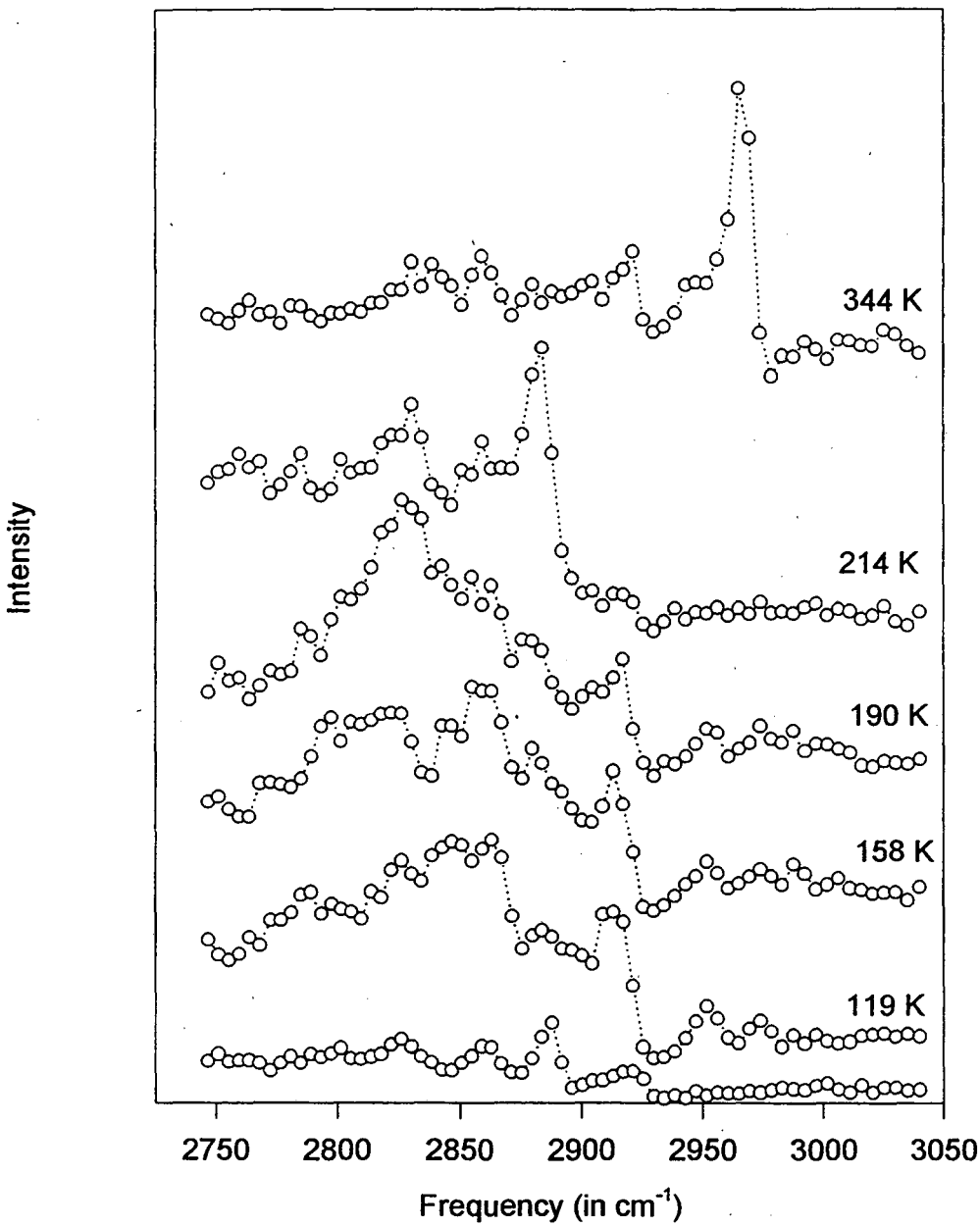
Intensity
344 K
214 K
190 K
158 K
119 K
2750
2800
2850
2900
2950
3000
3050
Frequency (in cm-1)

Fig. 7d

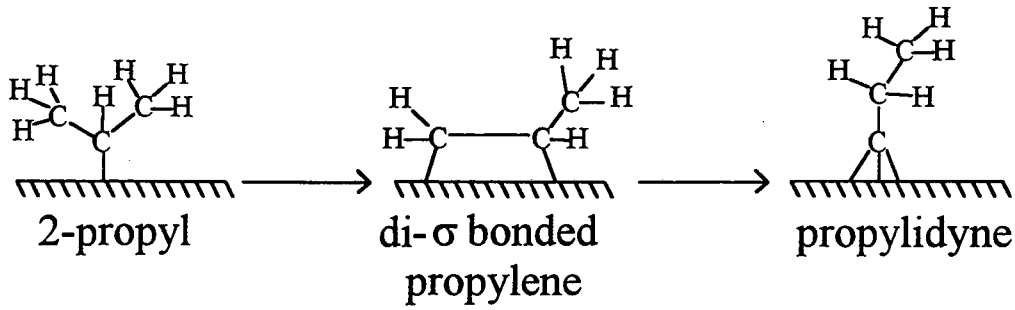

Fig. 7e

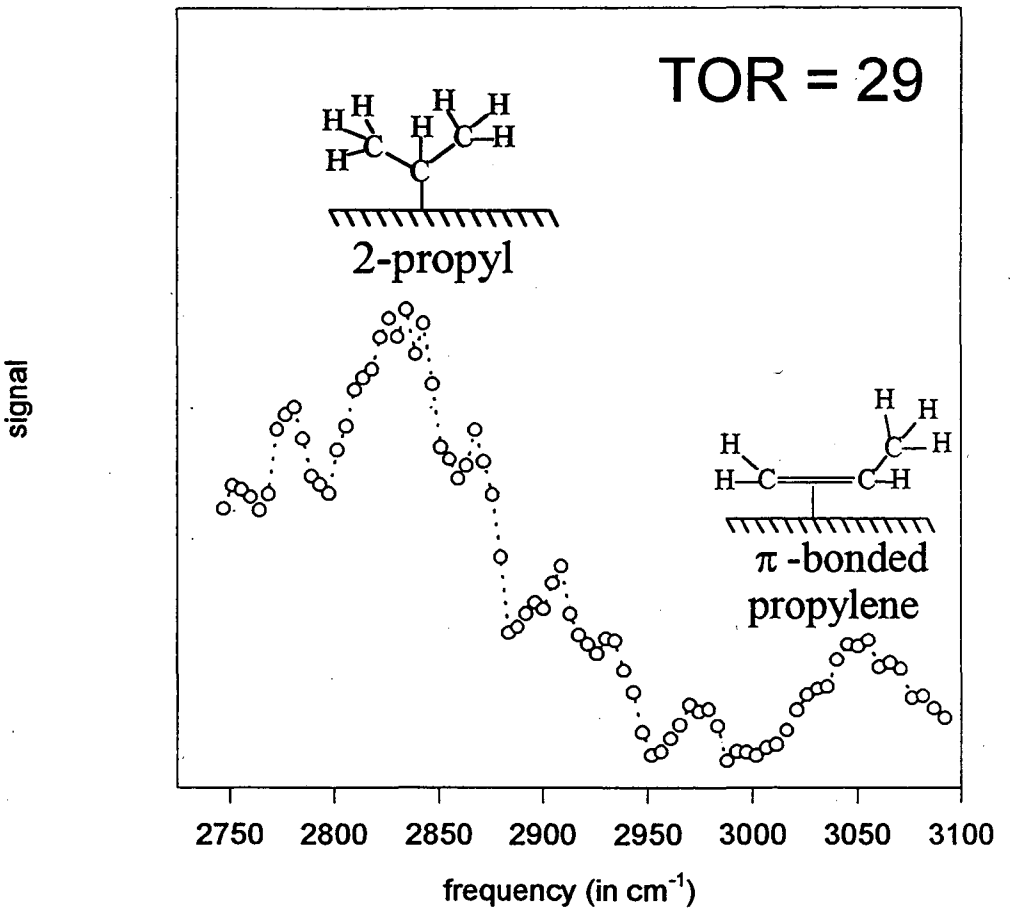
TOR = 29
2-propyl
π -bonded
propylene
signal
2750
2800
2850
2900
2950
3000
3050
3100
frequency (in cm-1)

Fig. 8a

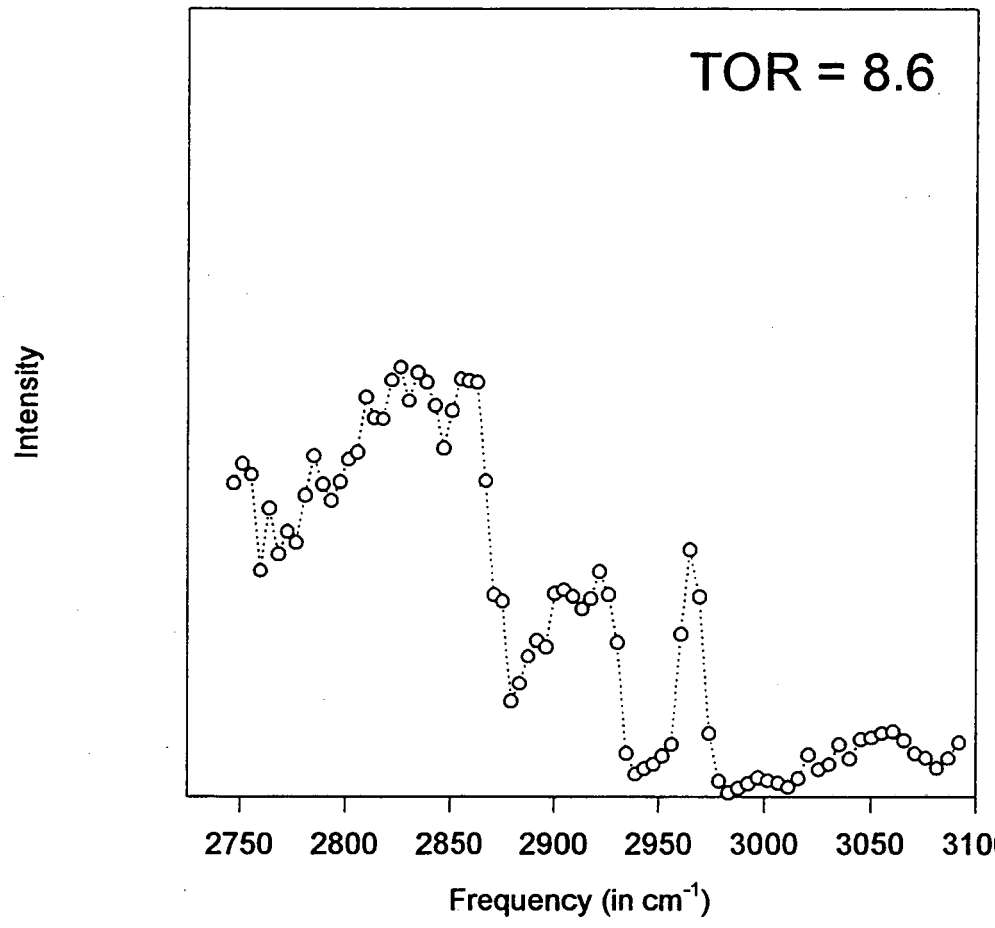
TOR = 8.6
Intensity
2750
2800
2850
2900
2950
3000
3050
3100
Frequency (in cm-1)

Fig. 8b

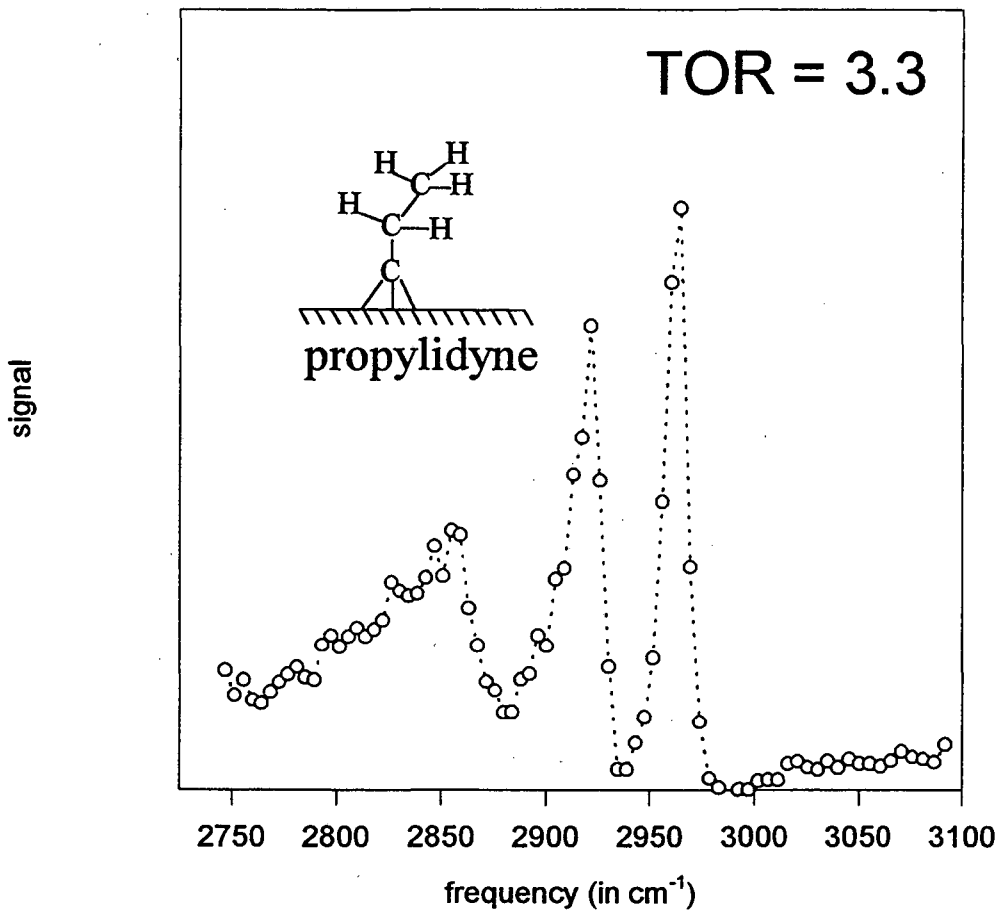
TOR = 3.3
propylidyne
signal
2750
2800
2850
2900
2950
3000
3050
3100
frequency (in cm-1)

Fig. 8c

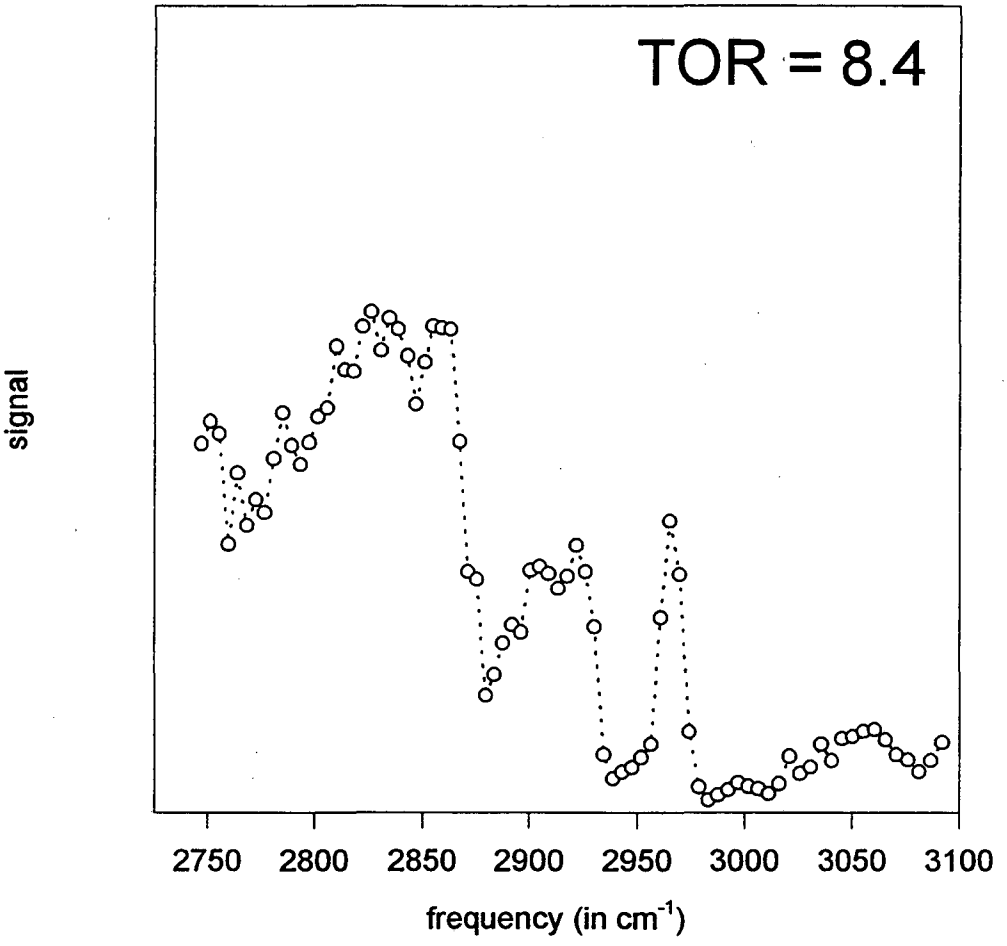
TOR = 8.4
signal
2750
2800
2850
2900
2950
3000
3050
3100
frequency (in cm-1)

Fig. 8d

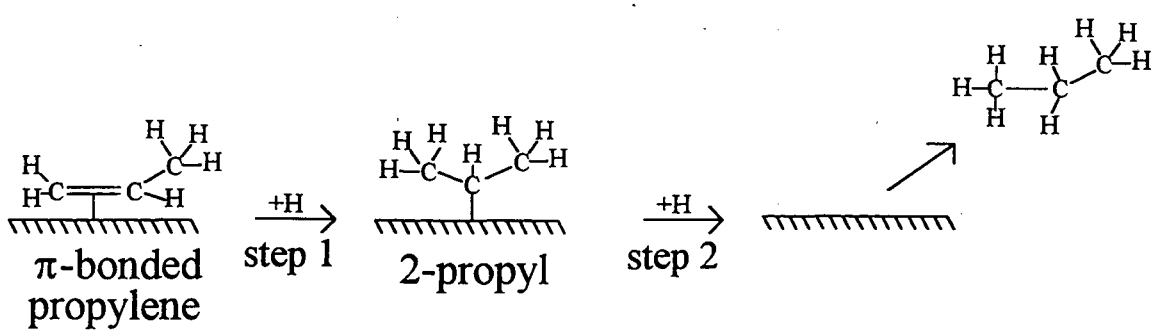

Fig. 9

Chapter 7

The Chemistry of Isobutene and Hydrogen on Pt(111)

The rate of hydrogenation of isobutene was monitored near ambient pressure over a Pt(111) single crystal by SFG. During hydrogenation 2-isobutyl groups and π-bonded isobutene species were the dominant surface species detected. Only small amounts dehydrogenated species such as isobutylidyne could be observed unless the surface was made very hydrogen poor. The hydrogenation rate was at least one order of magnitude lower than for 1-butene and cis 2-butene. Vacuum studies indicated that the rate of 2-isobutyl hydrogenation was much slower than that of 1-isobutyl, which may force isobutane production to proceed from π-bonded isobutene through the slow kinetic step of 1-isobutyl formation.

7.1 Introduction

The investigation of the surface chemistry of olefin hydrogenation has concentrated almost exclusively on the behavior of the smallest species, ethylene and propylene [1-9]. It has been shown for the case of ethylene that hydrogenation proceeds from a physisorbed intermediate, π-bonded ethylene (rather than from chemisorbed di-σ bonded ethylene), through an ethyl group to ethane [9] [Fig 1a]. The surface concentration of the key intermediate, π-bonded ethylene, was about 4% of a monolayer under conditions near zero order in ethylene pressure. This species most likely hydrogenates on atop sites consistent with (a) vibrational spectra, (b) the homogenous analog of this reaction, and (c) the structure insensitive nature of olefin hydrogenation. During catalysis the surface was covered under most conditions by a saturation coverage of the decomposition species, ethylidyne ($M{\equiv}CCH_3$). This species has been shown by isotopic labeling not to be involved in the reaction nor to hinder the rate of ethane formation to any appreciable extent [5, 10]. Ethylidyne resides primarily in the fcc three fold hollow site on Pt(111), but has been shown to be very mobile on the surface [11, 12].

Fewer studies have been conducted for higher olefins, most of which concentrated on the behavior of the next simplest olefin, propylene [13-16]. Under reaction conditions the first step to propylene hydrogenation was physisorption of the olefin as π-bonded propylene in analogy with ethylene hydrogenation. However, propylene hydrogenation is inherently more complicated than ethylene hydrogenation. The addition of the first hydrogen may either occur at the terminal or the internal carbon of the hydrocarbon. Under reaction conditions it was observed that 2-propyl groups were present in far larger concentration than 1-propyl groups. Also, 2-propyl groups were shown by vacuum experiments to be slightly more facile toward hydrogenation [13]. This led to the conclusion that 2-propyl groups along with π-bonded propylene were the key intermediates in propylene hydrogenation [Fig. 1b]

Beyond propylene and ethylene very few surface science investigations exist, which attempt to explore the behavior of olefin hydrogenation on transition metal catalysts. In fact, only a handful of studies exist studying the behavior of isobutene over a platinum catalyst [17-20]. In kinetic studies by Rogers et al. the hydrogenation rate of isobutene over a supported platinum catalyst was measured to be 20 times slower than propylene with an activation energy of 14.8 kcal/mol [18]. The reaction was found range between negative and zero order in isobutene and be slightly less than first order in hydrogen. Transmission infrared spectroscopy studies by Shahid and Sheppard investigated a supported platinum catalyst exposed to isobutene at room temperature. Evidence was found for di-σ bonded isobutene, π-bonded isobutene, and isobutylidyne species [Fig. 2]. Experiments, however, have not yet been undertaken which probe the vibrational spectrum of this system under reaction conditions.

It is the goal of this work is to study the surface chemistry of isobutene, its derivatives, and hydrogen on Pt(111) from ultra high vacuum to high pressure in order to investigate the role of all observable surface species and elucidate the reaction mechanism. To this end we have employed infrared-visible sum frequency generation (SFG), a surface specific vibrational spectroscopy to investigate the surface simultaneously with kinetic measurements by gas chromatography.

7.2 Results

(a) The Temperature Dependent Rearrangement of Isobutene on Pt(111) in UHV

Studies of the surface structure of isobutene on Pt(111) were carried out from 120 K to room temperature under ultra high vacuum (UHV) conditions. Exposing the clean Pt(111) surface to a saturation coverage of isobutene (4 L) at low temperature results in a vibrational spectrum that we assign to di-σ bonded isobutene (Fig. 3). The carbon-carbon double bond is broken and two new carbon metal single bonds are formed with the underlying platinum atoms. Four distinct peaks in the CH stretch range of the

vibrational spectrum are observed for this species. These are at 2825 cm^{-1}, 2855 cm^{-1}, 2890 cm^{-1}, and 2910 cm^{-1}. It is difficult to assign the features, but by analogy with di-σ bonded propylene, most of the intensity is likely to be from the CH_3 groups and their fermi resonances [13]. Shahid and Sheppard predict from the metal dipole selection rule that the strongest intensities might come at 2920 cm^{-1} from $\nu_s(CH_2)$ and at 2870 cm^{-1} for $\nu_s(CH_3)$ [19]. They assign two peaks from their own room temperature data of isobutene adsorbed on a supported platinum catalyst to di-σ bonded isobutene. These features are at 2925 cm^{-1} and 2910 cm^{-1} and, hence, do not correlate well with the single crystal work. Shahid and Sheppard note, however, that unpublished RAIRS data of di-σ bonded isobutene/Pt(111) at 90 K by Chester et al. has its dominant feature at 2895 cm^{-1}, which is in agreement with the present work [21].

A saturation coverage of the dehydrogenated species, isobutylidyne, can be formed on the clean Pt(111) surface by exposure to 4 L of isobutene at 295 K (Fig. 4). The most intense spectral feature at 2970 cm^{-1} is from the $\nu_{as}(CH_3)$ of the two terminal methyl groups in agreement with Shahid and Sheppard. In addition the lowest frequency peak at 2865 cm^{-1} is assigned to the $\nu_s(CH_3)$. The two intermediate peaks may be from a fermi resonance with a CH_3 bending mode and from the ν(CH). Shahid and Sheppard report that the RAIRS spectrum shows evidence for a $\delta_{as}(CH_3)$ at 1445 cm^{-1}. Therefore the 2880 cm^{-1} may be assigned to the fermi resonance and the 2920 cm^{-1} to the ν(CH).

The thermal evolution of isobutene/Pt(111) was followed by annealing the sample from 120 K to room temperature stepwise. Each annealing cycle consisted of heating to a predetermined temperature for 10 seconds and then allowing the sample to recool to 120 K where an SFG spectrum was recorded. Figure 5a shows the vibrational spectrum of the system annealed to 200 K for 10 seconds. The spectral features did not shift in position compared with the 120 K spectrum, but the relative intensities changed significantly. The 2890 cm^{-1} peak fell in intensity while the 2910 cm^{-1} feature grew stronger. The change in relative intensities most likely corresponds with a reorientation

of the di-σ bonded isobutene species on the surface. SFG is particularly sensitive to very small changes in orientation because spectral intensities varies with the dipole orientation as $\cos^6\theta$.

Further annealing the sample to 270 K yields a dramatically altered SFG spectrum (Fig. 5b). There are four distinguishable features at 2830 cm^{-1}, 2890 cm^{-1}, 2930 cm^{-1}, and 2975 cm^{-1}. The highest frequency peak corresponds well to a $\nu_{as}(CH_3)$, which is most likely from the formation of a small amount of isobutylidyne on the surface. The peak at 2930 cm^{-1} is unique to this spectrum and can neither be assigned to di-σ bonded isobutene or isobutylidyne. It, therefore, probably corresponds to the signature of an intermediate species. There are several possible intermediates in the formation of isobutylidyne from di-σ bonded isobutene. The two most likely pathways are shown in figure 6. The first candidate pathway would be through a 1-2 hydrogen shift to form isobutylidene followed by an elimination step at the α-carbon to form isobutylidyne. The other possible mechanism would involve C-H bond scission to form 1,1 dimethylvinyl which could undergo a 1,2 shift to from isobutylidyne.

For the analogous case of di-σ bonded ethylene decomposition to ethylidyne ($M{\equiv}CCH_3$), the preponderance of evidence points to an ethylidene intermediate [22]. Therefore, we tentatively postulate that the intermediate giving rise to the spectral features in figure 5b is isobutylidene. However, for a more definitive identification of this species an inorganic cluster analog would have to be synthesized and the vibrational spectrum from the intermediate matched to it. Further annealing of this system to room temperature yields isobutylidyne (Fig. 5c).

(b) Formation and Hydrogenation of 1- and 2-Isobutyl Groups

The preparation of 1- and 2-isobutyl moieties on the Pt(111) surface is achieved by adsorbing the corresponding iodides on the surface below 140 K and annealing the system above 170 K to break some of the C-I bonds by analogy with the case for ethyl

iodide [23]. To prepare the 1-isobutyl/Pt(111) system, 10 L (saturation coverage) of 1-isobutyliodide was exposed to the clean surface at 140 K. The system was then annealed to 205 K for 10 seconds and allowed to cool below 140 K before an SFG scan was taken (Fig 7a). The most intense feature at 2860 cm^{-1} is most likely from the $\nu_s(CH_3)$, while the feature at 2960 cm^{-1} is from the $\nu_{as}(CH_3)$. The wide variety of peaks observed is do to the low symmetry of this species. Indeed, there may be signal from CH, CH_2, and CH_3 species present.

Exposing the system in figure 7a to 1000 L of hydrogen at 205 K yielded figure 7b. The intensity difference in the spectra can be directly compared because the beam overlap and spacial alignment of the system was unchanged between experiments. In this case most of the spectral features remain, but the overall intensity has decreased due to the hydrogenation of some 1-isobutyl groups to isobutane. The decrease in intensity is approximately a factor of two to three for most spectral features.

Identical experiments were carried out for 2-isobutyl groups. The spectrum of 2-isobutyl/Pt(111) is shown in figure 8a. In this case broad signal from 2750 cm^{-1} to 2900 cm^{-1} is seen with two peaks at 2830 cm^{-1} and 2860 cm^{-1}. These features most likely represent the $\nu_s(CH_3)$ and a fermi resonance. The broadness of the spectrum from additional features at higher frequency such as the small peak near 2895 cm^{-1} may indicate that some of the 2-isobutyl has decomposed to di-σ bonded isobutene. The addition of 1000 L of hydrogen to this system at 205 K shows little evidence that 2-isobutyl groups can be hydrogenated under these conditions (Fig 8b). This is in striking contrast to 1-isobutyl (Fig 7b) where hydrogenation readily occurred under the same conditions.

(c) Isobutene Hydrogenation

In situ monitoring of isobutene hydrogenation at 295 K on Pt(111) was performed with 105 Torr H_2, 40 Torr isobutene, and 635 Torr He. The vibrational spectrum reveals

two distinct bands of signal in the CH stretch range (Fig 9a). The lower frequency range from 2780 to 2880 cm^{-1} corresponds well to adsorbed 2-isobutyl groups with the possibility of a small contribution from di-σ isobutene. The upper band, center around 3050 cm^{-1}, is readily assigned to π-bonded isobutene. The vibrational spectrum remained unchanged over several hours of reaction. Little evidence was seen for the decomposition product, isobutylidyne, during the reaction. Under these conditions the reaction rate is about 0.35 molecules of isobutene converted to isobutane per platinum site per second. This reaction rate is nearly a factor of twenty slower than measurements for the hydrogenation of the n-butenes under similar conditions [24].

Figure 9b shows the vibrational spectrum for the hydrogenation of isobutene under lower reactant pressures (20 Torr H_2, 5 Torr isobutene, and 760 Torr He) at 295 K. Under these conditions the turnover rate slowed to about 0.1 per site per second and the vibrational spectrum changed dramatically. The signal below 2900 cm^{-1} is still quite strong, but the peaks are much sharper. This most likely indicates an increase in the contribution from di-σ bonded isobutene compared with intensity from 2-isobutyl groups. The olefinic stretch range above 3000 cm^{-1} remains nearly unchanged, which indicates the concentration of the π-bonded species remains nearly constant. However, there are quite a few new peaks compared with the higher pressure regime in the range between 2900 and 3000 cm^{-1}. These can be assigned to 1-isobutyl groups and isobutylidyne.

7.3 Discussion

(a) Alkylidyne Hydrogenation

The hydrogenation of isobutene elucidates an important trend in olefin hydrogenation. First, as the size of terminal olefins increase the concentration of decomposition products present on the surface under reaction conditions decreases. Under conditions of 100 Torr H_2 and sufficient olefin (10's of Torr) such that the hydrogenation reaction is zero order in this reactant, ethylidyne dominates the surface during ethylene hydrogenation at

295 K [9]. It has been demonstrated by ^{14}C labeling experiments that a saturation coverage of ethylidyne hydrogenates at a rate at least five order of magnitude slower than the overall reaction rate [10].

Propylene hydrogenation with 100 Torr H_2 at 295 K shows that the dehydrogenation product, propylidyne ($M{\equiv}CCH_2CH_3$), could be easily removed from the surface during reaction [13]. The surface concentration of propylidyne would come to an equilibrium concentration of 5% of a monolayer regardless of whether the reaction was commenced on an initially clean Pt(111) surface or one with a saturation coverage of propylidyne. Equilibrium was established as fast as the surface coverage could be measured, an upper bound of ~5 minutes. In the case of isobutene hydrogenation, no isobutylidyne was detectable on the surface under reaction condition of 105 Torr H_2 and 40 Torr isobutene at 295 K, even though the detection limit of this species by SFG is less than 1% of a monolayer.

There are two possible reasons for the decrease in concentration of alkylidyne present on the surface during reaction; either the rate of alkylidyne formation is suppressed for increasing olefin size during hydrogenation, or the rate at which these species are removed from the surface by hydrogenation is suppressed, or a combination of both. It is clear from the vacuum work that the temperature of formation of these species from their respective di-σ bonded olefins is approximately the same [13, 22]. Indeed all these species form alkylidynes by room temperature. Therefore, it is unlikely that the formation rate of the alkylidyne species can account for the significant differences in alkylidyne concentration under reaction conditions. More likely, larger olefins are more readily hydrogenated than the smaller ones. The evidence for this stem from the fact that a saturation coverage of ethylidyne cannot be removed over hours of hydrogenation, while for propylene hydrogenation, the removal of propylidyne happens in minutes or less [9, 13]. In the case of isobutene hydrogenation, no isobutylidyne can even be formed until the hydrogen pressure is lowered well below 100 Torr (Figs. 9a and 9b).

The decrease in activation barrier for the insertion of the first hydrogen into the alkylidyne to form the respective alkylidene must stem from the nature of the β-carbon. In the case of ethylidyne the β-carbon is primary, whereas it is secondary in propylidyne and tertiary in isobutylidyne. Addition of the first hydrogen to all the alkylidynes occurs at the α-carbon to form their respective alkylidene species (Fig. 10). If the transition state for this step involves separation of charge, it would be expected that a tertiary carbon at the β position would be better able to stabilize the transition state than a secondary carbon, which in turn would be better than a primary carbon. Such separation of charge would occur if the transition involved, for example, α-hydride addition.

The most important consequence of the increasing rate of hydrogenation of the larger alkylidynes is the relative degree of cleanliness that prevails on the surface under reaction conditions. Indeed, during isobutene hydrogenation with 100 Torr hydrogen, the surface was essentially free of decomposition products.

(b) Kinetics and the Hydrogenation Mechanism of Isobutene

Isobutene hydrogenation proceeds from a physisorbed intermediate, π-bonded isobutene, through an isobutyl group to isobutane. Evidence for a physisorbed intermediate is readily found in the vibrational spectrum for this system where the amount of π-bonded isobutene is large. It is somewhat difficult to determine the di-σ bonded isobutene concentration because of overlapping intensities between 2-isobutyl and di-σ bonded isobutene. However, even if a significant amount of the low frequency intensity in the hydrogenation spectrum represents the di-σ bonded species, it is still unlikely that this is an important intermediate. It has been demonstrated for the analogous propylene and ethylene hydrogenation cases, that di-σ bonded olefins hydrogenate very slowly compared with their π-bonded counterparts [9, 13]. Therefore, the presence of a large quantity of π-bonded isobutene in the spectrum from figure 9a is a strong indication that the hydrogenation reaction proceeds almost exclusively through this species.

The addition of a hydrogen to form adsorbed isobutyl may take place either at the terminal carbon or at the internal carbon of the olefin bond (Fig 11). For terminal addition, a 2-isobutyl groups is formed, whereas a 1-isobutyl groups is produced from internal addition of a hydrogen atom. Figure 9a gives clear evidence that the surface concentration of 2-isobutyl group dominates that of 1-isobutyl groups during reaction at 105 Torr H_2. This is expected because terminal addition is far more favorable than internal addition, as has been previously shown both in gas phase and surface studies [13, 25, 26].

The preference for terminal addition, however, does not guarantee that 2-isobutyl groups are important intermediates in isobutene hydrogenation. The relative hydrogenation rates of 1-isobutyl and 2-isobutyl are also important. Indeed, the hydrogenation pathway through 1-isobutyl could become important, even for small surface concentrations of this species, provided its hydrogenation rate is significantly faster than that of 2-isobutyl. The vacuum hydrogenation spectra indicate that this is indeed the case (Figs. 7b and 8b). Therefore, the hydrogenation mechanism is somewhat ambiguous.

The rate of isobutene hydrogenation on Pt(111) is strikingly slow when compared with other butenes. Recent, results for isobutene, 1-butene, and cis butene hydrogenation compiled by Yang et al. show that isobutene hydrogenation is a factor of 20 slower than the other butenes under conditions of 100 Torr H_2 and 10 Torr butene at 295 K [24]. The reason for the substantial difference in turnover rate between isobutene and other butenes must stem from the fact that isobutene hydrogenates through 1- and 2-isobutyl, while all other butenes hydrogenate though 1- and 2-butyl intermediates. The important distinction between these pathways is that 2-isobutyl (the favored pathway for the initial hydrogen addition) contains a tertiary carbon attached to the metal while the 2-butyl species has a secondary carbon bonded to the underlying (111) surface.

The energy required to break the carbon metal bond in the case of 2-isobutyl is expected to be lower than for other butyl groups, but steric hindrance may prevent hydrogen from inserting into this species. This most likely causes a severe restriction of this pathway. Indeed, hydrogenation though a 1-isobutyl intermediate may represent the dominant pathway for isobutane production.

7.4 Conclusions

The rate of isobutene hydrogenation was found to be greatly suppressed compared with the hydrogen of straight chain butenes. This was attributed to the slow hydrogenation of 2-isobutyl, which may be prevented from hydrogen incorporation by steric hindrance. During reaction the concentration of the dehydrogenation product, isobutylidyne, was very small because of the relatively fast hydrogenation rate of this species. Under ultra high vacuum conditions it was observed that di-σ bonded isobutene dehydrogenates to isobutylidyne through an isobutylidene intermediate.

7.5 References

[1] I. Horiuti and M. Polanyi, Trans. Faraday Soc., 30 (1934) 1164

[2] C. Kemball, Proc. Chem. Soc., (1956) 735

[3] J. Schlatter and M. Bodart, J. Catal., 24 (1972) 482

[4] Y. Soma, J. Catal., 59 (1979) 239

[5] T. Beebe and J. Yates, J. Am. Chem. Soc., 108 (1986) 663

[6] S. Moshin, M. Trenary, H. Robota, J. Phys. Chem., 92 (1988) 5229

[7] R. Cortright, S. Goddard, J. Rekoske, and J. Dumesic, J. of Catal., 127 (1991) 342

[8] P. Cremer and G. Somorjai, J. Chem. Soc. Faraday Trans., 91, 20 (1995) 3671

[9] P. Cremer, X. Su, Y. Shen, G. Somorjai, J. Am. Chem. Soc., 118 (1996) 2942

[10] S. Davis, F. Zaera, B. Gordon, and G. Somorjai, J. of Catal., 92 (1985) 250

[11] U. Starke, A. Barbieri, N. Materer, M. Van Hove, G. Somorjai, Surf. Sci., 286 (1993) 1

[12] T. Land, T. Michely, R. Behm, J. Hemminger, G. Comsa, J. Chem. Phys., 97 (1992) 6774

[13] P. Cremer, X. Su, Y. Shen, G. Somorjai, submitted to J. Phys. Chem.

[14] G. Shahid and N. Sheppard, Spectrochimica Acta, 46a, 6 (1990) 999

[15] L. Lok, N. Gaidai, S. Kiperman, Kinetika i Kataliz, 32 (1991) 1406

[16] P. Otero-Schipper, W. Wachter, J. Butt, R. Burwell, and J. Cohen, J. of Catal., 50 (1977) 494

[17] J. of Catal., 24 (1972) 40

[18] G. Rogers, M. Lih, and O. Houen, AIChE J., 12 (1966) 369

[19] G. Shahid and N. Sheppard, Can. J. Chem., 69 (1991) 1812

[20] N. Avery and N. Sheppard, Proc. R. Soc. London A, 405 (1986) 1

[21] M. Chester, P. Gardner, and P. Pudney, see ref. 19 unpublished work

[22] P. Cremer, C. Stanners, J. Niemantsverdriet, Y. Shen, G. Somorjai, Surf. Sci., 328 (1995) 111 and references therein

[23] F. Zaera, Surf. Sci., 219 (1989) 453

[24] M. Yang and G. Somorjai, unpublished results

[25] R. Klein and M. Scheer, J. Phys. Chem., 62 (1958) 1011

[26] M. Yang, A. Tephyakov, B. Bent, in preparation

7.6 Figure Captions

Fig. 1 Mechanisms for ethylene and propylene hydrogenation.

Fig. 2 The structure of iobutenic moieties on platinum.

Fig. 3 The SFG spectrum of a saturation coverage of di-σ bonded isobutene on Pt(111) formed by exposing the clean surface to 4 L of isobutene at 120 K

Fig. 4 The SFG spectrum of a saturation coverage of isobutylidyne on Pt(111) formed at 295 K by exposing the clean surface to 4 L of isobutene

Fig. 5 The SFG spectra of the thermal decomposition of a saturation coverage of di-σ bonded isobutene measured at (a) 200 K and (b) 270 K

Fig. 6 The decomposition mechanism for isobutene/Pt(111)

Fig. 7 (a) The SFG spectrum of a saturation coverage of 1-isobutyl/Pt(111) formed from by adsorbing the corresponding iodide at 120 K and annealing to 205 K for 10 seconds. (b) The hydrogenation of (a) with 1000 L of H_2 at 205 K.

Fig. 8 (a) The SFG spectrum of a saturation coverage of 2-isobutyl/Pt(111) formed from by adsorbing the corresponding iodide at 120 K and annealing to 205 K for 10 seconds. (b) The hydrogenation of (a) with 1000 L of H_2 at 205 K.

Fig. 9 (a) The *in situ* SFG spectrum of isobutene hydrogenation with 105 Torr H_2, 40 Torr isobutene, and 635 Torr He at 295 K. (b) The *in situ* SFG spectrum of isobutene hydrogenation with 20 Torr H_2, 5 Torr isobutene, and 760 Torr He at 295 K

Fig. 10 A schematic representation of the comparison of the hydrogenation of ethylidyne, propylidyne, and isobutylidyne to their respective alkylidenes.

Fig. 11 Possible mechanisms for the hydrogenation of isobutene on Pt(111)

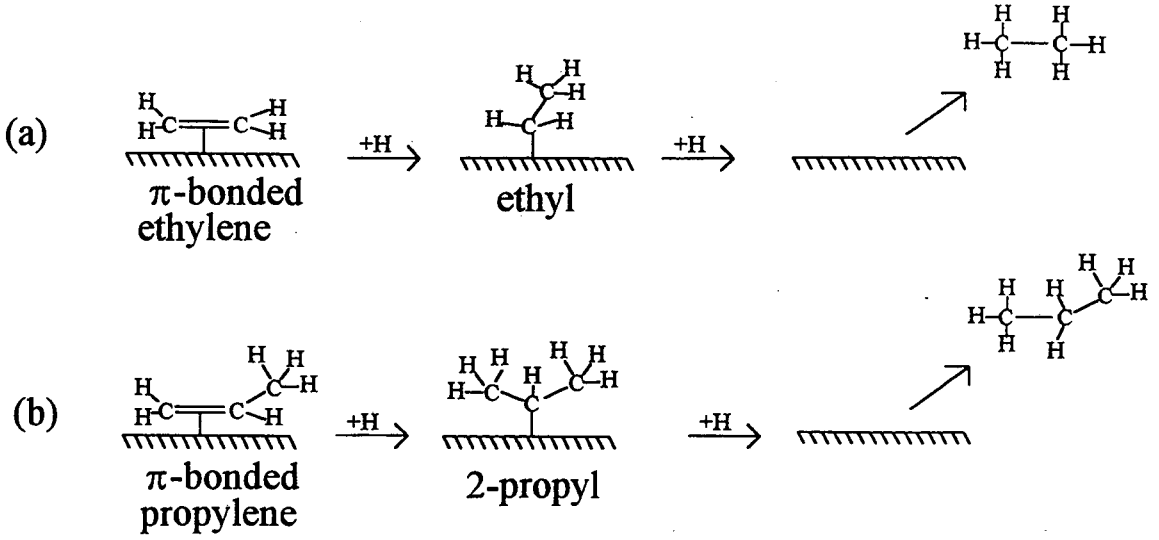

Fig. 1

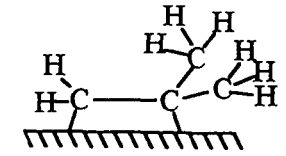

di- σ bonded isobutene

(A)

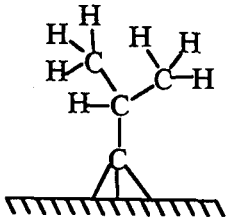

isobutylidyne

(B)

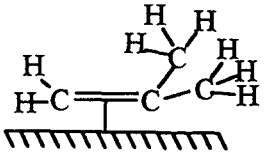

π-bonded isobutene

(C)

Fig. 2

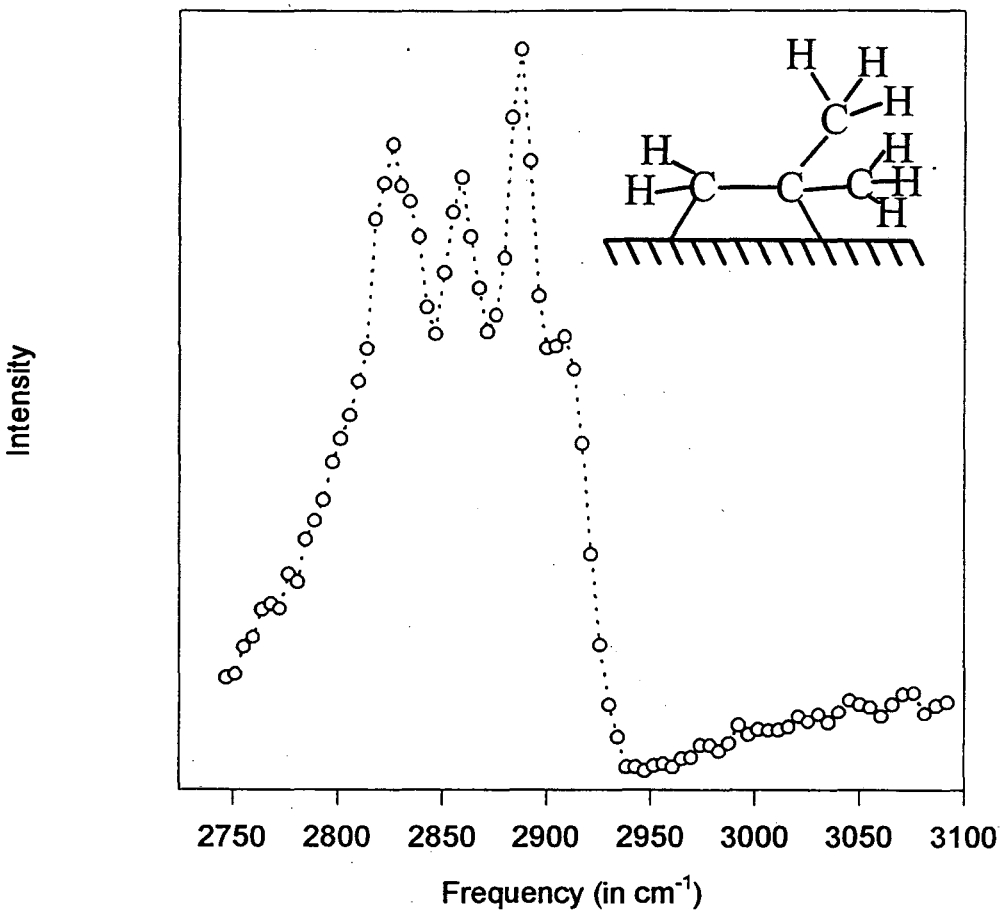
Intensity
2750
2800
2850
2900
2950
3000
3050
3100
Frequency (in cm-1)

Fig. 3

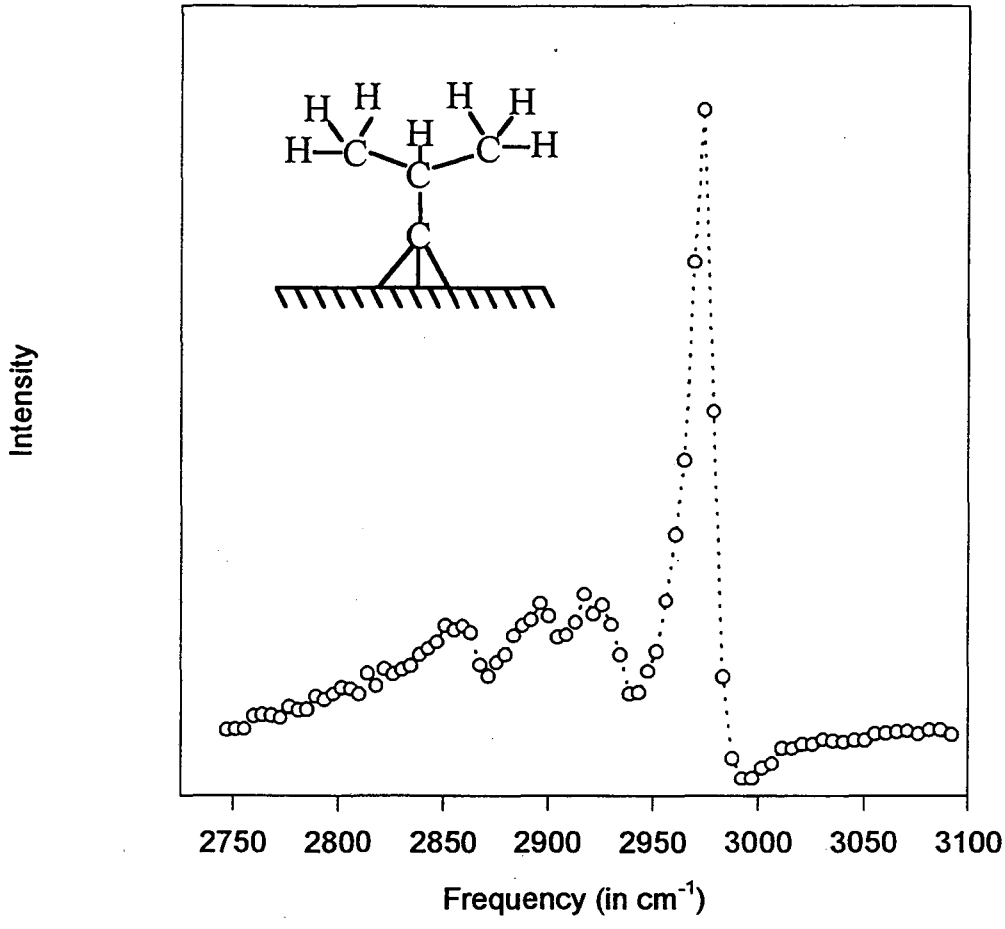
Intensity
2750
2800
2850
2900
2950
3000
3050
3100
Frequency (in cm-1)

Fig. 4

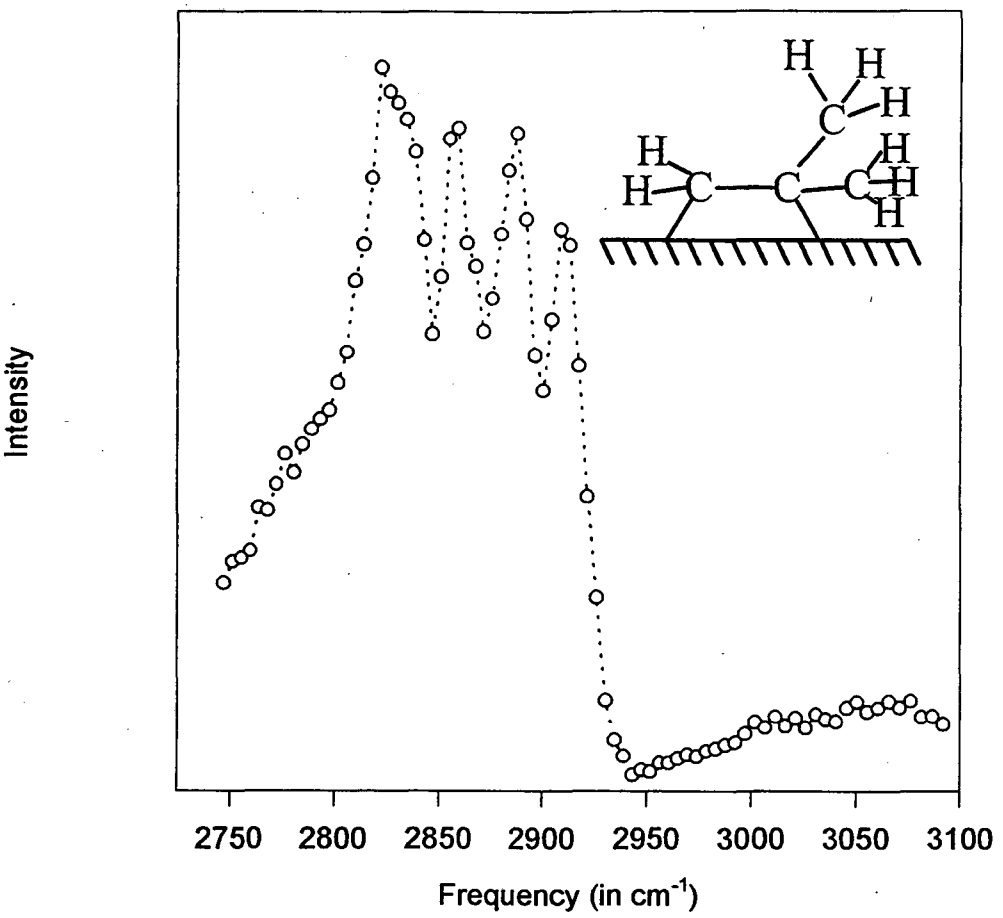
Intensity
H
H
H
H
H
H
H
H
C
C
C
2750
2800
2850
2900
2950
3000
3050
3100
Frequency (in cm-1)

Fig. 5a

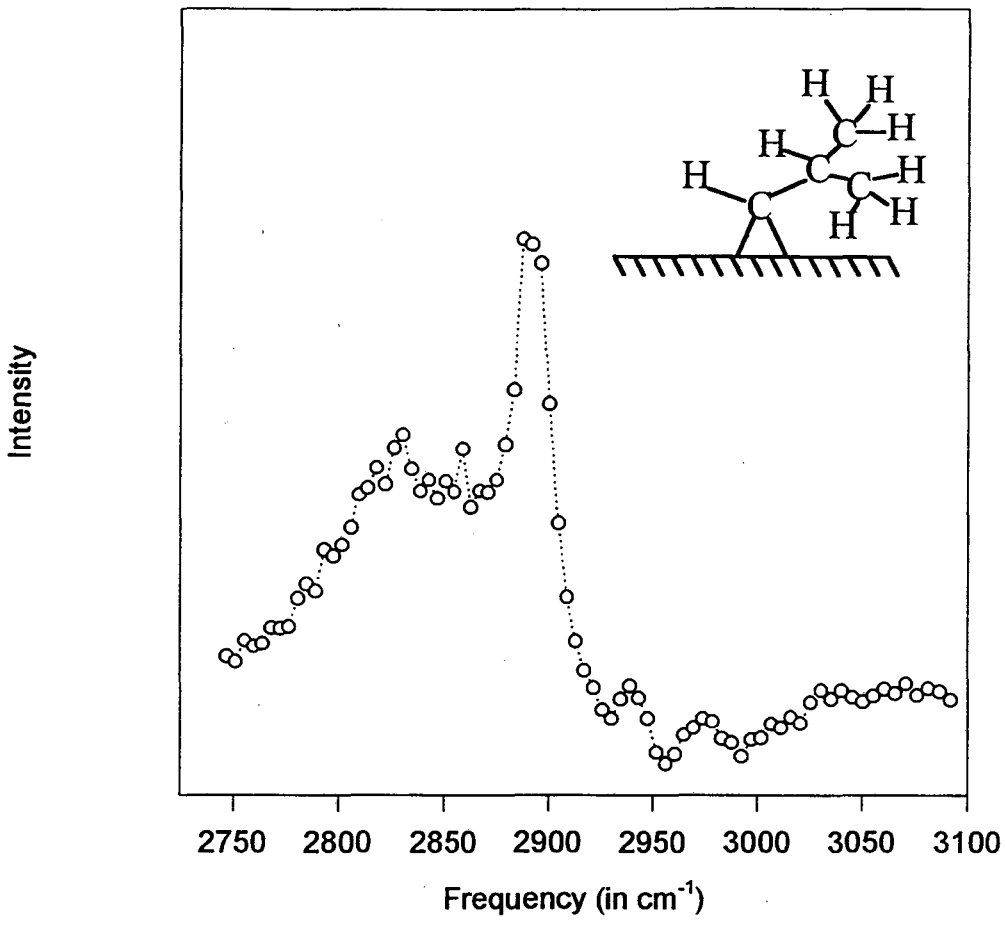
Intensity
H
H
H
H
H
C
C
C
H
H
H
H
2750
2800
2850
2900
2950
3000
3050
3100
Frequency (in cm-1)

Fig. 5b

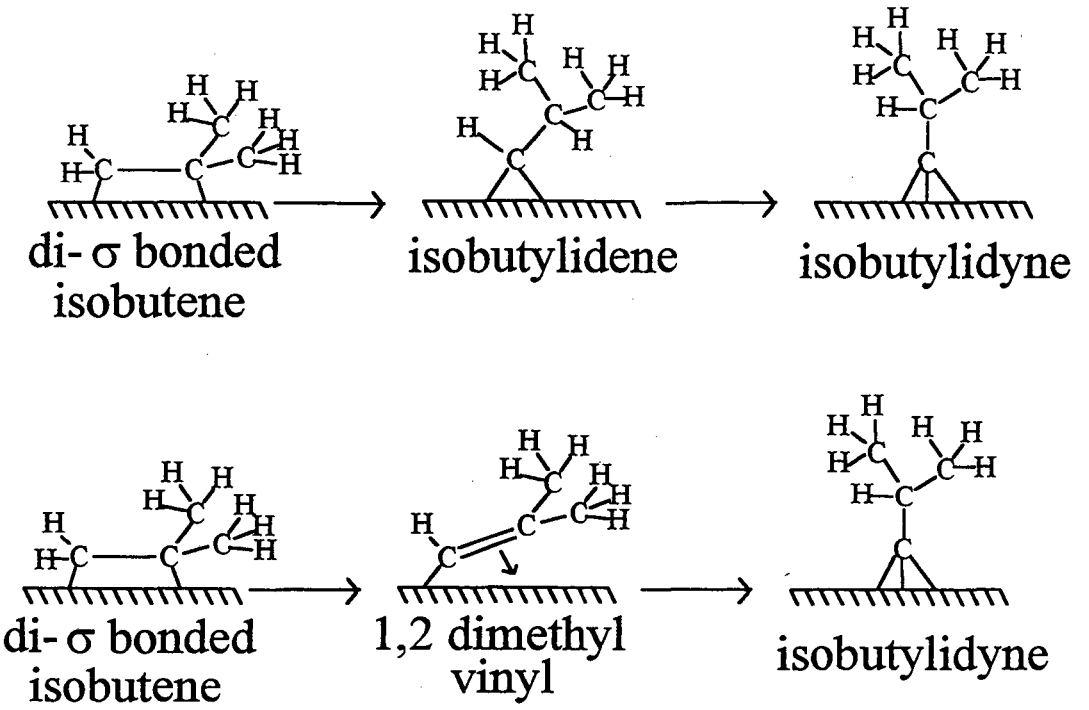
di- σ bonded
isobutene
isobutylidene
isobutylidyne
di- σ bonded
isobutene
1,2 dimethyl
vinyl
isobutylidyne

Fig. 6

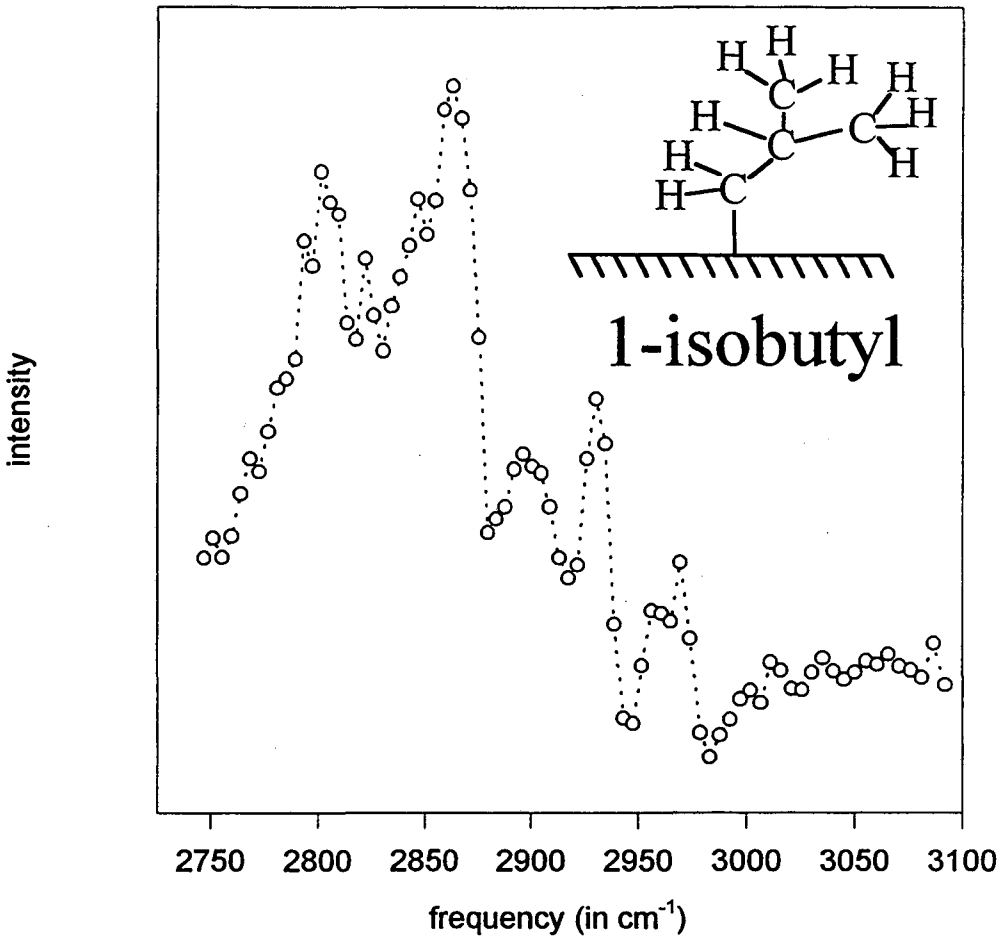
intensity
1-isobutyl
2750
2800
2850
2900
2950
3000
3050
3100
frequency (in cm-1)

Fig. 7a

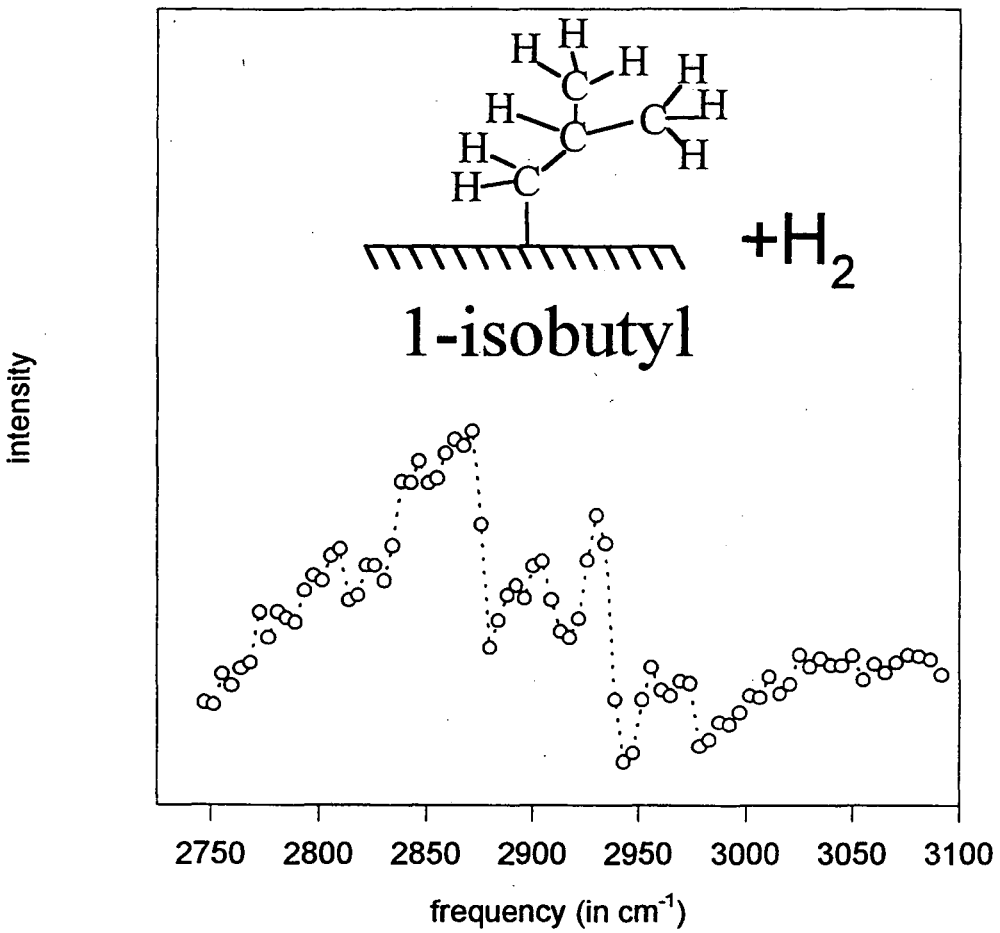
intensity
1-isobutyl
+H2
2750
2800
2850
2900
2950
3000
3050
3100
frequency (in cm-1)

Fig. 7b

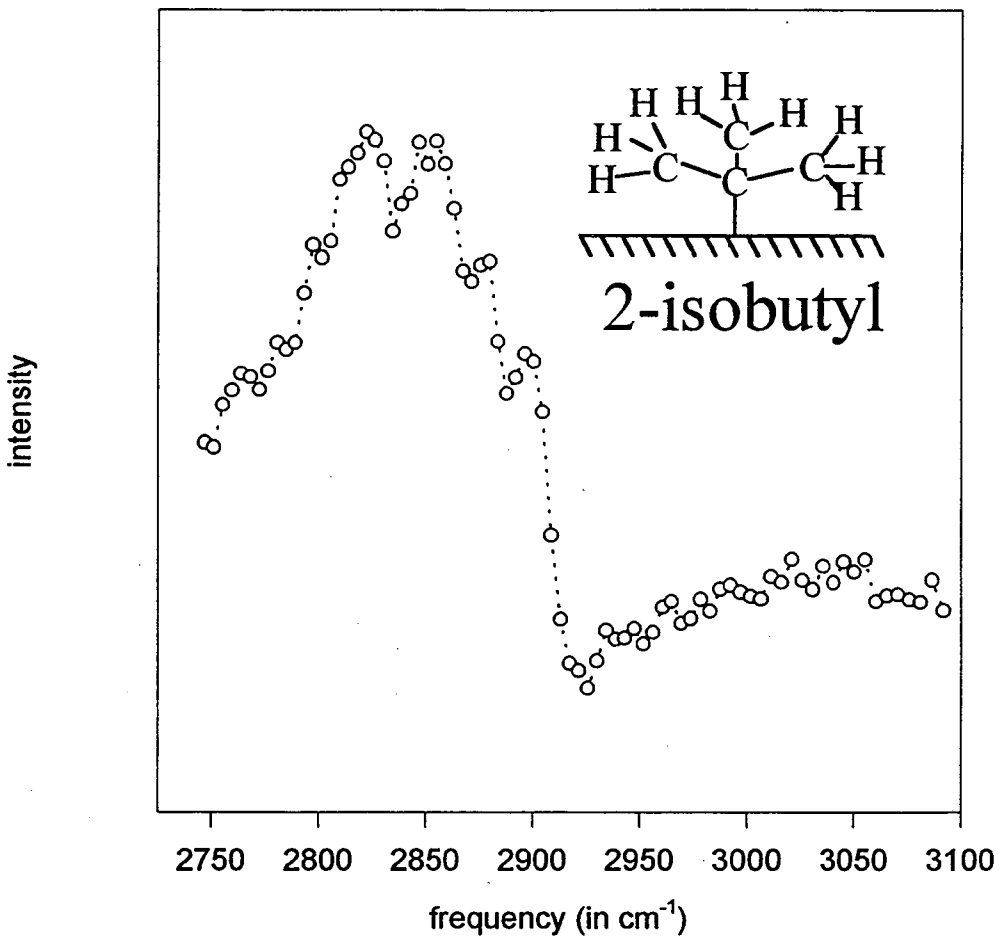
intensity
2-isobutyl
2750
2800
2850
2900
2950
3000
3050
3100
frequency (in cm-1)

Fig. 8a

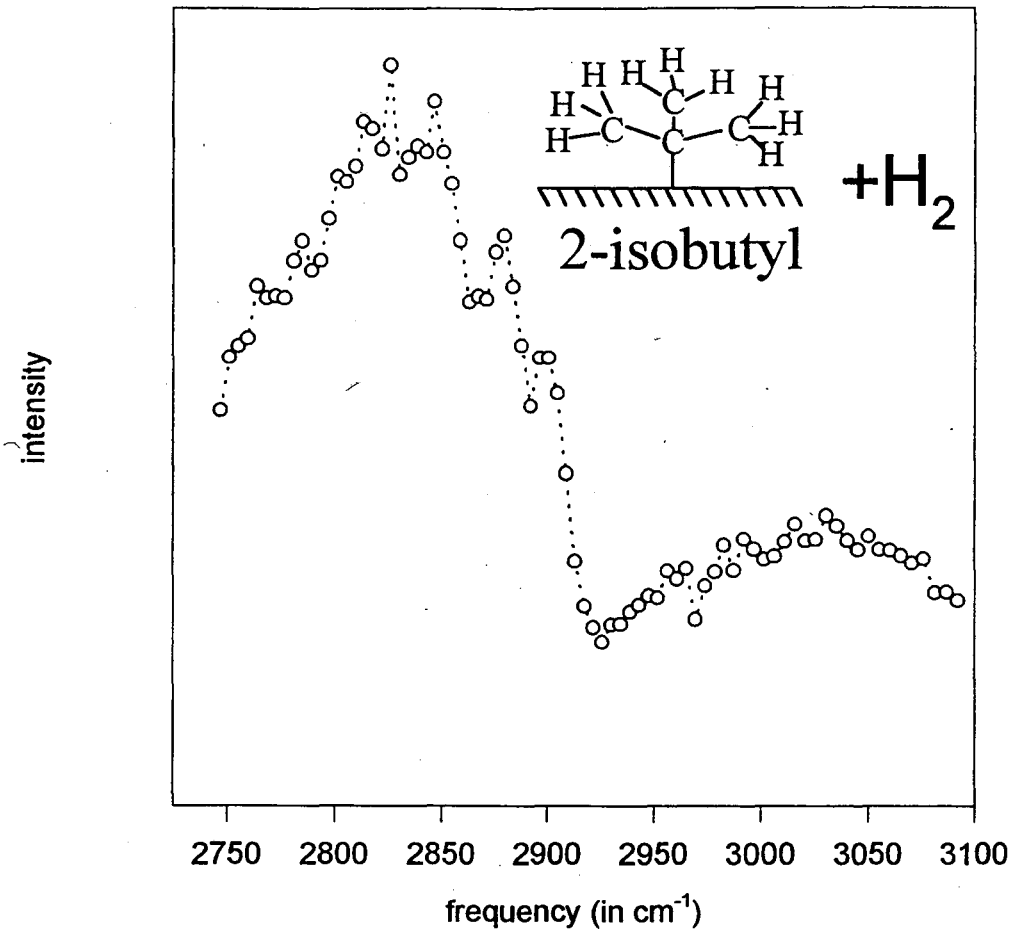
intensity
2-isobutyl
+H2
2750
2800
2850
2900
2950
3000
3050
3100
frequency (in cm-1)

Fig. 8b

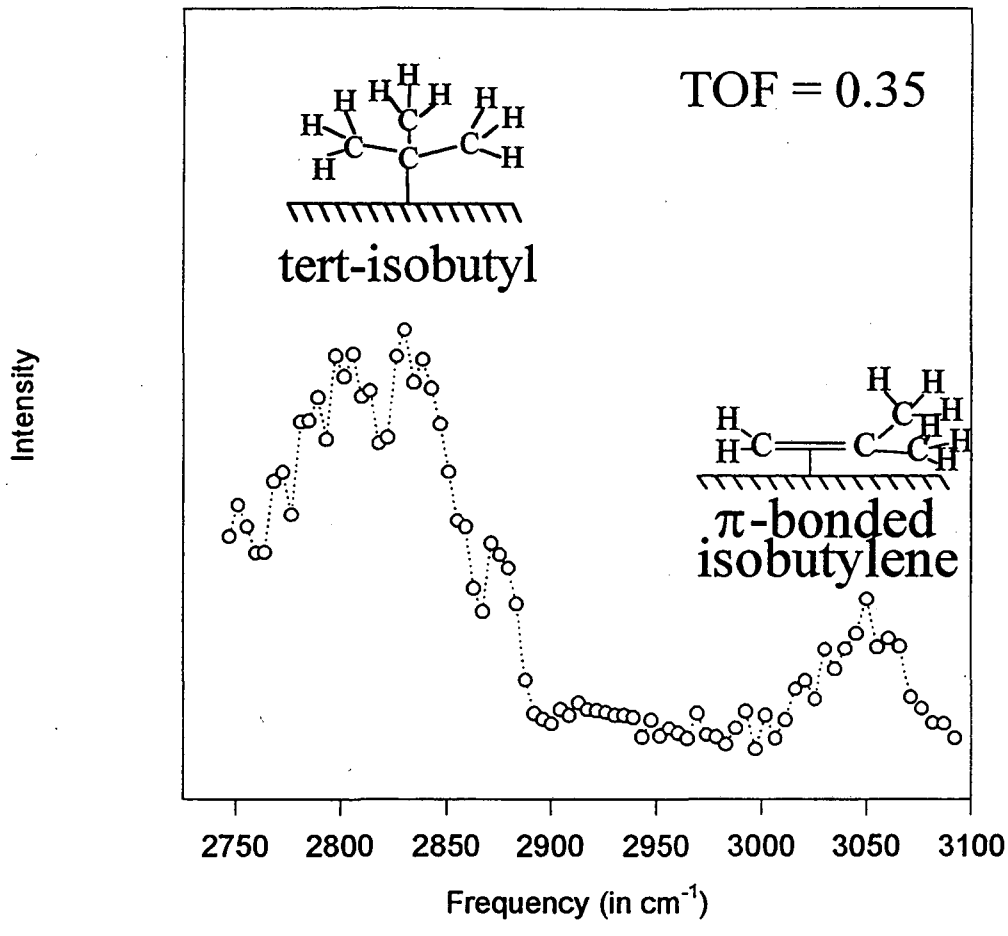
TOF = 0.35
tert-isobutyl
π-bonded
isobutylene
Intensity
2750
2800
2850
2900
2950
3000
3050
3100
Frequency (in cm-1)

Fig. 9a

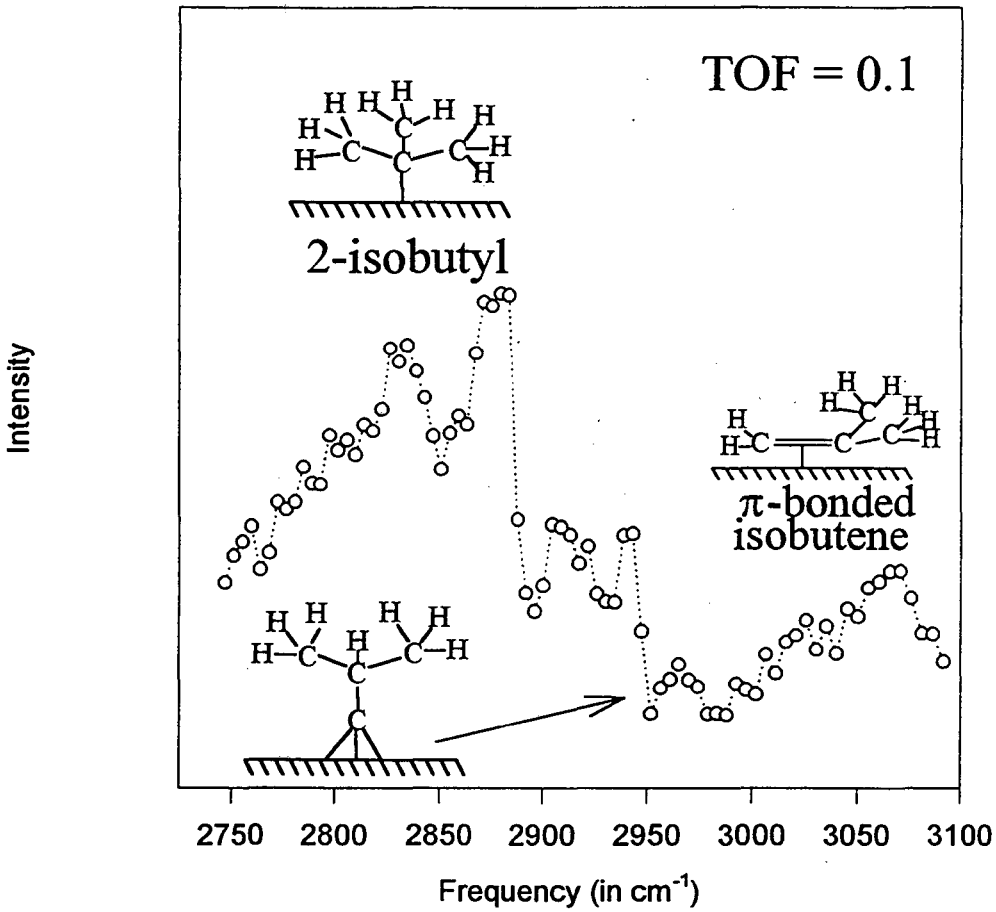
TOF = 0.1
2-isobutyl
π-bonded
isobutene
Intensity
2750
2800
2850
2900
2950
3000
3050
3100
Frequency (in cm-1)

Fig. 9b

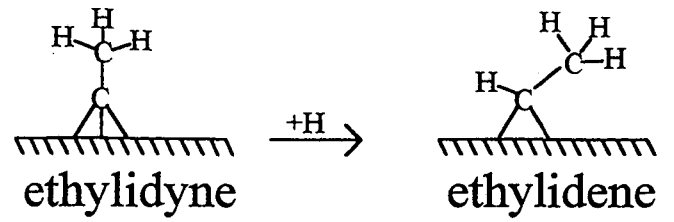
+H
ethylidyne
ethylidene
Slow

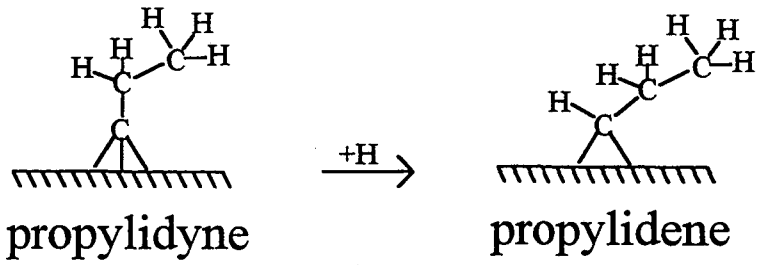
+H
propylidyne
propylidene
Fast

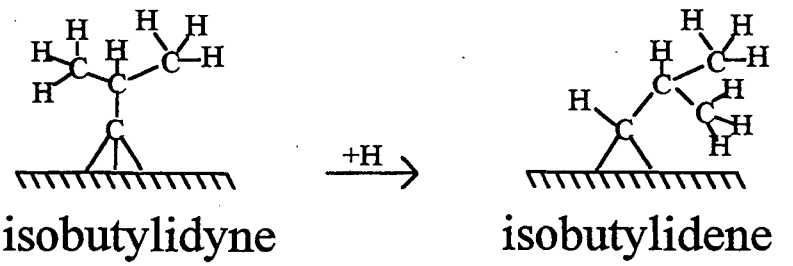
+H
isobutylidyne
isobutylidene
Faster

Fig. 10

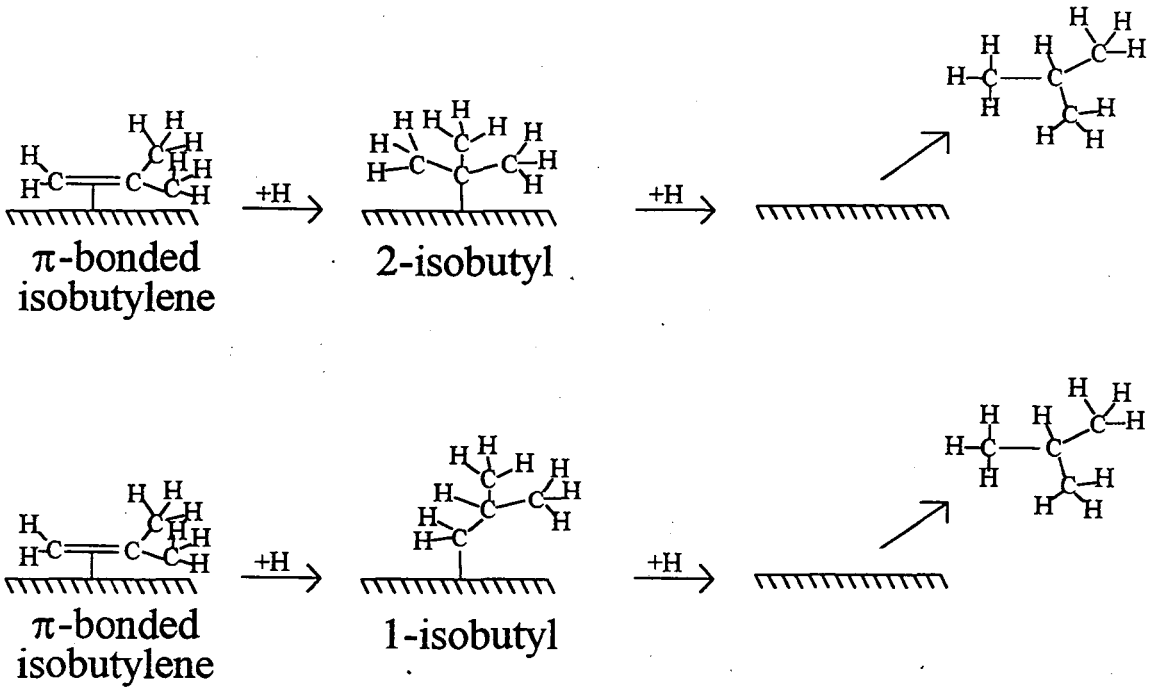
+H
+H
π-bonded isobutylene
2-isobutyl
+H
+H
π-bonded isobutylene
1-isobutyl

Fig. 11

Chapter 8

The Adsorption of Chiral Molecules on Achiral Surfaces: 2-Butanol/BaF_2

The vibrational spectra for (S) 2-butanol and racemic 2-butanol adsorbed on BaF_2 were monitored near 305 K. At this temperature it was found that the packing density of (S) 2-butanol was greater than for the racemate, while a small change in the molecular orientation could also be noted. This contrasted with the bulk liquid, where it has been found that the density difference between either of the entantiomers and the racemate is less than 0.1%.

8.1 Introduction

The behavior of enantiomers with respect to their racemate has been studied in great detail for many bulk systems [1]. Indeed it has been shown that many physical properties such as boiling point, melting point, density, and, viscosity differ for certain pure enantiomers with respect to their racemates. In most of the systems that show large differences in physical properties, the functional groups attached to the chiral center are all quite different. An example of such a system is α-(Trifluoromethyl)benzyl alcohol ($C_6H_5CHCF_3OH$). The enantiomers of this species freeze near room temperature, while the racemate remains a liquid to low temperature. On the other hand chiral systems exist for which there is little difference between the physical properties of the pure enantiomers and racemate. For this to be the case, there is usually little difference in at least two of the constituents attached to the chiral center. An example of this second case is $CH_3CH(C_9H_{19})(C_{10}H_{21})$. For this molecule, the two long alkyl chains are nearly the same length; therefore, the difference in interaction of either hand of this chiral pair with a chiral or racemic environment is approximately the same.

There are also borderline examples where it should be possible to enhance the differences in physical properties under certain conditions, but not others. Specifically, the behavior of chiral molecules could be very different in the bulk liquid then in an adsorbed monolayer. The origin of any difference would lie in the decrease in entropy in the monolayer.

The purpose of this paper is to identify such a borderline system (namely 2-butanol), where the differences in the physical properties of the racemate and enantiomer can be amplified by comparing the packing density and orientation of their monolayers at the BaF_2 interface. The density and molecular orientation of a monolayer of (S) 2-butanol is compared with (S&R) 2-butanol by infrared-visible sum frequency generation.

8.2 Experimental

Racemic 2-butanol and (S) 2-butanol were adsorbed on a BaF_2 surface by keeping the solid/vapor interface saturated with the alcohol at ambient vapor pressure. This was done by mounting a BaF_2 window on a sealed liquid cell filled with 2-butanol [Fig. 2]. Multilayers of butanol were prevented from fogging the BaF_2 window by resistive heating. This left only a single monolayer of butanol adsorbed at the BaF_2 surface.

The butanol/BaF_2 system was monitored by infrared-visible sum frequency generation in the CH stretch range. Spectra were taken for the SSP, PPP, and SPS polarization combinations.

8.3 Results

Figure 3a shows the vibrational spectrum for (S&R) 2-butanol/BaF_2 monitored with the SSP polarization combination. Three distinct features are observed in the CH stretch range. To obtain the proper assignments and peak strengths, the spectrum has been fitted with the standard nonlinear equation [2]:

$$\left|\chi^{(2)}\right|^2 = \left|\frac{A}{\omega_a - \omega_{ir} + i\Gamma_a} + \frac{B}{\omega_b - \omega_{ir} + i\Gamma_b} + \frac{C}{\omega_c - \omega_{ir} + i\Gamma_c} ke^{i\varphi}\right|^2 \qquad (1)$$

The form of the equation used assumes three resonant features (A, B, C) damped by Γ_i and a nonresonant background (k) which may have a phase relationship φ with respect to the resonances. The results are shown in table 1. The three resonances are at 2860 cm^{-1}, 2893 cm^{-1}, and 2951 cm^{-1}, and can be assigned to a fermi resonance, the $\nu_s(CH_3)$, and the $\nu_{as}(CH_3)$ respectively [3].

The identical experiment was repeated with (S) 2-butanol [Fig. 3b]. In this case the same three features were observed at approximately the same frequencies. However, in

this case the overall intensity of the spectrum was greater than from the racemic system. The fitting parameters revealed that the small fermi resonance near 2859 cm^{-1} is somewhat lower than in the first case, while the methyl symmetric and asymmetric stretches are higher [table 1].

The experiments were repeated using the PPP and SPS polarization combinations. Figures 4 a&b show the vibrational spectra for racemic 2-butanol and (s) 2-butanol respectively monitored by the PPP combination. Again the same three features are present (albeit in different ratios from the SSP case). The overall intensity is less than half of that obtained for SSP. The symmetric and asymmetric methyl stretches are substantially more intense for the levorotatory system than for the racemate; however, in this case the fermi resonance is also quite a bit stronger from the enantiomer. Another significant difference of changing the polarization combination is the blue shift in the apparent frequency fitted to the $\nu_{as}(CH_3)$ for the PPP spectra. This blue shift is most likely the result of a poor least squares fit rather than a significant spectral change. Alternatively, the problem may lie in the fact that both methyl groups from the 2-butanol molecules can contribute intensity to the $\nu_{as}(CH_3)$ feature at slightly different frequencies. This may lead to the broadening of the lineshape and the difficulty in fitting the spectrum with only three spectral features (eqn. 1).

SPS spectra yield dramatically different results (Figs. 5 a&b). There is a substantial nonresonant background that interferes with the resonant features. The strength of the fermi resonance and asymmetric stretch are stronger in the racemate, while the symmetric stretch is stronger in the (S) 2-butanol system. Both the symmetric and asymmetric stretch features are blue shifted with respect to the SSP polarization combination. Again, this may stem from probing of the two different methyl groups.

8.4 Discussion

2-butanol is a chiral molecule for which little difference can be noted between the physical properties of the racemate compared with a single enantiomer in the bulk liquid (table 2) [1]. Indeed, the density of the levorotatory molecule is only 0.09% greater than the racemate. However, the heat of interaction of left handed molecules with other left handed molecules is slightly greater than the interaction of left handed molecules with right handed molecules (accounting for the small density difference).

$$H_{\text{int}(S-S)} > H_{\text{int}(S-R)} \qquad (2)$$

The difference should be dominated by entropic contributions to the free energy near room temperature.

$$\Delta H_{\text{int}(diff)} < T\Delta S_{\text{int}} \qquad (3)$$

$$\Delta G_{\text{int}(diff)} = \Delta H_{\text{int}(diff)} - T\Delta S_{\text{int}(diff)} \qquad (4)$$

To amplify the difference in physical properties of the enantiomer with respect to the racemate, one must suppress the entropic term. There are two ways to achieve this:

{1} the temperature of the system may be lowered

{2} the entropy of the entire system may be decreased

Lowering the temperature is a crude approach. For example, a liquid system may freeze long before density changes, phase separation, or other differences become significant. The second approach, however, is quite simple. A reasonable reduction in the entropy can be achieved by reducing the dimensionality of the system from three to two. The primary effect of such a reduction is to reduce the three dimensional translational partition function to the two dimensional case:

$$q_{trans(2D)} = \frac{2\pi m}{h^2\beta} XY$$
$$q_{trans(3D)} = \left(\frac{2\pi m}{h^2\beta}\right)^{3/2} XYZ \qquad (5)$$

where q_{trans} is the translational partition function, m is the molecular weight of 2-butanol, h is Planck's constant and β is kT [4]. If one writes the entropy in terms of the partition coefficient, the free energy of interaction the equation becomes:

$$\Delta G_{int(diff)} = \Delta H_{int(diff)} - T(\frac{U - U(0)}{T} - NK \ln[q]) \quad (6)$$

Replacing the 3D transitional partition function by the 2D equation results in a difference of 10 kcal/mol in TΔS at room temperature! Therefore, it is expected that decreasing the dimensionality should have an observable affect on the free energy of interaction. This is indeed the case as can be seen from the 2-butanol/BaF_2 data.

The overall signal provided by the chiral monolayer is larger for all polarization combinations examined. For example the SSP spectral intensity of the enantiomer is more than 10% greater than for the racemate. This may not be totally due to an increase in number density from the racemate to the enantiomer. Some of the enhancement is probably due to differences in molecular orientation of the monolayer when only the pure enantiomer is present. This can be clearly seen by the fact that some of the spectral features are greater for the racemate with certain polarization combinations. Any orientational change is likely to be small, but significant.

The signal observed from the $\nu_{as}(CH_3)$ of the left handed molecule is approximately 4% greater for the average of the SSP and SPS combinations than is the case for the racemate. There is even a greater difference for the symmetric stretch. In that case the average of SSP and SPS is 18% greater for the enantiomer than it is for the racemate.

A definitive analysis of this system will require the decoupling of the orientation component from the number density. This could be achieved by deuterating either the ethyl or methyl group to yield absolute orientation information. However, a rough estimate of the increase in packing density of the enantiomer would be a few percent. This is very significant in light of the fact that the bulk liquid showed only a 0.09% increase in density for the pure enantiomer over the racemate.

8.5 Conclusions

Significant differences in the packing density and orientation between racemic and (S) 2-butanol were observed at the BaF_2 interface. This contrasts with the bulk liquid where the differences in physical properties are quite small.

8.6 References

[1] CRC Handbook of Chemistry and Physics, 61st edition, ed. by R. Weast, 1980, CRC publication

[2] Y. Shen, Surf. Sci., 299/300 (1994) 551

[3] L.J. Bellamy, The Infrared Spectra of Complex Molecules (Wiley, New York, 1975).

[4] P. Atkins, Physical Chemistry (W. H. Freeman and Company, New York, 1990)

8.7 Figure Captions

Fig. 1 Schematic representations of left and right handed molecules.

Fig. 2 Liquid cell apparatus for the chiral-SFG experiment.

Fig. 3 The SFG spectra for (a) racemic and (b) levorotatory 2-butanol with the SSP polarization combination.

Fig. 4 The SFG spectra for (a) racemic and (b) levorotatory 2-butanol with the PPP polarization combination.

Fig. 5 The SFG spectra for (a) racemic and (b) levorotatory 2-butanol with the SPS polarization combination

8.8 Tables

Table 1 The coefficients for (s) 2-butanol and racemic 2-butanol on BaF_2 for SSP, SPS, and PPP polarization

Table 2 Physical properties of liquid (S) 2-butanol and racemic 2-butanol

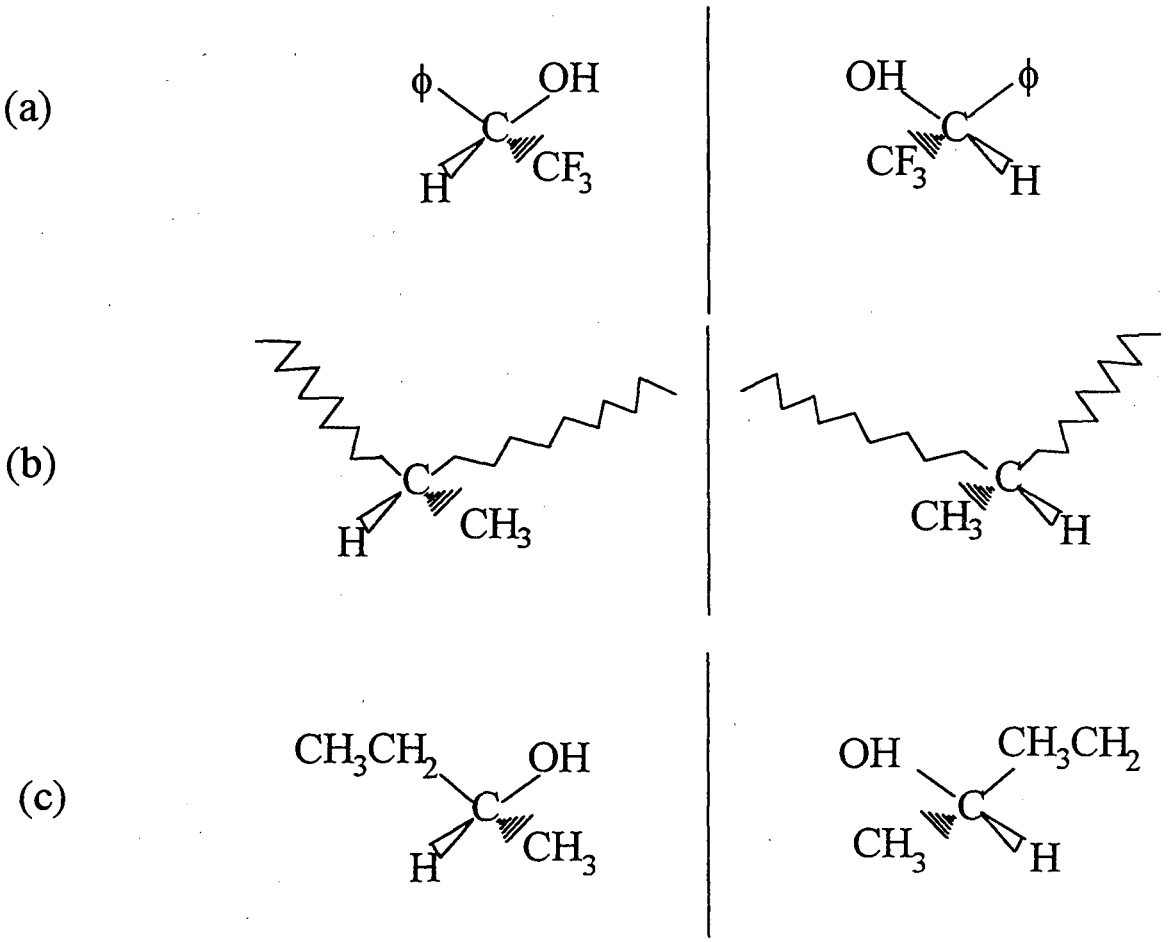
(a)
ϕ
OH
C
H
CF3
OH
ϕ
C
CF3
H
(b)
C
H
CH3
C
CH3
H
(c)
CH3CH2
OH
C
H
CH3
OH
CH3CH2
C
CH3
H

Fig. 1

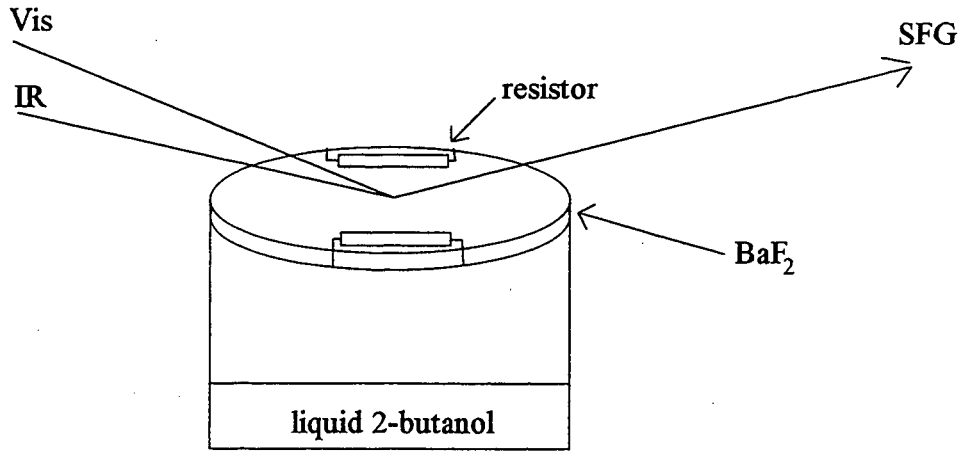

Fig. 2

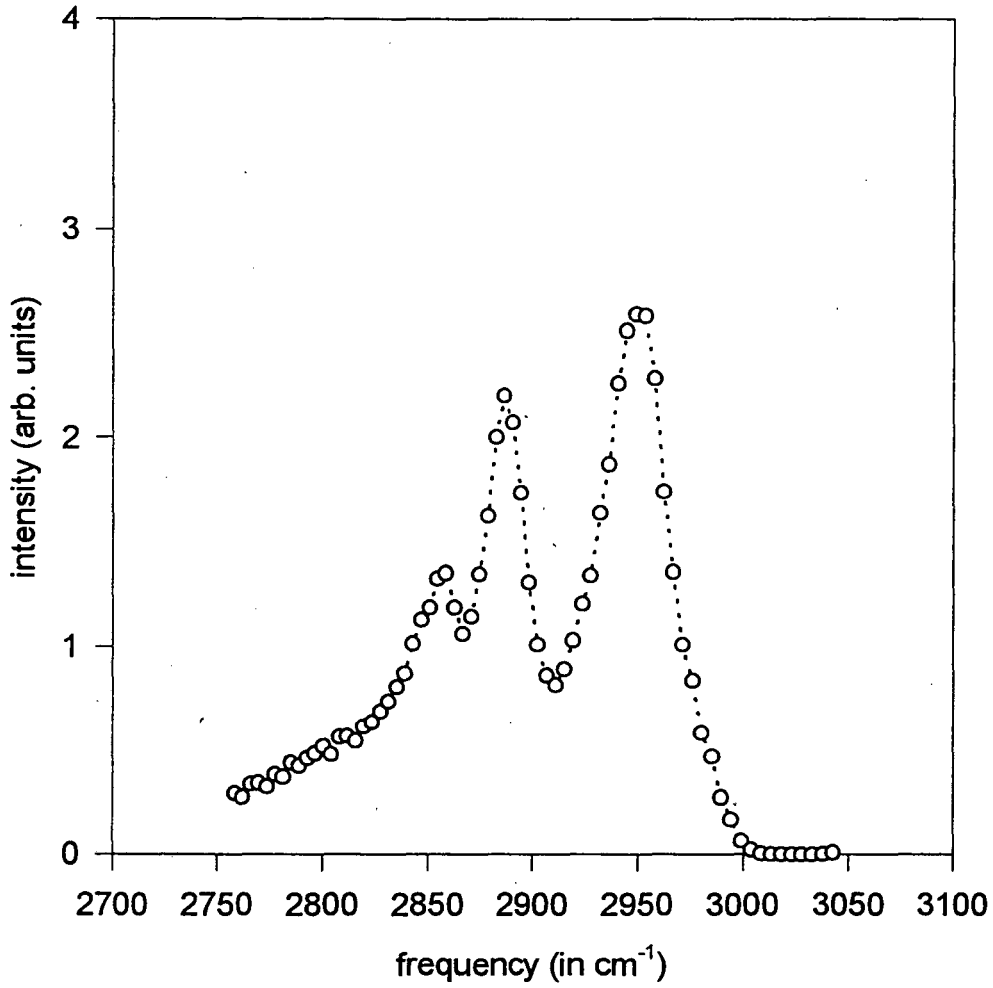
4
3
2
1
0
intensity (arb. units)
2700
2750
2800
2850
2900
2950
3000
3050
3100
frequency (in cm-1)

Fig. 3a

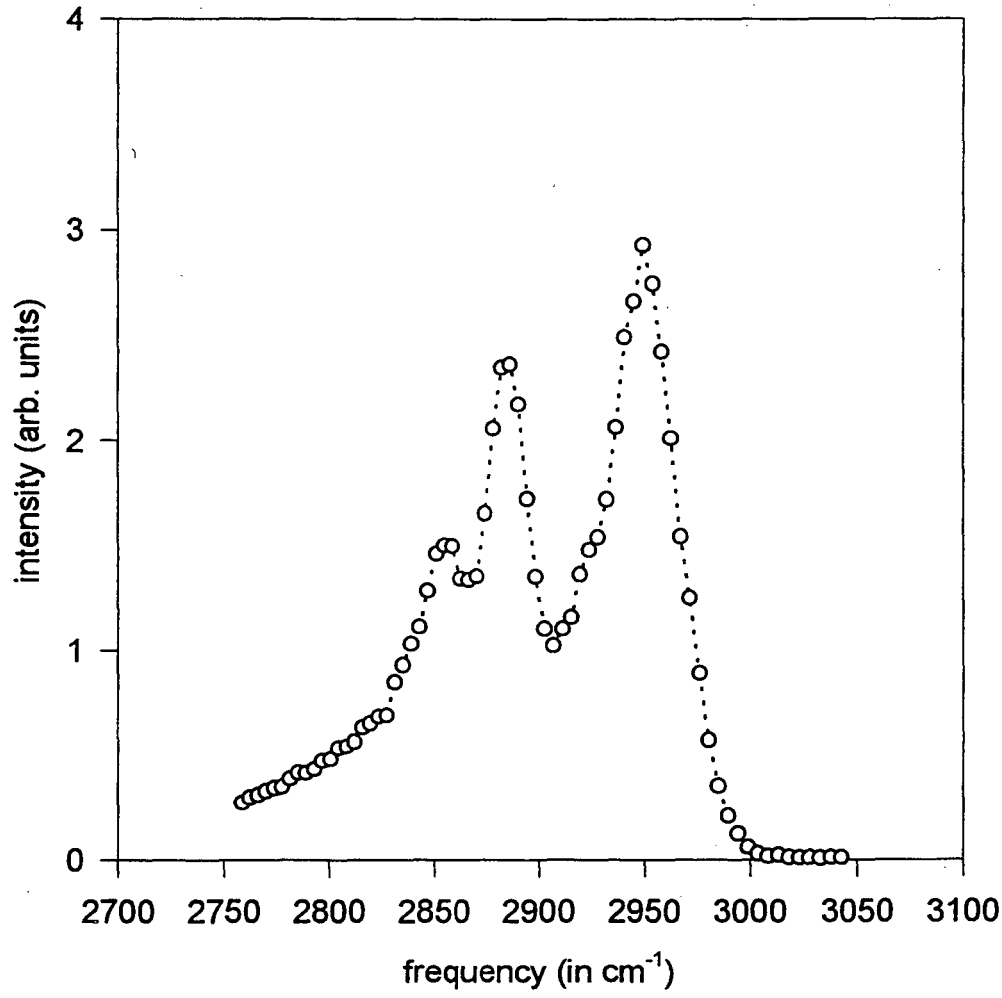
4
3
2
1
0
intensity (arb. units)
2700
2750
2800
2850
2900
2950
3000
3050
3100
frequency (in cm-1)

Fig. 3b

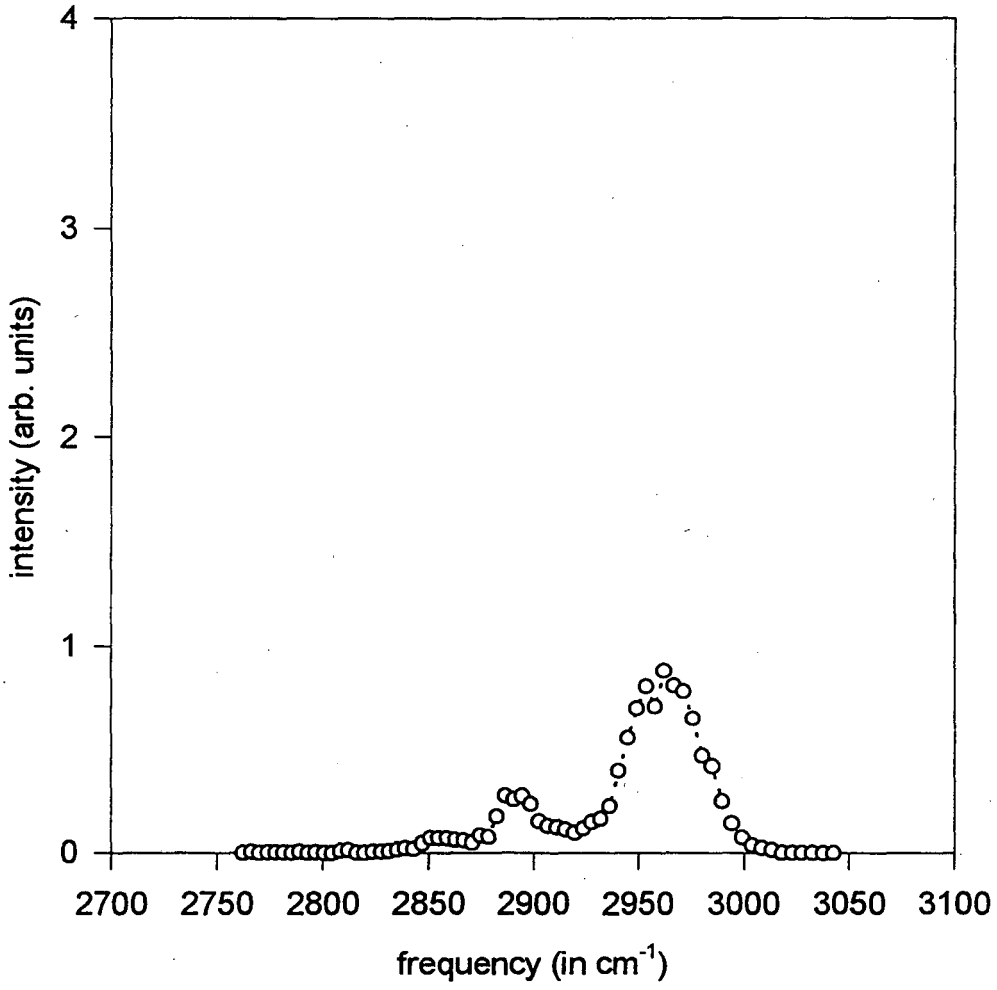
4
3
2
1
0
intensity (arb. units)
2700
2750
2800
2850
2900
2950
3000
3050
3100
frequency (in cm-1)

Fig. 4a

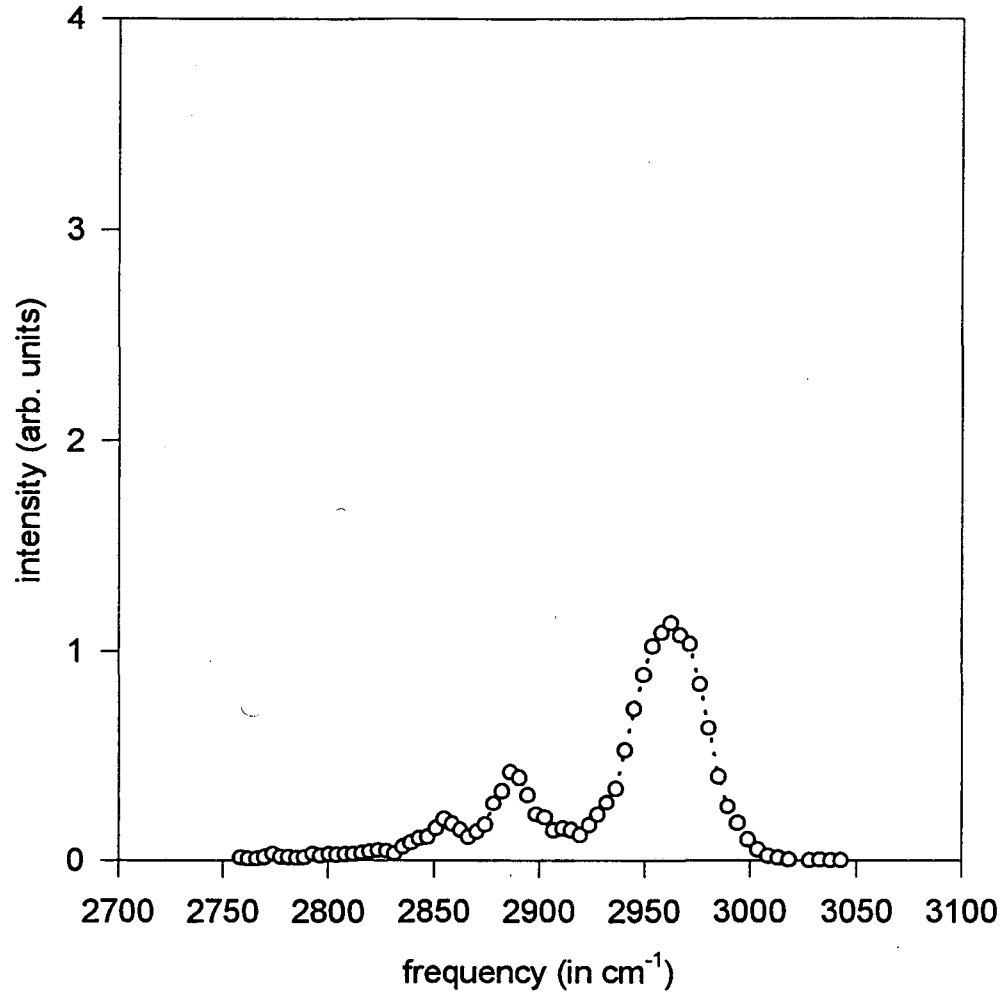
4
3
2
1
0
intensity (arb. units)
2700
2750
2800
2850
2900
2950
3000
3050
3100
frequency (in cm-1)

Fig. 4b

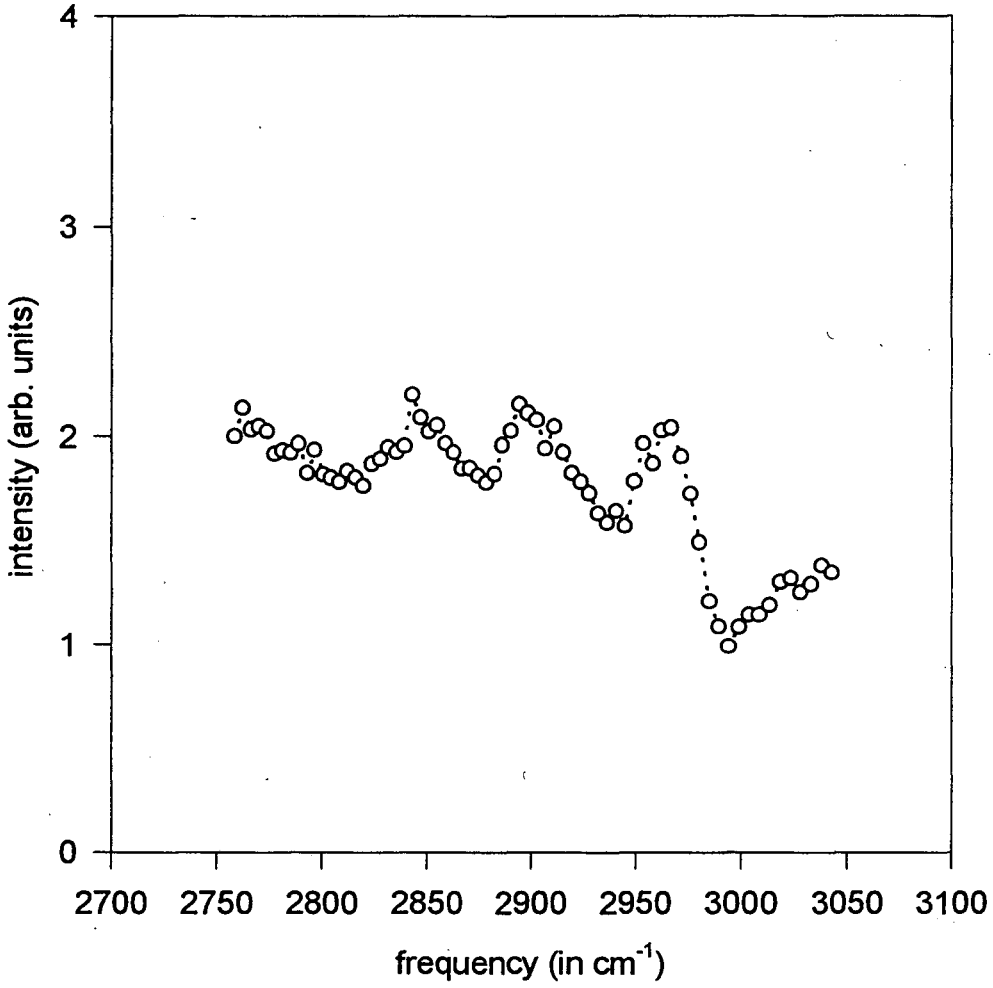
4
3
2
1
0
intensity (arb. units)
2700
2750
2800
2850
2900
2950
3000
3050
3100
frequency (in cm-1)

Fig. 5a

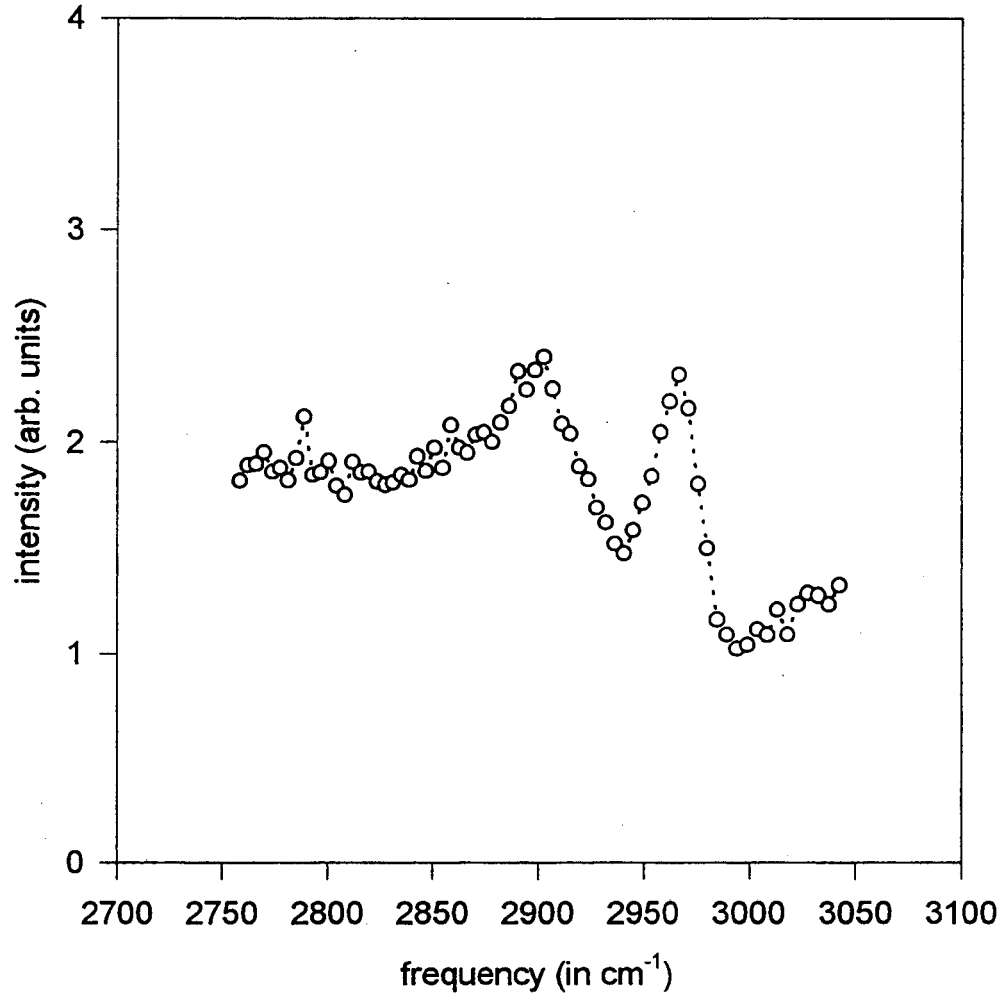
4
3
2
1
0
intensity (arb. units)
2700
2750
2800
2850
2900
2950
3000
3050
3100
frequency (in cm-1)

Fig. 5b

Table 1

	SSP (S)	SSP (S&R)	PPP (S)	PPP (S&R)	SPS (S)	SPS (S&R)
a	1.506	1.742	0.1330	*	-----	1.286
b	14.37	12.21	3.376	2.278	6.70	4.221
c	33.40	31.66	19.09	16.78	5.20	5.401
Γ_a	5.548	6.040	0.4654	*	-----	11.04
Γ_b	15.19	13.28	8.624	7.173	20.44	19.14
Γ_c	21.67	20.93	17.71	18.04	10.64	13.38
ω_a	2859	2860	2858	2858	-----	2860
ω_b	2891	2893	2894	2898	2913	2918
ω_c	2950	2951	2963	2863	2975	2977
k	0.350	0.348	0.0991	0.0520	1.23	1.277
θ	346°	351°	351°	347°	347°	359°

Table 2

	[α]	boiling point	density	η
(s) 2-butanol	+13.9°	372.5 K	0.8070 g/ml	1.3975
(s&r) 2-butanol	+0.0°	372.5 K	0.8063 g/ml	1.3978

Chapter 9

The Assignment of the Vibrational Spectrum For Ethanol at the Liquid/Vapor Interface

9.1 Results

The purpose of this work is to assign the CH stretch range of neat ethanol at the liquid vapor interface. In previous work by Stanners et al. three peaks were observed in this range at 2875 cm^{-1}, 2933 cm^{-1}, 2975 cm^{-1} [1]. The first two features were assigned to the $\nu_s(CH_2)$, $\nu_s(CH_3)$ respectively, while the small feature at higher frequency was assigned to either the $\nu_{as}(CH_3)$ or $\nu_{as}(CH_2)$.

In order to properly assign the CH stretch range we revisited this investigation with partially deuterated ethanols. An example of the vibrational spectrum for CH_3CH_2OH is shown in figure 1 for reference. The vibrational spectrum for CD_3CH_2OH revealed two peaks at 2875 cm^{-1} and 2975 cm^{-1} (Fig. 2), while the spectrum for CH_3CD_2OH gave rise to peaks at 2875 cm^{-1} and 2933 cm^{-1} (Fig. 3). Combining figures 2 and 3 yields a satisfactory approximation of the CH_2CH_3OH spectrum (Fig. 4).

Raman assignments for the CH stretch range of ethanol have been made by Kamogawa et al [2]. Their assignments are: $\nu_s(CH_2)$ at 2879.6 cm^{-1}, $\nu_s(CH_3)$ at 2927.1 cm^{-1}, and $\nu_{as}(CH_2)$ at 2972 cm^{-1}. Infrared data on partially deuterated ethanol reveal

that there is intensity near 2931 cm^{-1} for the CH_3CD_2OH species, which is most likely the $\nu_s(CH_3)$ [3]. However, the present work on CH_3CD_2OH shows that there is signal from the CH_3 group near 2875 cm^{-1} as well, we therefore conclude that the 2875 cm^{-1} feature in the CH_3CH_2OH spectrum derives intensity from both the $\nu_s(CH_2)$ and a the methyl group (probably a fermi resonance). Both signals at 2875 cm^{-1} are rather weak in their respective deuterated spectra [Figs. 2&3]. It is only the combination of these two feature that gives rise to strong signal near 2875 cm^{-1} (Figs. 1 and 4). Further, we assign the 2975 cm^{-1} feature exclusively to $\nu_{as}(CH_2)$, because no intensity is seen in that region from CH_3CD_2OH (Fig. 2).

9.2 References

[1] |C. Stanners, Q. Du, R. Chin, P. Cremer, G. Somorjai, and Y. Shen, Chem. Phys. Lett., 232 (1995) 407

[2] K. Kamogawa, S. Kaminaka, and T. Kitagawa, J. Phys. Chem., 91 (1987) 222

[3] H. Dothe, M. Lowe, and J. Alper, J. Phys. Chem., 93 (1989) 6632

9.3 Figure Captions

Fig. 1 SFG spectrum of neat ethanol.

Fig. 2 SFG spectrum of CD_3CH_2OH

Fig. 3 SFG spectrum of CH_3CD_2OH

Fig. 4 Combination spectrum of figures 2 and 3.

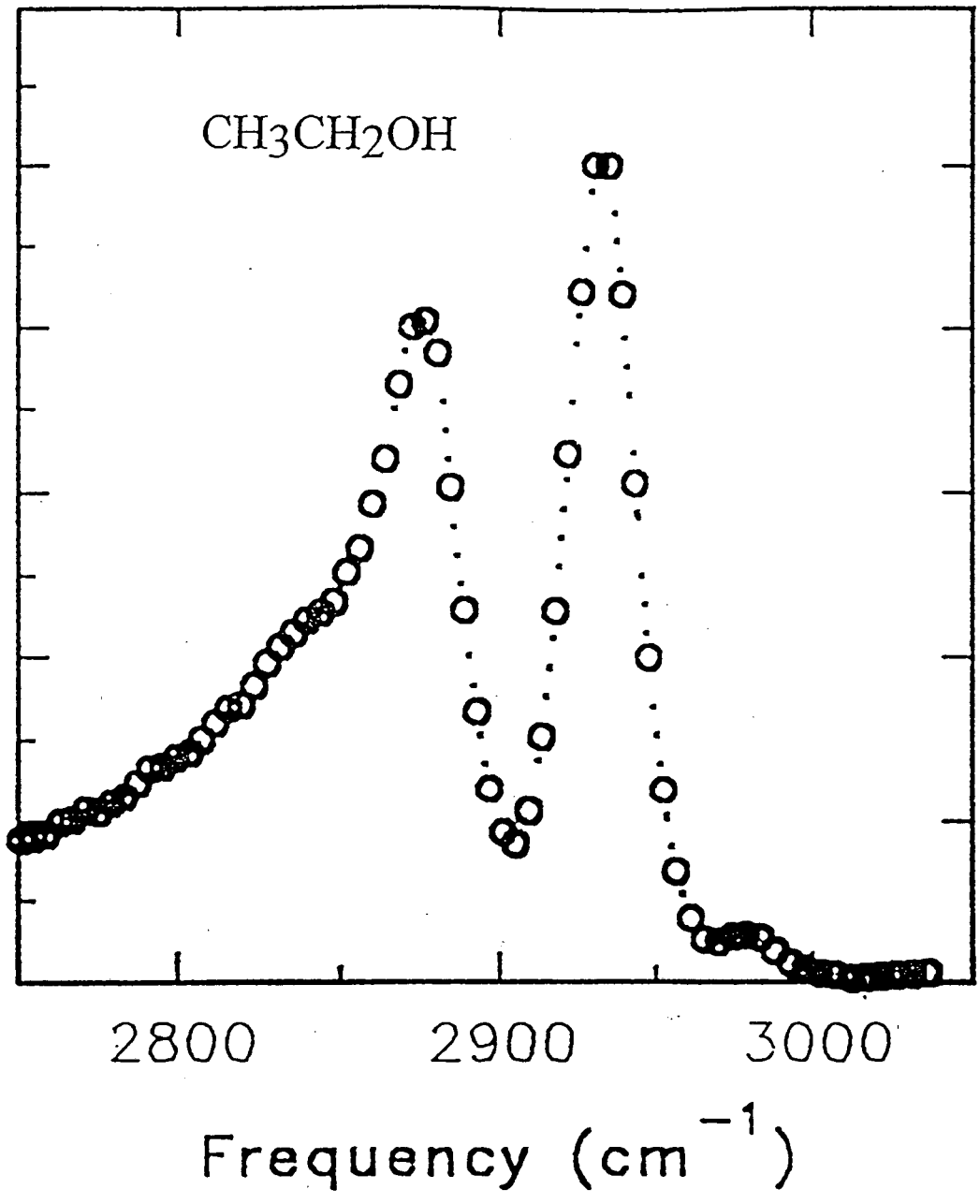

Fig. 1

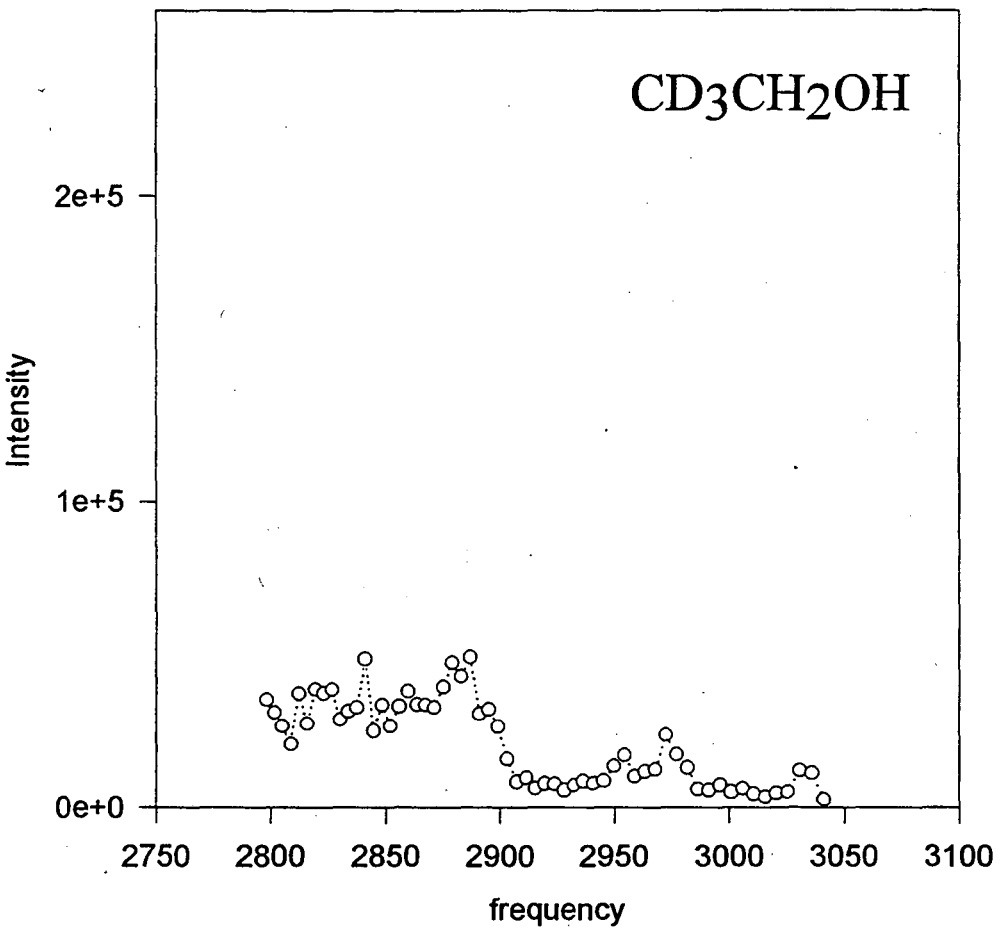
CD3CH2OH
2e+5
1e+5
0e+0
Intensity
2750
2800
2850
2900
2950
3000
3050
3100
frequency

Fig. 2

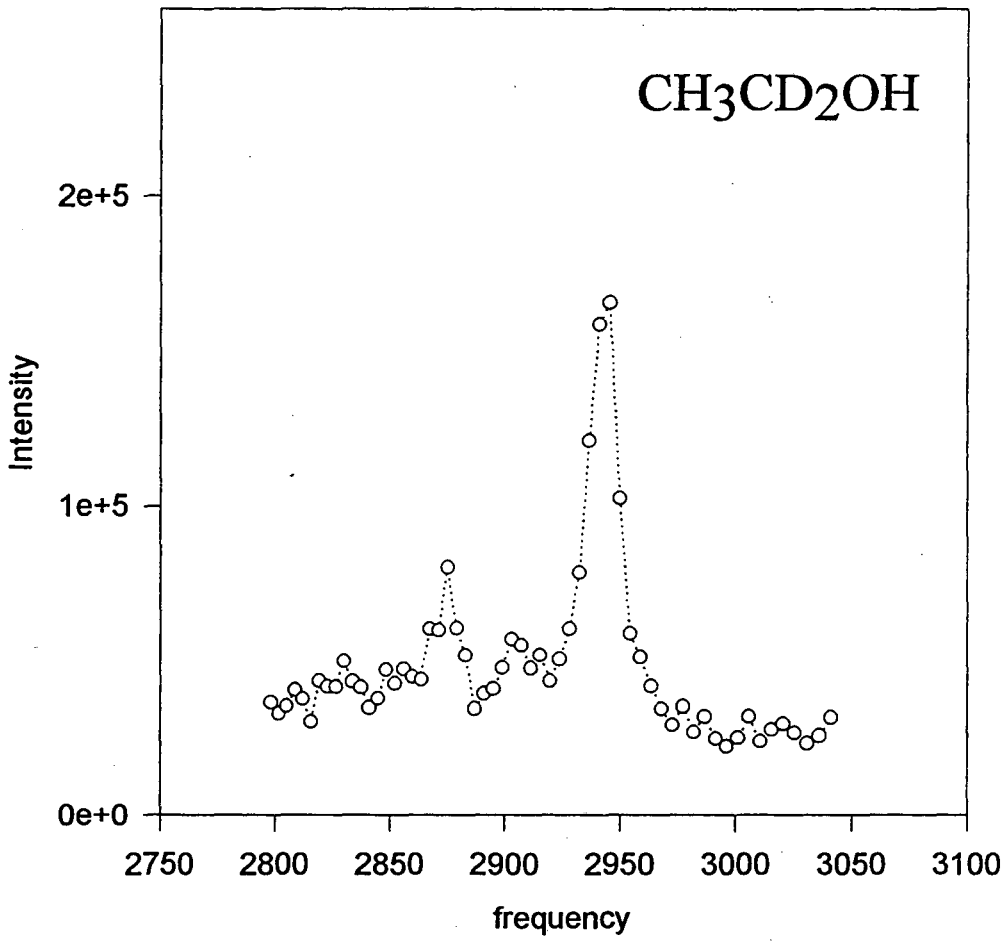
CH3CD2OH
2e+5
1e+5
0e+0
Intensity
2750
2800
2850
2900
2950
3000
3050
3100
frequency

Fig. 3

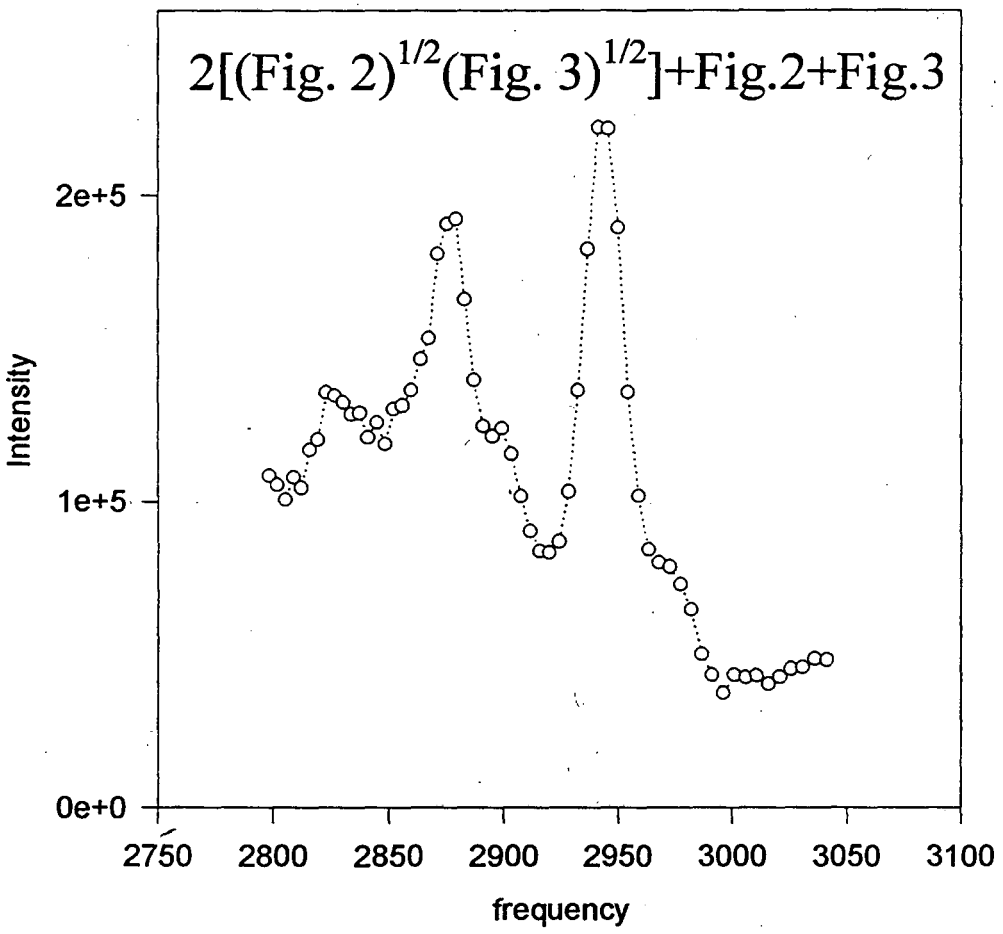
2[(Fig. 2)^1/2(Fig. 3)^1/2]+Fig.2+Fig.3
Intensity
2e+5
1e+5
0e+0
2750
2800
2850
2900
2950
3000
3050
3100
frequency

Fig. 4

Chapter 10

Conclusions

The surface science of heterogeneous catalysis has finally begun to focus on *in situ* studies of catalytic reactions as technology has advanced. This is true for model single crystals as shown by the present investigation of olefin hydrogenation on Pt(111) by infrared-visible sum frequency generation. Scanning tunneling/atomic force microscopy and UV Raman spectroscopy also hold great promise in this field. The latter would make an excellent compliment to SFG as it is more suitable on supported catalysts. On the other hand, STM/AFM will provide data about the morphology of the underlying catalyst that neither of the vibrational spectroscopies can provide.

The near term goal will be to concentrate on the differences between the species seen under ultra high vacuum conditions and the ones present on the surface during reactions at high pressure. It can already be seen from the present work that there are substantial differences. Under vacuum the species that reside on the surface are primarily chemisorbed while the species the "do" catalysis appear to be more weakly bound. This observation needs to be explored for a wide variety of systems including: ethylene oxidation, Fischer Tropsch synthesis, ammonia synthesis, methane coupling, and many others to see whether it holds true for both structure sensitive and structure insensitive reactions.

In the longer term *in situ* studies will ultimately need to concentrate on improving catalytic processes in real industrial settings. It appears that this should now be possible. Intermediate concentrations in reactions could be studied as a function of promoter concentration, temperature, reactant pressure, etc. Indeed, it may already be time to reconsider the role surface science can play in advancing commercial catalysis.

Ernest Orlando Lawrence Berkeley National Laboratory
One Cyclotron Road | Berkeley, California 94720

Prepared for the U.S. Department of Energy under Contract No. DE-AC03-76SF00098